Printing Conductive Paths for Electronic Functional Devices

SALAH MASWOUD

A thesis submitted to De Montfort University in partial fulfilment of the requirements for the degree of Doctor of Philosophy

Emerging Technologies Research Centre, De Montfort University, The Gateway, Leicester LE1 9BH, UK

Aug 2019

Printing Conductive Paths for Electronic Functional Devices

Salah Maswoud

PhD Supervisors:

Prof. Shashi Paul – 1st Supervisor

Dr. Iulia Salaoru – 2nd Supervisor

Dr. Sridhar Govindarajan – 2nd Supervisor

Emerging Technologies Research Centre, De Montfort University, The Gateway, Leicester LE1 9BH, UK

August 2019

Author’s declaration

I declare that the research work in this thesis was performed in accordance with the guidelines and regulation of De Montfort University and has not been submitted for any other degree nor qualifications at this university or any other academic institutions.

The work contained presented in this thesis has been conducted as a result of my own effort unless otherwise stated. The author must be acknowledged for any use of any part of this work unless for private study or academic purposes.

Salah Maswoud

August 2019

Acknowledgments

First, I would like to express my deep gratitude and indebtedness to my first supervisor, Prof. Shashi Paul, Head of Emerging Technologies Research Centre (EMTERC), for his academic and expert guidance, motivation, support and assistance that he has been offering.

Special thanks and appreciation are also due to the rest of my supervision team; Dr. Iulia Salaoru and Dr. Sridhar Govindarajan for their continuing recommendations and useful comments for this research work.

I am thankful to all EMTERC staff and students for their help, support and lovely times. Thanks also to all my friends inside and outside my second home, De Montfort University, with whom I have felt like they are my family during happy and hard times during this PhD journey.

Finally, my sincere gratitude, thankfulness and appreciation always go to Allah, my parents and all my family for being, forever, in my life, heart and mind.

Abstract

Printing inorganic and organic materials has been attracting plenty of researchers and scientists as an alternative to the conventional photolithography and electroless deposition methods due to the complications, time-consuming, size restrictions and high costs that these methods usually experience. Soft lithographic techniques and inkjet printing technology have offered simpler, lower costs and faster alternatives. One of the main objectives of this study is the contribution to these alternatives by utilising a cost-effective, simple and easy-to-use stamp printing machine in the deposition of metal patterns from poly(dimethylsiloxane) (PDMS) stamps onto treated glass substrates. Two drop-on-demand inkjet printers; one is a commercial desktop piezoelectric printer and a second thermal PEL printing and coating platform, were utilised to inkjet print functional materials. The cheap piezoelectric one used to deposit silver nanoparticles and poly(3,4-ethylenedioxythiophene)-poly(styrenesulfonate) (PEDOT:PSS) inks. By utilising this technology, innovative flexible information storage devices, electronic memory cells, were inkjet printed. All the components (silver electrodes and PEDOT:PSS active layer) of these memory devices were fully deposited by this simple desktop inkjet printer on a flexible substrate (ceramic coated PEL paper) at room temperature. The thermal printing machine, on the other hand, was employed to print graphene oxide on the PEL paper. These techniques also provide hope to develop environmentally friendly processes of fabrication used in the electronics and semiconductor industry and minimise the wastage of materials and power.

Table of contents

List of tables

List of figures

Printing Conductive Paths for Electronic Functional Devices

Chapter 1: Introduction

This chapter offers an overview on how stamp/transfer printing, soft lithography and inkjet printing technology emerged as alternatives to conventional deposition techniques. The motivations of this research and an overview of organisation of the thesis are included in this chapter.

1.1 Introduction

The focus on miniaturisation is of interest to a large number of researchers and scientists as it forms the foundation of modern and emerging technologies used in manufacturing and applications of micro and nanotechnology. That is due to its high efficiency, low consumption of power and cheap production costs when comparing with the macro industry. Therefore, the micro and nanofabrication methods have increasingly and continuously been developed to meet the requirements and advances in this field. Traditionally, the fundamental and prime fabrication methods used for manufacturing electronic devices and in the research laboratory are high-resolution lithographic techniques. Photolithography (optical lithography) has played a significant role in the semiconductor industry and made a major contribution to the fabrication process [1]. However, the increasing requirements and applications for high-resolution patterning of emerging small components and devices have led to the failure of the techniques that depend on photolithography due to optical diffraction and wavelength limitations of the used light. As a consequence, new approaches have been evolved to overcome the problems and the limitations of conventional lithographic techniques. One of which is the soft lithographic approach that was pioneered by the development of Microcontact Printing (μCP) by Whitesides and co-workers [2] at Harvard University, USA, and Metal Transfer Printing (MTP) [3] which was developed out of the soft lithographic technique to deposit metals. These techniques have been attracting many researchers and scientists and soon become one of the most commonly used methods for micro and nanofabrication. Despite the fact that these approaches, the microcontact printing (μCP) and metal transfer printing (MTP), were developed more than two decades ago and have been widely employed to pattern surfaces in micro and nanoscale for applications in chemistry, optics, electronics and nanobiotechnology, a simple, easy to use, cost-effective and automated instrument for the stamping and transfer printing processes has not been introduced.

One of the main objectives of this project is the utilisation of an automated deposition machine whose working principle is based on both microcontact printing and micro metal transfer printing processes using a cheap, easy to use, simple instrument and control system that enables it to precisely manipulate the stamping process where a fine movement and appropriate stamping pressure are needed to obtain distortion-free patterns with high resolution in a relatively large area within a reasonable time. The proposed technique is aimed to stamp/transfer micro and nanoscale patterns and expected to mass-produce the printed metal tracks with a reasonable budget and it is also anticipated to be viable for the industrial and commercial manufacturing field, especially, emerging technologies electronic devices both in micro and nanoscale devices such as the ones have been developed at Emerging Technologies Research Centre (EMTERC) including emerging electronic memories, photovoltaic solar cells, chemical and biosensors.

Another alternative way of depositing functional materials has emerged and been widely investigated is the non-contact inkjet printing technology. This technique has proven its reliability and cost-effectiveness as well as the reduction of wasted materials. It is also considered as one of the environmentally friendly techniques to replace the conventional deposition methods for the functional materials. In this study, the technique was utilised to deposit some functional material including, silver nanoparticles (Ag NPs), poly(3,4-ethylenedioxythiophene)-poly(styrenesulfonate) (PEDOT:PSS) and graphene oxide (GO) using a commercial desktop piezoelectric inkjet printer and a thermal inkjet printer. The commercial desktop printer was used to fully inkjet print information storage cells, specifically, two-terminal memory cells, on a flexible substrate. All the elements of these electronic memories were deposited by using the simple inkjet printer at room temperature. To the best of our knowledge, such inkjet printing of all the elements of these types of electronic devices on a flexible substrate using an ordinary commercial inkjet printer has not been reported.

1.2 Motivation of the research

One of the motivations of this work was the lack of a simple, easy to use, cheap, compact automated stamp printing system to deposit thin metals on glass substrates. The simple environmentally friendly inkjet printing technology was another motivation to endeavour to develop some new paths for this technique to fabricate flexible electronic devices.

1.3 Aims and objectives

This research work aims to print conductive paths for electronic device applications using two approaches; contact printing and non-contact printing, with the use of inexpensive materials and simple equipment. A functional electronic device was demonstrated during this study. The two techniques can complement each other for the fabrication of electronic devices as one can be used to transfer thin films (patterns) within nanoscales while the other is used for solution-based functional ink printings in the microscale.

1.4 Organisation of the thesis

This thesis is divided into 8 chapters as follows:

Chapter 1: this chapter offers an overview of how stamp/transfer printing, soft lithography and inkjet printing technology emerged as alternatives to conventional deposition techniques. The motivations of this research and an overview of the organisation of the thesis are included in this chapter.

Chapter 2: the chapter provides an overview of stamping/ transfer printing, printing methods for printed electronics (contact and non-contact). Micro-contact and micro-transfer printing techniques are discussed with more details because their working principles were employed in this research study.

Chapter 3: the chapter gives a brief description of the working principle of the techniques that were used for the optimisation and characterisation of the materials used in this research

Chapter 4: in this chapter, one kind of contact printing technique- the stamp printing machine, will be discussed, along with its design, manufacture and control. Then, the testing of the machine and the investigation of the stamp printed aluminium tracks on treated glass substrates will be discussed.

Chapter 5: this chapter will provide an overview about a non-contact printing technique, the inkjet printing technology; its background, working principle of some inkjet printing techniques, along with classifications and the factors and parameters that affect the quality of the inkjet-printed materials will be discussed.

Chapter 6: in this chapter, three functional materials will be investigated for inkjet printing; silver nanoparticles (Ag NPs), poly(3,4-ethylenedioxythiophene)-poly(styrenesulfonate) (PEDOT:PSS) and graphene oxide (GO). These materials were selected as they are relatively cheap, practical and environmentally friendly. Two drop-on-demand (DOD) techniques were employed to inkjet print these functional materials; a commercial desktop piezoelectric Epson Stylus P50 and PEL thermal inkjet printer.

Chapter 7: in this chapter, a novel electronic device, that was fully inkjet-printed by using the functional inks that have been discussed in detail in the previous chapters, will be discussed as an application of inkjet printing in the fabrication of functional devices.

Chapter 8: conclusion and future work.

Chapter 2: Stamping/Metal Transfer Printing

This chapter provides an overview of stamping/transfer printing. Micro-contact and micro-transfer printing techniques will be discussed in detail because their working principles have been employed in this research study.

2.1 Introduction

It is known that stamp printing and lithography have been widely used and applied in many applications and industries for centuries. Moreover, the combination of these two techniques introduced some soft lithographic methods such as microcontact printing, which was the very first demonstration and the initial start of soft lithography [2], and transfer printing. The proposed method that is introduced in this research study is a combination of stamp printing, microcontact printing (µCP) and micro transfer printing (µTP). Although these methods have been broadly and successfully used as alternative techniques to the photolithography methods [4], the microcontact printing has encountered some challenges such as the diffusion and edge disorder of the surface of self-assembled monolayers (SAM) [5] and the requirement of etching after printing to obtain the desired structure of the printed functional materials, which results in unwanted waste materials. Some developments and modifications of the µCP technique have been made to overcome some of these drawbacks and that has led to the discovery of new patterning and depositing techniques including micro fluid contact printing (µFCP) [6], nanotransfer printing (nTP) [7] and metal transfer printing (MTP) [8]. In metal transfer printing (MTP), a layer of metal, which is coated on prepared (with defined structures to be patterned) stamps, poly(dimethylsiloxane) (PDMS), is transferred to a film of polymer (substrate). Due to the pressure when the PDMS stamp is brought into contact with the substrate and the heating of the substrates, the formation of intimate junction between the coated metal layer on the PDMS stamp and the substrate's surface takes place. As soon as the stamp is separated from the substrate, the metal layers shaped by the structures on the stamp are patterned and transferred to the substrate. Zhe Wang et al [9] put the polymer substrate under controlled heating to ensure reaching a temperature below the melting point temperature (T_m) and higher or closer to the glass transition temperature (T_g) of the polymer. The metal-coated stamp was then brought into contact with the polymer substrate (poly(methyl methacrylate)) PMMA or

polystyrene (PS) coated silicon (Si) under a pressure of approximately 30 g/cm^2 (2.94 KPa). The coated PDMS and polymer substrate remained in contact until the substrate temperature cooled down to room temperature. Then, it was lifted off to leave the coated metal patterns, which were in contact with the polymer substrate, on the polymer substrate. They demonstrated the method by depositing gold (Au) lines of 50 µm width and aluminium (Al) squares of 5 µm^2 on PS/Si substrates.

Although there are more techniques such as photolithography [10], microcutting [11], micromoulding [12] and cold welding [13] that have been used to pattern metals, some require larger amounts of pressures which might lead to damage or deformation of the patterned metal and/or the substrate, and others need to use some aggressive chemicals and expensive materials/tools which results in increasing waste and costs. The metal transfer printing (MTP), on the other hand, depends only on the mechanical adhesion which is used as a driving force to achieve good metal deposition unlike the previous mentioned methods.

With the help of solvent vapour treatment and noncovalent surface force, Xinhong Yu et al. [14] were capable of transferring aluminium stripe patterns (10 µm) and gold rectangles (50 µm length and 20 µm width) from pre-patterned polydimethylsiloxane (PDMS) to polystyrene (PS) and (poly(methyl methacrylate)) (PMMA) substrates respectively. A subtractive stamping technique to pattern metal electrodes was demonstrated by Jennifer Yua and Vladimir Bulovic [15] with no requirement of pressure nor temperature or any kind of modifications, where they made use only of the kinetically controlled adhesion of the polydimethylsiloxane (PDMS) stamp to planar metal (Ag) electrode films on organic substrates.

Research work [16] utilising and functionalising b-cyclodextrin (βCD) self-assembled monolayers with both metal-coated elastomeric stamps and substrates has led to the supramolecular transfer printing of metals such as gold (Au) to functionalised silicon oxide

substrates. Chun-Hung Chen et al [17], on the other hand, deposited only certain metals (Cr and Ni, both are 70 nm thick) on polyethylene terephthalate (PET) substrate from a silicone mould, which was coated by antiadhesive layer before coating the metal, by introducing an infrared heating and a roller loading technique to ensure proper adhesion. Still, they were unable to deposit Al, Au and Ti with this method.

UV curing (partially and completely) of polymers was also used to provide a good network base and structure with good adhesion property to transfer gold films from completely cured UV-curable polymer to a partially cured UV-curable polymer [18]. Liang Fang et al [19] introduced a new technique of Tin-assisted transfer, where they utilised a releasing layer of Tin and electroplating to facilitate the process of transferring sub-micron linewidths of some metals including silver (Ag), gold (Au) and platinum (Pt) to flexible substrates.

Mei Zhu and Chengkuo Lee [20] were able to successfully transfer 80 nm thick, horseshoe-shaped aluminium (Al) patterns from oxygen plasma-treated polyethylene terephthalate (PET) substrate to polydimethylsiloxane (PDMS).

Z Wang et. al [21] used a soft lithographic technique to pattern metal layers (gold and aluminium) which were thermally evaporated and coated on pre-patterned PDMS stamp on a polymer substrate. In this technique, unlike other metal patterning methods including cold-welding and microcutting, the high pressure values are not required, which might deform the metal patterns as it uses mechanical adhesion forces for the patterning process. Aluminium films were also patterned using micromolding in capillaries (MIMIC) by generating a network of polymeric lines that are high enough to separate evaporated thin film to be electrically conductive lines [22].

Although various research groups have worked on printing metals, the novelty in this research project, is the capability of patterning metal tracks (aluminium) from PDMS stamps directly onto plasma-treated glass substrates using a cost-effective, simple, easy to use, environmentally friendly technique at room temperature and without the requirement of coating the stamp with any additional layers such as titanium that are used in some of the previously mentioned methods as a releasing layer to enhance adhesion of the metal to the substrate. The proposed adhesion is improved by using glass substrates that have been treated by oxygen plasma and controlling the pressure applied on the pre-patterned PDMS stamp and speed when it is brought in contact with the glass substrate. Besides, the utilisation of a cost-effective, easy to use, simple machine to carry out the metal deposition as the available techniques for aluminium printing are relatively expensive, time-consuming and/or sophisticated as the current deposition techniques utilise heat [23], solvent treatment [24] and/or take long processing times.

Aluminium was chosen due to many factors including:

- Inexpensive and easily deposited compared to other metals using different techniques such as thermal evaporator.
- Commonly used in solid-state fabrication; it comes after silicon and silicon dioxide as being the most used material in fabrication of electronic devices.
- The challenges encountered in printing the metal on glass substrates using a cost-effective technique in large areas as most work was carried out on polymer substrates as mentioned earlier.

2.2 Stamping/Transfer Printing: Background Information and Literature review

The fabrication and applications of micro and nanotechnology have been attracting a great deal of attention from both academia and industry. This can be attributed to the interesting properties that many of these technologies have including high efficiency, small size and low power consumption when compared to the macro industry. Moreover, the production costs are lower. Hence, the techniques that are used for the micro and nanofabrication have constantly undergone development and optimisation in order to meet the requirements of the rapidly advancing field. Photolithography (optical lithography), which is one the conventional high-resolution lithographic techniques, has been used as a prime fabrication method in the semiconductor industry. However, this technique failed to meet the increasing requirements and applications of nanoscale components and devices due to the optical diffraction and wavelength limitations of the used light. Therefore, the development and optimisation of new approaches and methods have been researched and introduced to overcome the issues and limitations associated with the conventional lithographic techniques. One of these approaches is a soft lithographic technique pioneered by the development of Microcontact Printing at Harvard University, USA, as mentioned earlier. This technique has been attracting many researchers and scientists and shortly become one the most commonly used methods for the micro and nanofabrication in academia and industrial field [25] [26] [27] [28].

Microcontact printing has been widely employed for patterning surfaces in the micro and nanoscales in many applications including micro-electro-mechanical systems (MEMS) [29], microelectronics [30] and biology [31] since it was developed, and recently there has been intense interest in developing a microcontact printing system combining the low budget, versatility and being small in size. However, there is no standard, cheap automated instrument representing the technique yet. In this work, the aim is to utilise a cost-effective, simple, automated instrument for the printing, which will be able to print materials from micro to

nanometre scales of desired sizes and patterns and suitable for mass production in a reasonable budget.

2.2.1 Printing methods for printed electronics

The following section provides an overview of some techniques that have been used in the printing and the fabrication of electronics. These techniques can be divided into two main categories depending on the mechanical contacting behaviour between the system that delivers the ink and the receiving substrate. The two categories are; contact and non-contact printing.

2.2.1.1 Contact printing methods

In these techniques, the delivery system of the ink physically contacts the substrate which is somehow considered to be a disadvantage as this might have a negative effect on the substrate and/or the delivery system. Some of these methods are briefly explained in the next sections.

a) Flexography

The technique employs a polymer with patterned structures for printing. A roller controls the ink that to be transferred to a cylinder which has the pre-patterned polymer and finally, the receiving substrate, which is attached to another cylinder (impression cylinder), holds the patterned ink simply by utilising the pressure of the impression cylinder. Different types of ink including solvent and water-based inks were printed using this process. Moreover, conducting silver electrodes [32] were successfully printed by this method.

b) Screen printing

This process also depends on a mechanical pressure to print the ink from a pre-patterned solid mask. Although this technique is considered to be slow and its resolution is quite low compared to other techniques, its capability of generating thick layers (including dielectric materials) and large areas make it find some applications in printed electronics industry [33] [34].

c) Gravure printing

The mechanical pressure also plays a major role in this technique. A metallic cylinder, which is engraved with the structures and patterns to be printed, is soaked in an ink unit. The receiving substrate is positioned between this cylinder and another cylinder where both cylinders rotate in a reverse direction, the patterned ink is then transferred from the inked pre-patterned metallic cylinder to the substrate by mechanical pressure. The quality and the printing speed of the roll to roll printing method is high. However, the mechanical pressure might have a bad impact on some substrates that can not bear high pressures. Low viscosity inks are printed with this technique such as the one used to print conductive silver lines [35].

d) Lithography

The micro and nanofabrication methods are generally achieved by two approaches: top-down and bottom-up methods. In the top-down approach, the desired structures are obtained by gradually removing the undesired materials from the bulk substances. The bottom-up approach, on the other hand, the desired materials are constructed or assembled by building up molecules and atoms.

One of the most widely used top-down fabrication techniques is lithography, which is the core fabrication method for semiconductor devices [36], where a light or electron beam is used to remove the undesired structures from the resist and as the wavelength of the light is the main

element of several lithographic methods, the fabrication of small-sized features requires sophisticated tools and devices which leads to increasing the cost of the technique.

Lithographic fabrication techniques can be generally classified into three categories; the mask lithography, the scanning lithography and the soft lithography.

In the mask lithography, a physical mask is used as a resist in order to pass the irradiation to the substrate, an example of this is photolithography which has been widely used as the basic fabrication techniques in the semiconductor industry for ages, however, due to the increasing need to fabricate significantly tiny materials, photolithographic techniques failed to meet the requirements of the nanofabrication even with using shorter wavelengths of light reaching near, deep and extreme ultraviolet UV and X-ray spectrum, as these types of fabrication require smaller wavelengths (few nanometres) sources.

In the scanning lithographic techniques, on the other hand, energetic and subatomic particle waves including ions and electrons (wavelength of approximately 1 nm) are used for the patterning of the desired resists. Electron Beam Lithography, Focused Ion Beam Lithography, Scanning Probe Lithography and Dip Pen Lithography are some of the techniques that belong to this category. Although the scanning lithography has overcome the high resolution limitations of the mask lithography, it is more expensive and slower than the mask lithography [37].

All the previous methods mentioned above are considered as conventional lithographic techniques where-in most of which the resolution is mainly obtained and restricted either by the optical diffraction limitations of the used light or the energetic particle waves resulting in low resolutions or high capital and operational costs respectively when dealing with nanoscale materials. In addition, although these methods have shown a great deal of success for the fabrication of structures and materials that are sensitive to radiation, especially on flat glass or

semiconductors wafers and surfaces in microelectronics, they face daunting challenges to keep up with the need of patterning materials in applications such as biotechnology, flexible printable electronics (non-planar surfaces) and large area patterning.

To overcome all of this, soft lithographic techniques (non-conventional lithography and subdivided from contact lithography [38]), whose concepts are taken from old simple lithographic processes and techniques like stamping and moulding, have been developed in terms of introducing new substances and chemicals, and how they are processed. In these methods, van der Waals forces, wetting and kinetic factors play a major role in determining the high resolution of the patterned micro and nanomaterials. Soft lithographic techniques make use of elastomeric stamps and soft moulds made of polymers (polydimethylsiloxane PDMS most widely used) to pattern structures in the micro and nano regime, these stamps and moulds are cast and cured in contact with rigid masters that have the desired features and are usually fabricated by conventional lithography. The capital and operational costs are significantly low compared to the conventional ones.

Two of soft lithographic techniques; microcontact printing and microtransfer printing, will be discussed in more details in next the section 2.2.1.3 and 2.2.1.5 respectively.

2.2.1.2 Non-contact printing techniques

These methods, unlike the contact printing ones, the delivery unit of the ink has no physical contacts with the target substrate and this gives the advantage of printing on a broad range of substrates. Moreover, they control the quantity of the materials to be deposited as they can interface with computer-controlled software to translate any digital information to control the printhead achieving controlled structures and features. The non-contact printing technique can be classified into three main categories based on the mechanism that the materials are deposited:

a) Energy beam based techniques

This process makes use of high energetic beams to deposit different patterns of thin films. Some of these beams include focused ions and laser. An example of this method is Laser Induced Forward Transfer (LIFT) [39].

b) Flow based techniques

This technique employs mechanical pressure (using a pump in some cases) on an ink unit (reservoir) to continuously but precisely dispense it on a substrate. The delivery of the ink is continuous which is different from inkjet printing, which is ejected as individual droplets. Fused Deposition Modeling (FDM) [40], an additive manufacturing technique, is an example of this category.

c) Droplet based techniques

This process includes two techniques, the aerosol jet and inkjet printing. In the aerosol jet (spray) printing, an aerosol of droplets from the ink to be deposited is generated (by pneumatic atomiser), carried and ejected out through the nozzles usually using gases which provide the right kinetic energy to print the materials. The inkjet printing, on the other hand, involves the formation and ejection of serials of a controlled quantity (volume) of droplets of fluid (ink) from a reservoir chamber travelling through a nozzle with a velocity of several metres per second reaching the desired substrate at defined positions. This technique will be discussed in more details in chapter 5.

The schematic diagram, in figure 2.1, presents the main classifications of the printing techniques; contact and non-contact and their main sub-branches.

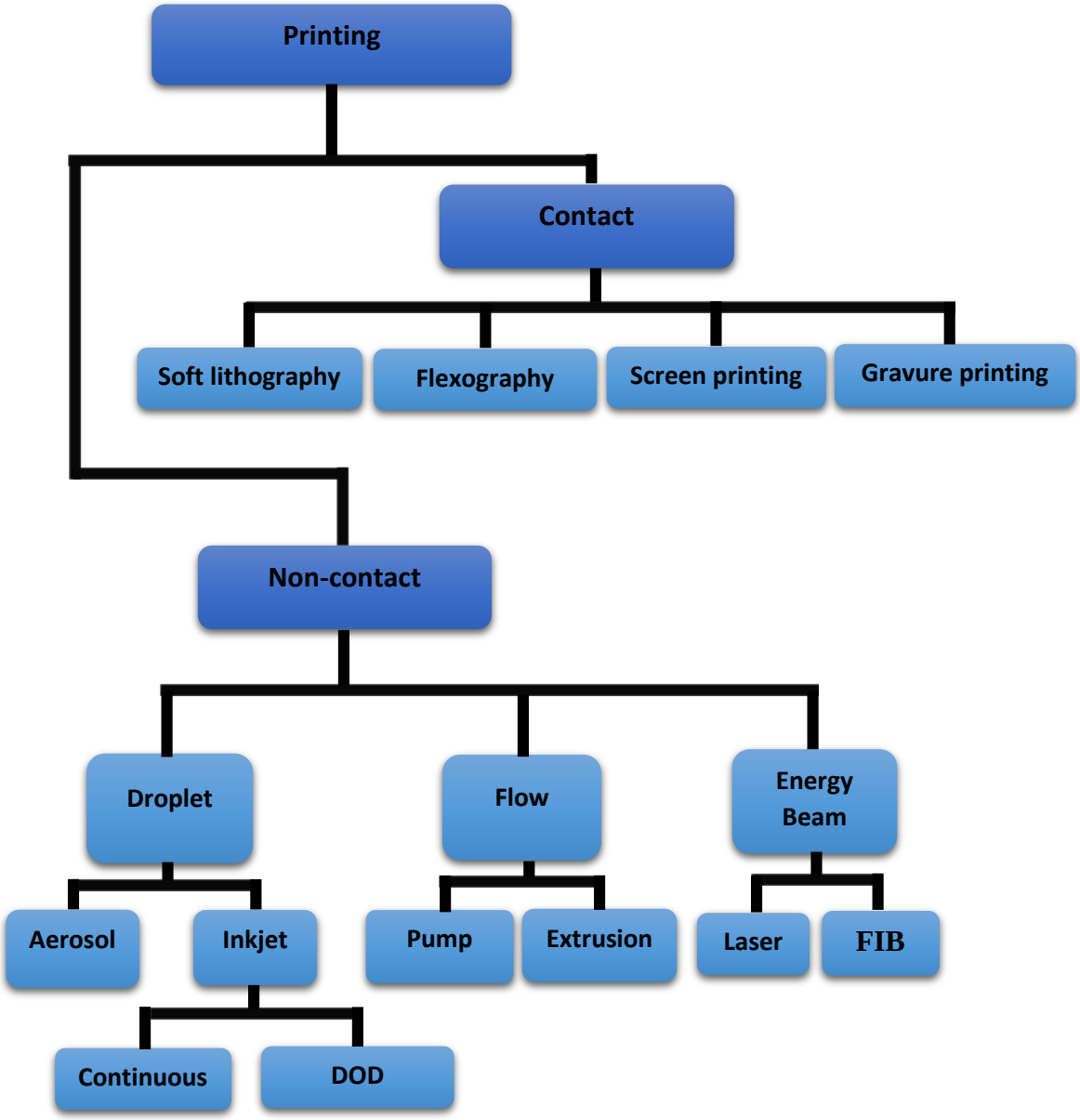

***Figure 2.1**: a schematic diagram presents main classifications of the printing techniques; contact and non-contact and their main sub branches.*

2.2.1.3 Microcontact printing (µCP)

Microcontact printing (µCP) is a simple and inexpensive technique that has been widely employed to pattern surfaces, mainly by using monolayers, in micro and even nanoscales [41] for applications in chemistry [42], electronics [30], nanobiotechnology [31] [43]. This technique is based on two steps: the fabrication of the desired elastomeric stamps and printing [44]. The transfer of the patterns is commonly achieved by coating (inking) the stamps with monolayers molecules able to create covalent and noncovalent bonds with the substrate and form an intimate conformal contact between the surface of the substrate and the molecules on the stamp features. These monolayer molecules replicate the stamp patterns in the surface of the substrate. Figure 2.2 exhibits a simple schematic diagram of the process of µCP.

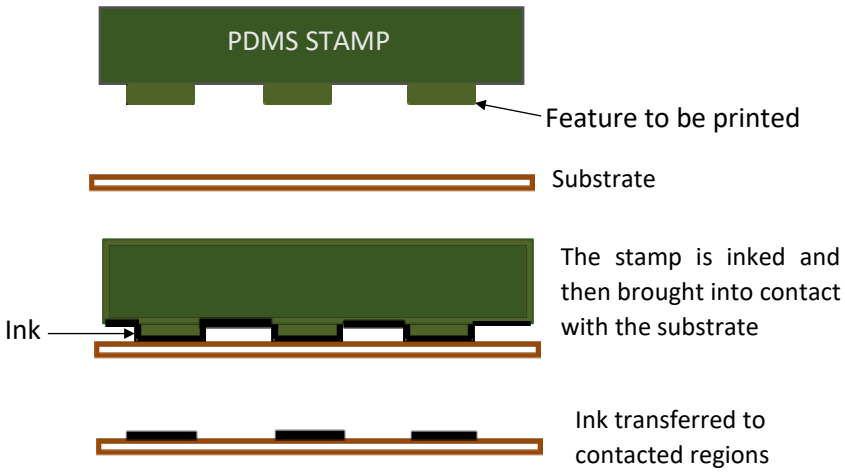

Figure 2.2: *a simple schematic diagram shows the main steps of microcontact printing using an inked PDMS stamp and a target substrate.*

µCP is usually carried out by three methods and configurations based on how the stamp is placed on the surface of the substrate:

a) **The planar method**: where the stamp is positioned on the substrate. This configuration is simple, as can be seen in figure 2.2, and has achieved high resolutions.

b) **The rolling method***:* in this technique, the stamp is rolled over the surface as shown in figure 2.3. The rolling set up has been widely used for patterning large areas in a single printing (more than 50 cm^2) [44].

c) **The curved method:** here, the substrate, usually cylindrical one, is rolled in between a clean and an inked stamp as presented in figure 2.4. This method makes patterning curved shapes obtainable and accessible [45, 46].

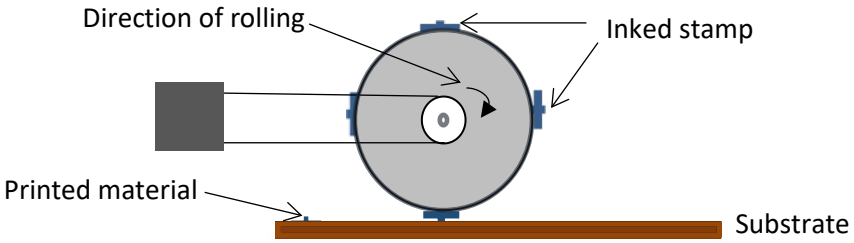

Figure 2.3: *Microcontact printing rolling technique; an inked stamp rolled over the substrate.*

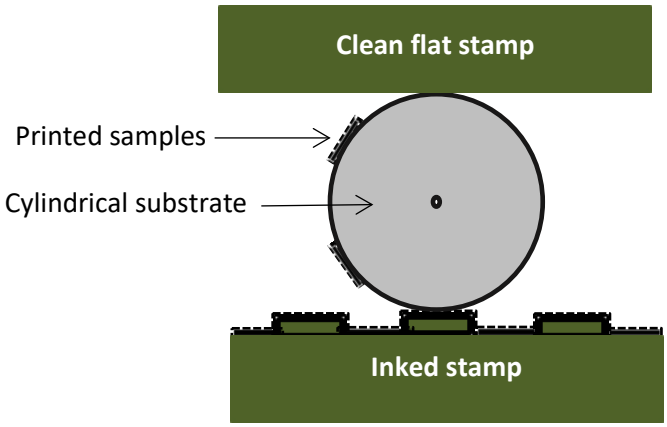

Figure 2.4: *Microcontact printing curved technique; rolling a substrate (cylindrical shape) between inked stamp and clean one.*

As mentioned earlier, µCP was first developed to replace conventional lithographic techniques, but as the flexibility and bendability of the elastomeric stamps facilitate the printing on nonplanar and uneven surfaces, the technique has found applications in various fields such as MEMS, biotechnology, and optics. In addition, the simplicity, the high throughput, the high efficiency and low budget of the soft lithographic technique have significantly contributed to

the success that it has experienced academically and industrially. Moreover, the materials used to accomplish the μCP process can easily be assembled, inexpensive and not hazardous comparing with conventional lithographic methods which they tend to be expensive, sophisticated and some use toxic materials. Other advantages of μCP include versatility, repeatability, mass production, the ability to pattern in large areas and work in and out of clean rooms. However, the printing technique has encountered a few hurdles, one of which is the mechanical stability of the elastomer stamp which sometimes causes alignment issues. Due to all these advantages, the μCP technique has become one of the most promising methods for micro and nanofabrication.

The self-assembled monolayers (SAMs) (ink) is one of the essential requirements for μCP. The self-organisation of the molecules or atoms due to covalent and noncovalent bonds is called self-assembly [47] and it can be achieved by placing a substrate in a solution of the molecules of interest, taking the substrate out of the solution and then rinsing it. After rinsing, self-assembled monolayers of the molecules remain on the surface of the substrate. There are several kinds of SAMs depending on the way they attach to each other, one of which is the electrostatic self-assembly as it uses electrostatic forces for the assembly. Hexadecanethiol (HDT, n=15) is considered to be one of the most widely used as an ink in the literature. An example of this is the immersion of a gold substrate into a solution of alkanethiolate molecules to achieve SAMs of alkanethiols (hexadecanethiol HDT) on gold [48, 49]. SAMs are patterned by means of many techniques but the most popular one is μCP. In the μCP, thiols, which were the first to be employed [50], and silanes SAMs [51] have been widely deposited. The patterning procedure can be briefly described as; a pre-fabricated stamp with desired features is inked with SAMs molecules and then applied to a substrate to transfer the SAMs. In the end, using a suitable etching material to remove uncoated areas on the substrate is adequate to leave the patterned structure of interest on the substrate.

Different substrates can be used, however, careful selection of ink should be taken depending on which one is capable of the formation of sufficient organised SAMs on certain substrates; thiols, for example, are usually used on noble metal substrates [52] while silanes are commonly employed on non-metallic surfaces [53].

2.2.1.4 Recent work on microcontact printing (µCP) systems

Although the µCP technique [2] and the MTP method [3] have been widely used in the surface patterning process (in micro and nano scales) for applications in many fields including electronics, chemistry and nanobiotechnology, a standard, cost-effective and automated instrument for the stamping and transfer printing processes has not been introduced. Lately, there has been intense interest to develop a µCP system which is cheap, versatile and small in size. A large number of laboratories, especially, in an academic set up, use manual patterning techniques which lead to inaccurate, inconsistent results and lack reproducibility. The majority of recent studies focused on the mechanical actuation [54] and electrostatic phenomenon [55] for µCP. Chakra et al. introduced an instrument for the automated µCP in which a computer-controlled pneumatic actuator was used [56]. Gesim also presented the µCP3.0 [57] which makes use of the pneumatic actuation for the stamping process. In microelectronics applications, few proposals for instrumental µCP machines have been provided, such as roller based instruments [58] and magnetic assisted µCP [59] where a magnetised material (iron) injected on the top of the stamp (this causes restrictions on the stamp size) and the magnetic field source placed under the substrate to achieve a controlled magnetic pressure on the stamp. Moreover, to the best of my knowledge, there is no simple, cheap instrument focused only on the metal transfer printing at room temperature and has not been carried out manually. Besides, all the previously proposed systems make the µCP process more complicated, bulky, expensive and some are incapable of working in aseptic conditions.

2.2.1.5 Micro transfer printing (μTP)

The idea of transfer printing was started in the 1750s by J Sadler and G Green [60] as a technique to decorate ceramics and porcelain enamels (pottery) utilising engraved metal (steel and copper) plates that take monochrome patterns to be transferred by pressing against the materials needed decoration. However, the transfer printing in micro and nano fabrications involves methods that assemble functional materials for different applications and it has expanded to cover a wide range of materials and applications including transferring metals in the fabrication electronics industry.

Micro transfer printing is a technique based on the deterministic assembly mode of the transfer printing developed at the University of Illinois, US (see section 2.2.1.7). This technique resulted from continuing research started by dry transfer printing of silicon ribbons [61] using moulded stamps, such as PDMS, to assemble microscale structures. In this technique, a pre-patterned stamp is brought into contact with donor substrates (with functional materials to be deposited) followed by contact with the receiving (acceptor) substrates, as illustrated in figure 2.5 (c). The process is based on the adhesion and release of the functional material at the interfaces between the viscoelastic stamp and the target substrates. As the stamp is made of a viscoelastic (elastomeric) material, the strength of its interface adhesion depends on the speed at the moment the interface is broken. Therefore, the transfer or printing in this method is based on controlling the adhesion and the fracture at all interfaces: the ink and the donor substrate, the ink and the stamp and the ink and the receiver substrate. When a viscoelastic stamp is brought into contact with an ink on a donor substrate, two interfaces are generated: one is between the ink and the stamp, while the other is between the ink and the donor substrate. When an elastomeric PDMS stamp makes a contact with inks on a donor substrate, conformal contact driven by van der Waals interaction [62] occurs. The adhesion between the elastomeric stamp and the ink on the donor substrate is mainly sensitive to the speed at which the stamp is

separated from the donor substrate. If a sufficient peeling speed is used in the separation of the stamp from the donor substrate, and the strength of the adhesion is enough, the coatings on the donor substrate are lifted from the substrate to the stamp's surface. Then, when the patterned stamp makes contact with a receiving substrate, it is separated with a lower peeling speed which results in a weak adhesion to the patterned stamp allowing the coatings to adhere to the surface of the receiving substrate, separating them from the stamp. One can refer to the work of Feng et al. for further details on understanding the kinetically controlled process involved in ink/pattern transfer to and from the stamp, and the critical speed determination for transfer printing [63]. The forces involved in the stamping process will be discussed in the following sections.

This kind of transfer printing can be classified into three main basic modes [64] as shown in figure 2.5:

a) **Additive Transfer:**

   It involves using an inked stamp with the material to be printed. The inked stamp is then brought into contact with the target substrate before peeling off to leave the desired material on the substrate.

b) **Subtractive Transfer:**

   This method uses a donor substrate and a structured stamp. The stamp is brought into contact with the coated donor substrate with the material of interest. When the stamp is removed, the structures on the stamp will contain the material of interest and it can be used as additive transfer printing while the donor substrates have the remaining deposited material which can be used for different application as well.

material of interest and it can be used as additive transfer printing while the donor substrates have the remaining deposited material which can be used for different application as well.

c) **Deterministic Assembly:** a fabricated (micro and nano patterns) coated donor substrate and a stamp are used in this technique. Contacting and peeling the stamp into and from the pre-structured coated substrate leaving the stamp with the desired inked structures which are transferred to a receiving substrate when it is contacted by the stamp.

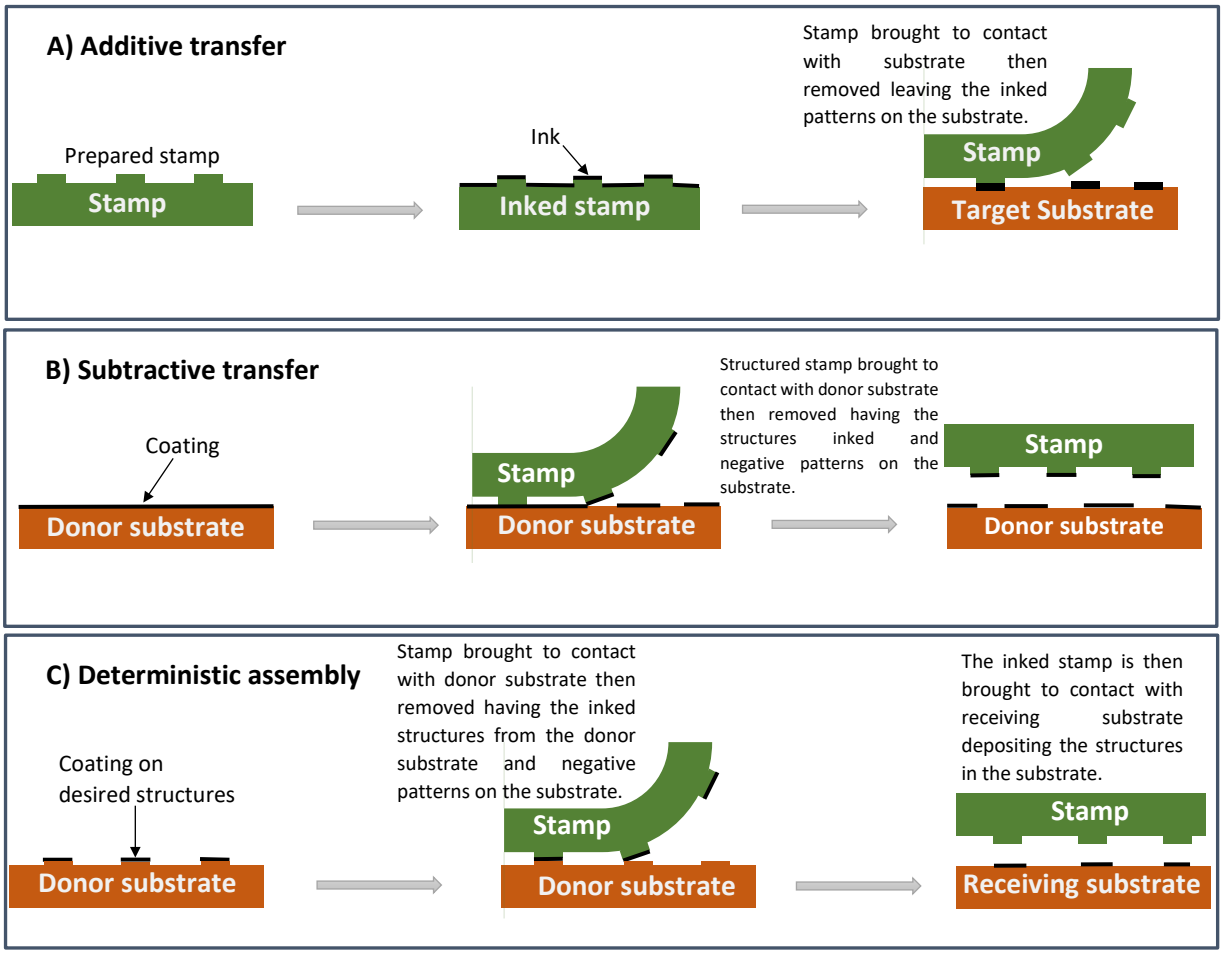

Figure 2.5: *schematic diagram illustrates the three main basic modes of the transfer printing; a) additive transfer, b) subtractive transfer and c) deterministic assembly.*

This versatile printing process has broadly been employed in many fields and industrial applications such as printing metals including copper [66] and other metals [66], integrated circuits on flexible substrates [67] and photovoltaic (PV) panels [68]. Furthermore, some commercial companies adopted the technique including Sempruis and X-Celeprint.

The mechanism of the micro transfer printing technique can be divided into two main categories; the bonding mechanism and the de-bonding mechanism, which are briefly explained in the next sections.

a) Bonding Mechanism

When an elastomeric PDMS stamp is brought into contact with a substrate with desired features, conformal contact takes place and the adhesion energy of this contact is based on molecular forces which are responsible for binding two materials including van der Waals forces/interactions, molecular interaction, covalent bonds and surface chemical bonds along with the forces resulted from the dissipative process in the elastomeric polymer [69]. The bond formation occurs in a small interface area where the distance between the polymer's atoms/molecules and the target substrate should be less than 1 nm (this is the chemical bond length between atoms in a material). Thermodynamic work of adhesion (Wa) defines the generation of chemical bonds (in the interface) between two materials. This work can be expressed as:

$$W_a = \gamma_s + \gamma_l - \gamma_{sl} \quad \text{.....2.1}$$

Where, γ_s is the surface energy of the solid (substrate), γ_l the surface energy of the liquid (polymer) and γ_{sl} is the interfacial energy between the polymer and the substrate. For a good wetting process, the interfacial energy (γ_{sl}) is required to be stronger than the sum of (γ_l and γ_s) which represents the surface tensions of the polymer and substrates interfaces with air. This will be discussed in detail in chapter 5 section 5.2.4

The polymer has a low resistance to spread (flow) and this is defined by its rheological (viscous) properties while the material of the substrate should have a good interfacial surface to allow spreading/wetting driven by adhesive forces.

b) De-bonding mechanism

Most of the measurements that are related to adhesion are focused on the de-bonding process and rupture factors as the adhesion between two adhered materials can be identified by the energy/unit area which is required in the process of separating them. When an elastomer polymer is brought into contact with a solid substrate (surface), the determination of the adhesion forces can be estimated by the molecular forces (which is responsible for binding two surfaces together) and the forces resulting from the dissipative process in the elastomeric polymer [69,70].

The energy release rate (G) which is the energetic driving force for an extending crack, it relates the stored energy in the elastomer to the area of contact that is decreased during separation.

When a stamp is peeled off a substrate with a peeling force (F) in a steady-state velocity (v) as shown in figure 2.6, the energy release rate (G) J/m^2, can be related to the peeling force as:

$$G=\frac{F}{W}\ [64] \quad \ldots\ldots 2.2$$

Where, (w) is the width of the contact area.

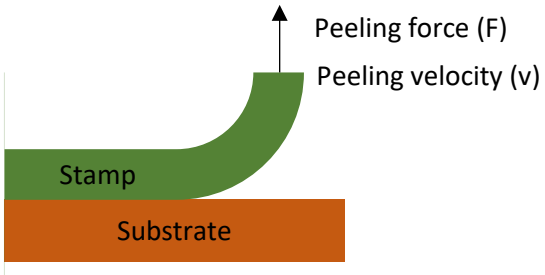

Figure 2.6: *a stamp is peeled off a substrate by a peeling force (F) and a peeling velocity (v).*

When the PDMS stamp is picked up from the donor substrate carrying the thin film and then brought into contact with the receiving substrate to print this thin film, two different energy release rates occur. A critical energy release rate for the thin film/donor substrate ($G^{film/substrate}$) which is independent on the peeling velocity when both materials are elastic and a critical energy release for the stamp/thin film ($G^{stamp/film}$), this depends on the peeling velocity (v) as the stamp is viscoelastic and it equals to $G^{stamp/film}$ multiplied by (v). As the dissipation energy of a viscoelastic material is increased when the peeling velocity is increased. The critical energy release for the stamp/thin film can be expressed as:

$$G^{stamp/film} x\ v = G_0 [1 + (\frac{V}{V0})^n] \quad \text{.....2.3}$$

Where, G_0 is the critical energy release rate when the peeling velocity is approaching (0), v_0 is a reference peeling velocity (when the critical energy release rate doubles G_0) and (n) is a scaling parameter.

When (G) in equation (2.2) reaches $G^{film/substrate}$, it means that the stamp can lift the thin film from the donor substrate, as presented in figure 2.7 (left), with a peeling force (F_{pickup}).

$$F_{pickup} = w\ G^{film/substrate} \quad \text{.....2.4}$$

Stamping/printing the thin films from the stamp to the target substrate as shown in figure 2.7 (right), on the other hand, takes place when (G) reaches ($G^{stamp/film}\ x\ v$), where the stamp can print the thin film on the target substrate with a peeling printing force ($F_{printing}$):

$$F_{printing} = w\ G^{stamp/film}\ x\ v \quad \text{.....2.5}$$

The peeling velocity at which both energy release rates are the same is called the critical velocity (v_c) as can be seen in equation 2.6.

$$G^{film/substrate} = G^{stamp/film}\ x\ v_c \quad \text{.....2.6}$$

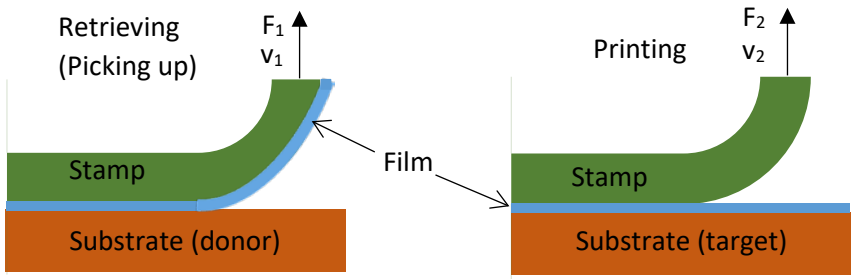

Figure 2.7: *a stamp retrieving (left) and printing (right) a film from a donor substrate to a target substrate.*

The pickup and print process relationships with the energy release rates and peeling forces and velocities can be summarised/simplified as in table 2.1.

Table 2.1: *a summary of relationships between energy release rates and peeling forces and velocities that determine the pickup or printing process.*

Process/Energy/Force/velocity	Energy Release Rate	Peel Forces	Peel Velocity
Pickup (retrieve)	$G^{film/substrate} < G^{stamp/film}$ *x* v	$F_{pickup} < F_{printing}$	$v > v_c$
Print	$G^{film/substrate} > G^{stamp/film}$ *x* v	$F_{pickup} > F_{printing}$	$v < v_c$

It can be concluded that the adhesive forces between thin films on the substrate and the stamp can be driven by (attributed to) the separation (peel) velocity rate.

2.2.1.7 Recent progress in micro transfer printing (µTP)

Most of the recent work on developing the micro transfer printing technique has focused on controlling the speed at which the stamp separates from the substrates. A Carlson and his group [70] used a pneumatic actuator to control the contacting and separation of the stamp with and from the substrates. Another work was demonstrated by A Carlson et al. [71] when they introduced shear while printing to weaken the force that is required for the stamp and printed

object (ink) interface to be broken. However, J Eisenhaure et al. [72] used a different polymer (shape memory polymer) instead of the PDMS stamp as a stamp material for the printing technique. Moreover, a different stamp releasing method was invented by Saeidpourazar et al. [73] where they used laser to generate heat to produce thermal mismatches at the surface between the stamp and printed materials. They called the invention “laser micro transfer printing”.

Regarding the machines and instruments that have been developed for the micro transfer printing, the automated micro transfer machine, which was introduced Rogers et al. [74] at the University of Illinois at Urbana-Champaign, US, is a good example of a successful instrument for the printing technique.

A different stamp, OrmoStamp, was used by R Nagel et al. [75] to transfer thin film of gold on a silicon substrate by means of nanotransfer printing (nTP).

2.2.1.8 PolyDimethylsiloxane (PDMS) stamp

Whitesides and co-workers [2] used an elastomeric stamp, PolyDimethylsiloxane (PDMS), in the first development of the microcontact printing. The PDMS stamps have been in interest of a lot of researchers and scientists because of many advantageous properties over other stamps such as poly(methylmethacrylate) (PMMA):

- The ability to adhere to metals.
- The compatibility with bio-materials, rigid and flexible substrates and being chemically inert which makes it easily separated from moulded structures that have been cured on [76].
- The porosity of PDMS tends to increase the possibility of adsorption of several molecules [77].
- Being optically transparent and good dielectric.

- The high viscosity and elastomeric nature: the ability to experience conformal contact to the surface over large areas, mixing with a curing agent to increase the rigidity or the flexibility.
- The capability of curing at room temperature, 48 hours, or heating, the higher temperature, the quicker is the curing time, for example, at 100°C curing time is 35 minutes and at 150°C is 10 minutes [78].

Although the PDMS stamps have shown lots of advantages, they encounter some drawbacks. On the main disadvantages of PDMS stamps is the issues related to the aspect ratio (the height to the width ratio) of the patterned materials. The aspect ratio of the relief features on the PDMS stamps was found to be between 0.2 and 2 in order to obtain distortion-free patterns [79] and that is due to the fact that the stamps are relatively flexible and soft and have a Young`s modulus of 1-2 MPa. If the patterned features are higher than the rated aspect ratio, they are likely to collapse or experience pairing due to the weight of the patterned structures themselves. On the other hand, structures which below that range cannot withstand the stamping pressure and result in sagging [80]. Figure 2.8 shows some of the deformations that occur to the stamps; pairing and sagging. Some proposals to overcome this drawback have been presented, one of which is the synthesis of a tough PDMS stamp [81], which has improved the aspect ratio to be within this range 0.02 to 5, but made the stamps unsuitable for uneven substrates and surfaces. Moreover, composite stamps were proposed [82] combining soft and hard PDMS stamps. These stamps have shown the capability of patterning nanoscale features [83].

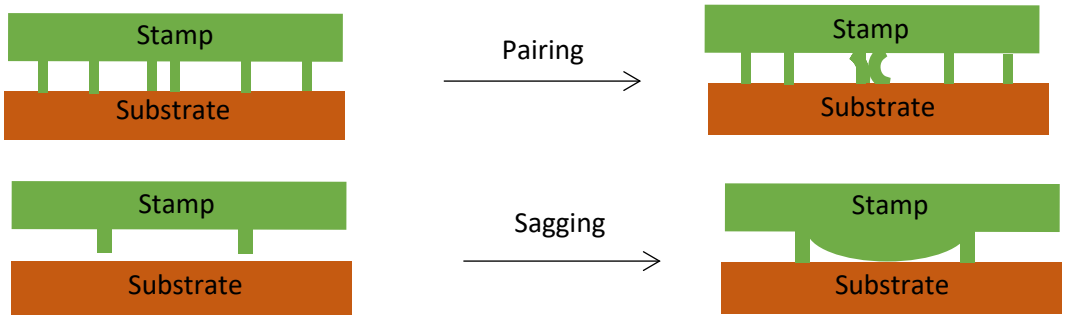

Figure 2.8: *the most common stamp deformations; pairing and sagging.*

Another problem that PDMS stamps face is the minor distortions to the stamps due to the difference in the thermal expansion coefficients during the thermal curing against specific masters such as silicon which has a thermal expansion coefficient of $2.6x10^{-}6\ K^{-1}$ while the PDMS stamp's is $3.1x10^{-4}\ K^{-1}$ [84]. This difference causes minor distortions to the stamps when using masters that expand slightly more or less than the PDMS. To overcome this problem, the curing temperature can be lowered, however, this will increase the curing time. Moreover, hard support can be used to back the PDMS stamp to minimise the distortion, especially while releasing stamps from masters [85]. Stamps with three layers were also developed [86]. These stamps provide bendability for uneven surfaces, rigidity for the stamp stability and the easiness during peeling off the master.

In recent years, there has been an awful lot of research to develop stamp printing including light-stamping lithography (LSL) where the author(s) employed a UV induced surface bonding to directly transfer the contact surface of the PDMS to a substrate [87], the UV induces the development of chemical bonds between a PDMS stamp and a substrate.

Philips, IBM and Gesim have also been developing and optimising stamps. IBM introduced a technique [88], an Invar sheet was used as stiff support for the PDMS stamp to achieve the rigidity of the stamp while preserving the capability of bending on uneven surfaces. Relatively large areas were patterned with trivial distortions. Philips, on the other hand, proposed another

method [89]; a thick PDMS stamp attached to flexible glass support was developed to obtain the stiffness and the bendability of the PDMS stamp at the same time. This arrangement succeeded to pattern large areas free of defects such as sagging. Gesim presented a different arrangement [90] where a diaphragm PDMS stamp and electric motors were used to provide a precise conformal contact and areas in the range of millimetres were successfully printed with approximately free defects.

Applied pressure during printing is of great interest for the ones develop stamps, the amount of pressure (P) needed to produce a conformal contact between two surfaces can be calculated by [91]:

$$P = \pi E^* \Delta / \lambda \quad \text{.....2.7}$$

$$\text{And } E^* = E_a/(1-\nu_a^2) + E_b/(1-\nu_b^2) \quad \text{.....2.8}$$

Where, E* is the bulk modulus of two surfaces (a) and (b) with two-dimensional sinusoidal roughness of wavelength λ and amplitude Δ, whereas E and ν are the Young`s modulus and the Poisson ratio of the surfaces respectively.

It is clear that the required pressure depends on the bulk modulus of the two surfaces. As a result, a precisely controlled pressure is required when dealing with solid surfaces to avoid tiny relief structures from collapsing.

One of the main objectives of this project is the utilisation of an automated deposition machine whose working principle is based on both microcontact printing and micro metal transfer printing processes and using an electromechanical device and electronically controlled system that enable it to precisely manipulate the stamping process where a fine movement and appropriate stamping pressure are needed to obtain distortion-free patterns with high resolution in a relatively large area within a reasonable time. The proposed technique is aimed to stamp/transfer micro and nanoscale patterns and expected to mass-produce the printed metal

tracks with a reasonable budget and it is also anticipated to be viable for the industrial and commercial manufacturing field, especially, emerging technologies electronic devices both in micro and nanoscale devices such as the ones have been developing at Emerging Technologies Research Centre (EMTERC) including emerging electronic memories, photovoltaic solar cells, chemical and biosensors.

Chapter 3: Fabrication and Characterisation techniques

This section gives a brief description of the working principle of the techniques that were used for the optimisation and characterisation of the materials used in this research.

3.1 Thermal evaporator

The thermal evaporation is one of the techniques which is broadly used to deposit thin-film materials; inorganic materials including metals and organic materials on substrates. The materials that are to be deposited are loaded on a heating filament (made from high melting point materials like tungsten and put at the bottom of the chamber) in several shapes including boats, baskets and coils. The evaporation of the required material starts when the materials reach vaporisation point by heating the filament due to the high current passing through it. As this process takes place under high vacuum and in a very low pressure, approximately $4x10^{-6}$ mbar, the evaporated materials travel upwards to settle and accumulate on the target substrates, which are placed on the top of the chamber, to form films. The thicknesses of the deposited films on the substrates are monitored and measured by a quartz crystal placed inside the chamber parallel to the target substrates. This crystal uses the piezoelectric effect to evaluate the mass-thickness, where a mechanical strain (increase or decrease in the rate of evaporated mass of the material on the crystal) causes a change in the frequency and electric potential of the crystal, which correlates to the mass of the deposited material, and in turn the thickness of the deposited film. Figure 3.1 presents a simple diagram of a basic thermal evaporator.

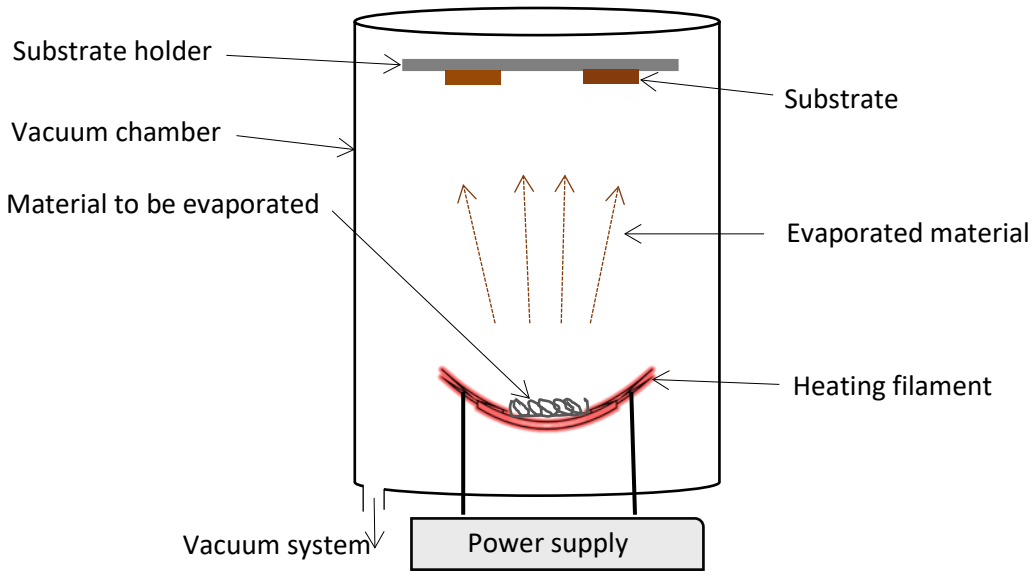

Figure 3.1: *a simple diagram of a basic thermal evaporator.*

3.2 Scanning Electron Microscopy (SEM)

Scanning electron microscopy (SEM) is a technique used to generate images of samples by applying a beam of high energised electrons sent from an electronic gun made from a sharp tungsten filament placed under high vacuum. The use of electrons which have short wavelength instead of light that has longer wavelength makes the scanning electron microscopy suitable for imaging in micro and nanoscales. The energy that is associated with this beam of electrons can be adjusted from 100 eV to 30 keV. After supplying current to the electronic gun, a strong electrostatic field draws current of the filament and a beam of electrons is produced and travels through condenser lenses and scanning coils before bombarding the substrate. The electrons impact the materials on the substrates, the materials absorb the energy of the electrons and re-emit signals containing information related to the surface morphology and topography of the materials are produced and as a result, images are generated. Figure 3.2 simply illustrates the basics of scanning electron microscopy SEM and its main components. Analysed substrates are preferable to be conductive to provide an electric path for the electrons and to obtain better image resolution, so nonconductive ones are usually coated with thin layers of gold or carbon.

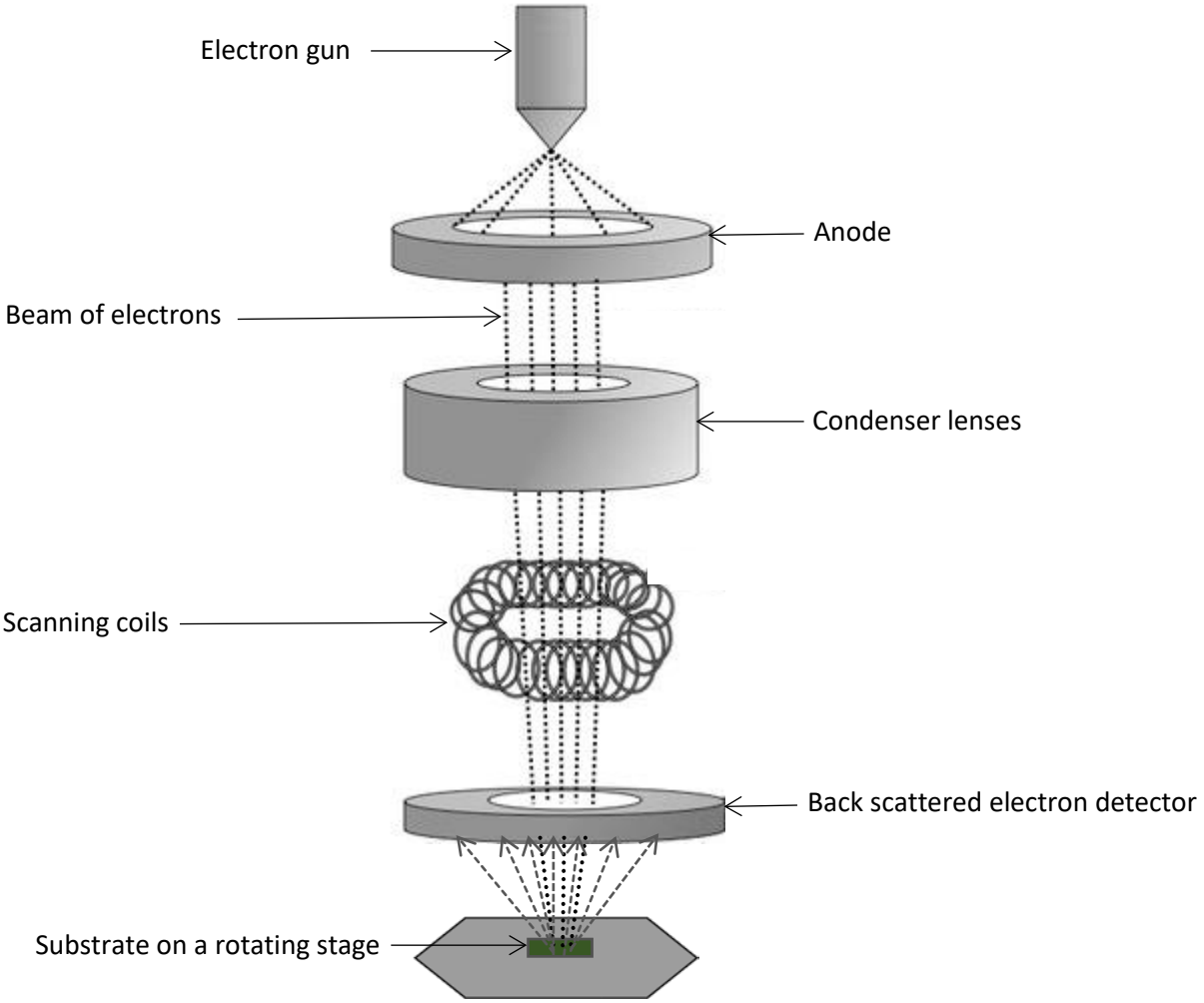

Figure 3.2: *the main components of scanning electron microscopy SEM.*

3.3 Thickness measurement techniques

Profilometer and ellipsometer are the main thickness measurement methods that have been used in this work, their working principles are illustrated with the help of the visual presentations as follows:

3.3.1 Profilometer

Profilometry is a process in which the topography of the surface of the sample can be detected and as a result, the thickness and stress of films, depth of the etched materials and the sample roughness can be evaluated. The profilometer uses a sharp probe (diamond stylus tip) with radius in the nanometre scale to scan the surface of the substrate and produce a line scan so different measurements can be taken easily. A basic structure and a simplified working principle of a stylus profilometer and can be been in figure 3.3**.**

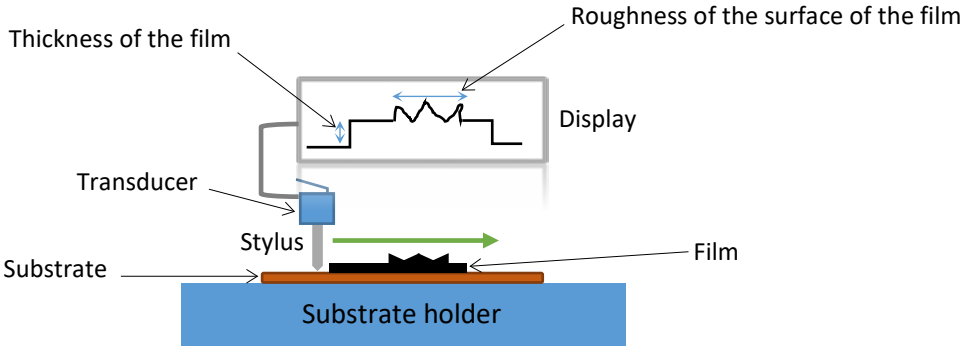

Figure 3.3*: a basic structure and a simplified working principle of a stylus profilometer.*

3.3.2 Ellipsometer

Ellipsometry is a non-contact and non-destructive measuring technique can be employed to characterise the refractive index, thickness and roughness of the surface of the samples by means of laser light and Fresnel`s equations [92]. As this method depends on changing the polarisation of the light while transmitting it through the layer of interest, the samples are preferably to be reflective substrates such as silicon substrates. A schematic diagram of an ellipsometer is presented in figure 3.4.

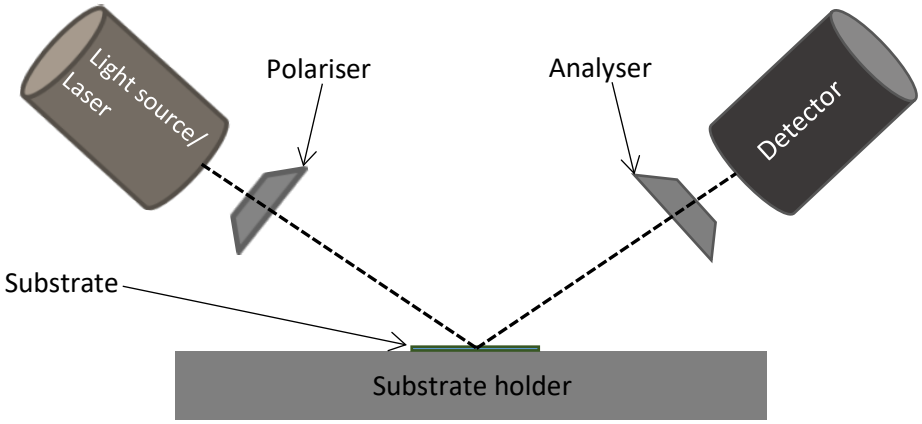

Figure 3.4: *a schematic diagram of an ellipsometer.*

3.4 Electrical measurement techniques

In this work, the electrical measurements including Current-Voltage (I-V) and resistivity measurements have been performed by using Hewlett Packard HP4140B picoampere Meter/DC Voltage Source and 4-probe set-up based on Van Der Pauw method. This picoampere can source current from 1pA-10 mA and DC voltage range is (0 - ±100 v). The IV measurements are carried out by means of Agilent programmes and probe stations.

3.4.1 Sheet Resistance Measurements

The set up (figure 3.5) used to measure the resistivity of the thin film printed material is based on Van Der Pauw method where measurements are carried out by contacting four corners of the thin film. This eliminates errors such as the ones from the wire/cable and contact resistances. The programme for this measurement was designed at EMTERC led by Dr K Manjunatha and Prof S Paul. Current is sourced through two contacts and voltages are calculated from the other two, and this is repeated for every two different contacts, then an average voltage is taken into consideration when measuring the resistivity and sheet resistance using this equation:

$$Rs = \frac{\pi}{ln2} x (V_{23}/I_{14}) \quad \text{.....3.1}$$

Where, Rs is the sheet resistance of the thin film (Ω/□), V_{23} is the voltage measured between 2 and 3 contacts and I_{14} is the current fed through 1 and 4 contacts. For better results, the average value of the resistance is calculated after switching the contacts around all the terminals. The supplied current is advisable to be low to prevent self-heating of the printed thin films due to Joule effect power dissipation.

The resistivity can be calculated using this equation:

$$\rho = Rs\ x\ Thickness\ of\ thin\ film\ x\ Correction\ factor \quad \text{.....3.2}$$

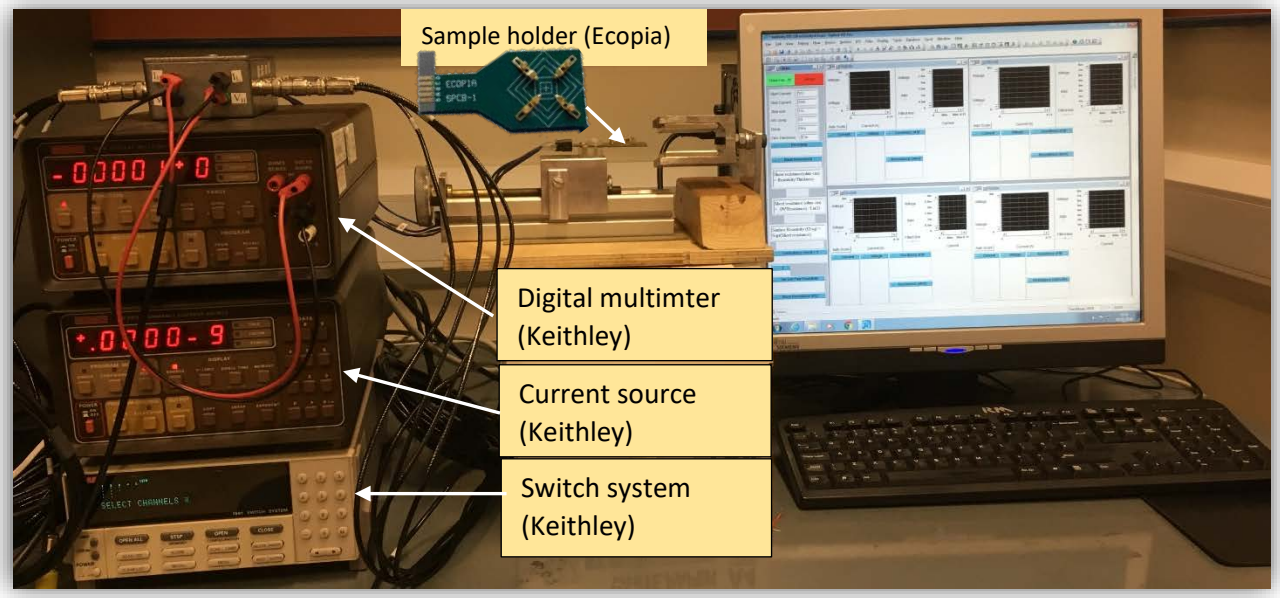

Figure 3.5: *the set up for the resistivity measurements using Van Der Pauw technique.*

3.4.2 4-probe measurement technique

In this technique, four probes are placed (with equal spacing between each other) on the thin film of interest. The sourced current is passed through the two outer probes while the voltage is measured across the two inner ones. This set-up, as shown in figure 3.6, is widely used in

the resistivity measurements of thin film as it is designed to eliminate the errors caused by the resistances of the electrical contacts.

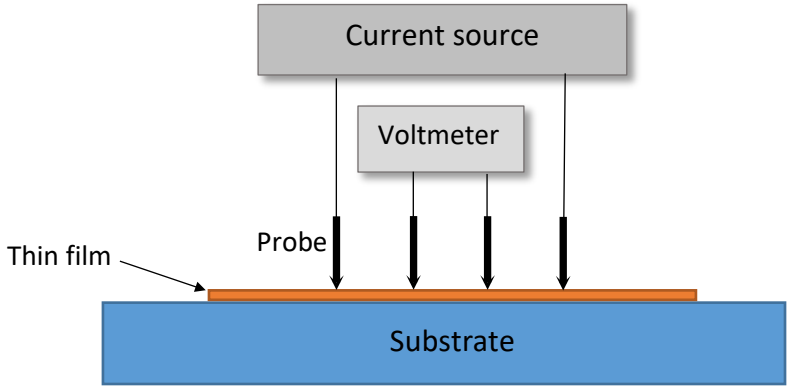

Figure 3.6: *schematic diagram of a 4-probe technique.*

The electrical resistivity of a thin metallic film that has a thickness which is much smaller than its length can be measured using this equation:

$$\rho = \frac{\pi}{\ln 2} \cdot \left(\frac{V}{I}\right) \cdot d \text{ [93]} \quad \text{.....3.3}$$

Where, (V) is the voltage drop between two inner probes on the thin film, (I) is the current passing through the outer probes on the thin film and (d) is the thickness of the thin film.

3.5 Tensiometer (Torsion Balance)

This instrument (figure 3.7) is used to measure the surface or interfacial tension of fluids by using a platinum ring (DuNouy ring). The measurements are carried out in a quick time (less than a minute) which is useful when measuring colloidal suspensions whose surface tensions change rapidly. The device is levelled then the DuNouy ring is attached to the hook. First, the index pointer should be set to zero. The fluid to be tested is put in a container to be positioned on the movable platform below the ring. Then, the platform is moved till the ring is slightly immersed (just under the surface of the fluid; come into contact with the fluid) in the fluid. By gently moving the index pointer until the ring suddenly detaches from the liquid surface and at that moment the indication of the pointer shows the surface tension of the test liquid which can directly be read from the instrument in Newtons per metre.

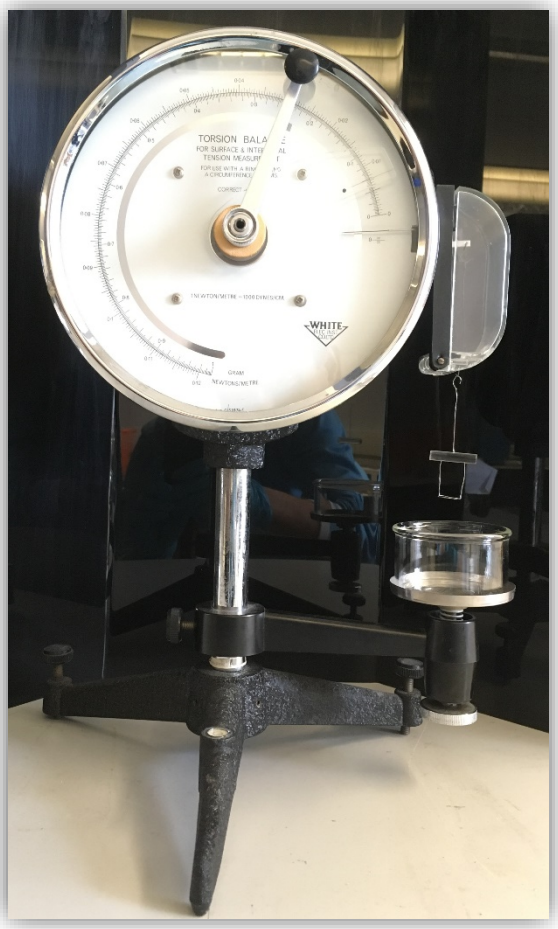

Figure 3.7: *the torsion balance used in this research to measure the surface tension of the materials of interest.*

3.6 Goniometer (Contact Angle Measurements)

The contact angle measurements are crucial in the investigations of the wetting of the ink on the substrates. Figure 3.8 exhibits the goniometer used in this research which was CAM200 KSV NIMA (Biolin Scientific, Sweden), it is based on video and imaging analyses (user-programmable and computer-controlled) and can be used to measure contact angles (static and dynamic), surface and interfacial tensions and solids' free surface energies when equipped with the right software. The fluid to be investigated is filled into the syringe, and then it is placed in the holder above the adjustable sample stage which needs to be spirit levelled when samples are put on it. The syringe is adjusted while observing by the camera to be placed in the middle

and just on the top of the substrate. It is necessary to ensure that the drop that is ejected out of the syringe is fully visible by the camera as the instrument, as mentioned earlier, depends on video and image analysis of the drop before and after impacting the surface of the substrate.

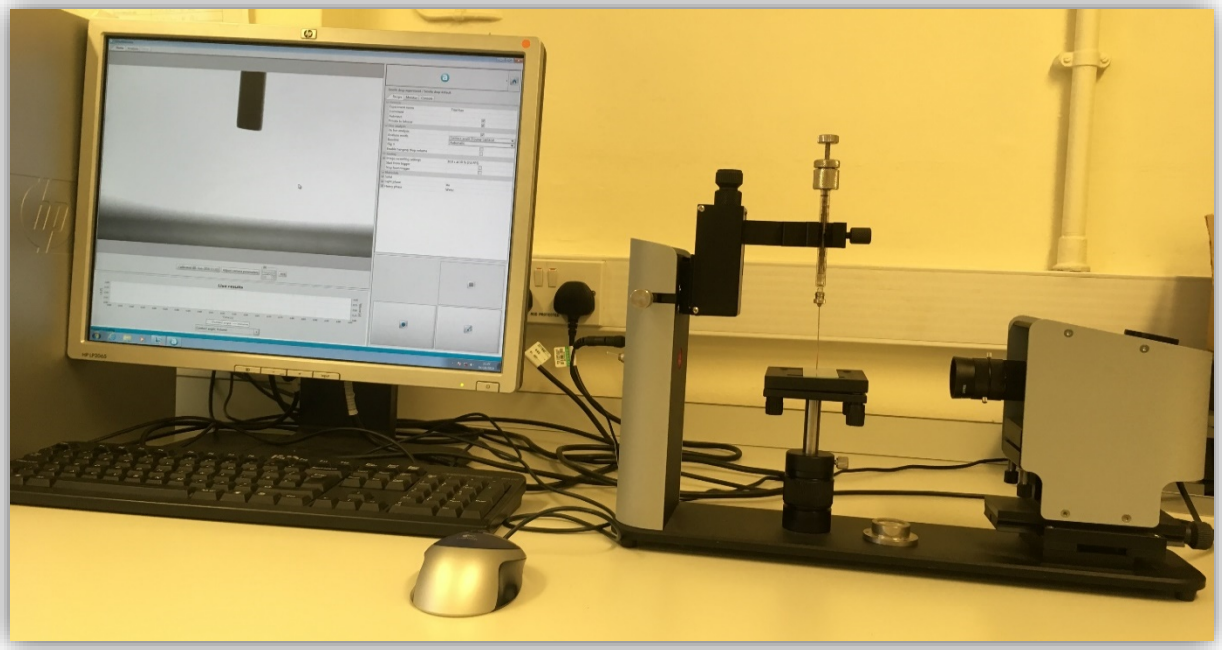

Figure 3.8: *the goniometer system that was used in this research for contact angle measurements.*

The working principle is based on Young's equation (see eq.3.4), which provides a quick understanding and explanation on the wettability of liquids on solid surfaces.

$$\gamma_{sg} = \gamma_{sl} + \gamma_{lg}\cos(\theta) \quad \text{.....3.4}$$

Where, γ_{sg} is the solid-gas surface tension, γ_{sl} is the solid-liquid surface tension, γ_{lg} is the liquid-gas surface tension and (θ) is the contact angle between the liquid and the solid, as shown in figure 3.9. More details can be found in chapter 5, section 5.2.4.

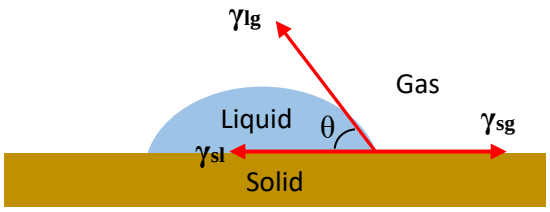

Figure 3.9: *a drop of liquid making a contact angle of (Θ) and the surface tension components of the liquid, solid and gas.*

3.7 Viscometer

Figure 3.10 shows the viscometer used in during the PhD study, it is Brookfield DV2T viscometer. It measures the viscosity of Newtonian fluids or apparent viscosity of non-Newtonian liquid at different angular velocities and shear rates during specified periods. First, the spindle is completely immersed in the cylinder that contains the test fluid. Then, the spindle is rotated at a certain rotational speed for a specific time. The exerted force created by the spindle rotation at a constant angular velocity in the fluid is manipulated to obtain the viscosity of the liquid in centipoise cP (cps) or milliPascal seconds (mPa.s).

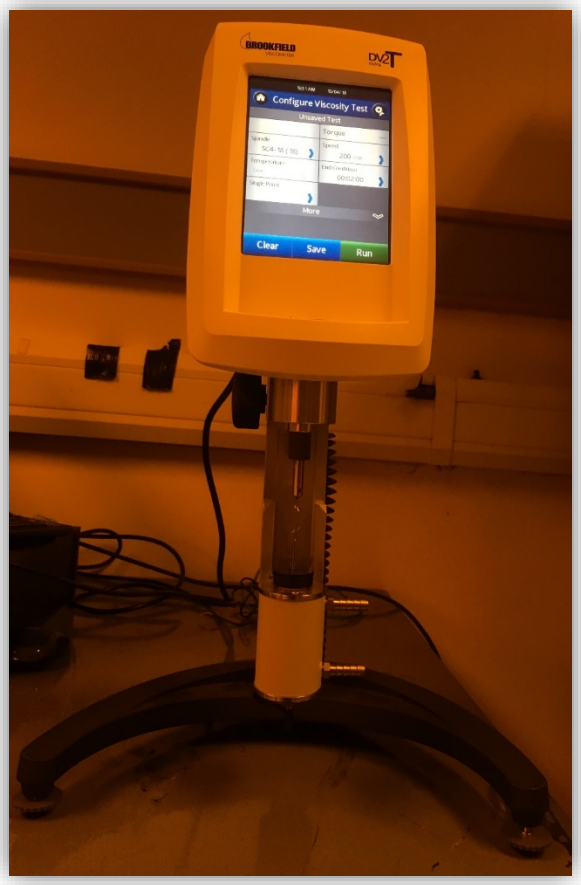

Figure 3.10: *the viscometer that was used in this research for measuring the viscosity of the liquids of interest.*

3.8 RF Plasma Barrel Etcher

This equipment is used to treat the surfaces of substrates by exposing them to plasma (ionised gas). Different gases are used for different purposes, such as oxygen is used to remove organic materials and hydrogen for etching over metals and silicon. The process gas is pumped into a vacuum chamber with a fixed flow rate to maintain the pressure, followed by radio frequency (RF) excitation to ionise it. The plasma chemically reacts with the sample material and results in volatile products that can be evacuated using a vacuum pump. The PT 7100 RF Plasma Barrel Etcher (Bio-Rad, California, US) that was used in this work is shown in figure 3.11.

Figure 3. 11: *PT 7100 RF Plasma Barrel Etcher that was used in this research for treating the surface of the substrates.*

Chapter 4: Contact Printing: Stamping/Transfer Printing

In this chapter, one contact printing technique utilising the stamp printing machine, will be discussed, along with its design, manufacture and control. Furthermore, testing of the machine and the investigation of the stamp printed aluminium tracks on treated glass substrates will be discussed.

4.1 The Stamp/Transfer Printing Machine

4.1.1 The design, manufacture and automation control of the utilised machine

The printing machine was designed by using an electric cylinder attached to a threaded rod, which acts as a support to provide a stationary position and stabilisation for the electric cylinder and avoid vibrations while the actuator moves, as presented in figure 4.1. The electric cylinder, LDZBB5L-100A5 [94] from SMC Pneumatics (Milton Keynes, United Kingdom), is a linear actuation device with an inbuilt DC stepper motor (high accuracy and fine resolution in small ranges are needed), was selected due to its inexpensive costs, manual and automating operations, high performance and reliability to provide the required movements needed for the stamping process. A directional control driver, LC3F212-5A5B [95] supplied along with the electric cylinder from SMC Pneumatics (can be operated automatically and manually and used also for the motor protection from high current), was used to control the motor by a simple set up, as shown in figure 4.2, which consists of:

a) **Power supply:** a 24 DC power supply to feed the main terminals of the directional control driver with (24 Vdc, 1.3 A) and power control terminal of the driver by the use of 3 KΩ to reduce the current to 8 mA**.**

b) Waveform generator: Agilent 33220A 20 MHz waveform generator is used to generate a 5V square wave to be applied to the phase control terminals (which control the travelling direction of the actuator: extension or retraction) of the driver where a precise programmed control for the motor can be achieved.

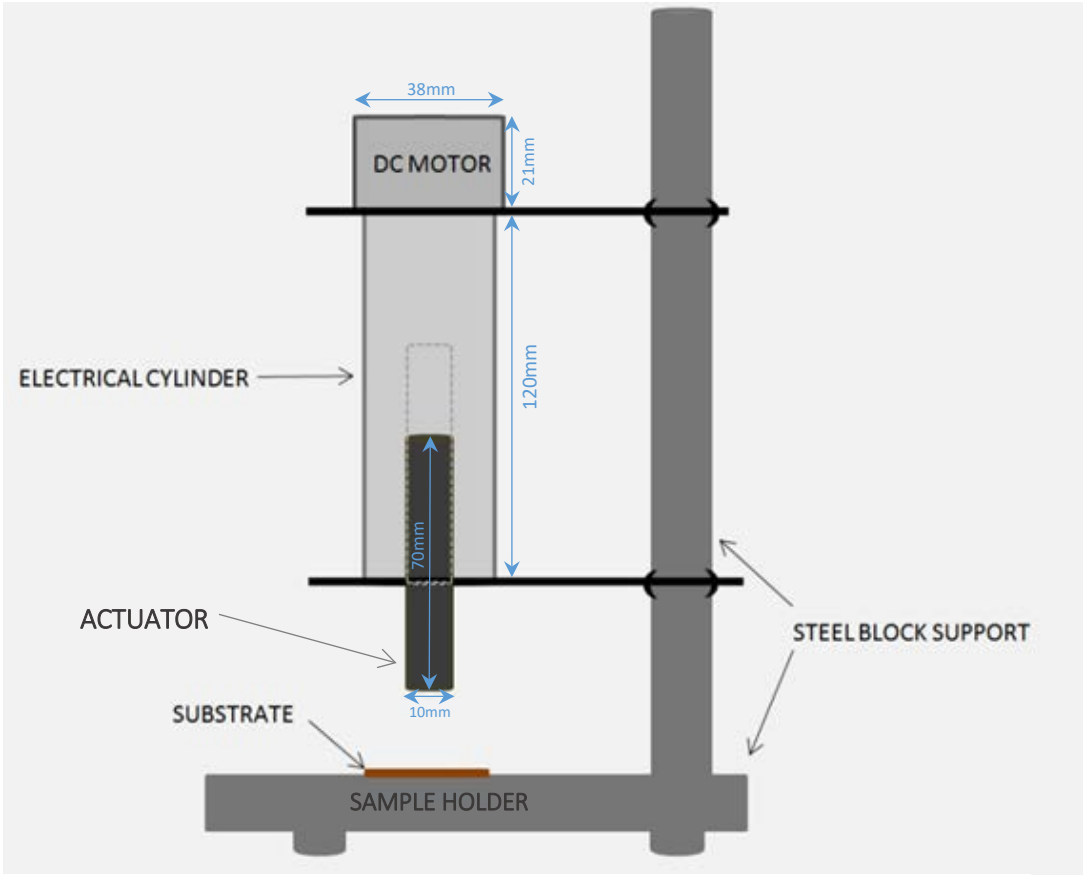

Figure 4.1: *the architecture design and main components of the utilised stamp printing machine.*

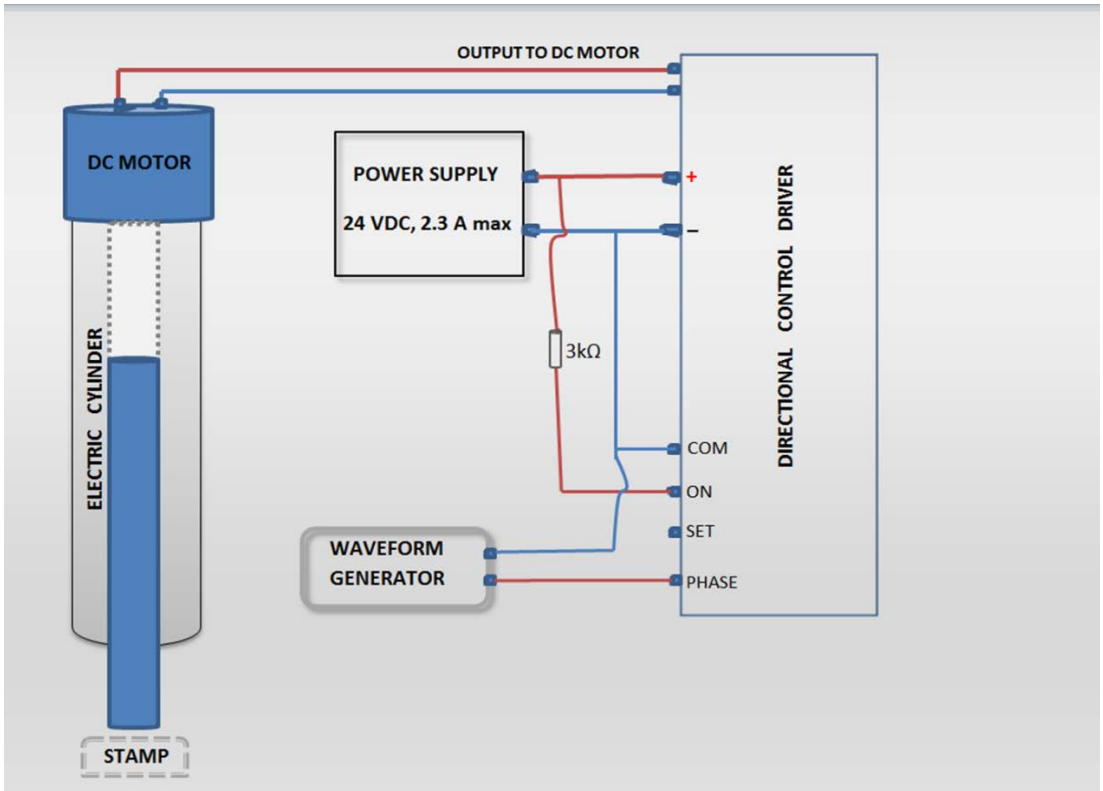

Figure 4.2: *set up of the control unit for the electric cylinder DC motor using only a directional control driver, a power supply and a waveform generator.*

4.1.2 Automation and programming

Agilent Visual Engineering Environment (VEE) software has been used for the control of the directional control drive LC3F212-5A5B through the waveform generator 33220A (20MHz) used in this work. Agilent VEE is a visual language environment that has been widely employed to automate, design and test instruments and electronic devices such as waveform generators, oscilloscopes and thermometers due to its simplicity, functionality, flexibility, high performance and compatibility with several industrials standards. The programme`s main functional icon called object, so basically the programmer connects these objects in a specific way, similar to block diagrams, according to the devices to be tested or controlled.

The Agilent VEE programme that was designed to automate the stamping process in the proposed printing machine can be found in the appendix (figure A1).

An Arduino-based microcontroller (UNO R3), programmed and coded by Eng. V Pracas and Dr K Manjunatha at De Montfort University, was also used to control the speed of the actuator and the force sensitive resistor (FSR) to calibrate the proposed printing machine.

4.1.3 PDMS Stamp preparation

The process of the stamp preparation commenced with the design and manufacture of the stamp casting assembly set (casting unit) which is shown in figure 4.3, consists of Teflon holders for: the master and the stamp carrier (figure 4.3 b and c), and a stainless steel stamp holder (figure 4.3 a). Two types of masters (masters are generally fabricated by conventional micro or nanofabrication method such as photolithography [96]) were used; one is at the bottom of the base of the casting set where defined four lines were engraved (0.5 mm depth and widths of 0.5, 1, 1.5 and 1.5 mm) at the mechanical workshop at De Montfort University, an example of which is presented in figure 4.4 a (more microscopic images showing the dimensions of these lines (tracks) can be found in the appendix, figure A.2), and the other master (stencil) was

already prepared and been used at printed electronics laboratories as shown in figure 4.4 b, it was simply made by laser printing some features and figures on a transparent plastic sheet. The lab masters come in different sizes and figures, the ones were used are in the size 2cm x 2cm to fit in the base (tray) of the casting kit, images of which can be seen in figure 4.4 c.

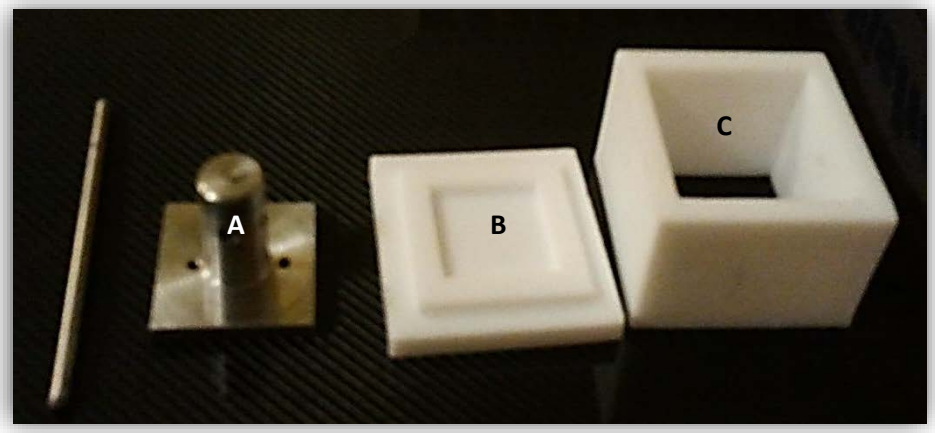

Figure 4.3: *the main parts of the stamp casting assembly set; a) stainless steel stamp holder, b) Teflon master holder and c) Teflon stamp carrier holder.*

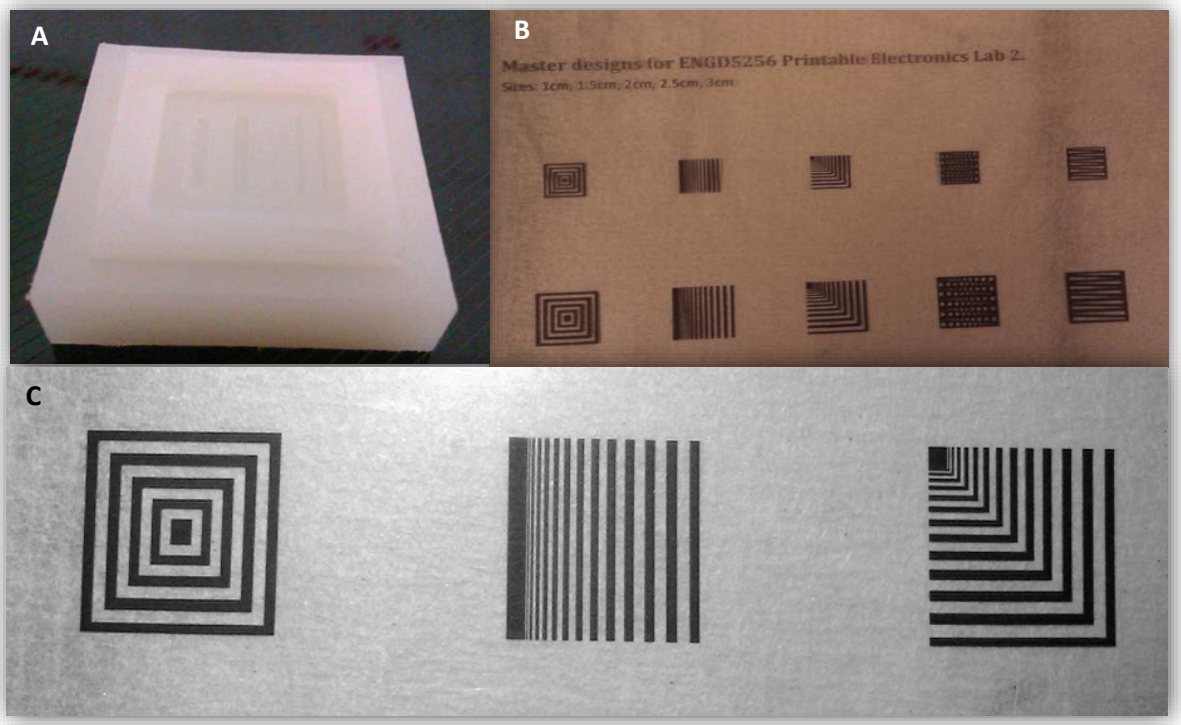

Figure 4.4: *the stamp masters used in this research; a) lines engraved in the base of the casting unit, b) printed electronics laboratory masters, and c) the laboratory stamp masters that were used to test the stamp printing machine.*

The PDMS silicone polymer was chosen to be the prime material for the stamp to be used in the proposed printing machine due to the advantages and outstanding properties that PDMS-

based stamps have as discussed earlier. The PDMS stamp is a mixture of two parts: the base (silicone elastomer) and the curing agent (silicone resin solution), the most widely used in academia and industry is Sylgard 184 from Dow Corning, Midland, Michigan, USA [97].

After having mixed and stirred the two components thoroughly for at least two minutes; it is recommended that for each 10 volume parts of the silicone base, 1 volume part of the curing agent should be mixed to obtain a good stamp (the more curing agent, the more inelastic and rigid the stamp is [98]), the mixture was desiccated under low vacuum at room temperature to degas until all air bubbles that were formed after mixing were disappeared as there is no fixed time to be certain that the bubbles have been completely removed due to the high viscosity of the PDMS components.

The following step was to gently pour the air-bubble-free fluid into the stamp casting unit which has the masters placed in. Then the whole casting unit was put inside a desiccator to remove any remaining bubbles. Finally, the curing process was taken place in an oven, 100°C for 35 minutes. During curing, the mixture is crosslinking and solidifying making it practical to replica mould on the master that has the desired features. The masters were peeled off and the final shapes of some of the cast PDMS stamps were as presented in figure 4.5. The surface of the cured PDMS was rough and it was hard to achieve a smooth surface due to the nature of the PDMS and the Teflon base used. A brief visual demonstration of the whole process of the preparation of a PDMS stamp is presented in figure 4.6.

Figure 4.5: *some of the PDMS stamps that were cast with some masters for purpose of testing the stamp printing machine.*

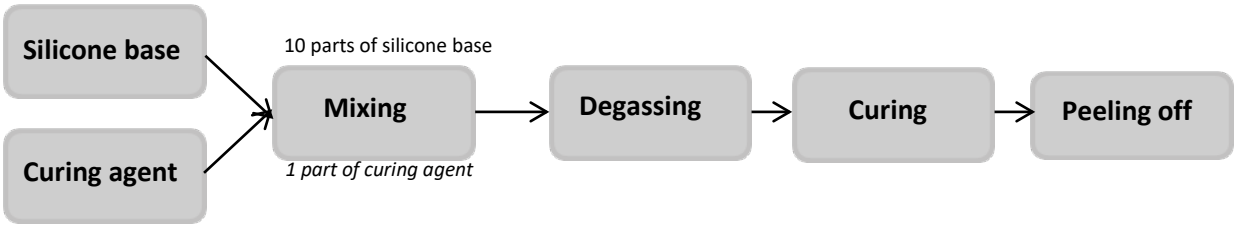

Figure 4.6: *a brief visual demonstration of the process of making PDMS stamps.*

There are some parameters and precautions which were observed while carrying out the process of the PDMS-based stamp preparation that should be taken into consideration for the optimisation of the stamps. These can be briefly explained as follows:

- The two components of the PDMS stamp should be mixed and whisked vigorously to ensure the uniformity of the cross-linked casting stamp.
- Stress and pressure on the stamp holder are preferred to be as low as possible while pouring the PDMS elastomer mixture into the casting assembly set.
- The casting unit should be kept flat to even the PDMS mixture and avoid deformations in the stamp due to the creation of air bubbles and left for a sufficient period of time, particularly, after pouring the PDMS liquid and before putting in a hot oven, to allow the mixture to settle in in a homogenous uniform condition.
- Curing time is noticed to be as long as possible and this is done by lowering the curing temperature, 48 hours at room temperature, to achieve excellent casting as the shear modulus of the cured stamp depends on several parameters including the curing temperature and the proportion of the curing agent.

4.1.4 Calibration of the stamp printing machine

In order to calibrate the proposed machine, a force sensitive resistor (FSR) (controlled by the Arduino microcontroller) and different weights of a fixed area were required. The FSR was mounted on a movable holder as shown in figure 4.7. Vials were filled with salt of different weights; 7, 10, 12.5, 15, 17.5 and 20 g. The vials were placed on the FSR in turns, and as seen in figure 4.8, the sensor output (in mV) increased with the increase in weight. Pressure values (in KPa) corresponding to the weights were derived from the following equation:

Pressure = Force/Area= mass (Kg) x acceleration of gravity (m/s^2) / $\pi r^2(m^2)$ …….……4.1

Where, r is the radius of the bottom area of the vial. As for the pressure unit, one kPa is equal to 101.972 kilogram-force per square meter. It is also worth noting that the maximum weight (pressure) was 20g (7.6 kPa) due to limitations of the FSR.

Figure 4.7: *an FSR mounted on a movable holder and vials filled with different salt weights.*

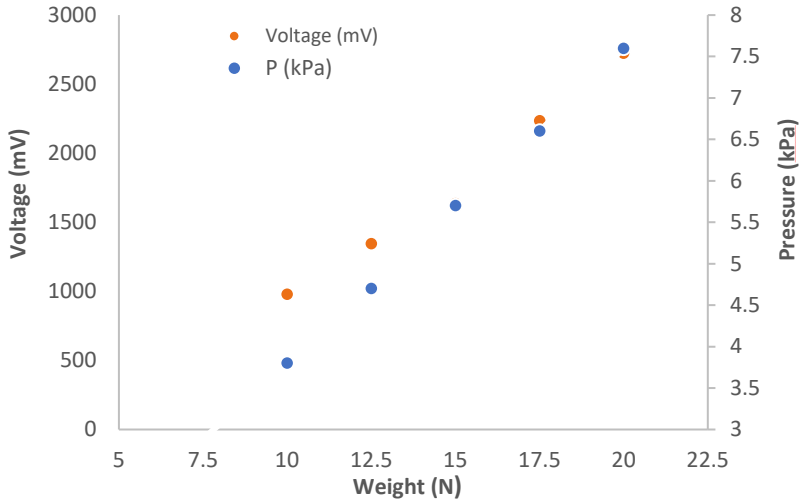

Figure 4.8: *the corresponding sensor outputs to different weights along the derived pressure values in kPa.*

Having calibrated the pressure values for the stamp printing machine, the next step was to evaluate the specific values for the pressure, speed of the actuator and contact time of the PDMS stamp with the substrate. In addition to the afore-mentioned pressure values, the actuator speed range was between 5-30 mm/s while the contact time was between 5-60 s. The speed of the actuator was controlled by the Arduino microcontroller.

Double-sided tape on paper was used as a substrate to determine the optimum parameters (pressure, speed and contact time) for the transfer of 150 nm aluminium (Al) coated on glass slides purchased from Sigma Aldrich (Dorset, United Kingdom) to the used substrate. The substrates were placed on the FSR, then the (Al) coated glass was attached to the actuator. The pressure values, range of the speed of the actuator and the contact time were investigated, as shown in table 4.1, in order to optimise the critical parameter values for the transfer to take place. It is was found that a minimum pressure of 6.6 kPa is required for the transfer of aluminium from the glass slides to the used substrate. Moreover, from the experiment, the required speed of the actuator and contact time for a good transfer were between 10-20 mm/s

and 15-30 s, respectively. As shown in figure 4.9, the transfer of aluminium from the glass slides to the tape when applying the optimum control parameters mentioned before.

Table 4.1: *testing the control parameters; pressure, speed of actuator and contact time for the aluminium transfer from the glass to the double-sided tape.*

Pressure (KPa)	2.7						3.8						4.7						5.7						6.6						7.6					
Speed (mm/s)	5	10	15	20	25	30	5	10	15	20	25	30	5	10	15	20	25	30	5	10	15	20	25	30	5	10	15	20	25	30	5	10	15	20	25	30
Contact time (s)	5	15	30	40	50	60	5	15	30	40	50	60	5	15	30	40	50	60	5	15	30	40	50	60	5	15	30	40	50	60	5	15	30	40	50	60

Transfer of aluminium from glass to double-sided tape: RED=unsuccessful and GREEN=successful

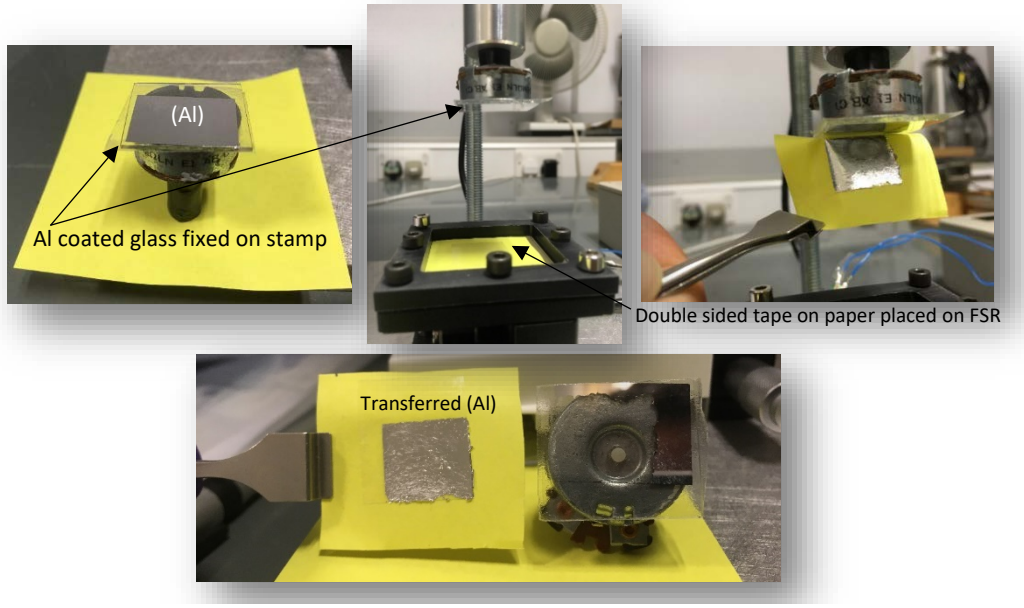

Figure 4.9: *the transfer of aluminium from the glass slides to double-sided tape when applying the optimum control parameters; pressure is more than 6.6 kPa, actuator speed is between 10-20 mm/s and the contact time is in the range of 15-30 s.*

4.1.5 Deposition of thin films on stamps

After having finished PDMS stamp preparation, different stamps with several patterns were subjected to depositions of thin films by means of a thermal evaporator. Figure 4.10 shows a number of PDMS stamps placed on the substrate holder at the top of the thermal evaporator to be ready for aluminium deposition.

Aluminium, 99.99% pure purchased from Sigma Aldrich (Dorset, United Kingdom), was chosen to start with due to the fact it has plenty of advantages including availability, cheapness, commonly used in semiconductor devices, good electrical and thermal properties and the ability to adhere to the PDMS stamp. 50, 150, 200, 250 and 300 nm layers of aluminium were deposited on the patterned of the different stamps by using the thermal evaporator with these parameters were taken into consideration: vacuum pressure of $4x10^{-6}$ mbar (to avoid contamination and increase the deposited thin film quality by eliminating scattering and the collision between the atoms) and current of 20 A. The rate of evaporation is important here to obtain a layer of aluminium that does not adhere strongly with pre-patterned PDMS stamps, facilitating easier transfer of the aluminium layer from the stamp to the substrate. As the migration rate of the evaporated atoms is higher than the rate of newly arriving evaporated atoms to achieve layer by layer growth and builds islands that are strongly bonded with each other and the substrate, when the deposition rate increases the size of the critical nuclei decreases and the nucleation barrier becomes smaller [99]. Therefore, in this work, a quick and rapid deposition rate for the evaporated aluminium was selected > 1.5 nm/s for all PDMS stamps. When the desired thickness of the evaporated aluminium was observed on the control panel (monitor) of the thermal evaporator for each specified thickness, the evaporator temperature was allowed to cool down (approximately one hour) before taking out the stamps with aluminium deposited patterns. The aluminium (Al) deposited stamps can be seen in figure 4.11.

Figure 4.10: *PDMS stamps inside the thermal evaporator for (Al) deposition.*

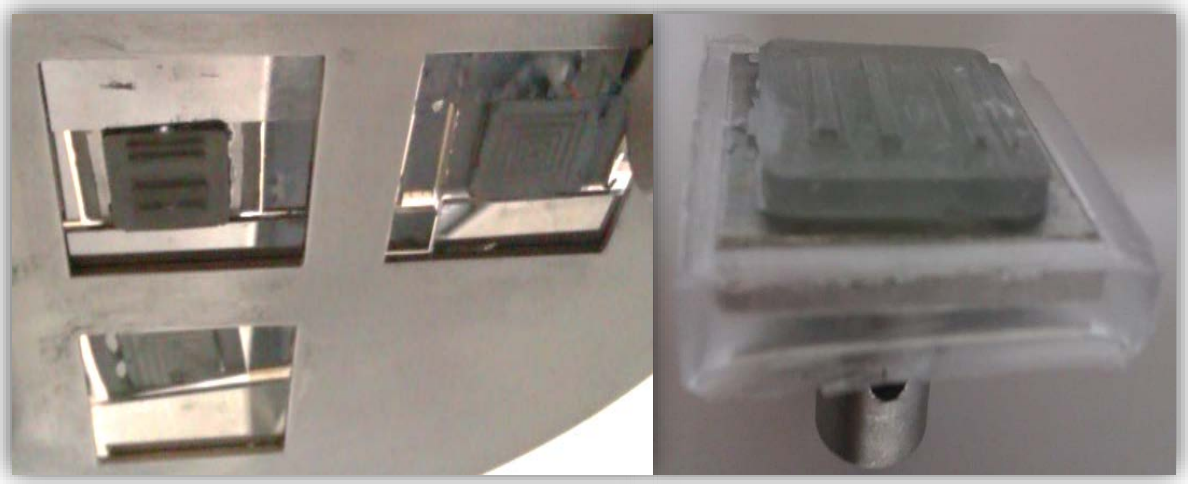

Figure 4.11: *some of the PDMS stamps after (Al) deposition.*

4.1.6 Printing metal paths on glass substrate

The automated stamp/transfer printing machine was initially tested by using the PDMS stamps that had been thermally evaporated and deposited on by aluminium thin films of thicknesses of 50, 150, 200, 250 and 300 nm. As corning glass substrates, purchased from Sigma Aldrich (Dorset, United Kingdom), were used as test substrates for the printing process, it should be carefully cleaned to ensure purity.

4.1.6.1 Cleaning the glass substrates

First, it should be noted that the whole cleaning process was carried out in a laminar airflow bench in a clean room to ensure a clean environment free from dust and chemical contamination of the substrates.

The glass substrates were cleaned as follows: firstly, the glass substrates were placed in a solution containing 95% of 18MΩ De-Ionised (DI) water and 5% Decon-90 before sonicating in an ultrasonic bath for half an hour. Then, they were rinsed in 18MΩ DI water using the same ultrasonic bath for 5 times. Secondly, the substrates were placed in acetone and then isopropyl (different beakers) to be sonicated for 15 minutes. 2 minutes of ultrasonication rinsing with 18MΩ DI water was done again for 5 times before drying with nitrogen. Finally, the glass substrates were baked on a hot plate at 150 °C for an hour. This is a widely used procedure for cleaning glass substrates in laboratories, more information can be found here [100].

4.1.6.2 Substrate Treatment: Plasma Etching and Chemical surface modification

As the aluminium tracks that are to be transfer printed from the PDMS stamps to the treated plasma glass substrates, and the surface energy of the PDMS stamp is relatively low 19.8 mN/m [101] while the surface energy of the aluminium is 840 mN/m [101], the adhesion of the evaporated aluminium to the PDMS stamp is weak, which makes the transfer printing process

applicable when the right pressure applied, time of contact and optimised surface of substrates along with the right peeling off speed of the stamp from the substrate. Hence, before the process of the stamp/transfer printing took place, the cleaned glass substrates were subjected to oxygen plasma treatment to increase the surface energy of the substrates, forward power of (approximately 100 watts) and reflected power (less than 5 watts). However, different times of the plasma treatment were investigated; 1, 2, 5, 10, 15 and 20 minutes.

The water contact angle with untreated glass is 32° (±2°) while water rinsed glass is 25° and plasma-treated ones are <10° [102]. The surface energy of a glass substrate is 310 mJ/m^2 [103].

The plasma-treated glass substrates were then investigated by contact angle measurements to evaluate the best wetting and the highest surface energy of the substrates. Figure 4.12 presents some of the results obtained of the contract angle measurements, more results will be included in the appendix (figure A.3).

4.1.6.3 Contact Angle Measurements

The glass substrates that were treated by oxygen plasma for 15 minutes were selected for the proposed stamp/transfer printing machine demonstrations as the obtained contact angle is the lowest which is 10° which means that it has the highest surface energy and wetting.

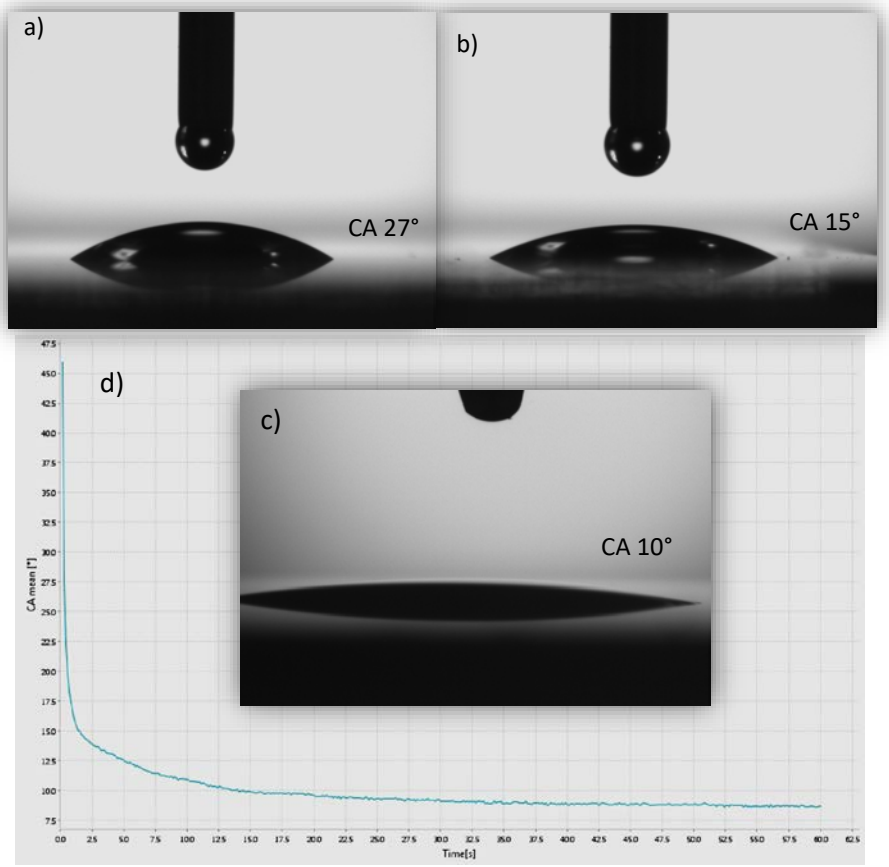

***Figure 4.12*:** the contact angle measurements using water drops on oxygen treated plasma glass substrates; a) plasma for 1 min, measured contact angle (CA) is 27°, b) for 5 min, CA is 15°, c) plasma for 15 min, CA is approximately 10° and d) the goniometer software contact angle results for the 15min oxygen plasma treated glass.

4.1.6.4 Testing the stamping machine

As the automated stamping/transfer printer has been constructed, a programme control on the electric cylinder motor was achieved and different PDMS stamps were prepared with several patterns where thin films of aluminium were deposited on, all materials and components required to test the machine were on hand and accessible.

First, a patterned PDMS stamp with aluminium deposition was attached to the end of the actuator of the electric cylinder as shown in figure 4.13. A cleaned and 15-minute oxygen

plasma-treated corning glass slide (thickness of 2 mm) was placed on the steel support, exactly where the attached stamp contacts, to ensure intimate contact between the stamp and the glass substrate (see figure 4.14). The control parameters were set to the optimal values discussed earlier (stamp pressure of 6.6-7.6 kPa, speed of actuator of 10-20 mm/s and stamp/glass contact time of 15-30 s) to achieve a good transfer of Al patterns to the treated glass substrates. In the end, the printed samples were then taken to be investigated via current-voltage (IV) probe stations for electrical measurements, optical microscopy and SEM for imaging and surface topography/morphology measurements, and profilometer for thickness measurements.

Figure 4.13: *a patterned PDMS stamp attached to the actuator of the electric cylinder.*

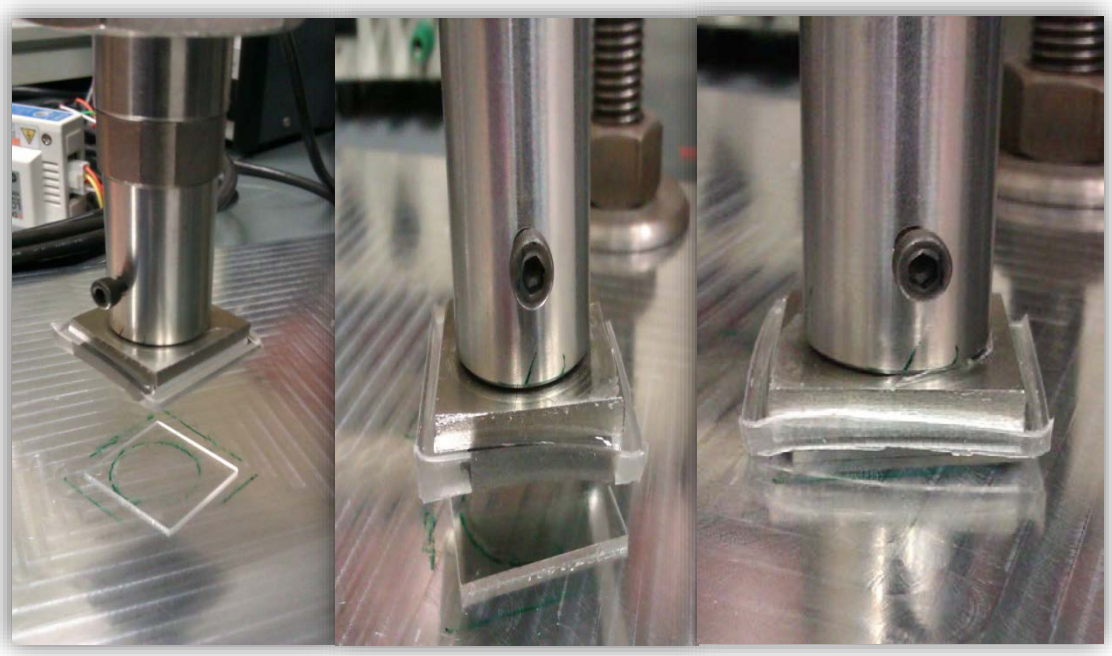

Figure 4.14: *placing a glass substrate to ensure an intimate conformal contact between the stamp and the substrate.*

The same procedure was also carried out using different substrates including p-type silicon wafers and flexible substrates and then they were partially analysed with some of the equipment mentioned previously to evaluate the quality of the printing and the versatility of the machine. However, as the main focus here only on using glass substrates, the printing results of some of these substrates is only included in the appendix because they might be used for future studies.

4.2 Results and Discussion

The quality, adhesion and electrical properties of the aluminium printed patterns and tracks on the oxygen plasma-treated glass substrates were investigated by using an optical microscope, SEM microscopy, adhesion test (scotch tape test) and current-voltage (IV) measurements. The transfer of Al to clean but not treated glass substrates was unsuccessful, and for this reason, the measurements were performed only on O_2 plasma-treated substrates.

4.2.1 Optical Microscope and SEM

The substrates with printed Al were initially investigated by optical microscopy and scanning electron microscopy (SEM) to obtain clear and informative images of the printed patterns to evaluate the quality of the stamp printing of the aluminium. The measurements were commenced with these techniques due to the fact that they are non-destructive techniques as the substrates are subjected to more tests and investigations.

When printing the aluminium tracks from the pre-structured and patterned stamps to clean glasses, the transfer was so poor and hardly not much of the aluminium was transferred as shown in figure 4.15. This can be attributed to the low surface energy of the glass as the deposited aluminium has a higher surface energy as stronger bonding forces are required to overcome the adhesion bonding between the aluminium tracks and the PDMS stamp, which results in difficulty of the stamping printing even when investigating with different actuator speeds, stamp contact times and higher pressure values, especially, the aim here is not to use high temperatures to heat the substrate. Therefore, there are two proposed methods here to achieve a good aluminium transfer printing; the first is to reduce the bonding and adhesion between the interface of the PDMS stamp and the aluminium tracks, however, this was already done by using a quick and rapid evaporation rate of the aluminium, as mentioned previously, to obtain a weak adhesion between the metal and the stamp. Moreover, as the Young's modulus of stamps is 2 MPa which is much less than aluminium thin film Young`s modulus of 70 GPa [104], the aluminium thin layer can be fractured on the PDMS stamp.

The second method is increasing the bonding strengths of the aluminium and the glass substrate interface to enhance the aluminium transfer printing and overcome the weak bonding between the metal and the stamp and this was tackled by treating the glass substrates with oxygen plasma to increase the surface energy of the substrate.

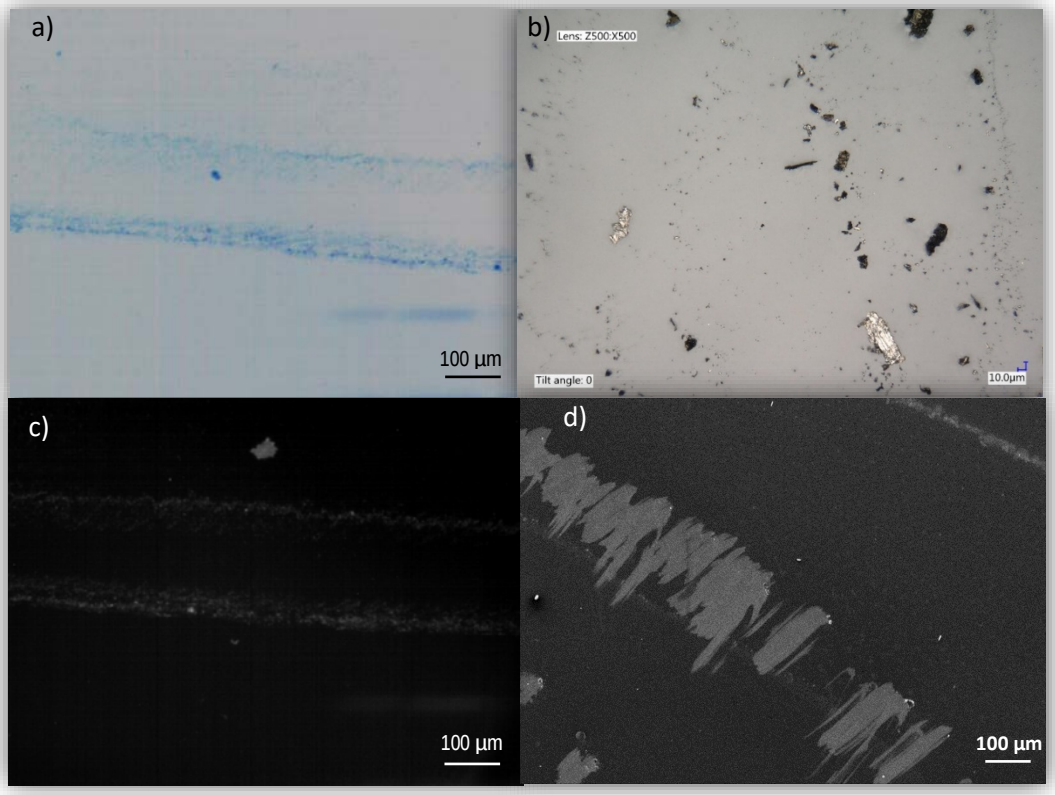

Figure 4.15: *optical microscope images (a, b and c) and SEM image (d) of distorted stamp printed aluminium films on glass. For SEM images: Electron High Tension (EHT)=20KV and Working Distance (WD)=23mm.*

After introducing these two methods and re-performing the stamp printing with the optimised control parameters in place, good results were obtained as can be seen in figure 4.13 which shows optical microscope images of stamp printed aluminium tracks/patterns on 15min plasma O_2 treated glasses. The stamp printed metal tracks appear to be continuous without any distortions even at the sharp edges of the track.

The optical microscopy images, shown in figure 4.16, present the transfer of aluminium layers (tracks) of (200 - 250 nm) thickness (to be measured by a profilometer in section 4.2.3) and (300 µm – 1.5 mm width) from the PDMS stamp to glass substrates treated oxygen plasma, as it can be observed that the aluminium tracks were successfully printed without any deformation especially at the corners of the tracks.

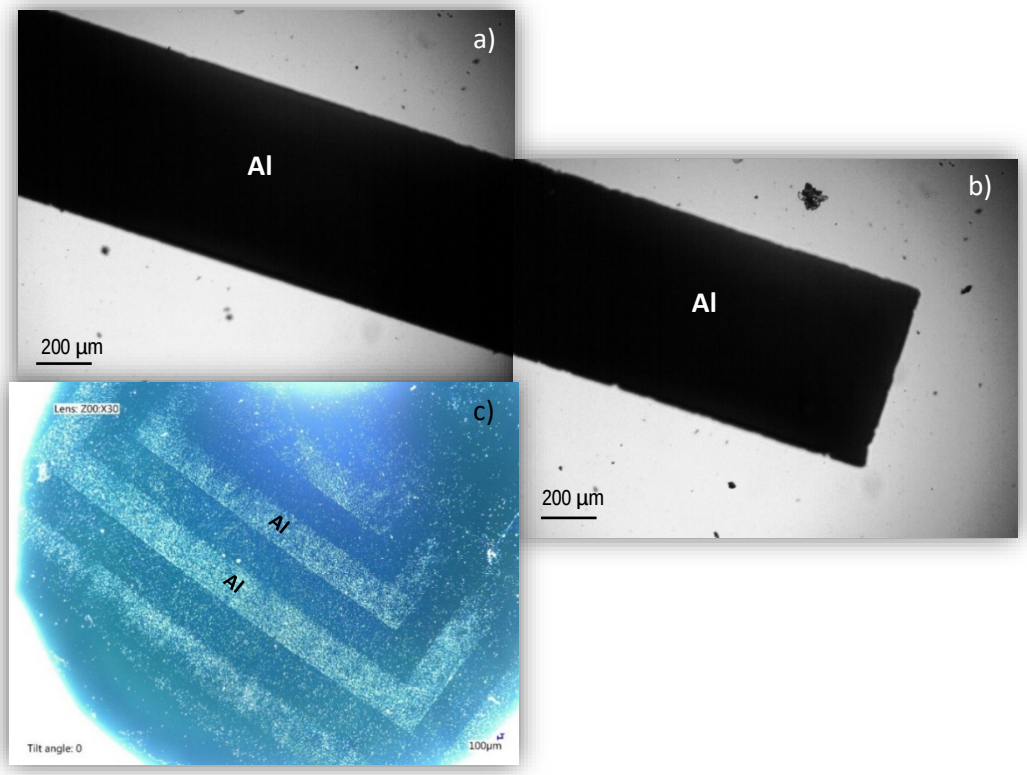

Figure 4.16: optical microscopic images for printed aluminium tracks; a) the centre of the track and b) the edge of the track shown in (a), and c) aluminium patterns (tracks with 90° curves) on oxygen plasma treated (15 min) glass substrates.

The aluminium tracks were successfully transferred this time after establishing a conformal contact between the stamp and the oxygen plasma-treated glass substrate with a stamp pressure of 7 kPa, peeling speed of 15 mm/s to lift the stamp away from the substrate. The aluminium remained adhered to the treated substrates might be due to the kinetically adhesion force as the glass substrate has now surface energy which is high enough to overcome the weak bonding between the aluminium and the PDMS stamp.

SEM, on the other hand, was performed on glass substrates with different thicknesses of stamp printed aluminium (smaller thicknesses of aluminium, 50nm) as presented in figure 4.17. The SEM images revealed that the transfer of the thin films of aluminium from the stamps to the substrates was successfully achieved, however, not completely. It is worth noting that minimum contact time was taken into consideration as the Al thickness was very small, and therefore to avoid any delamination of the printed Al.

Moreover, the other control parameters were set to maximum values for a quick transfer with adequate transfer force.

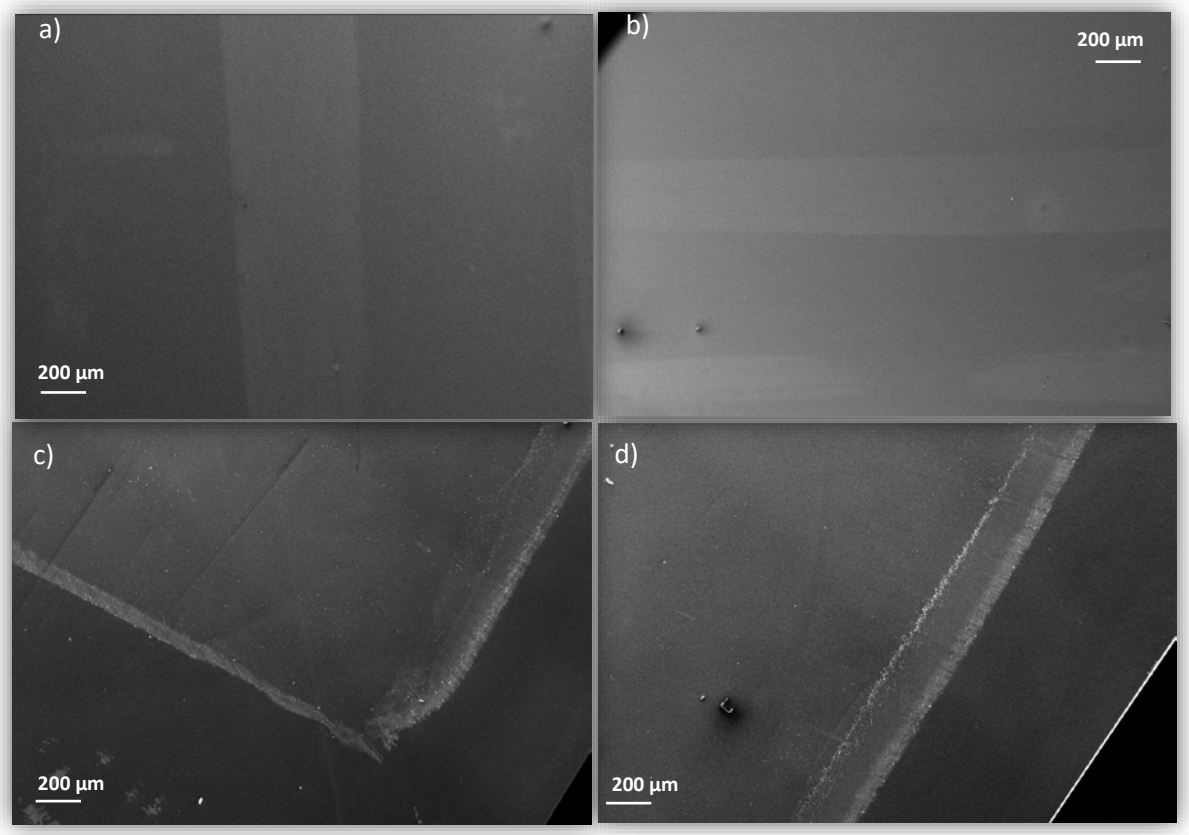

Figure 4.17: *SEM images of different stamp printing patterns of aluminium thin films (50 nm) on oxygen plasma treated (15min) glass substrates. EHT=20KV and WD=13mm.*

From the analysis of SEM images, it can also be observed that neither sagging nor collapsing of the different widths of the patterned aluminium tracks was experienced during the printing process, but a change in the width of the same track (of approximately 60 µm) and a cut in another were observed on some images such as the one in figure 4.18 and this might be due to the fact that during the stamp preparation some tiny distortions on the line patterns had already existed and the stamp was not totally flat and even, and/or the rough surface of the PDMS stamp.

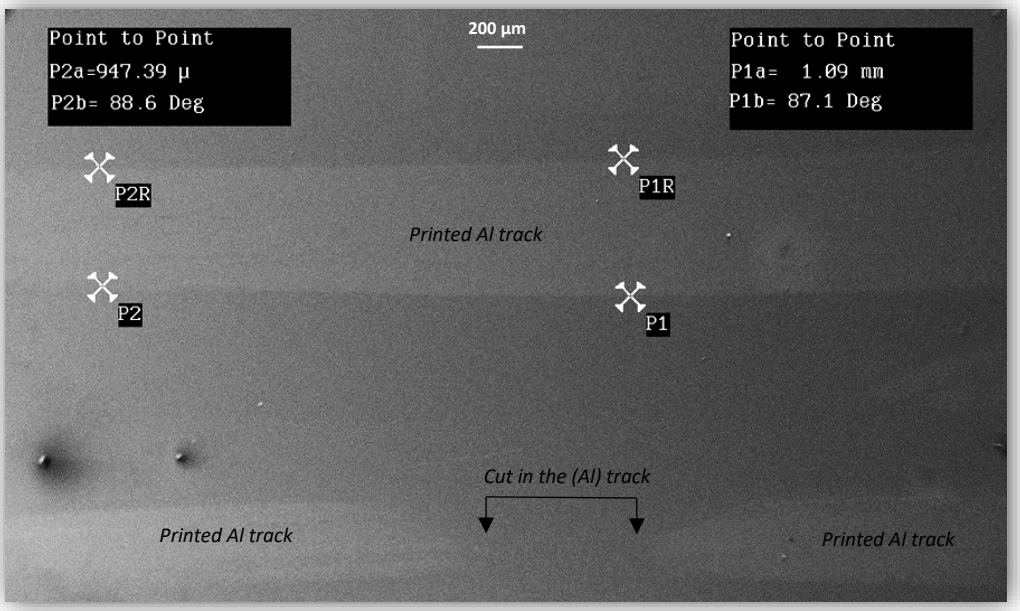

Figure 4.18: SEM image shows a slight difference (of approximately 60 µm) in a printed aluminium track width and a cut in another, printing on oxygen plasma treated (15 min) glass substrates. EHT=20kV and WD=13mm.

4.2.2 IV Electrical Measurements

It is worth noting that most of the IV measurements were performed only on the successful aluminium stamp printed tracks that were printed when applying the optimal control parameters: pressure of the stamp, speed of the actuator and contact time between the PDMS stamp, on O_2 plasma-treated glass substrates which were discussed in section 4.1.6.4.

The IV measurements were performed by using an HP4140B picoammeter. Figure 4.19 shows the IV characterisation of the aluminium transfer printed tracks (50 nm thick) from the PDMS stamp to an oxygen plasma-treated glass substrate. It can be seen that the stamped aluminium was not conductive; as the passing current in pico-amperes which means that the printed aluminium tracks behave like an insulator as they are discontinuous and appear to have cracks/cuts as described earlier through observations of the SEM images.

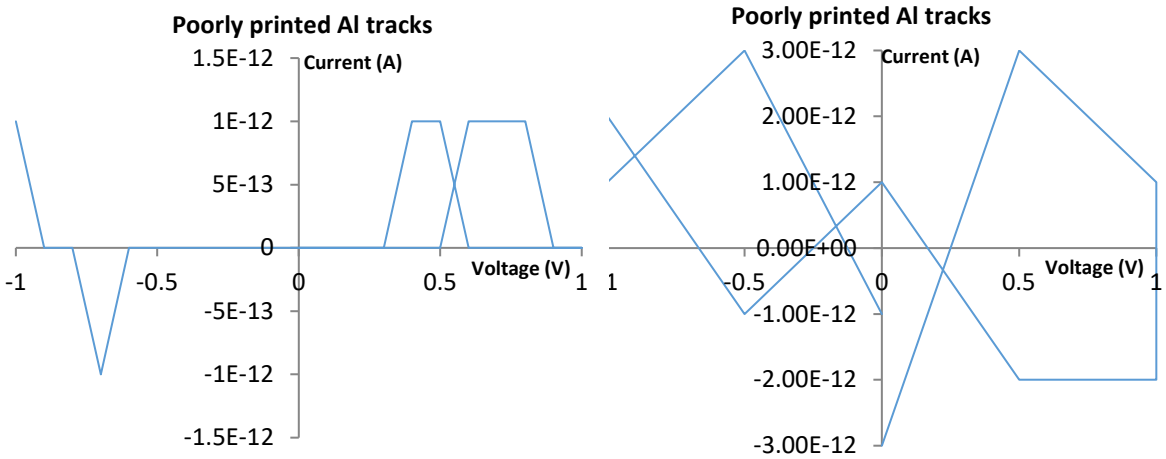

Figure 4.19: *IV measurements for first tested stamp printed tracks that show no conductivity due to the deformation in the printed Al.*

Electrically conductive aluminium tracks (200 nm thick) were stamped from the pre-patterned PDMS stamps on oxygen plasma (15 min) glass substrates when applying the right amount of the stamping pressure (7 kPa) with proper contact time between the stamp and the substrate (15 s) and adjusting the right speed of removing the stamp away from the substrate (10 mm/s). Applying these control parameters results in good stamping/transfer of aluminium tracks with electrical conductivities close to that of bulk aluminium. Table 4.2 summarises the conductivity of the printed Al in relation to the control parameters.

Conductivity of printed (Al) tracks: GREEN is conductive and RED is not conductive.	Control parameters		
	Pressure (kPa)	Actuator speed (mm/s)	Contact time (s)
	2.7	N/A	N/A
	3.8	N/A	N/A
	4.7	N/A	N/A
	5.7	5	5
	6.6	10	15
	7.6	15	30
	N/A	20	40
	N/A	25	50
	N/A	30	60

Table 4.2: *stamp printed (Al) conductivity with the control parameters; pressure, actuator speed and contact time.*

Many physical properties including the resistivity and sheet resistance of metals change with the thickness of the film of the metal. Many factors including the thickness of the film, the rate of the deposition, the grain boundaries and the temperature affect the resistivity of the thin films [105]. The collisions of the electrons with the surface of a material become crucial with decreasing the thickness of the thin film of the material. The electrical resistivity, as well as the

sheet resistance, usually increase with the decrease of the thickness in metals especially when it is in the range between the electron mean free path and specific coalescence limits. This concludes that the thin metal electrical conductivity increases when the thickness of the thin film increases until it reaches the same quantity as the bulk metal`s conductivity and remains constant [105]. The electrical resistivity in thin films is also influenced (increased) by the electron scattering at thin-film surfaces and interfaces and at grain boundaries as described in Fuchs-Sondheimer [106,107] and Mayadas-Shatzkes [108] models when the thickness and/or the particle grain size of the thin film (printed layer) is in the same order with the electron mean free path.

The resistivity of thin metallic layers and films with dimensions where the length is much larger than the thickness of the thin film can be determined by the 4-probe technique using this equation:

$\rho = \frac{\pi}{\ln 2} \cdot (\frac{V}{I}) \cdot d$ (eq.3.3 mentioned in section 3.4.2: 4-probe technique)

Where, (V) is the voltage drop measured between two internal electrodes on the metallic thin film, (I) is the current passing through the thin film through the external electrodes and (d) is the thickness of the thin film.

As it is known that the resistivity of the bulk aluminium is in a range of 2.65 to 2.82×10^{-8} Ω.m, this range was taken as a reference for all the resistivity measurements carried out in this work.

The resistivity of a stamped/ transfer printed aluminium track of thicknesses of 200 nm, on an oxygen plasma-treated (15 min) glass substrate was calculated using equation 3.3 and the IV measurements shown in graph 4.20 and it was found to be 1802×10^{-8} Ω.m; this is significantly higher than the bulk resistivity which can be due to fine discontinuities and tiny gaps that might exist in the stamped/ transfer printed aluminium film. Moreover, the exposure of the aluminium

to the atmosphere might have led to the formation of a layer of aluminium oxide (Al_2O_3) which is an electrical insulator and this might alter the surface properties of the printed aluminium.

More IV measurements were carried out on better stamped/ transfer printed aluminium tracks where different amounts of pressure were applied (between 6.6-7.6 kPa) from the PDMS stamp on the treated glass substrates, different peeling off velocities and contact times, as presented in the figures 4.20-23. Resistivity values of $1325x10^{-8}$, $691x10^{-8}$ and $681x10^{-8}$ Ω.m were determined from equation 3.3 and graphs 4.21, 4.22 and 4.23 respectively, with the last two values being quite similar. This indicates that the resistivity of the stamped aluminium tracks decreased, and hence the conductivity ($1/\rho$) increased, when higher pressure and speed values were applied, which could be due to more materials transferred from the stamp to the glass substrate. Moreover, in all graphs, an ohmic behaviour of the stamped printed aluminium lines can be noted.

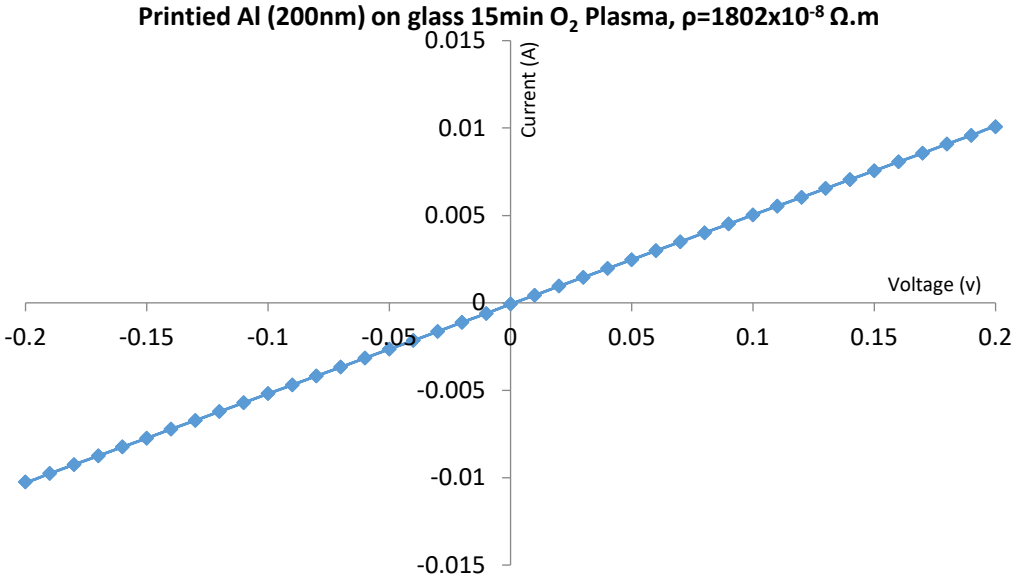

Figure 4.20: *IV characteristics for stamp printed 200nm Al on O_2 plasma treated glass showing ohmic contact behaviour with resistivity of $1802x10^{-8}$ Ω.m. Control parameters; pressure (P)= 7 kPa, actuator speed (v)=10 mm/s and contact time (t)=15 s.*

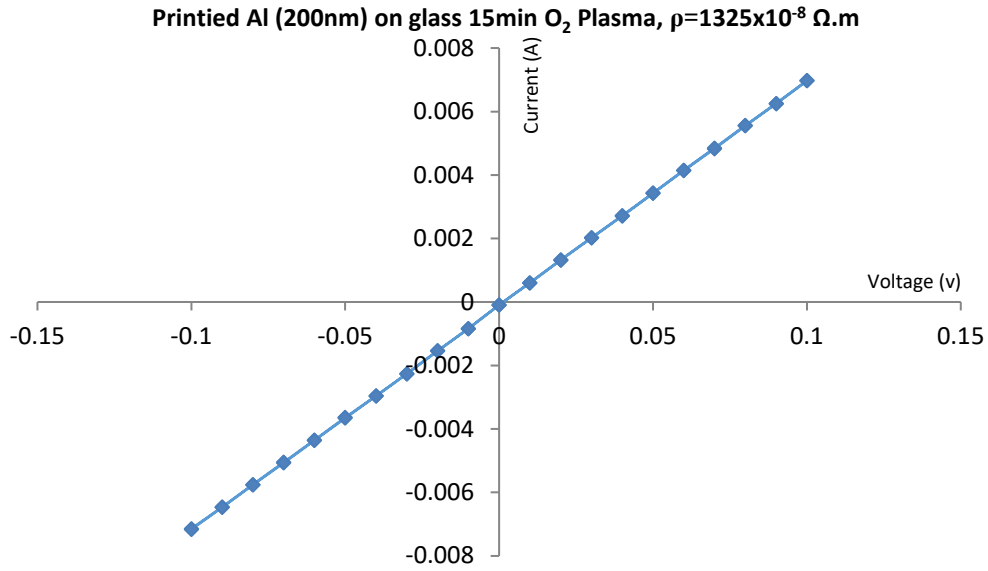

Figure 4.21: *IV characteristics for stamp printed 200nm Al on O_2 plasma treated glass showing ohmic contact behaviour with resistivity of 1325x10^{-8} Ω.m. Control parameters; P= 6.6 kPa, v=15 mm/s and t=15 s.*

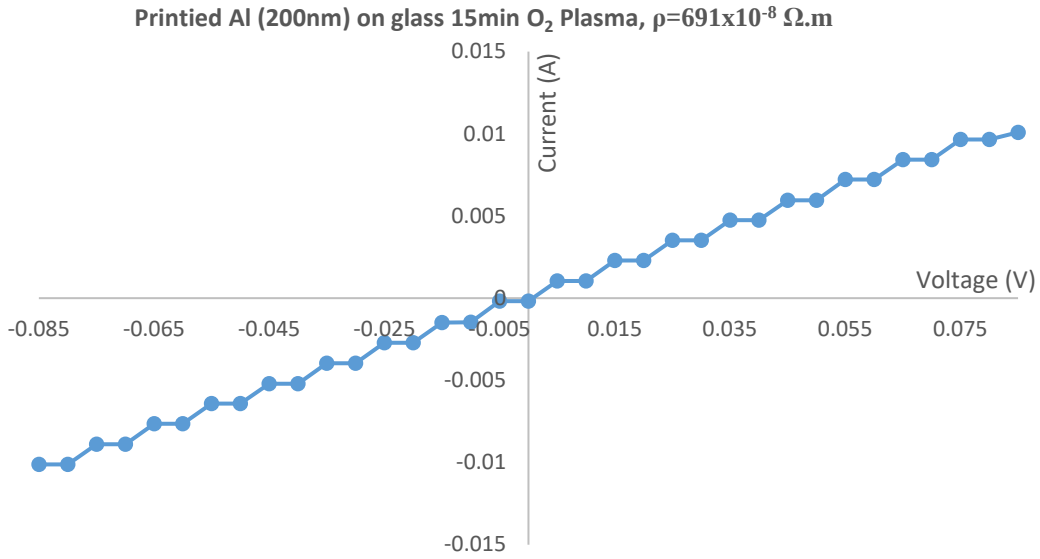

Figure 4.22: *IV characteristics for stamp printed 200nm Al on O_2 plasma treated glass showing ohmic contact behaviour with resistivity of 691x10^{-8} Ω.m. Control parameters; P= 7 kPa, v=15 mm/s and t=10 s.*

Form the resistivity measurements shown the figures 4.20-23, it can be concluded that a pressure higher than 7 kPa, a range of actuator speed of 10-15 mm/s and contact time between 10-15 s are the desired control parameters to obtain a good conductivity of the printed Al. More resistivity measurements on successful stamp printed aluminium (200 nm) on O_2 plasma-

treated glass substrates with different control parameters, and more details presented in the figures can be found in the appendix (figure A.4).

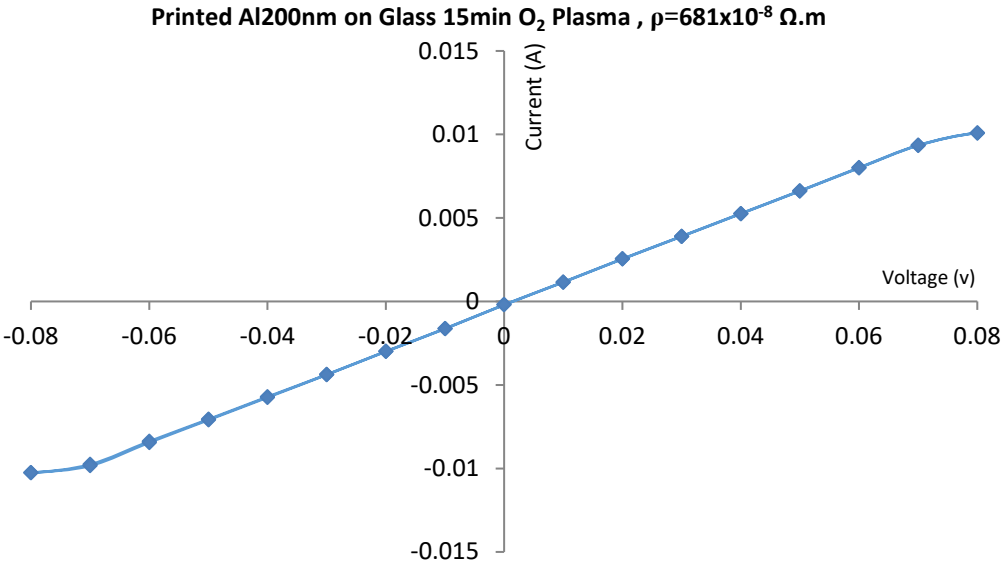

Figure 4.23: *IV characteristics for stamp printed 200nm Al on O_2 plasma treated glass showing ohmic contact behaviour with resistivity of 681x10^{-8} Ω.m. Control parameters; P= 7.6 kPa, v=15 mm/s and t=15 s.*

4.2.3 Thickness measurement by a profilometer

The thickness of the stamp/transfer printed aluminium tracks was measured by using a profilometer. As this instrument is one of the destructive techniques that was used in this research, its measurements were planned to be performed as the last investigation for the printed aluminium tracks. Good results were obtained regarding the thickness of the patterned materials. Oxygen plasma-treated (15 min) glass substrates with transfer printed aluminium tracks from the PDMS stamps with defined tracks of thicknesses between 200 and 250 nm, and widths ranging from 300-600 µm were subjected to evaluation using this equipment and the thicknesses of the printed aluminium tracks were observed. As described earlier, the amount of the pressure of the PDMS stamp on the substrate should be monitored, as at very low scales such as nanometres, the pressure should be precisely controlled to avoid the failure of the transfer of the patterns from stamps to the substrates because of low pressure or damage to the transferred patterns if the pressure is too high. Therefore, the desired control parameters

discussed in the previous section were employed. The profilometer observations, however, as can be seen in graphs 4.24 and 4.25, show results of measuring the thicknesses of the stamp printed aluminium on the treated glass which are 200-250 nm and these values are similar to the evaporated aluminium thickness on the stamp before carrying out the stamp printing. It can be concluded that the stamping/transfer printing machine is capable of patterning aluminium tracks and patterns.

To be noted; in all presented graphs, the width of tracks is approximately 300 and 600 µm and thickness 200-250 nm, more graphs can be found in the appendix (figure A5 and A6).

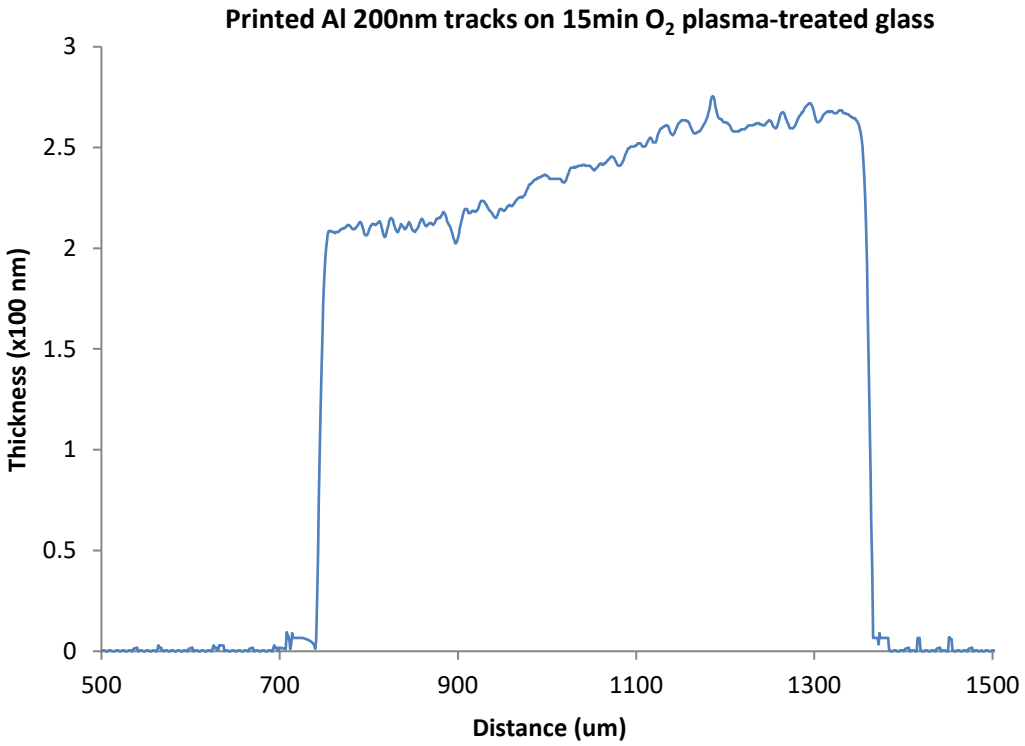

Figure 4.24: *a profilometer measurement of stamp printed aluminium (width 600 µm) on 15-minute O_2 plasma treated glass showing thickness of 200-250 nm.*

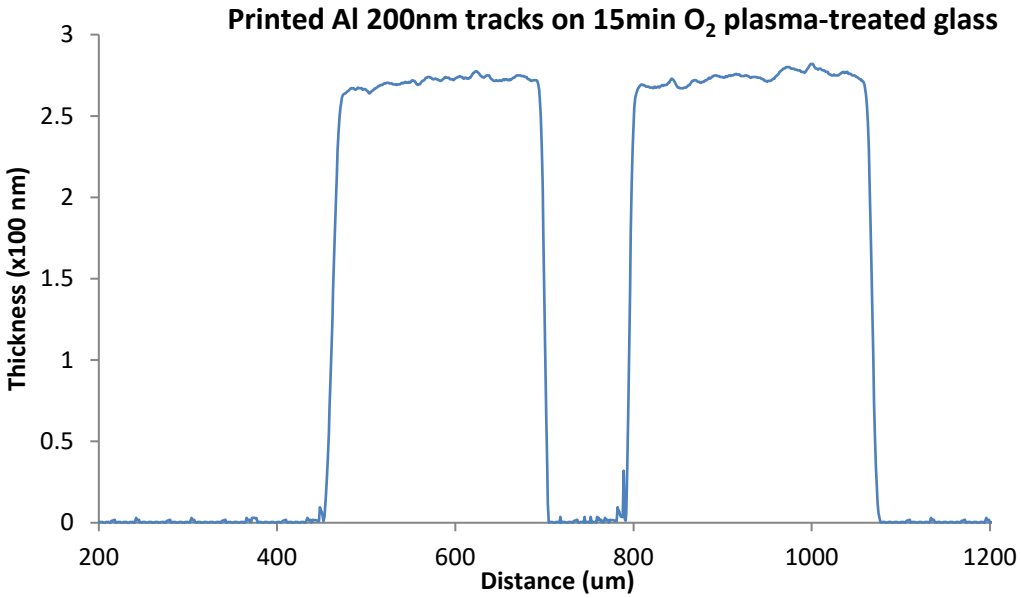

Figure 4.25: *a profilometer measurement of stamp printed aluminium (width 300 µm) on 15-minute O_2 plasma treated glass showing thickness of approximately 250 nm.*

4.2.4 Adhesion (tape) test

A quick adhesion test to evaluate the strength of the adhesion of the transferred aluminium patterns on the oxygen plasma-treated (15 min) glass substrates. A scotch tape test was performed on some of the printed tracks, and the transfer printed metal suffered some damages and peeled off in some areas from the glass substrate when an external mechanical force applied to it as can be noticed in figure 4.26 b. This means that the printed Al did not completely adhere well on the glass, however, more investigations are required to verify this, but could not be performed due to time limitations.

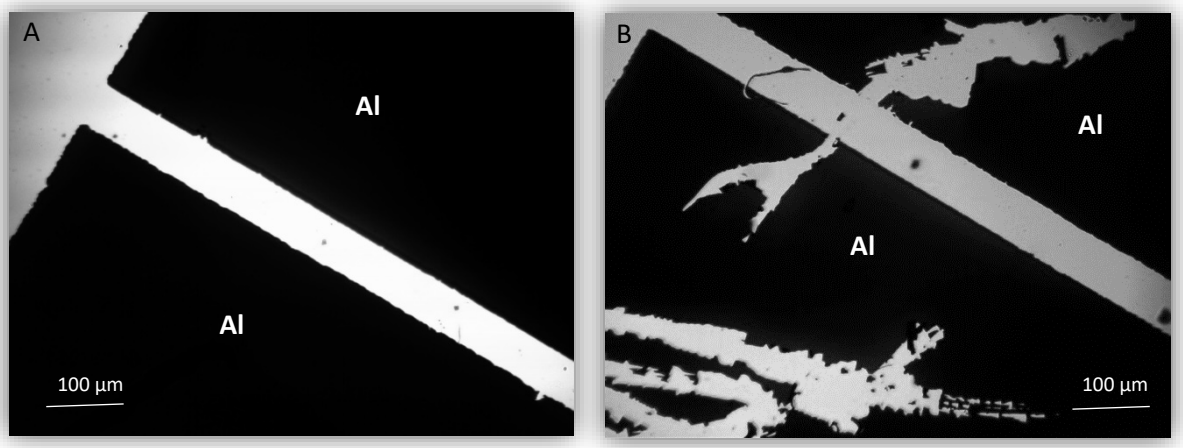

Figure 4.26: *optical microscope images show the stamp printed (Al) on glass a) before the adhesion test and b) after the adhesion test.*

4.3 Conclusion

As a result of the lack in developing a simple, easy to use, cheap, compact automated stamp printing machine, it has been the motivation for utilising such a system which consists of cost-effective components. The control on this stamp printing machine achieved. Test of the machine showed promising results of pattering micro and nanoscale aluminium tracks (thickness of 50, 150, 200, 250 and 300 nm) on oxygen plasma treated glass substrates with basic manipulation and control of the stamping pressure of the PDMS stamp on the glass substrate, the speed of the actuator which results in the control of the velocity of the peeling off process of the PDMS stamps and the contact time between the patterned PDMS stamp and the substrate. It was concluded that a pressure value of 7-7.6 kPa, an actuator speed of 10-15 mm/s and contact time of 10-15 s are the range of desired control parameters to achieve a good transfer of aluminium tracks from the coated PDMS stamps to O_2 plasma-treated glass slides. More inorganic materials such as copper are also to be investigated by the machine in future work. Some distortions and deformations in some of the deposited aluminium tracks were observed and they are highly likely to be due to the amount of the pressure applied on the PDMS stamp, therefore, pressure (force) sensors are to be implemented in the machine to ensure optimum force is applied on the stamp for each specific pattern to gain a high resolution printing free of defects.

Chapter 5: Inkjet Printing

Although the previously discussed stamp printing technique was able to transfer nanoscale and microscale patterns, it was unable to do so with solution-based materials (inks). Therefore, an inexpensive simple solution-based technique was required. This chapter will provide an overview about a non-contact printing technique, the inkjet printing technology; background, working principle of some inkjet printing techniques, classifications and the factors and parameters that affect the quality of the inkjet-printed materials.

5.1 Introduction

The era of inkjet printing technology is believed to have started when Savart demonstrated in 1833 that the fluid dynamics laws control the jets of the liquid that break into a series of drops [109]. Two decades later, J Plateau related the drop size and the diameter of the jet [110]. However, Lord Rayleigh [111] was the founder of the basics of the current inkjet printing technology when he was carrying out some research on the instability of jets of fluids [112], and then in 1951 when Rayleigh's findings were translated into a practical inkjet machine by R. Elmqvist of Siemens-Elema in Sweden [113]. In 1858, William Thomson (later Lord Kelvin) was able to manufacture the first similar inkjet printing device (a recording device called the Siphon recorder), which was used to record telegraph messages by means of electrostatic forces. At Stanford University in the US, Dr Sweet introduced a continuous inkjet technology in 1965 [114] which was the first of its kind that is based on regular applied pressure on the ink to obtain a stream of uniform and separated (spaced) droplets. Approximately 10 years later, IBM adopted this idea when they commercialised the 4640 (later known as 6640) printer in 1976. Another different jetting technology, drop-on-demand (DOD), appeared in 1977 when Siemens developed the work done by S. I. Zoltan [115] to introduce a piezoelectric printer (PT80) with a twelve-jet printhead that is able to generate fast and reliable printouts. Finally, Mark Naiman of the Sperry Rand Corporation patented his work in 1965 [116] which was about the thermal inkjet printing. However, Canon and Hewlett-Packard (HP) invented two inkjet printers, they described them as; "Bubble jet" and "Think jet", respectively, and they claim that those are the first to be developed of the thermal inkjet technology.

Inkjet printing is one of the Additive Manufacturing [117] techniques which forms, controls and deposits tiny droplets of inks onto the substrate. The printing technology is undoubtedly able to revolutionise the electronic devices manufacture industry, which includes materials selection, design, fabrication steps and device configuration/structure. Three main components

are involved in this technology: ink, printhead (cartridge) and substrate. The appropriate functionality/properties of these components such as ink properties, right driving voltage waveform (pulse amplitude/width) and a suitable substrate will ensure a high quality printed pattern and a reliable and a reproducible process. The factors driving this continuous interest are mainly attributed to digital and additive patterning, its efficiency in material use, large area capability, low cost, compatibility with rigid/flexible substrates. Indeed, in the last years, the inkjet printing deposition method has been increasingly and extensively researched as an alternative deposition and fabrication technique to the conventional subtractive techniques including lithography and etching. A large interest is currently undergoing to fabricate both organic [118,119] and inorganic materials [118,120,121] on flexible and rigid substrates. Additionally, the 3D inkjet printing (IJP) technology is considered to be one of the most promising technologies to obtain environmentally friendly electronic devices with zero harmful radiation, very low heat generation and inexpensive production costs. Subsequently, plenty of materials and electronic devices, including metal nanoparticle inks [122], polymers [123], resistors for memory applications [124], organic light emitting diodes (OLEDs) [125] and printed circuit boards [126] have been completely or partially inkjet printed. To summarise, the simplicity and high throughput of inkjet printing technique in depositing a large number of materials such as metals and polymers have had a significant impact on developing and manufacturing flexible electronic devices including thin film transistors, sensors and memory devices, a full description of that can be found here [127]. A large number of structures and configurations such as lines, tracks, coatings and arrays have been inkjet printed due to the fact that this deposition technique is compatible with polymers, nanoparticles and functional inks on a wide range of substrates. Moreover, the precise control of the volume of the printed material and the drop position (location) because of the high repeatability of the drop ejection mechanism make it possible to anticipate the dimensions of the deposited patterns, which in

many cases, are complex in a single pass deposition without the need for post-treatment processes [128]. The ink properties, on the other hand, play a major role in controlling the jetting behaviour and the drop speed and volume (drop formation), drop impact and the spreading (wetting) process on the substrates and the final morphology of the deposited material [129]. Hence, the ink formulation, Newtonian and non-Newtonian properties of the fluid, and the main parameters including the surface tension, the contact angle, pH, viscosity, solvent evaporation rate and density have to be taken into consideration and monitored to ensure high quality printing and adhesion between the droplets and the substrate.

5.2 Classifications of inkjet printing

With regards to the working principle of the printheads, the inkjet printing technology can be divided into two main categories along with few others as described in figure 5.1. The following section provides a review of the major inkjet printing techniques.

5.2.1 Continuous inkjet

This type of inkjet printing is commonly employed to deposit a wide range of information including texts, names and logos of different products and packages in industry. This inkjet technology is known as ‘continuous’ due to the fact that the drops are created continuously. Briefly, this high speed and non-contact printing technique working principle can be defined as a continuous series of ink droplets are ejected out of a nozzle due to pressure at high frequencies (between 50KHz-175KHZ).

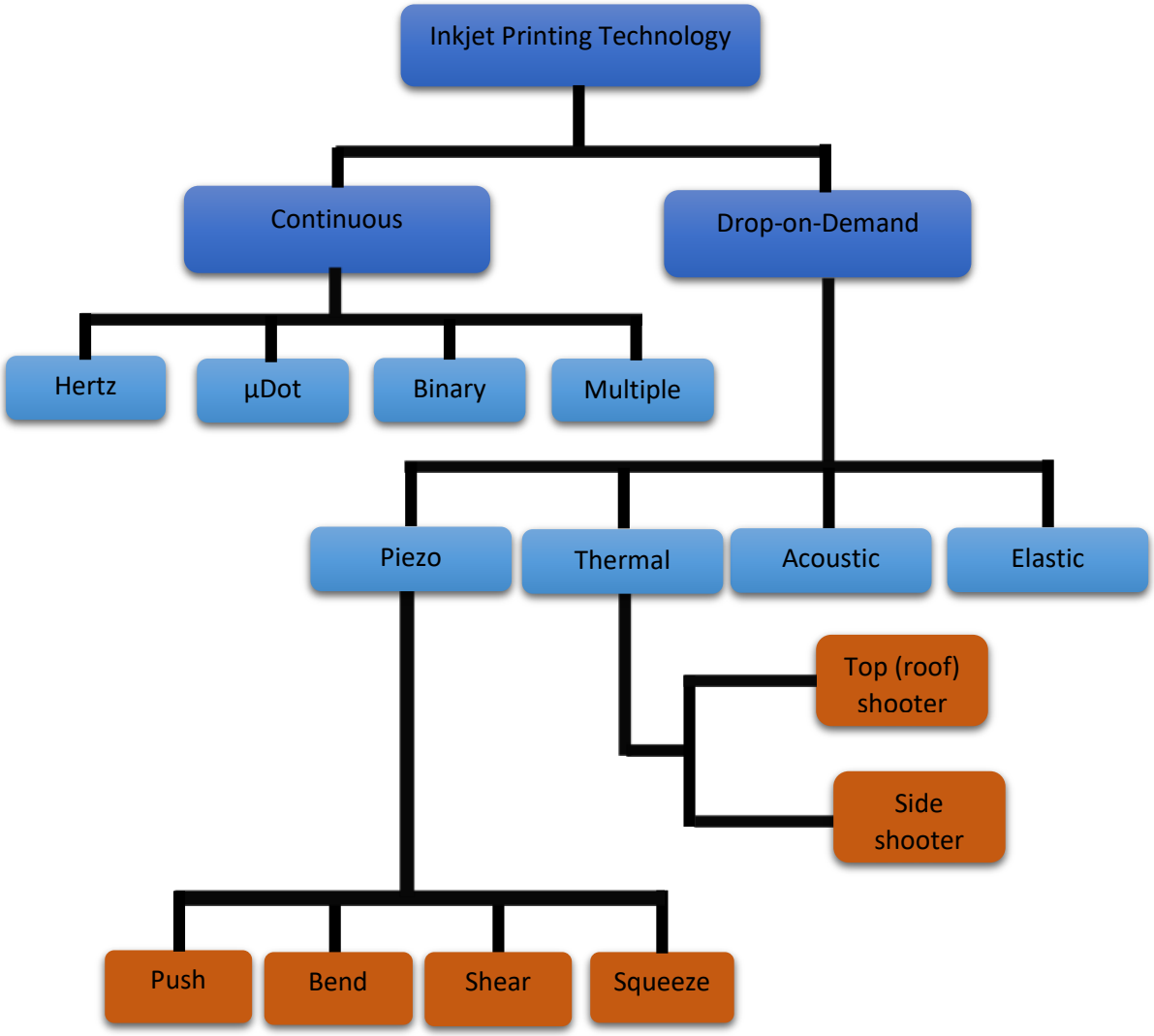

***Figure 5.1**: a block diagram presents main classifications of inkjet printing technology based on the working process of the printheads.*

A vibration source produces acoustic waves that break the ink into drops at regular periods (intervals). Smaller droplets are formed from the ejected ink at a specific wavelength, hence, tiny deviations (perturbations) start to develop. Although, under ordinary circumstances, the anticipation of the size of the tiny droplets and the discontinuity (breakup) points of the ejected jet is not easy and seems to be impossible, modifying the frequency of the pressure waves can result in a uniform stream of droplets. Weber and Lord Rayleigh [130] mathematically related

the velocity of the ejected jet, the diameter of the nozzle and modulation frequency. Figure 5.2 exhibits a simple explanation of the working principle of continuous inkjet printing technology. Charging electrodes, which are responsible for charging the droplets (charging field), and electrostatic filed deflectors (plates), which are used to direct the droplets (deflection field), are employed for the selection of particular droplets from the uniformed jet of the drops. For this reason, conductive (electrically) inks are widely used in this method. In the charging electrode stage, the droplets, in the presence of the electrostatic charging field, become electrostatically charged and break up. If the charging electrode has a positive potential, the electrons gather closer to the positive potential source and when the droplet breaks up, the electrons get trapped and as a result, the droplet becomes negatively charged (which is proportional to the potential applied to the charging electrode). In the end, higher charged droplets are directed by the electrostatic deflection field to the desired position on the printed surfaces (substrates) while uncharged (or less charged) droplets are redirected and collected to be reused. The potential across the reflectors (plates) and the distance between them determine the strength of the reflector's electric field which determines the degree of the droplet deflection. The droplet deflection amount can also be predicted from the droplet exposure period to the electric field, the droplet speed and the length of the plates. The exposure of the recycled ink to the ambient atmosphere which causes ink degradation and the complexity of this process are some of the main drawbacks that play an important role to make it not broadly employed to print functional materials.

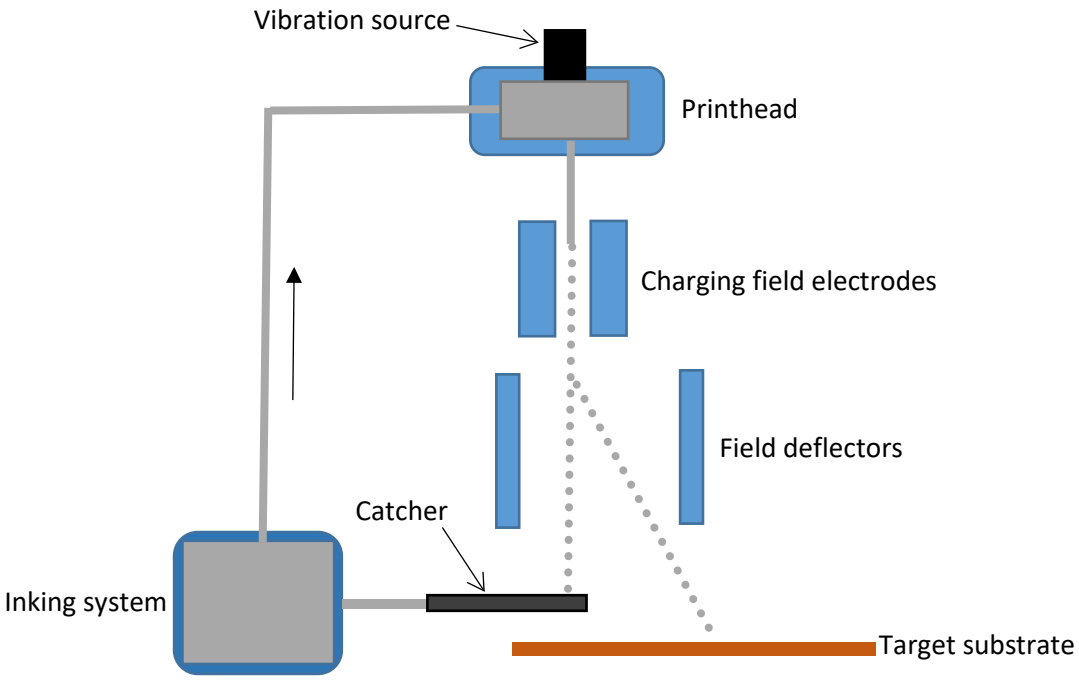

Figure 5.2*: a simple explanation of the working principle of continuous inkjet printing technology.*

5.2.2 Drop-on-Demand

As the name suggests, this printing technology is generating droplets only when required. The droplet position control, the design of the system and the ink flexibility along with its direct jetting (dispensing) process (no need to recirculate the ink) make the technique more favourable when high-resolution printing is required. This technology has many types depending on how the droplets are generated, however, here we discuss in details only the ones that were used to carry out the research and these are Thermal and Piezoelectric inkjet printing.

5.2.2.1 Thermal Inkjet Printing

This printing technology is widely used in desktop printers and its working principle based on heating thin films, resistive elements usually built in the ink reservoir near the nozzles, in which when heated by electric current creates bubbles in the ink due to the ink vapourisation as presented in figure 5.3. The ink is insulated from the heat by these bubbles which they cause

pressure inside the chamber and as they start to collapse when the heating element is turned off, the ink motion towards the collapsed bubbles due to the decrease (change) in volume (volume contraction). All of this generates transient pressure wave force ink droplets to be ejected out of the nozzle. The momentum and velocity of propelling the droplets into the substrate are acquired from the ink acceleration and the bubbles creation and collapsing. The displacements of ejected droplets are refilled (by capillary action) again with ink in preparation for next droplet formation (deposition). The whole cycle takes place in roughly 10µs. The ink degeneration and degradation (functional properties loss) due to the thermal process make this technique not so popular when printing functional materials.

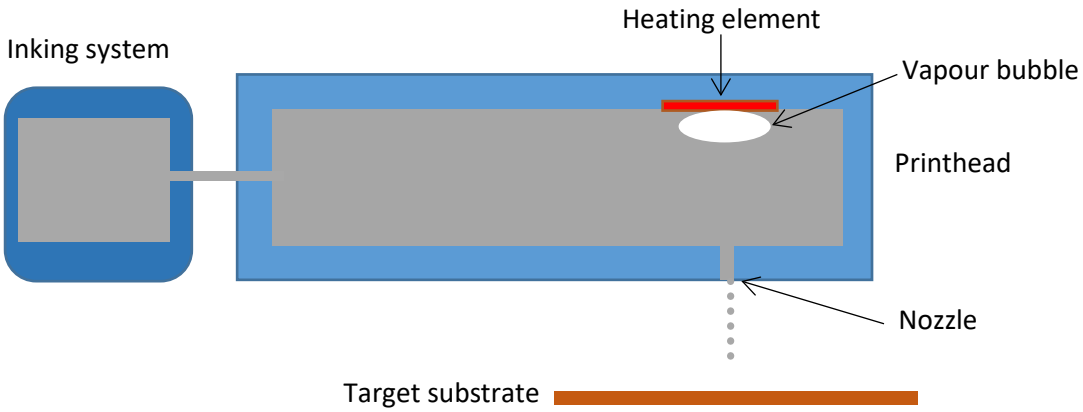

Figure 5.3: *a simplified diagram of the working principle of thermal inkjet printing technology.*

5.2.2.2 Piezoelectric Inkjet Printing

In this printing technology, a piezoelectric element is used to generate the droplets [131]. When an electric energy is applied to the piezoelectric element, a mechanical deformation (expansion or contraction) in its shape occurs and this causes a change in the ink volume in the chamber which increases the pressure that ejects the droplet from the nozzle. Acoustic resonances might also cause oscillations in the ink which create droplets by breaking the ink stream. This inkjet

printing is usually divided into four modes based on the piezoelectric deformation mode used to form the droplet [132].

a) **Push (bump)-mode piezoelectric inkjet printing:** S Howkins (Exxon Company) patented [133] this technology. Although Brother, Hitachi and Epson are all developing the technique, Trident is the main leading company optimising push-mode printheads. Figure 5.4, shows the mode`s design. After applying electric voltage to the piezoelectric material, it is pushed towards the ink chamber wall to cause the ejection of the droplet. A thin layer (membrane) is mounted between the piezoelectric element and the ink to avoid any interaction.

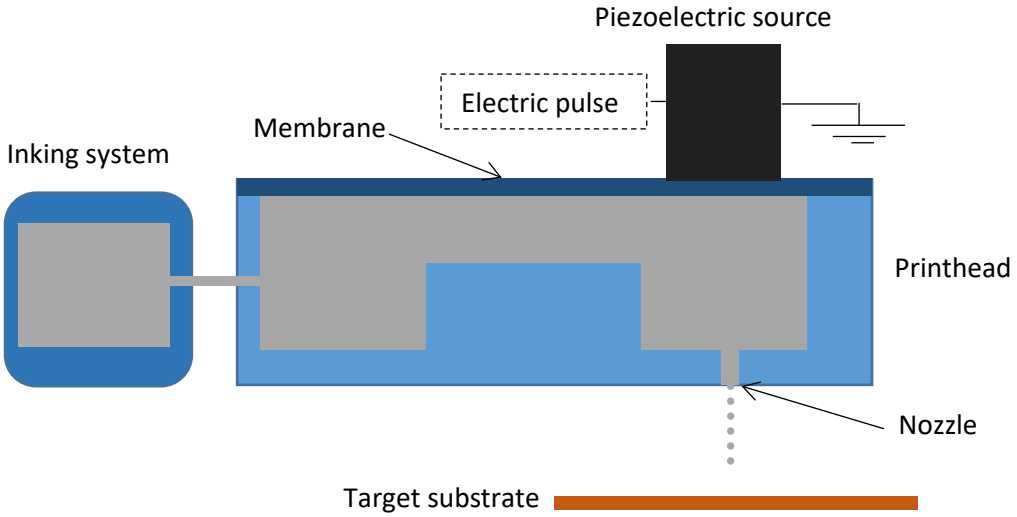

***Figure 5.4**: a push mode piezoelectric inkjet printing design.*

b) **Bend-mode piezoelectric inkjet printing:** These printheads were patented by Stemme at Chalmers University [134] and Kyser and Sears (Silonics company) [135]. Despite the fact that Xerox, Tektronix and Kyocera are among the companies which have been selling these printheads, Epson is one of the main companies that is developing them. As illustrated in figure 5.5, the inner side of the ink chamber is constructed of the

piezoelectric element bonded with a thin layer of a diaphragm while the outer side has a conductive diaphragm. When potential pulses are applied, the diaphragms are bent and this induces pressure in the ink chamber causing the formation of droplets.

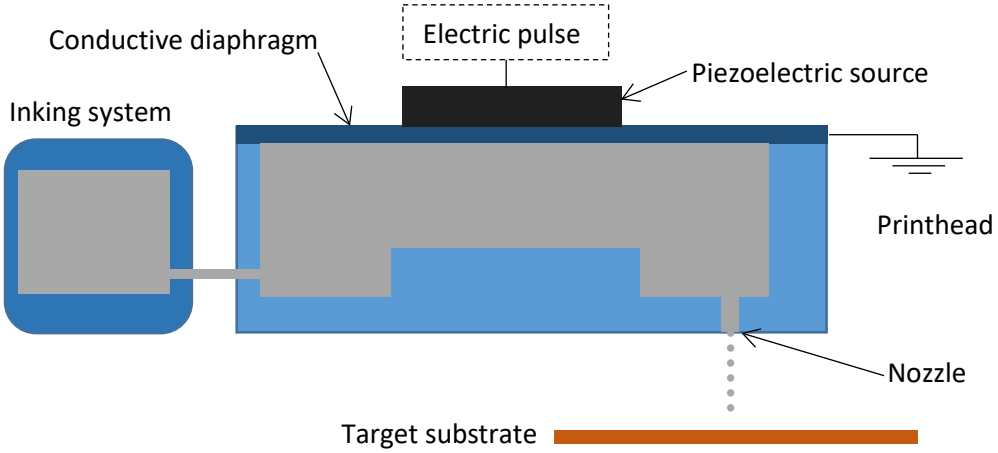

Figure 5.5: *a bend mode piezoelectric inkjet printing design.*

c) **Shear-mode piezoelectric inkjet printing:** This mode was developed by K Fishbeck and A Wright of Xerox Corporation [136], Fujifilm Dimatrix and Xaar are the developers of shear mode printheads. The piezo element shear deformation changes the shape of the top part (half) of the chamber (channel) as shown in figure 5.6, and this causes another deformation in the bottom part (half) and all this results in inversed (V) shape chamber (channel). The deformation and chamber shape change create the ejection of the droplet.

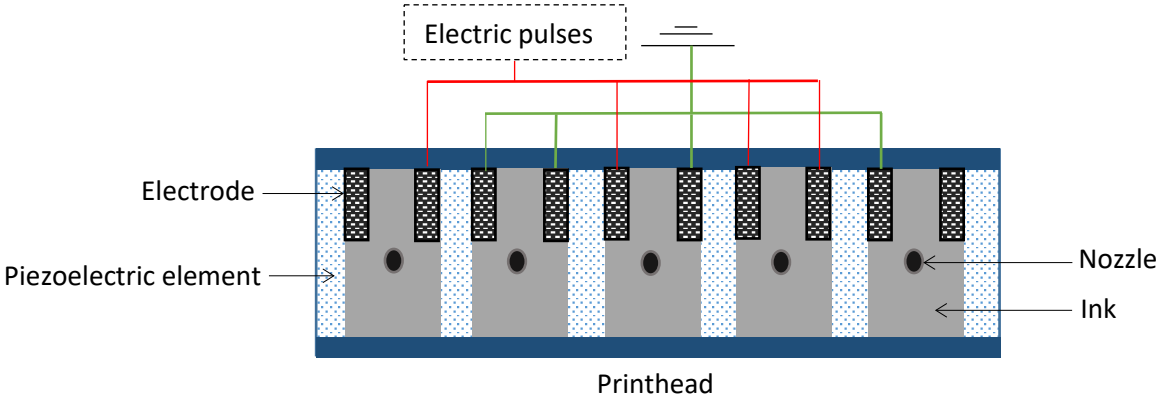

Figure 5.6: *a shear mode piezoelectric inkjet printing design.*

d) Squeeze-mode piezoelectric inkjet printing: Zoltan (Clevite Company) introduced this mode in 1972 [137]. The electrical excitation to piezoelectric elements makes them to deform which results in ink squeezing inside the chamber and being ejected out of the nozzle as droplets as seen in figure 5.7.

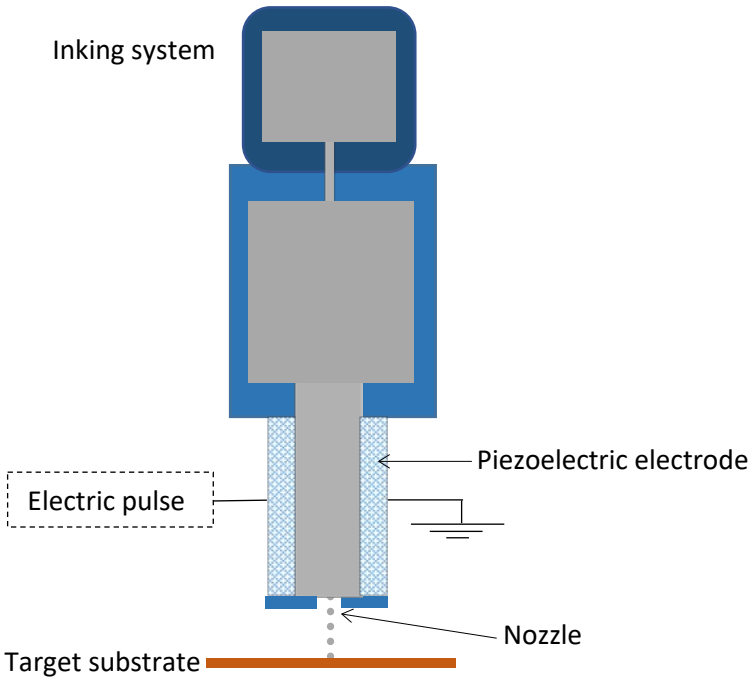

Figure 5.7: *a squeeze mode piezoelectric inkjet printing design.*

Multi nozzle print heads have also been used where different techniques are employed. They are higher throughput compared to the single ones and more capable of printing on large areas as several droplets can be deposited parallelly from various nozzles. Nozzle clogging due to ink particles blockage, complications in the precise control of all nozzles and the ink property limitations, on the other hand, are some the issues that these nozzles face.

In general, although the thermal inkjet printheads were more commonly used due to lower manufacturing costs, the piezoelectric printheads are more favoured nowadays, especially, after being continuously developed which led to low production costs, its capability to pattern wider range of materials, and the requirement of relatively high temperature to create bubbles in the thermal printing method, which limits the range of inks, for example, biomedical inks and inks with high vapour pressure are highly susceptible to degradation with high temperature. Moreover, the piezoelectric printheads function under smaller pressures that assist to keep a stable meniscus after the formation and ejection of the droplet and this prolongs the life of the heads. As a result, the piezoelectric inkjet printheads are used in almost all industrial inkjet printing technologies including Microfab Technologies, Xennia and Konika Minolta IJ Technologies.

For a detailed description of printhead printing technology, one can look at [138].

5.2 Printing factors and parameters

There are some important parameters and factors that determine the quality of the printing and these include: the ink (physical and chemical properties), the substrate (physical and chemical properties) and the printhead (shape/diameter of the nozzle, waveform width and amplitude). The next sections will discuss some of these parameters and factors.

5.2.1 The ink

One of the major challenges when employing the inkjet printing technology in depositing the functional materials is a proper ink formulation [139]. In addition to the basic and essential requirements for conventional inkjet printing inks, more attention needs to be paid when formulating metal-based inkjet printing inks as the main purpose of the deposition is to obtain electrically conductive patterns with good resolution and adhesion properties to the substrates. The main role of the ink is to deposit functional materials onto a substrate and as it plays a major role in controlling the processes during the inkjet printing such as the ejection of the droplets, jetting stability, the wetting of the droplets and the interaction between the droplets and the substrate, formulating the ink is of great interest and importance to meet the essential requirements for a successful high quality inkjet printing. Therefore, the physical and chemical properties of the ink including the surface tension, the viscosity, the contact angle, the pH, the solvent evaporation rate, the density and the droplet behaviour (volume and speed) should be taken into consideration in the ink formulation process along with the effect of each property on the ink's overall performance from storing the ink outside and inside the cartridges, through jetting out of the printheads and the interactions with the substrate to healthy and environmental risks [140]. To sum up, a good inkjet printing ink should have/be:

- Compatible with all materials involved in the printing process including the printheads and the substrates.
- Controlled and stable physical and chemical properties.
- Soluble additives during the ink's lifetime and good evaporation rate during and after printing.

5.2.1.1 Main ink properties

The physical and chemical properties of the ink play a major role in the determination of important factors such as the jetting behaviour, droplet speed and formation and all these factors influence the quality of the printing.

a) The stability of the ink

A good ink should reserve its properties for a long time. The particle zeta potential and the dielectric constants of the dispersed-particle solutions are some of the parameters that significantly influence the ink's stability. Polymeric dispersants including Disperbyk and Tego Dispers are added to the ink (aqueous and non-aqueous) to enhance its stability. One of the most common issues, which affect the ink stability, is the aggregation (flocculation) of dispersed particles (pigments) due to Van Der Walls forces, which cause the particles to aggregate when approaching each other [139]. Some techniques used to tackle this challenge including the adsorption of the particles` surfaces with a material that has a positive or negative electrical charge which leads to electrostatic repulsion when the particles approach each other and protects the particles from aggregation (agglomeration). This type of stabilisation is called electrostatic stabilisation. A similar mechanism is also used to achieve the stability of organic solutions is steric stabilisation where the particles are surrounded by an adsorbed coating of sterically bulky molecules including nonionic polymers [141].

A good indication of the stability of the ink can be anticipated by the pH of the ink and its electrolytes (if existed). The electrical repulsion, mentioned above, usually depends on the pH of the ink whereas the electrolytes may cause flocculation of the charged particles during long storage periods. For this reason, the electrolyte concentration is advisable to be so low and the pH is high.

Inks that contain pigments are less stable than the ones that have dyes, as the dye inks are thermodynamically stable because all ingredients dissolved in one solvent whereas the pigment-containing inks have only a kinetic stability.

b) The surface tension

The surface tension of the ink plays a major role in the formation of the droplets and their wetting and spreading onto the substrate. It is the force controlling the droplet shape and responsible for the droplet separation from the printhead. When the surface tension of an ink increases, the driving force required to a specific droplet speed increases. Contrarily, lower surface tensions can cause air suctions in high-speed droplets. Surfactants such as siloxanes and alkoxylated polyalcohols are added to the ink to modify its surface tension. Significant care should be taken when adding these surfactants as tiny changes in their concentration might well lead to a huge alternation in the surface tension of the ink. For this reason, checking the surface tension of the stored ink before printing is so important as surfactants' concentration (if surfactants added) might have changed due to their adsorption on the particles or the walls of the ink container [139]. Values of surface tensions for piezo and thermal printheads are usually different for each printer and printing process.

It is worth mentioning that if no surfactants are added and the surface tension of the ink is only from the solvent medium, the value of the surface tension remains constant (static surface tension). However, when adding surfactants, both static and dynamic surface tensions are taken into consideration. There are many methods to measure the surface tension of an ink including DuNouy ring (for static surface tension) and The Maximum Bubble Pressure Method (dynamic surface tension) [142]. A tensiometer (Torsion Balance) based on the DuNouy ring technique was used during the research.

c) The viscosity

This ink property is one of the most crucial factors that affects the ink's stability, jettability and droplet formation. To understand it, ink can be imagined to be sheared between a bottom fixed plate and a top moving plate (with constant velocity (V)), the distance between the two plates being (h). In thermodynamics, this type of flow is called Couette Flow, when the ink`s flow speed decreases to zero, a shear flow of a velocity of $\upsilon = V(\frac{y}{h})$ occurs. A laminar flow (smooth-and-parallel layers that have different flowing velocities) takes place and the ink speed ranges from max (V) at the top moving plate to the lowest value 'zero' at the stationary plate. As each layer flows faster than the one underneath it, a force due to the layers' friction is created; the direction of this force is opposite to the layers' motion. In order to maintain a contact velocity for the moving plate, an external tangential force (F) is applied to the ink, and this force is directly proportional to the ink's velocity (υ) and the area of each plate (A) and inversely proportional to the distance between the plates (h), this can be shown in this equation:

$$F=\eta.A.\frac{\upsilon}{h} \quad \text{.....5.1}$$

Where η is the viscosity of the ink which represents the physicochemical nature of the ink.

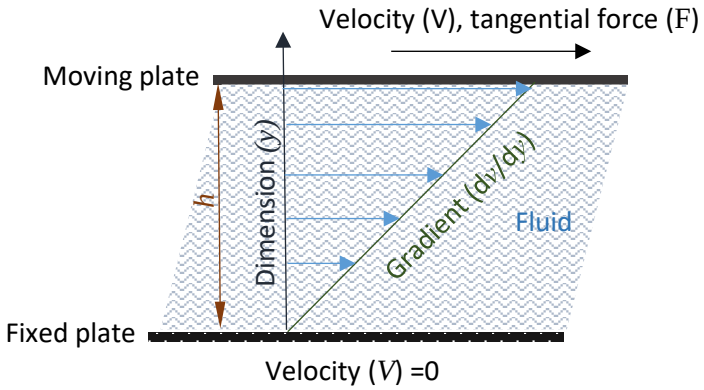

Figure 5.8: *Couette Flow between two parallel plates; a moving plate and a fixed plate.*

However, the ratios of $(\frac{\upsilon}{h})$ and $(\frac{F}{A})$ are called the shear rate ($\dot{\gamma}$) and shear stress (τ) respectively. The shear stress is responsible for ink flowing in a specific direction and pattern, and the alternation of the deformation of the ink per time is defined as the shear rate. Newton's law of viscosity (shear stress= η. shear rate) expresses the relationship between the shear stress and shear rate where the proportionality coefficient (η) is known as the viscosity coefficient (called the viscosity) which determines and evaluates the resistance of the ink towards deformation and change. In the SI units, the unit of the viscosity is ($N.s/m^2$) while in the CGS system is ($dyne.s/cm^2$), the latter is known as a poise (P). Some values of viscosities of different materials can be seen in table [5.1].

Table 5.1: some values of viscosities of different materials.

Material at 25°C	***Viscosity (mPa.s, cP)***
Water	0.894-1
Blood	3-4
Olive oil	80-100
Honey	2000-10000
Ethanol	1-6
Ethylene glycol	16.9

A flow curve, which identifies the ink's flow behaviour, is basically a curve that shows the relationship (correlation) between the shear stress (τ) and shear rate ($\dot{\gamma}$). A viscosity curve, on the other hand, is relating the viscosity (η) and the shear rate ($\dot{\gamma}$). In Newtonian inks, the flow of the ink follows shear stress and shear rate, where a linear relationship and constant ratio exist, hence, the viscosity of the ink depends only on the pressure, the temperature and the chemical composition of the ink. In addition, the forces applied to the Newtonian ink have no effect on the viscosity. However, in non-Newtonian inks, the nonlinear relationship between the shear stress and shear rate reflects on the viscosity of the ink, therefore, as well as the previous factors (the pressure, the temperature and the chemical nature of the ink) the applied forces influence the viscosity. Water and oil are Newtonian fluids, and pseudoplastic (shear thinning) fluids and dilatant (shear thickening) fluids are some kinds of non-Newtonian fluids.

To sum up, Newtonian inks have a fixed viscosity over a broad range of shear stresses and rates while non-Newtonian fluids have different changeable viscosities with respect to various shear rates and stresses and that is why the Newtonian inks are the most commonly used ones for inkjet printing.

The viscosity of the ink can significantly influence the jetting stability of the ink and it is modified by using several additives such as ethylene glycol. The inkjet ink viscosity should be within a certain range to achieve good inkjet-printed patterns. Inks with high viscosity require high driving voltage to create the pressure to form a droplet while very low viscous inks can result in satellite droplets. The piezoelectric printheads work well with inks that have a viscosity between 4-20 cP, while the viscosity for the thermal ones should be lower than 3 cP.

The instrument used in this work to measure the viscosity of fluids is called viscometer.

The density of the ink has an effect on the jetting process. More energy is required for the jetting of droplets of inks as the density increases due to the increase in the kinetic energy of the ink.

The concentration of the pigments (particles) in the ink, conductivity and dielectric property of the ink are of great importance as well. The pigment concentration in most of the conventional inks is less than 10% w/w while in unconventional inks including conductive inks can be more than 50% w/w. However, although the more particles, the more expectations to achieve conductive patterns, aggregation may be the main issue that needs to be addressed as the particles might be in contact which can lead to nozzle clogging. Filtration tests are highly recommended to evaluate the ink and prevent ink aggregation. For nonconductive inks, charging agents are usually added, especially, for the printers that work on the droplet deflection by electric fields such as continuous inkjet printers.

The focus here will be on the conductive inks which include: nanoparticle inks (colloidal suspensions of nanoparticles in water or organic solvent such as colloidal nanoparticles silver used in this research study) and conducting polymer inks that include polymers which have conjugated pi-electron system in them to achieve conductivity such as PEDOT:PSS ink (used in this work). Other kinds of conductive inks including organometallic inks (metal-organic compounds in solvents such as silver organic compound in toluene), carbon nanotubes, graphene oxide inks were briefly investigated/studied.

5.2.1.1 Main components of an ink

The basic components of the ink can be divided into:

a) **The functional materials**: These are the main ingredients of the ink and they can be metal, metalorganic or polymer precursors in the state of molecules, nanowires, nanoparticles.

b) **The carrier solvents**: These solvents are usually responsible for the ink polarity and boiling point of the ink which is so crucial when curing the ink. Moreover, they identify the nature of the ink which can be water-based (water is the main ingredient), organic (organic solvent dominates the composition of the ink), crosslinks monomers and reactive solvents like UV inks (polymerisation reaction might take place after triggering the ink). The carriers can also affect the surface tension, viscosity and overall stability of the ink and its components.

c) **The additives**: These can include a lot of materials such as surfactants, humectants, dispersants, binders (resins), wetting modifiers, rheological modifiers, photo-initiator, bactericides and fungicides. Each one is added to achieve a specific property for a certain function. They are involved in the preparation of the ink to modify some of its properties. For instance, surfactants such as siloxanes are used to modify the surface

tension of the ink. Furthermore, to control the ink evaporation and help limiting the coffee-ring effect, humectants like glycols and alcohols are added to the ink. The dispersants (polymers such as styrene-acrylic acid-methacrylic acid copolymer), on the other hand, are used to protect the ink from agglomeration and precipitation (condensation). Another important additive to the ink is the binder (polymers such as acrylic resin and vinyl chloride) which works as an adhesive to help transferring the ink to the substrate, the resins can also be used as a protector (resistance against abrasion) and a viscosity modifier. The wetting and rheology modifiers are added to control the surface tension and viscosity of the ink to improve the wetting on the substrate and jetting stability. Finally, biocides and fungicides are usually added to avoid the growth of fungus and bacteria in some inks.

Defoamers can also be added to the ink to resolve issues created in inks due to the presence of bubbles [143].

5.2.2 The substrate

The physical and chemical properties of the surface of a substrate such as the surface energy, planarity, roughness and homogeneity play a major role when a droplet of an ink impacts on it. Furthermore, the interactions between the ink and the substrate are controlled by the surface energy of the substrate and the surface tension of the ink, this interaction strongly influences the resolution of the printed layers and the ink spreading. The wettability and adhesion of the final inkjet printed material are determined by the properties of both the ink and substrate. Moreover, the surface energy (wettability) of non-porous, smooth substrates along with the surface tension of the ink are the main factors that determine the final diameter of the ejected droplets. Porous substrates including paper, on the other hand, have other properties that effects the print quality such as the influence of the capillary forces created by the porosity of the

substrate on the ink, causing adsorption or absorption of the ink and that results in separating the functional materials from the ink's solvent. The interaction between the droplet and the surface of the substrate is complex and governed by many forces including gravitational, inertial and capillary forces. For good inkjet printing, the surface tension of an ink is recommended to be at least 10-15 points lower than the substrate's surface energy [144]. The surface treatment (physical or chemical) of the substrate is sometimes required to optimise the printability of the substrate by many techniques such as plasma etching for cleaning the substrate and chemical functionalisation for tuning the surface energy of the substrate including its hydrophobic/hydrophilic behavior.

5.2.3 The inkjet printing droplet impact

The properties of ink and the surface of a substrate significantly influence the ink's droplets when impacting the substrate's surface and determine their behaviour and final shape. Surface tension, contact angle, viscosity and density are among the main properties of the ink that have the most effect and the different types of surfaces including hydrophilic, hydrophobic, smooth, rough, homogeneous and inhomogeneous can result in six sequences when a droplet impacts a dry surface [145]. These possible sequences of the ink morphologies on a dry substrate include deposition, prompt splash, corona splash, receding breakup, partial rebound and complete rebound.

The size of the droplet and its impact speed also affect the droplet behaviour. In most cases, the ink droplets wetting of dry and smooth substrates can undergo five phases:

1. Kinematic.
2. Spreading.
3. Relaxation/oscillation.

4. Wetting.

5. Equilibrium.

In the kinematic phase, when the droplet collides the substrate`s surface, the shape of a large amount of the area of the droplet that is not contacting the surface does not change. As soon as the diameter of the droplet contacting the surface of the substrate is the same as the droplet diameter, the next phase takes place, the spreading phase. In this phase, the contact area expands and most of the initial kinetic energy of the droplet is largely consumed. As soon as the spreading reaches its maximum state, the oscillation or relaxation phase might occur depending on the properties of the surface of the substrate. Droplets that impact hydrophilic surfaces are usually experiencing initial oscillation then expanding due to the capillary effects before reaching the equilibrium phase. A hydrophobic surface, on the other hand, might make the droplet retract and reduce its contact line with the surface and can lead to a complete rebound when colliding against super-hydrophobic substrates.

5.2.4 Wetting and contact angle

It is known that as soon as a droplet of ink (liquid) is positioned on a surface of a solid substrate, it starts to spread till no forces are applied on it; equilibrium state, creating an angle with the solid surface, known as the contact angle (θ). The wettability (wetting process) of the droplet measurements and studies can be carried out by involving the contact angle that it makes with the solid surface of the substrate. The contact angle can be defined as the angle (at the intersection) between the liquid-solid interface line and the liquid-gas interface line. This angle expresses the wetting degree when the drop interacts with the solid surface. An indication of high wettability and good droplet spreading on the surface when the contact angle (CA) is less than 90^{o} as the droplet contact with the surface increases and it largely spreads on it. A complete spreading and wetting and the droplet becomes completely flat along with the surface when the

contact angle is 0º. However, larger contact angles (more than 90º) indicates low wettability and the droplet tends to bead up on the surface as the contact area between the droplet and the surface decreases and a compact droplet is formed, as seen in figure 5.9, where more details are also expressed such as the surface energy and hydrophobic/ hydrophilic surface of the substrate. Some factors and parameters such as certain equilibrium conditions, temperature, time, topography and dirty free surfaces should be taken into consideration when measuring the contact angle [146].

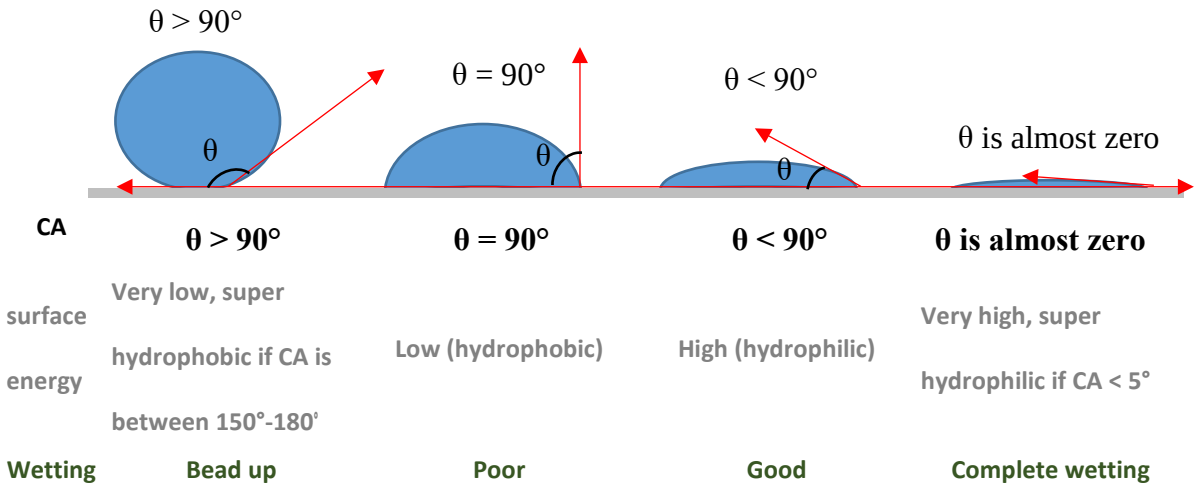

Figure 5.9: *the effect of contact angle and the free surface energy of the substrate on the wetting of a liquid of a solid substrate.*

The surface tension of the liquid determines the shape of the droplet. As shown in figure 5.10, neighbouring molecules inside the bulk of a pure fluid (liquid) are equally pulled to each other in all directions and a balanced force (net zero) is achieved. At the surface, on the other hand, the molecules could not have this balanced force as they do not have neighbouring molecules in every direction, therefore, neighbouring molecules under the surface pull the ones at the surface inwardly and internal pressure is created. Therefore, to achieve the lowest possible surface free energy, the fluid (liquid) contracts in the area at the surface by intermolecular

forces which are known as the surface tension. Although, as mentioned earlier, these forces, the surface tension forces of liquid, determine the droplet shape, external forces such as gravity might also influence the determination of the shape of the droplet.

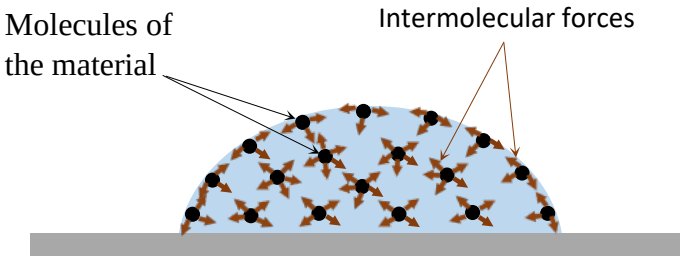

Figure 5.10: *how the surface tension determines the shape of a drop of a liquid.*

Thomas Young was studying the wetting process of liquids and developed an equation in 1805 relating the surface tensions of liquid-gas, solid-liquid and solid-gas by the mechanical equilibrium of a drop [147]. This equation is called Young`s equation and it provides a quick explanation and understanding about the wettability of known liquids on solids and can be used to obtain specific wetting properties by altering the surface tension/energy components, this equation can be expressed as:

$$\gamma_{sg} = \gamma_{sl} + \gamma_{lg}\cos(\theta) \quad \text{.....5.2}$$

Where, γ_{sg} is the solid-gas surface tension, γ_{sl} is the solid-liquid surface tension, γ_{lg} is the liquid-gas surface tension and (θ) is the contact angle between the liquid and the solid, as can be seen in figure 5.11.

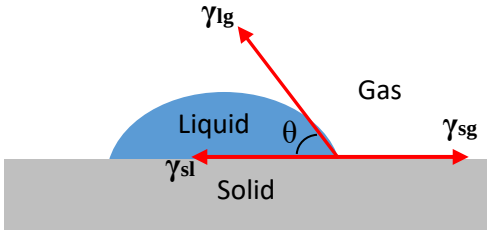

Figure 5.11: *a drop of liquid making a contact angle of (ϑ) and the surface tension components of the liquid, solid and gas.*

As been mentioned earlier, this simple equation can provide a lot of important information about the wettability of liquids on solid surfaces. However, some considerations and assumptions are usually required to be taken into consideration such as the properties of the solid surface which needs, in many cases, to be not only rigid but also smooth and homogenous and mechanical stability and equilibrium of the liquid where spreading is assumed to have occurred and the liquid have stabilised. Based on Young`s equation, each solid-liquid-gas interaction system has a unique defined contact angle which has, in fact, a maximum value called the advancing contact angle (θ_a) and a lowest limit known as the receding contact angle (θ_r). The advancing contact angle (θ_a) takes place just before the liquid contact line with the solid starts to move to cover the un-wetted areas, while receding contact angle (θ_r) refers to the opposite situation where the liquid-solid contact line retracts back leaving, what was initially wetted, uncovered. Therefore, the advancing contact angle (θ_a) is always larger than the receding contact angle (θ_r) [148]. The range between the advancing and receding contact angles is called the contact angle hysteresis [149]. Although no one has completely and thoroughly explained this hysteresis, the main factors that cause it.

5.2.5 The jettability of the ink

In the physical chemistry field, it is believed that the main forces that control and act on the ink in the inkjet printing are the gravity force ($\rho l^3 g$), viscous force ($\eta l \upsilon$), the surface tension force (γl) and the inertia force ($\rho l^2 \upsilon^2$), where (ρ) is the density, (l) is the characteristic length scale (typically the nozzle/droplet diameter), (g) is the gravitational acceleration, (η) is the ink`s viscosity, (υ) is the velocity of the jetting ink and (γ) is the surface tension of the ink [150].

Several dimensionless factors/numbers are relating these forces, these include; Reynolds number (Re), the Weber number (We) and the Ohnesorge number (Oh).

The Reynolds number (Re) expresses the ratio between inertial to viscous forces, it identifies the fluid`s flow regime, low Re means laminar flow while high Re means turbulent flow. It can be expressed as;

$$Re=\frac{va\rho}{\eta} \quad \text{.....5.2}$$

Where, (a) is a characteristic dimension of the nozzle (m). The Weber number (We) is described as the balance between the inertial forces and the capillary forces. The flow of the fluid can be characterised at the interface of two fluids by this number. It is also used to identify the mechanism of the droplet formation when the fluid interacts with the surroundings. This number can be expressed as;

$$We= \upsilon^2 a\rho / \gamma \quad \text{.....5.3}$$

Whereas the Ohnesorge number (Oh) provides a relationship between the viscous, inertial and surface tension forces as expressed in the following equation:

$$Oh=\frac{\sqrt{We}}{Re}=\frac{\eta}{\sqrt{a\rho\gamma}} \quad \text{.....5.4}$$

The inverse of the Ohnesorge number is usually recognised as Z which is an important number in the determination of the stability of the droplet ejection. Moreover, printability range is defined as $4<Z<14$ [151] where the upper bound is restricted by the formation of satellite droplets and the lower limit is defined for viscous forces at higher Z numbers.

5.2.6 Droplet formation

The physical and chemical properties mentioned earlier, the amplitude and the width of the driving waveform and the shape of the nozzle are the main parameters and factors that can be optimised for the droplet formation.

Some relevant parameters that should be generally realised in inkjet printing are the satellites (satellite droplets), the time of flight, droplet pitch and line pitch. Firstly, the satellites are tiny

droplets that are unintentionally and undesirably formed during the ejection of an ink and they influence the quality of the printing. Secondly, the time of flight is the period between the nozzle ejection and recycling the ink in the gutter. Finally, the droplet pitch defines the distance between the centres of two droplets in the x-direction, and the distance in the y-direction is called line pitch

5.2.7 Ink curing/drying

One of the most important steps in the process of inkjet printing is curing the ink (ink drying). Although thermal sintering is the conventional method to cure most metal nanoparticle inks, other approaches have been used such as UV [152] UV radiation curing, chemical [153], plasma [154] and microwave sintering [155].

In the curing process, thermal sintering, the ink is subjected to a change from a liquid state to a solid-state and this is essential after the inkjet printing of the nanoparticles ink to help weld/bond the particles together and obtain continuous connectivity (electrical percolated path) [156] by the evaporation of the solvent of the ink leaving behind only the ink`s functional materials and achieve optimal profiles and good conductivities of the printed silver nanoparticles. The curing temperature has to be much lower than the bulk melting point of the material of interest. Generally, when the size decreases the melting point decrease due to the fact that the nanomaterials cohesive energy changes, as moving the surface atoms requires only very low energy because of the few bindings they create with each other at the free surface comparing to the ones in the bulk material which are evenly surrounded [157,158].

During the curing and drying process of the inkjet-printed materials, some defined shape patterns and phenomena can occur which might have an impact on the distribution and the morphology of the printed functional materials. This includes the coffee ring effect which is first studied by Deegan et al. [159] and it indicates the deposition of the particles of a material

at the edges when a droplet of the material dries. This effect can be explained by realising the fact that at the edges, the evaporation rate is higher than the one in the centre which induces a capillary flow to replenish the evaporated liquid from the edges by the one from the centre as shown in figure 5.12.

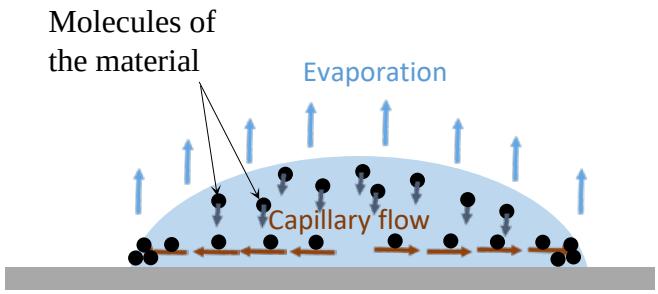

Figure 5.12: *a schematic simple explanation of the cause of the coffee ring effect.*

Chapter 6: The Inkjet Printing of Functional Materials

In this chapter, three functional materials will be investigated for purpose of inkjet printing: silver nanoparticles (Ag NPs), poly(3,4-ethylenedioxythiophene)-poly(styrenesulfonate) (PEDOT:PSS) and graphene oxide (GO). These materials were selected due to their outstanding properties, practicality and the very low negative impact on the environment and humans. Moreover, these materials have been studied in the electronics industry such as in the fabrication of memory devices as electrodes (Ag) and active layers (PEDOT:PSS and GO). Two DOD techniques were employed to inkjet print these functional materials; a commercial desktop piezoelectric Epson Stylus P50 from Epson (Suwa, Japan) and a PEL thermal inkjet printer from Printed Electronics Limited (PEL) (Tamworth, United Kingdom). Besides the simplicity and cost-effectiveness of these two printers, depending on the properties of the ink, thermal printer used for the water-based inks, while the piezoelectric one for the solvent-based inks.

6.1 Inkjet Printing (IJP) of Silver Electrodes from Silver Nanoparticles (Ag NPs) Ink

6.1.1 Background on the inkjet printing of silver nanoparticles ink

Conductive inks such as silver (Ag), copper (Cu), gold (Au) and conductive polymer inks have been extensively studied in recent years [154, 156, 160, 161]. However, the nanostructured/nanoparticles Ag ink has been of special interest due to many advantages for both the metal and ink properties including:

- Affordable and cheap when compared to others.
- Stable for a few years.
- Can be used with a wide range of ink vehicles including ethanol and tetradecane.
- The silver very low affinity for O_2 makes it more resistive to oxidation than many other metals including copper.
- In addition to their high electrical conductivity, the Ag nanoparticles and nanocomposites also show interesting chemical and optical properties that can be employed in many applications include imaging and sensing [162].
- Shaping and controlling the dimensions of the silver nanoparticles are not complicated [163].

The synthesis of the silver nanoparticles is usually done using bottom-up solution technique where zero-valent silver compounds/salts dissolved in a solvent and Ag nanocrystals are grown as these precursors are reduced to zero-valent atoms. Silver nitrate is the most widely used precursor to produce silver nanocrystals as most other silver compounds/salts are difficult to dissolve in many solvents and this is soluble in polar solvents. Capping agents such as metal ions/atoms, polymers, organic molecules and surfactants are manipulated to shape the nanocrystal. Polyvinylpyrrolidone (PVP) [164] and bromine anions [165] are the two most

employed capping agents for shaping the silver nanoparticles as they react with the silver nanocrystal {100} planes/facets (the side surfaces of the Ag nanocrystal) while behaving passively with other facets/planes which leads to adding more Ag atoms to the other facets/planes such as {111} facets/planes.

The Ag nanoparticle ink needs to meet crucial requirements to be used in inkjet printing to avoid drying out, agglomeration and clogging the printhead, reduce aggregation of the particles and limit the coffee-ring effect. In addition, the ink's viscosity and surface tension have to be suitably adjusted due to their important role in the droplet size determination, the satellite droplet formation, the droplet position and wetting on the substrate. That is why the formulation of this ink has attracted a lot of attention from academia and industry. As mentioned before, the main ingredients when formulating an ink are the functional materials, here, silver nanoparticles (as a metal precursor), which should be high enough to obtain conductivity and the carrier solvent (solution). The carrier solution could be water (should be completely pure to avoid contaminations), organic-based solvents or cross-links monomers. Additives (small quantities) including surfactants, humectants, dispersants, binders, wetting modifiers, rheological modifiers, bactericides and fungicides might well be involved in the preparation of the ink to modify some of its properties. For example, as previously explained in chapter 5, surfactants are used to optimise the nanoparticle surfaces by forming a coating on them to make them attract or repel causing flocculation or stabilisation respectively. They have both hydrophilic and hydrophobic properties so they can also alter the surface tension of the ink. However, biocides and fungicides are not usually added to the silver nanoparticles ink as it has antibacterial behaviours (properties) itself.

Most of the nanoparticles silver inks have Ag nanoparticle with spherical shape (from 5 to 100 nm in diameter) [166]. A lot of research has been taking place employing this ink in inkjet printing. Conductive lines (approximately 80 μm width) with resistivity of 3 μΩ cm were inkjet

printed using spherically shaped colloidal Ag nanoparticles ink (diameter of 5-7 nm, dispersed 10% by weight (10wt%) in α–terpineol), and the printed lines were cured at 300 °C for 10 mins: the resistivity was approximately twice that of the bulk resistivity of 1.6 μΩ cm [167]. Moreover, an ink of approximately 50 nm Ag nanoparticles dispersed 25 wt% in water and diethylene glycol (DEG) was inkjet printed to achieve $1.6x10^{-5}$ Ω cm of 130 μm conductive lines after being baked for 3 mins at 260 °C, this value is close to the silver bulk resistivity which is 1.6 μΩ cm [168].

After inkjet printing of the nanoparticles ink, thermal sintering is performed as it is crucial, as explained earlier, to achieve a conductive inkjet printed silver after the evaporation of the carrier solvent. The curing temperature has to be much lower than the bulk melting point of silver; it is anticipated that the silver nanoparticles (in nanometers) have significantly lower sintering temperatures and melting point than bulk silver of approximately 250 °C [169] for the nanoparticles and 962 °C for the bulk metal. This significantly low melting point of the nanoparticles is due to the large surface atoms to inner atoms ratio. As the aim here is to have a surface self-diffusion of the particles to initiate nanoparticles neck formation, hence particles bonding and not to solid to liquid phase change. The inkjet-printed silver nanoparticles layers are basically the assembly and togetherness of these nanoparticles that their mean diameter is increased by curing.

6.1.2 Testing the silver nanoparticles ink

The ink which was used here in the inkjet printing of silver patterns is a nanoparticle silver ink purchased from Printed Electronics Limited (PEL) (Tamworth, United Kingdom). It contains 60-70 nm of silver particles (40%wt) in a solution of ethanol and ethylene glycol, along with some compounds including buffering agents and surfactants to modify the ink's rheological properties and some of organic and polymeric substances. Furthermore, for the prevention of

the agglomeration and precipitation, polymer chains are used to coat the silver nanoparticles. Prior to the inkjet printing of the purchased nanoparticle silver ink, the main properties such as the viscosity, the surface tension, pH are required to be investigated to ensure good inkjet printability and adhesion. All the measurements were carried out at least 3 times per sample and an average amount was taken into consideration.

To start with, the viscosity of the ink was measured by a viscometer (Brookfield DV2T viscometer) and it was 4±2 cP (at spindle speed of 200 rpm and shear rate of 264 in 60 s) which is comparable to the manufacturer datasheet (6 cP) and it is within the range the piezoelectric inkjet printer was capable of printing (4-20 cP). Secondly, 34±1 mN/m was the obtained for the surface tension of the ink from a tensiometer and that is also in good terms with the data sheet (35 mN/m). Furthermore, the pH of silver ink was measured by a pH meter and was 9±1. Finally, the contact angle and wettability of the ink were carried out using CAM200 KSV NIMA goniometer and the results of ink contact angles with the PEL paper, silicon, glass, plastic coated with indium tin oxide (ITO) were 38°±2°, 13°±1°, 29°±1° and 25°±2° respectively. The contact angle measurement of the silver nanoparticles (Ag NPs) ink on a ceramic coated PEL paper is shown in figure 6.1. As can be seen in figure 6.1 b, the evolution of the silver droplet with time occurs in two steps; one after 5 s and the other at 10 s. After the second step, the contact angle remained constant at 38°. This change in the contact angle with time might be attributed to the quick infiltration of the carrier solvent into the porous surface of the paper substrate due to capillary forces.

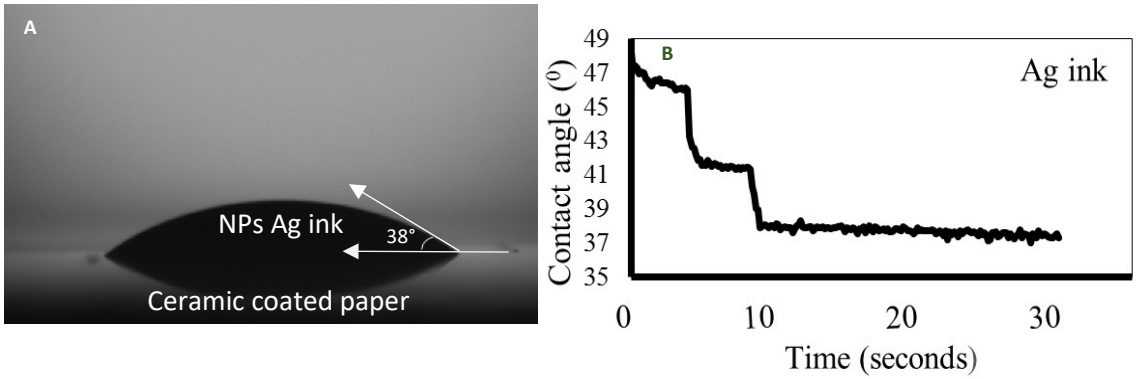

Figure 6.1: *the contact angle measurements of NPs Ag ink on ceramic coated paper; a) an image shows the ink droplet making a contact angle of 38° with the paper and b) the time that the droplet takes to settle down.*

6.1.3 Printing the silver nanoparticles ink

Having tested the main properties and factors that are crucial to achieve a high-quality inkjet printing of nanoparticle silver and obtained good results which are within the range of which they should be for printing and the print head, the ink was used to print utilising piezoelectric Epson Stylus P5O desktop printer onto ceramic coated paper from PEL. The printer functions by means of a piezoelectric squeeze mode printhead [170] and its main specifications are:

- 90 nozzles per colour (printhead).
- 65 µm nozzle orifice diameter.
- Minimum droplet size is 1.5 pl (picolitre).
- Printing resolution is 5760 x 1440 DPI (dots per inch).

It is worth mentioning here that there were no modifications done to the printer in order to print the silver ink. The nanoparticle ink was initially filtered using a 5µm filter to remove large particles (if any existed) to avoid blocking the nozzle, then ultrasonically stirred for 30 mins to ensure good dispersion and uniformity. The next step was to fill the ink in the cartridge which was done by using a syringe. For each cartridge, some specific changes in the associated interface such as the brightness and contrast were required to achieve good printouts. Different shapes and tracks were successfully inkjet printed on ceramic coated PEL paper with various

layers ranging from 1-10. Curing then took place at 120 °C for 5 minutes (recommended by the supplier, PEL) to help evaporate the solvents. Printing on plastic coated with ITO, on the other hand, encountered some issues due to the flexibility of the plastic when rolling inside the printer which caused distortions in some patterns. Silicon and glass substrates were also investigated and promising results achieved, however, using this inkjet printer, some modifications were required as the position where to locate the sample was chosen to be instead of the CD holder, and because the aim here was only to print on flexible substrates (ceramic coated PEL paper) this has been postponed to be carried out in future work.

The quality of the patterned silver was investigated by means of LAOPHOT-2 optical microscope (fitted with Nikon camera DS-Fi1), scanning electron microscopy (SEM), Current-Voltage (IV) and sheet resistance measurements, profilometer, mechanical stress (bending) test and scotch tape (adhesion) test.

6.1.4 Results and Discussion

It was observed that the silver nanoparticle ink requires at least 4 passes of inkjet printing of the ink to achieve conductive thin layers of the silver ink and this can be attributed to the fact that the silver particles are separated and disconnected when printing 3 passes or lower. However, from 4 prints and higher, and, obviously, after curing and evaporating the organic solvents, the particles start to connect with each other to establish a continuous path for the electric current. Figure 6.2 presents some of the first trials (10 passes) of printing the nanoparticle silver ink whose conductivities were initially investigated by a simple digital multimeter and exhibited promising results. The electrical resistivity measurements and analysis will be discussed in section 6.1.4.3.

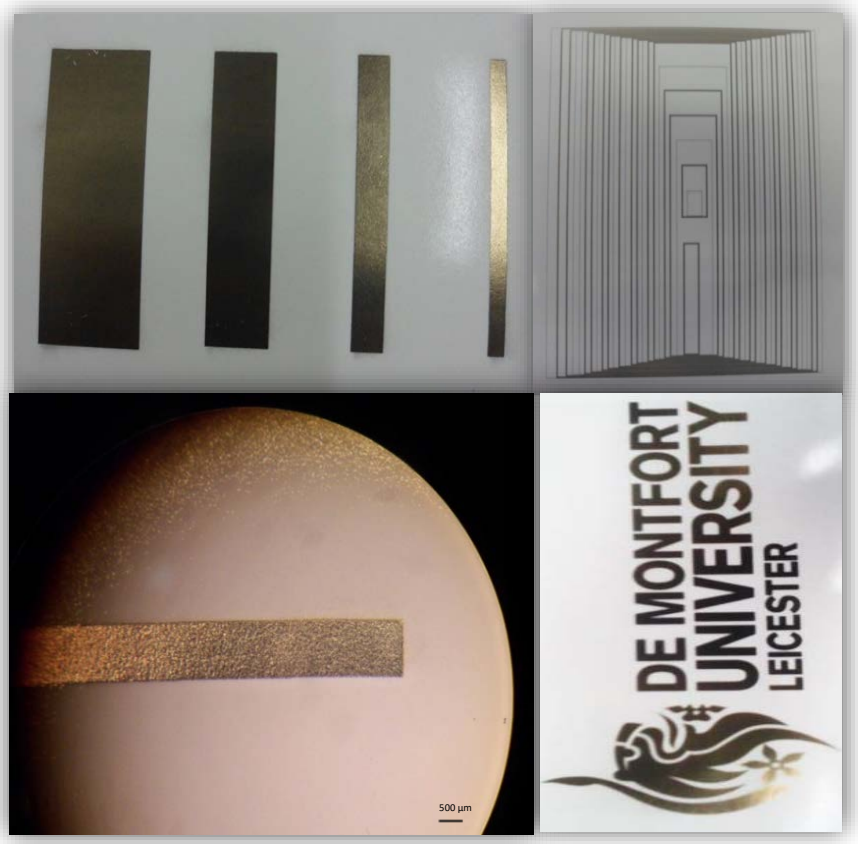

Figure 6.2: *photographs and optical microscope images of the first trials (10 passes) of printing the nanoparticle silver ink with different shapes and patterns; a) photograph of printed tracks with different widths, b) photograph of printed lines and curves, c) optical microscope image of 1-mm-width track and c) photograph of printed DMU log along with the university name.*

6.1.4.1 Optical microscope imaging of silver ink printed tracks

The quality of the inkjet-printed nanoparticle silver layers was initially assessed by Nikon LABOPHOT-2 optical microscope, fitted with Nikon Camera DS-Fi1.

Firstly, the microscope was used to obtain a microscopic image of the surface of a PEL ceramic coated paper as shown in figure 6.3 to be as a reference for further observations.

Individual droplets of the printed silver can be seen in the microscope images shown in figure 6.4 when an approximately 90 µm wide track was inkjet printed (3 passes).

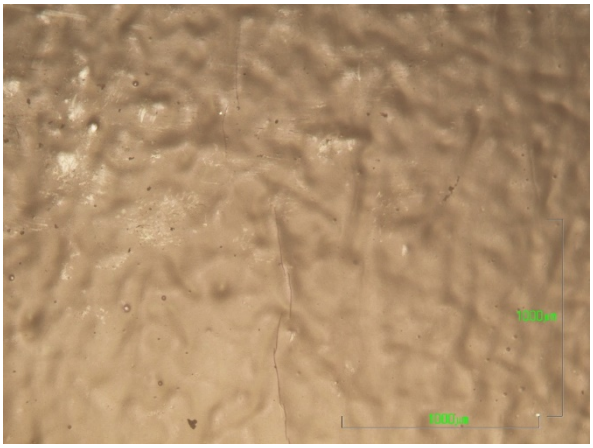

Figure 6.3: *a microscope image of the surface of ceramic coated paper.*

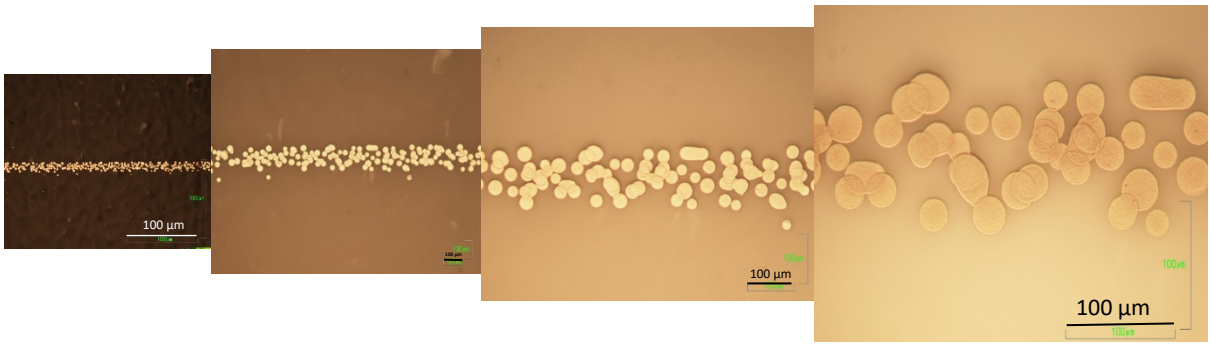

Figure 6.4**:** *microscope images of inkjet printed NPs Ag track of 90 µm width; magnifications of 5x, 10x, 20x and 40x (left to right).*

The optical microscope images presented in figure 6.5 provide a visual illustration of the different inkjet printed layers (passes) of the silver particles. In printed layers equal to or less than 3 passes (figure 6.5 (a) and (b)), the printed particles are separated and disconnected, and as a result, they are not able to conduct electricity. However, the connectivity and the formation of paths for the electrons to pass through when an electrical field is applied to are only applied to the printed layers which had undergone inkjet printing of 4 passes or more (figure 6.5 (c), (d), (e) and (f)). For the application of the inkjet printing of functional materials that will be discussed in chapter 7, a 10-pass inkjet-printed silver, as shown in figure 6.5 (f), will be used as electrodes for the proposed electronic memory device to ensure their electrical conductivity.

Figure 6.5 also shows optical microscopic images of the inkjet-printed Ag NPs with different passes; one pass, three passes, four passes, five passes and ten passes.

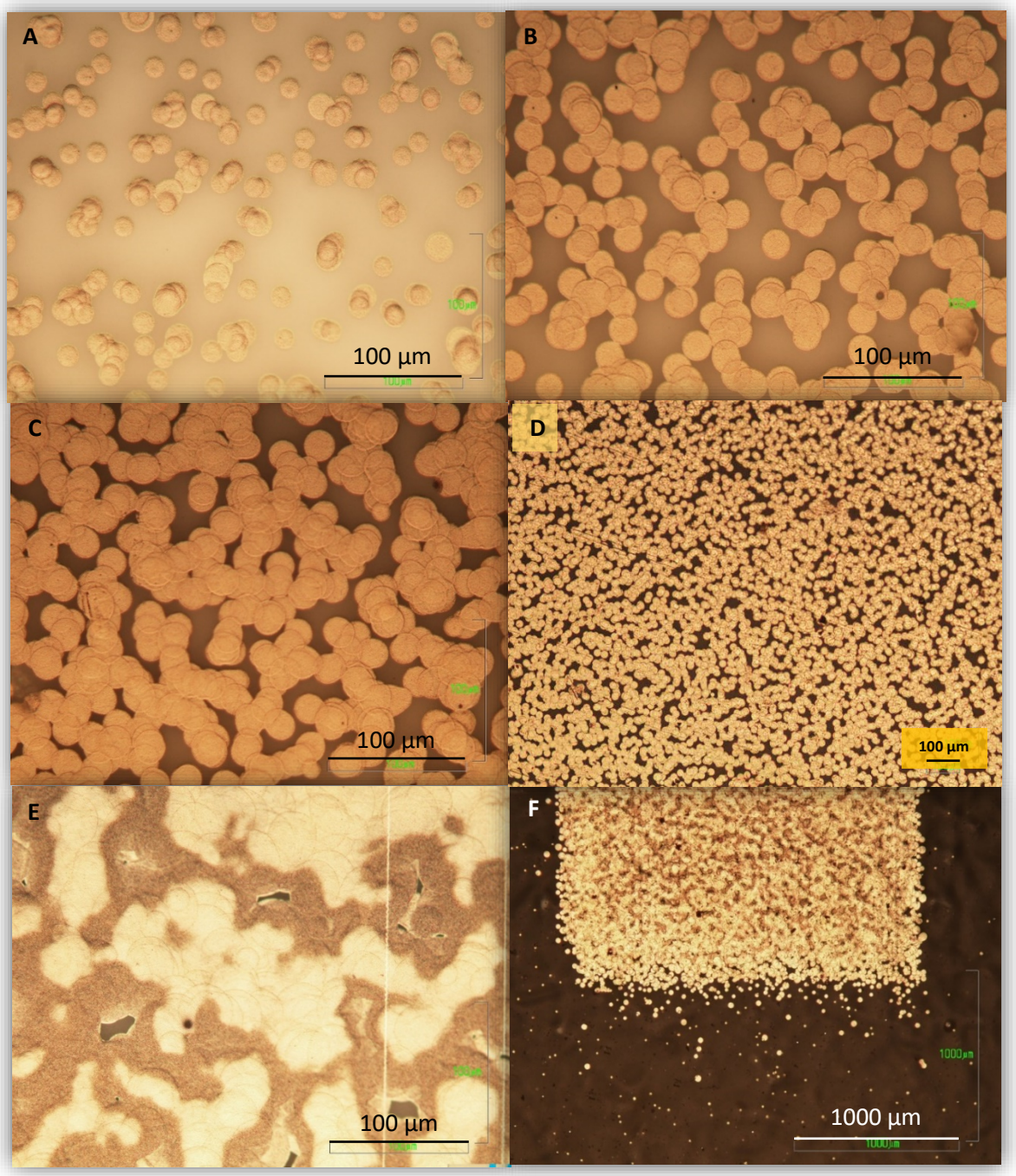

Figure 6.5**:** *optical microscopic images of the inkjet printed NPs Ag with different passes; a) one pass, b) three passes, c) four passes, d) five passes, e) ten passes and f) a conductive track that can be used as an electrode.*

A quick analysis was carried out using SEM to evaluate the diameter of the nanoparticle silver droplet and it shows that it is in a range of 20-23 µm as presented in figure 6.6.

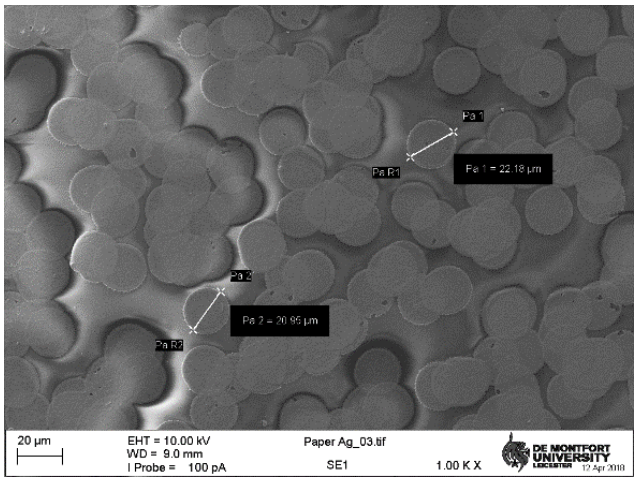

***Figure 6.6**: SEM image of inkjet printed droplets of NPs Ag with diameter evolution of single droplets (20-23 µm).*

6.1.4.2 Thickness measurements of the inkjet printed silver nanoparticles

Several techniques have been investigated to determine the thickness of the inkjet-printed silver nanoparticle ink including profilometer, optical microscope and SEM. The profilometer did not show any good results, however, both SEM and the optical microscope provided a good estimation of the thickness of the printed silver.

a) Profilometer (thickness) measurements of inkjet printed Ag NPs ink on paper

The profilometer's diamond tip did not move smoothly over the flexible substrate (ceramic coated paper) and as a result, the output data, as presented in figure 6.7, was incorrect as the tip requires a solid substrate to achieve a sensible, readable output.

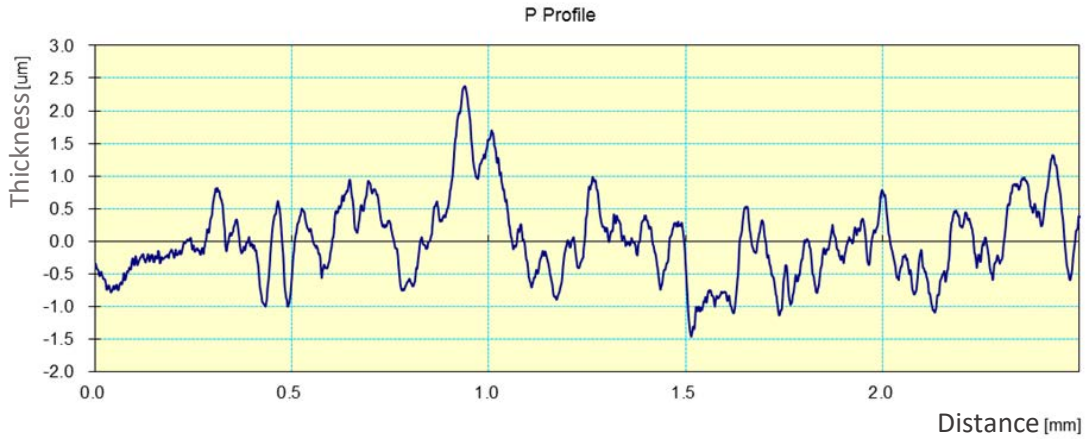

***Figure 6.7**: a profilomter's output of inkjet printed Ag NPs on a ceramic coated paper, the tip of the diamond was not able to carry out the measurement due the porous and flexible surface of the ceramic coated paper.*

b) Optical microscope thickness measurements of inkjet printed Ag NPs ink on ceramic coated paper

A Nikon LABOPHOT-2 optical microscope, fitted with Nikon Camera DS-Fi1, was used to measure the thickness of 5-layer inkjet-printed silver on PEL paper. All optical microscope images have a scale of 100 µm as a reference for the dimensions of the patterns. The printed sample was put in a vertical position (cross-section) so the view and the focus from the microscope lens can be only the interface between the metal thin film and the paper. Figure 6.8 exhibits images of the optical microscope which show a thickness of the inkjet-printed nanoparticle silver of 23±3 µm which what was anticipated and in agreement with some literature (taking into consideration the kind of printer, ink and the substrate used here are different for the reported thicknesses). 1.5 µm for a single layer line and 6 µm for a five-layer line reported by Perelaer et. al when they inkjet-printed silver ink with a particle size of 8.9 nm and Ag content of (30wt%) on a glass substrate using an Autodrop printer from Microdrop Technologies [171]. Joubert et. al also reported thicknesses (4.7, 37.3 and 21.7 µm) when they

printed silver ink (12 nm particles, Ag 6 wt%) on different photo paper substrates (Epson, Penguin and Whatman) respectively, using a Fujifilm Dimatrix printer [172].

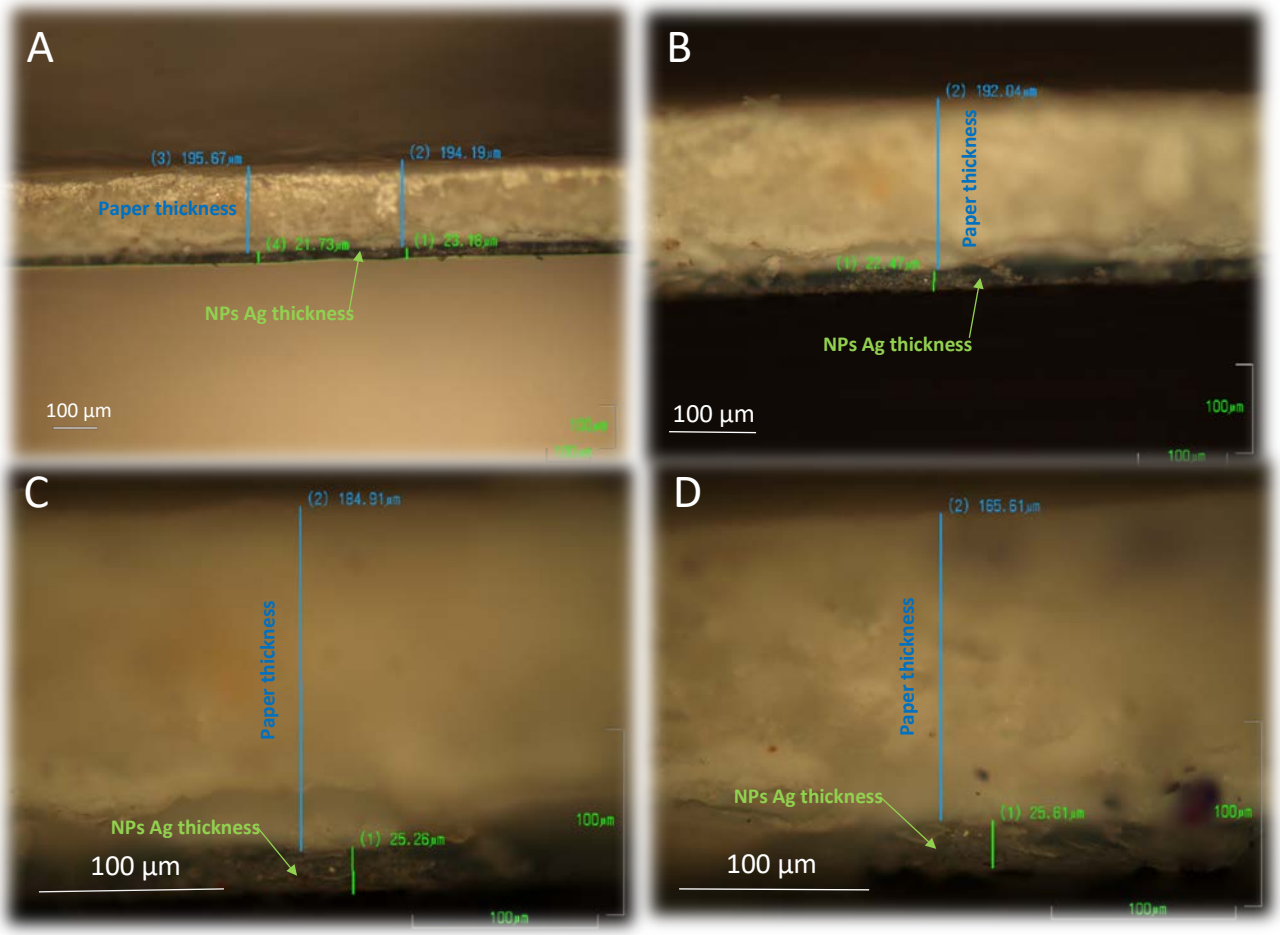

Figure 6.8: *optical microscope images for the evaluation of the thickness of 10-layer inkjet printed Ag NPs in different magnifications; a) 10x, b) 20x and both c) and d) 40x.*

c) SEM thickness measurements of inkjet printed Ag NPs ink on paper

SEM imaging was also considered to estimate the thickness of a 10-pass thin film of inkjet printed silver nanoparticles. As a reference, a 5 nm gold-coated PEL ceramic coated paper was analysed by SEM as can be seen in figures 6.9. Again the substrate was positioned vertically to allow clear viewing of the printed silver layers interface with the paper as shown in figure 6.10 a. A higher magnification (5k) was required to be able to distinguish the metal layers and

as it can be seen in figure 6.10 d, the thickness is approximately 23 µm which is in the range explained in the optical microscope measurements.

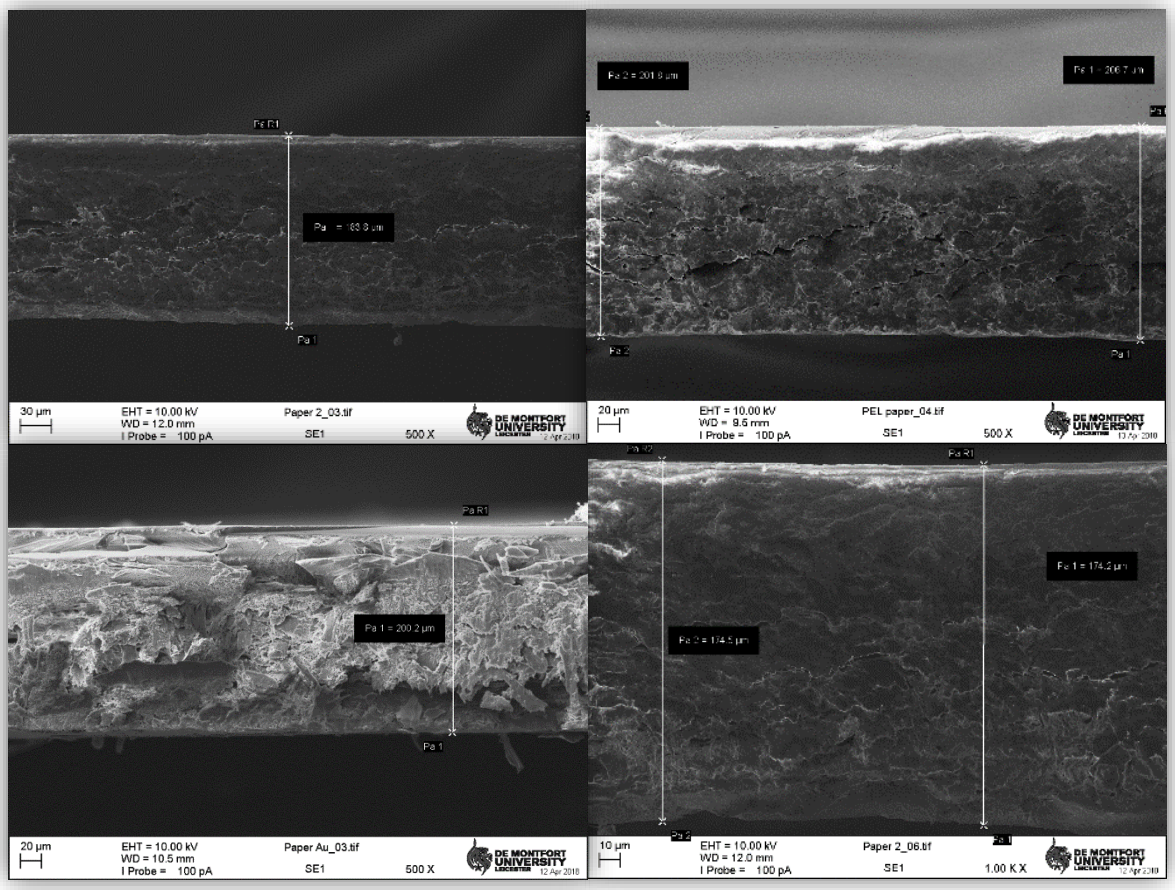

Figure 6.9: *SEM images of PEL ceramic coated paper coated with 5 nm layer of gold, the thickness of the paper appears to be between 170-200 µm.*

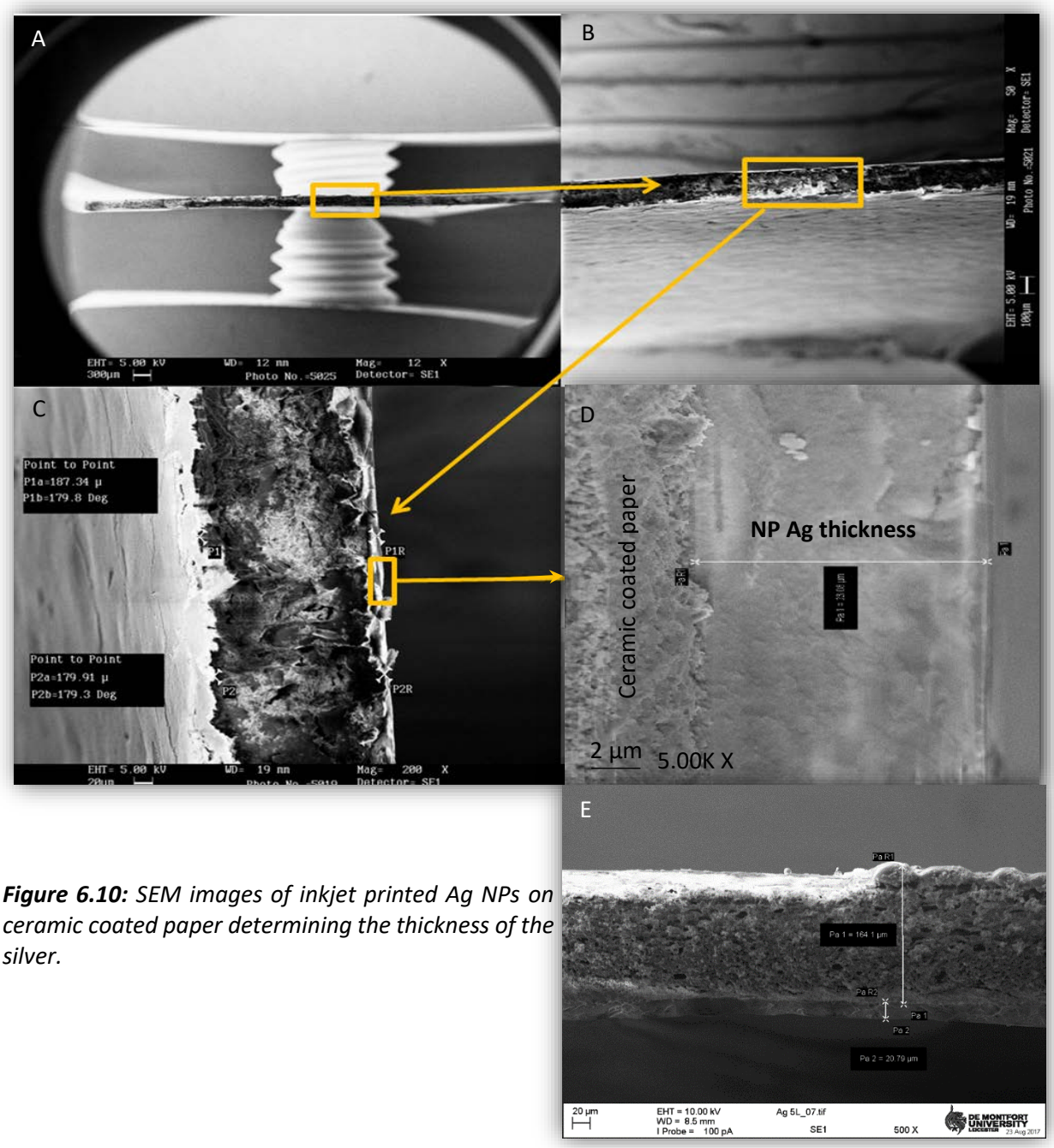

Figure 6.10: *SEM images of inkjet printed Ag NPs on ceramic coated paper determining the thickness of the silver.*

6.1.4.3 Resistivity and electrical measurements on inkjet printed silver nanoparticles ink

As mentioned earlier in chapter 4, unlike in bulk materials where the influence of the sample boundaries on the total resistivity can be usually neglected, the resistivity of thin films such as the inkjet-printed silver layers is certainly affected by scattering both at the thin film surfaces and interfaces and the grain boundaries of the silver particles as the thickness and/or the particle

grain size (diameter) of the thin film (printed layer) is/are in the same order with the electron mean free path as described in Fuchs-Sondheimer and Mayadas-Shatzkes models [106-108].

The resistivity of thin metallic layers and films with certain dimensions such as the case when length is much larger than the thickness of the thin film can be determined by using this equation:

$\rho = \frac{\pi}{\ln 2} \cdot (\frac{V}{I}) \cdot d$ (eq.3.3 mentioned in section 3.4.2: 4-probe technique)

Where, (V) is the voltage drop between two points on the inkjet-printed silver thin film, (I) is the current passing through the thin film and (d) is the thickness of the thin film.

As after the curing process for the inkjet-printed silver nanoparticle ink, the printed layers might be micro-structured as polycrystalline thin films and this might have an influence on some properties including the conductivity of the printed metal. Therefore, different methods including normal 2-probe, 4-probe IV measurements and Van Der Pauw methods were used for the electrical measurements on the inkjet-printed silver for comparisons and an attempt to achieve more precise results. All the electrical measurements were performed on the 5-pass inkjet printed Ag NPs on ceramic coated paper.

a) 2-Probe IV Measurements

The resistance of the 5-layer inkjet printed nanoparticle silver ink was measured by 2-probe IV measurements technique and it was approximately 13 Ω as can be seen in graph 6.11.

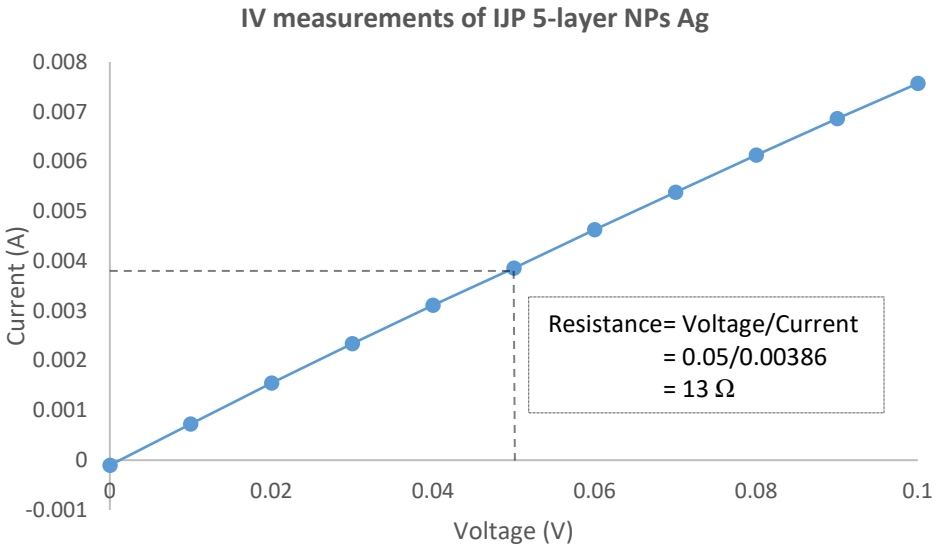

***Figure 6.11**: 2-probe IV measurements of inkjet printed NPs Ag (5 passes).*

b) 2 and 4 probe IV Measurements:

A different 2, 4- probe IV measurement instrument (programmed by J Glover at De Montfort University) was used to measure the resistance of the inkjet-printed NPs Ag on ceramic coated paper, the programme set up for this can be seen in the appendix (figure A7). The measured resistance in the 2-probe and 4-probe IV measurements were $R_{2\text{-probe}}$ =13.88 Ω and $R_{4\text{-probe}}$ = 81.95 mΩ respectively, as can be seen in figure 6.12.

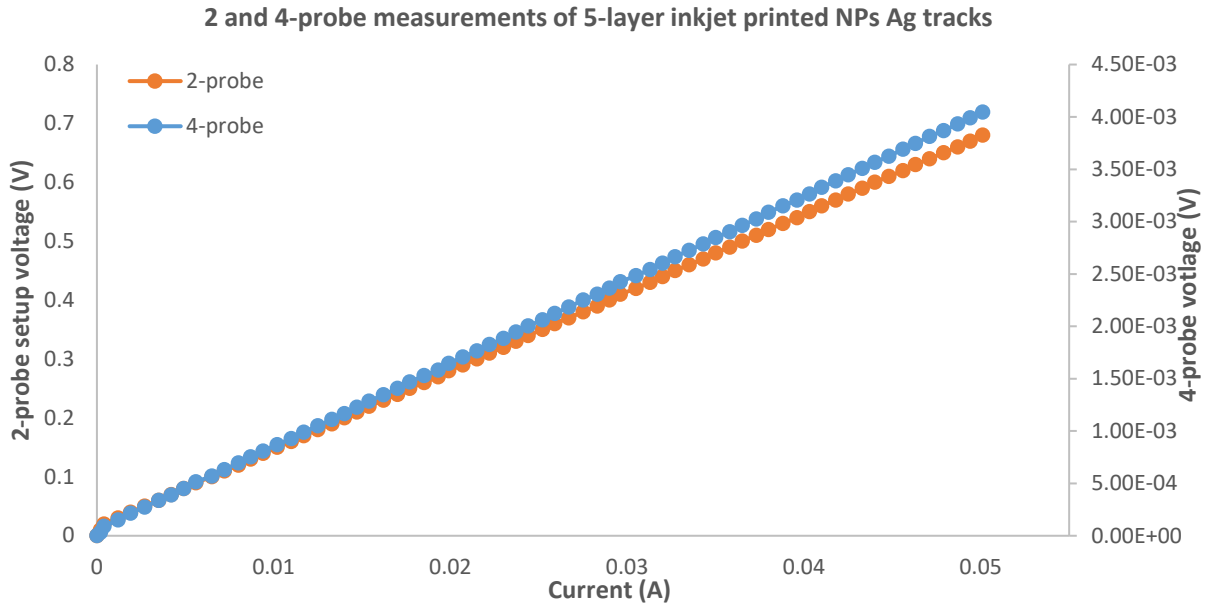

***Figure 6.12:** 2 and 4-probe IV measurements of 5-layer inkjet-printed NPs Ag on ceramic coated paper.*

c) Van Der Pauw method

The resistivities of the 5-layer inkjet-printed silver thin films measured by Van Der Pauw method for two edge locations; probes are 6mm and 4mm apart, are 290.5×10^{-8} Ω.cm (2.91 μΩ.cm, R_S 0.1263 Ω/□) and 400×10^{-8} Ω.cm (4 μΩ.cm, R_S 0.1739 Ω/□) respectively. These results are similar to the reported (Kim et al. reported 3.2 μΩ.cm [173] sheet resistance of an inkjet-printed silver on a paper is 0.3 Ω/□, 0.024 Ω/□ sintered by laser [174] and 1.9 Ω/□ sintered by infra-red [175]. Figure 6.13 shows a comparison of the reported values with measured values. Although they are slightly larger than the resistivity of the bulk silver (1.59×10^{-8} Ω.m), they are within the range of the silver nanoparticle ink specification from the supplier.

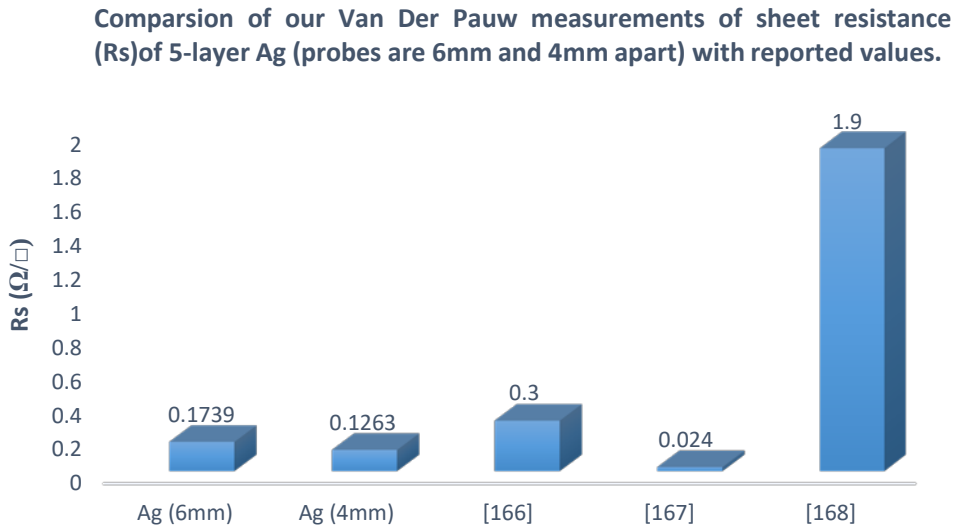

Figure 6.13: *comparison of our sheet resistance measurements using Van Der Pauw (probes are 6mm and 4mm apart) of 5-layer printed Ag with reported values.*

Comparison between two setup measurements for the same printed silver nanoparticles ink (5-layer inkjet-printed Ag) to investigate the effect of different current values and different steps and intervals (1m-10mA, step 1mA) and (1μ-1mA, step 10 μA) on the printed thin films. From figure 6.14, the resistivity of inkjet-printed silver does not change dramatically with the change of the current value and step interval which means that the inkjet-printed thin film metal is

stable and robust and withstands small amounts of current (microamperes) as well as slightly higher values (few milliamperes). Therefore, they can be employed in many electronic devices such as the electronic memory device that will be discussed in chapter 7.

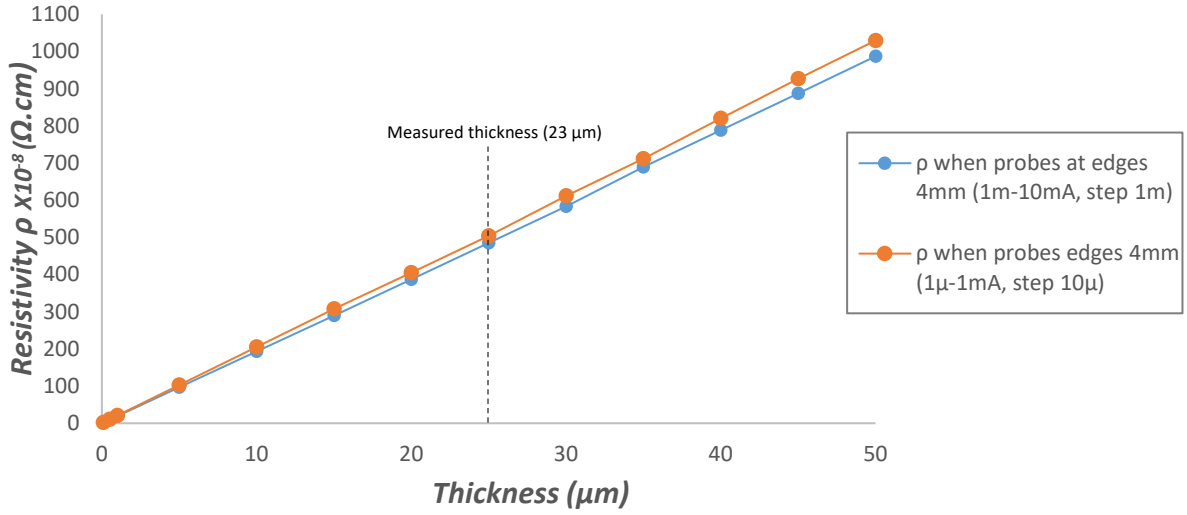

Figure 6.14: *resistivity measurements of 5-layer inkjet printed NPs Ag on ceramic coated paper by Van Der Pauw method with different current scale values and steps, probes are 4mm apart.*

Resistivity (ρ) measurements of the 5-layer thin film of inkjet-printed of silver nanoparticle ink were also performed at edges at two different spaces between the probes (distance between probes 6mm and 4mm) as shown in figure 6.15. The current scale is 1-10 mA, step 1 mA for all measurements unless stated differently.

It is worth noting here, measurements shown in figure 6.14 and 6.15) that the thicknesses of the printed silver layers were estimated and the results were obtained from the software (simulations) attached to the Van Der Pauw setup.

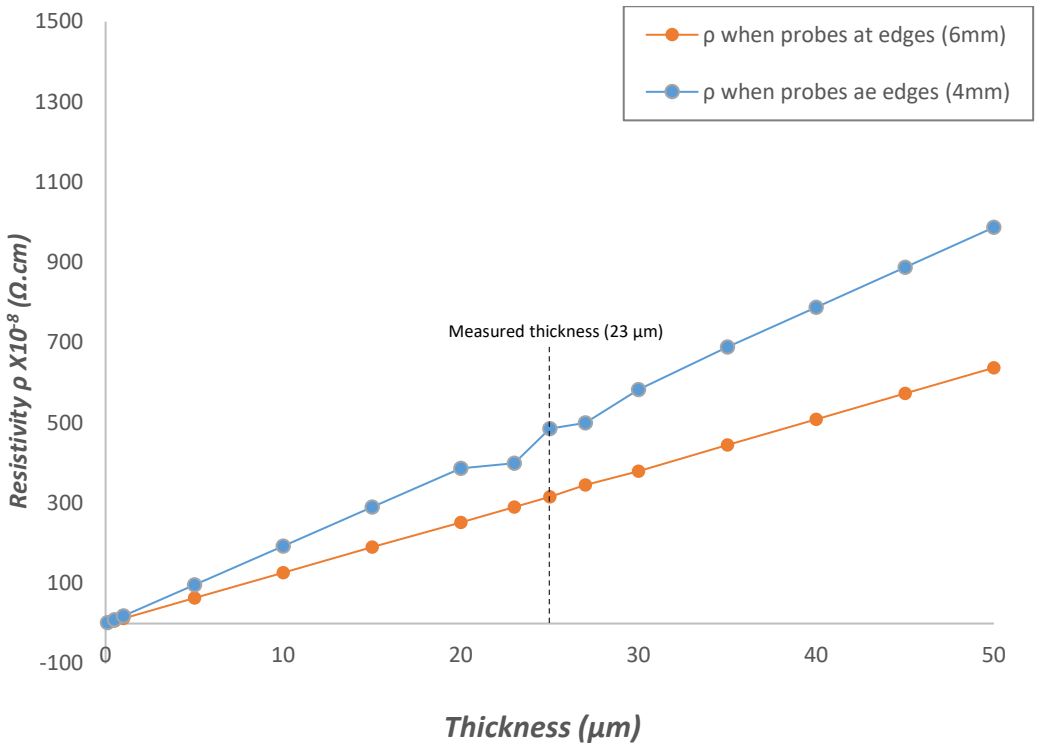

***Figure 6.15**: resistivity measurements of 5-layer inkjet printed NPs Ag on ceramic coated paper by Van Der Pauw method where probes positioned at two different distances (6mm and 4mm apart).*

Based on the resistivities of the 5-layer inkjet-printed Ag measured by Van Der Pauw and taking into consideration the dimensions of the printed tracks as shown in table 6.1, which summarises the results of all the methods used for the resistivity/ resistance measurements, it can be concluded that although the resistance and resistivities values measured by different techniques are not exactly the same, they are close and within the range the ink supplier suggested. Therefore, the inkjet-printed silver nanoparticle carried out in this work using a desktop inkjet printer can be used for the electronic memory application that is discussed in chapter 7.

***Table 6.1**: a summary of all measurements results for all used techniques for the resistivity/resistance measurements of inkjet printed Ag NPs on ceramic coated paper.*

5-layer inkjet printed NPs Ag on PEL ceramic coated paper								
Technique		Resistivity (Ω.m)	Length ((mm)	Width (mm)	Thickness (µm)	Sheet resistance (Ω/□)	Calculated Resistance (Ω)	Measured Resistance (Ω)
Bulk silver		$1.59x10^{-8}$	10	2	23	0.69 m**	3.5 m	NA
			20	4	23	0.69 m**	3.5 m	NA
Van Der Pauw	Probes 6mm apart	$2.91x10^{-8}$	20	6	23	0.1263	4.2 m	16.5m
	probes 4mm apart	$4x10^{-8}$	20	4	23	0.1739	8.7 m	21.9 m
2-probe (IV)		$1.59x10^{-8}$*	20	4	23	0.69 m**	3.5 m	13
2-probe (IV) ***		$1.59x10^{-8}$*	20	4	23	0.69 m**	3.5 m	15
4-probe (IV) ***		$1.59x10^{-8}$*	20	4	23	0.69 m**	3.5 m	86.5 m

*Resistivity of bulk silver was used in the resistance calculation. ** Sheet resistance values are estimated using the bulk resistivity of the silver. ***Programmed by G Lover at DMU

6.1.4.4 Mechanical stress (bending) test:

Bending tests and mechanical stress effects on the 4-layer inkjet-printed Ag on ceramic coated PEL paper was performed to investigate the resistance of the printed metal to bendability and the strength of its structure. The mechanical stability of the printed patterns using inkjet printing technology is essential to investigate its potential and look at the exploitation of this technology for flexible electronics. For this reason, this test was performed on all the IJP patterns in this work.

Prior to performing the aforementioned test on the printed substrates, the surface behaviour of the ceramic coated PEL paper before and after the bending test was investigated by means of an optical microscope to anticipate the test's influence on the paper alone. Figure 6.16 presents microscopic images of the ceramic coated paper in different states; flat, smooth bending (approximately 45°), and sharp bending (approximately 75°). It can be observed that the surface of the ceramic coated paper has undergone some changes, especially, in the sharp bending test, which might affect the printed material on it. Hence, this should be taken into consideration when performing the test. Optical microscopic images of printed samples were

taken to be a reference before performing the test are shown in figure 6.17. The smooth and sharp bending tests applied to the samples can be seen in figure 6.18.

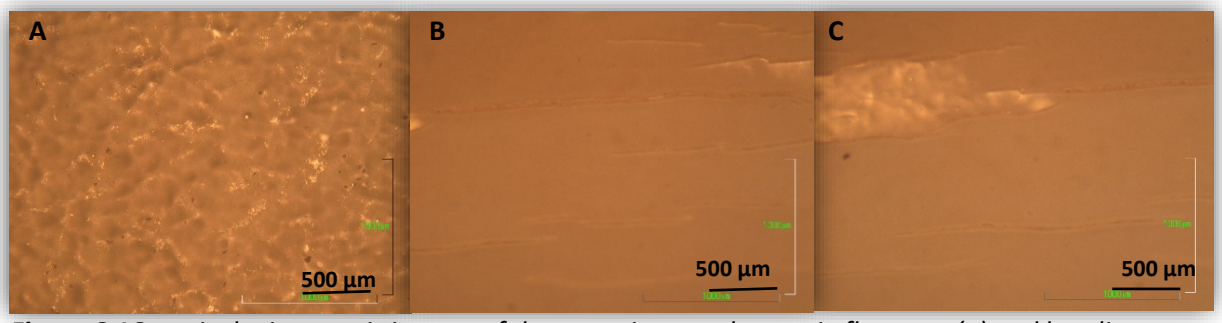

Figure 6.16: *optical microscopic images of the ceramic coated paper in flat state (a) and bending state; smooth (b) and sharp (c).*

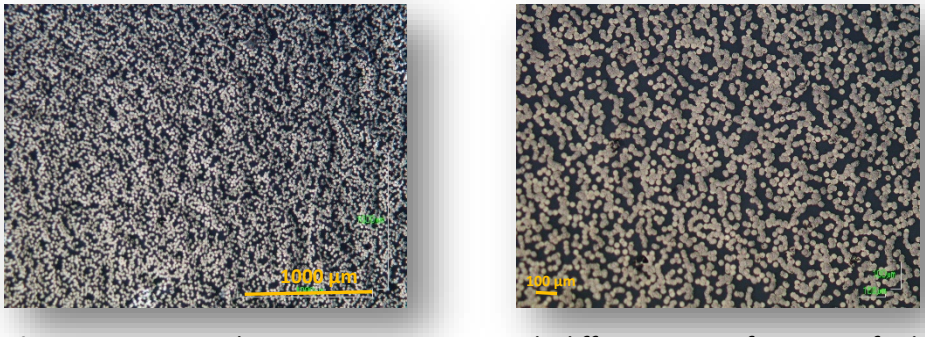

Figure 6.17: *optical microscopic images with different magnifications of inkjet printed Ag before performing the bending test.*

Figure 6.18: *photograph of smooth (a) and sharp (b) bending of the IJP silver.*

A smooth bending was initially carried out on the IJP silver, and after leaving the samples for 5 days, microscopic images were taken, as presented in figure 6.19, while the samples were in

two states; a bending state where the sample was kept bent and a flat state upon removal of the bending stress.

In the bending state, it can be observed that some cracks and deformations occurred in both smooth and sharp bending, with larger distortions occurring under the sharp bending. In the flat state, these deformations remained with shrinking of the crack in the smooth bending. The ceramic coating and surface of the paper might have influenced this and caused distortions in the printed silver, therefore more investigations with different bending and mechanical stress analysing techniques are required to conclude these results.

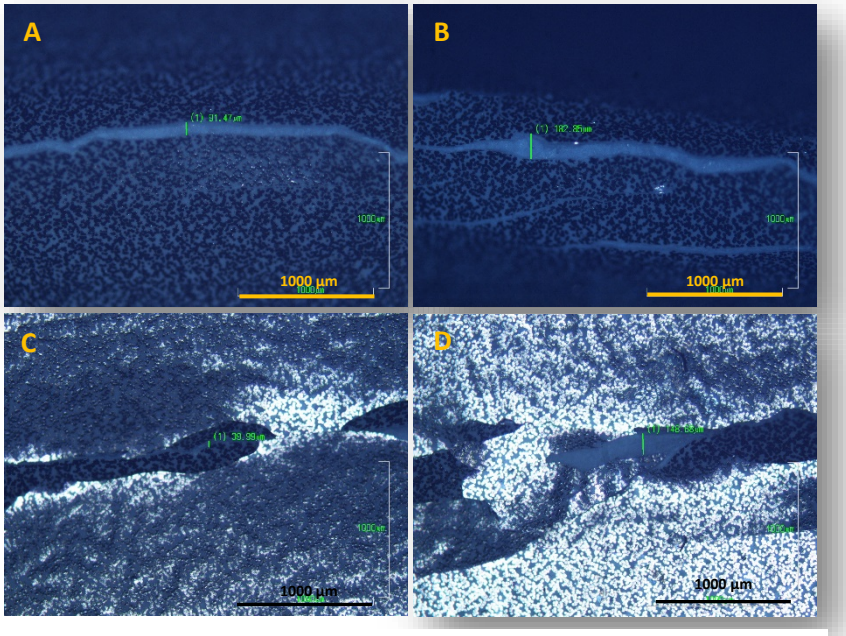

Figure 6.19: *optical microscopic images of IJP silver after performing the bending test; bending state: a) smooth and b) sharp bending, and flat state: c) smooth and d) sharp bending.*

6.1.4.5 Adhesion test

Although this test provides an indication and general understanding of the adhesion of two materials by means of a simple tool (scotch tape), it is not considered to be a precise investigation for the evaluation of adhesion, as it is prone to human error, susceptibility in the application and removal of the tape onto and from the sample. This test was selected to provide

a quick indication on the strength of the adhesion of the inkjet-printed silver to the ceramic coated paper. The inkjet printing technology requires a good adhesion behaviour between the IJP patterns and the substrate to achieve a reliable and optimised performance for potential exploitation in the flexible electronics industry.

Five-layer inkjet-printed silver on ceramic coated paper samples were subjected to the scotch tape test. The tape (approximately 30 mm wide) was positioned on the printed area till the edge where the interface between printed silver and the PEL paper can be seen. Manual, gentle pressure was applied along the tape to ensure that the tape contacted the printed silver. After a few seconds, the tape was peeled off from where the edge of the printed silver was, until the end of the tape in a single fast motion. In figure 6.20, it is clear that no deformation nor delamination occurred especially on the top and middle of the test area (figure 6.20: a, b, d, e, h and i). Furthermore, the adhesive layer was transferred and attached to the printed silver which can be explained in terms of both the adhesive forces between the substrate and the Ag printed layers, and the cohesion forces within the Ag printed layers must be stronger than the adhesive forces between the adhesive layer and the plastic film (backing material). It was demonstrated [176] that the incorporation of the Ag nanoparticles in ceramic improves some mechanical properties, including fracture roughness without altering their hardness and elastic characteristics. Therefore, this strong adhesive force between the printed layers and the ceramic coated paper are attributed to the formation of the ceramic-silver composites in the sintering process.

In the bottom area, on the other hand, despite the fact that the printed patterns remained adhered to the substrate, the adhesive layer of the tape was only partially transferred to the top of the printed layers as shown in figure 6.20 (c, f and j), which could be due to the fact that lower pressure was applied when removing the tape comparing to the pressure at the top and middle areas.

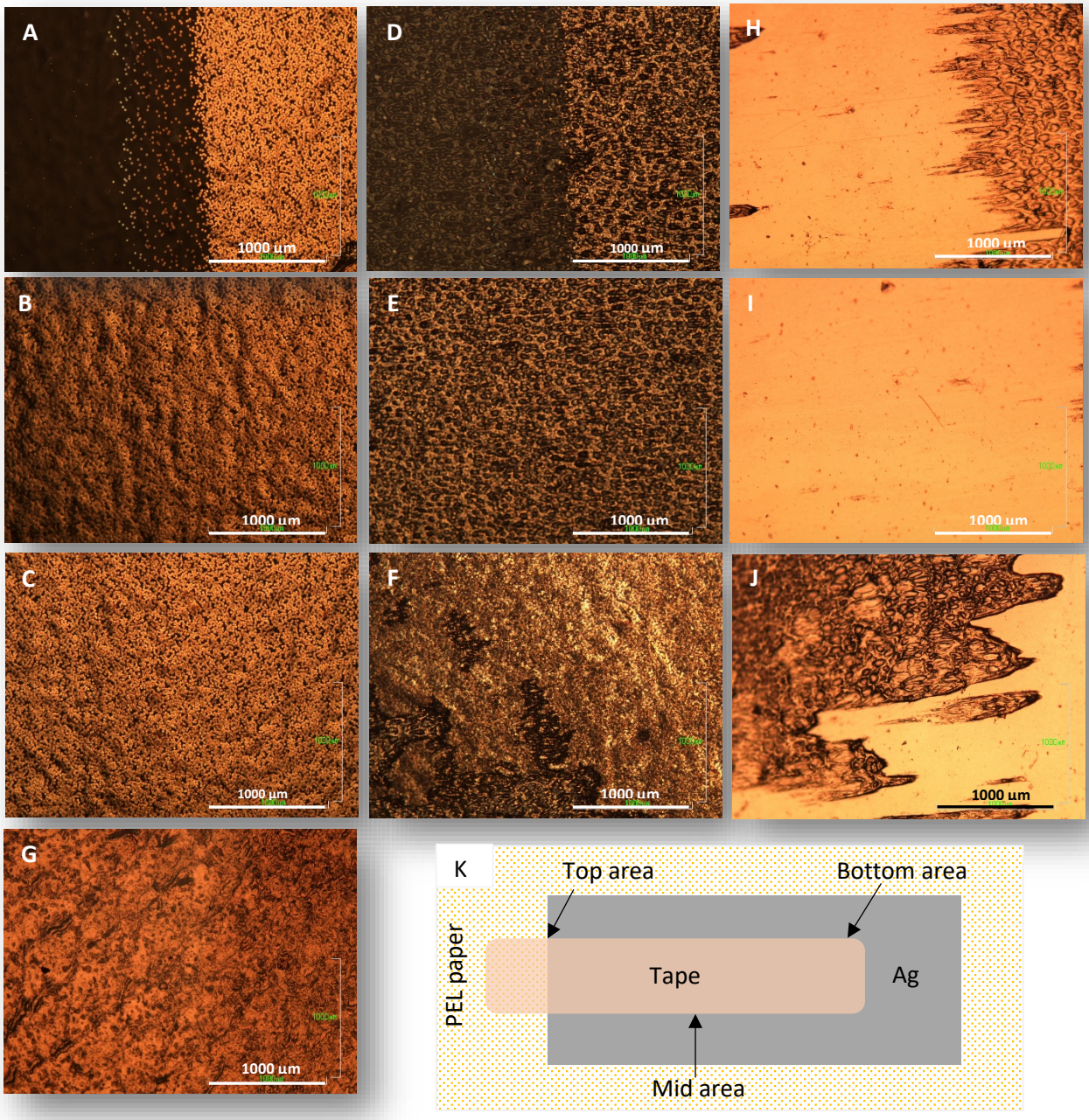

Figure 6.20: *optical microscopic images of the IJP silver and* ***before performing the tape test****; a) top area of the printed Ag, b) mid area and c) bottom area, and* ***after performing the tape test****; d) top of the printed Ag , e) mid, and f) bottom area. Microscopic images of the used tape; g) before the test and after the test; h) top, i) mid and j) bottom area. A schematic diagram showing the tape test set up (k).*

6.2 Inkjet Printing (IJP) of PEDOT:PSS

6.2.1 Background on the inkjet printing of PEDOT:PSS

The intrinsically conductive polymer PEDOT:PSS consists of PEDOT: poly(3.4-ethylenedioxythiophene) doped with PSS: poly(styrenesulfonate) anions [177]. The presence of conjugated pi-electron in the polymer is the main reason for its conductivity. Although that PEDOT was conductive (approximately 300 S/cm) and stable when it was chemically polymerised [178], it is insoluble which limited its application. It was till doping the electrolyte PSS [179], which is water-soluble, during the PEDOT polymerisation to develop an electrically conductive (1-10 S/cm) high stable polymer that is soluble in water. The reduction of Coulomb interactions between the positively charged PEDOT and the negatively charged PSS results in the hopping rate enhancement and conductivity [180].

The polymer finds a lot of applications such as organic light emitting diodes (OLED), organic photovoltaic (OPV), electromagnetics and optoelectronics mainly in sensing applications and as an electrode material or hole transport/injection layer in organic electronic devices [181,182] because of its high oxidation resistance, thermal stability, optical transparency through visible light region, near Infrared IR and near Ultraviolet UV, high work function and conductivity which is improved along with morphological and optical properties, by adding organic solvents or the treatment of the PEDOT:PSS film with solvents including glycol and DMSO [183,184]. Moreover, the application of mechanical pressure (load) on PEDOT:PSS alters its electrical properties as it is a piezoresistive material which has made it useful to be used in some mechanical sensors [185]. PEDOT:PSS, on the other hand, has some drawbacks. The acidic property of the doped PSS might affect its lifetime in some applications.

Many reports have investigated the effect of some parameters such as the treatment and the temperature of the substrate that including annealing and the drop spacing [186]. The thickness of the PEDOTPSS films was subjected to extensive research as well [187].

An increasing interest in low-cost solution-based depositing techniques has attracted many research and industrial and manufacturing fields as an alternative to the conventional production methods which are considered to be expensive, complicated, high waste and contamination. Despite the fact that spin coating is a cheap, easy and fast technique to deposit PEDOT:PSS, it has many issues including material waste and limited spatial resolution (only coating the whole surface) which can be a major drawback in the manufacturing of electronic devices. Inkjet printing has overcome many of these obstacles and is considered to be one of the most commonly and widely used solution processing methods due to its simplicity, low deposition costs, low-temperature patterning, compatibility with a wide range of substrates, no contact and maskless processing. The inkjet printing of PEDOT:PSS has attracted a great deal of attention for many applications to develop and optimise the technique to obtain high quality and resolution deposition. Mabrook [188] inkjet printed PEDO:PSS thin films to work as chemical sensors for ethanol and methanol detection. When exposed to these gases, the morphology of the PEDOT:PSS thin film changes which leads to a change in the conductivity of the sensors. A desktop printer was used to pattern 600 nm thickness of conductive PEDOT:PSS on PET substrate [189]. And a memory device (Ag/PEDOT:PSS/Ag) with two processes; inkjet for printing the silver electrodes and spin coating for the PEDOT:PSS deposition [190].

6.2.2 Testing the PEDOT:PSS ink

Prior to the inkjet printing of the purchased poly(3,4-ethylenedioxythiophene)-poly(styrenesulfonate) PEDOT:PSS in 2% ethylene glycol monobutyl ether/water (3:2) ink (Sigma Aldrich), the main ink properties needed to be investigated to ensure good quality printing. All the measurements were performed at least 3 times for each sample and an average amount was taken into consideration.

Firstly, the viscosity of the ink was measured by a viscometer (Brookfield DV2T viscometer) and it was found to be 14±2 cP (at a spindle speed of 200 rpm and a shear rate of 264 in 60 s) which is comparable to the manufacturer data-sheet (4-10 cP). The viscosity of an ideal ink for inkjet printing was advisable to be between 4-20 cP, the measured viscosity for the PEDOT:PSS ink was within this but might be slightly higher than quoted values. However, this does not mean that the ink might not be good for inkjet printing as this measurement was conducted at an angular velocity of only 200 rpm (shear rate of 264) which was the maximum that the used equipment is restricted to whereas, for a better indication of viscosity, the measurement should be taken under higher shear rates. During the inkjet printing, the shear rate is anticipated to be higher, so the ink's viscosity might decrease and produce a good quality inkjet printing.

Secondly, 33±2 mN/m was the obtained surface tension of the ink from tensiometer (Torsion Balance), measurements were carried out 3 times. The measured value of the ink's surface tension was very similar to that suggested in the ink's data-sheet (35-38 dynes/cm, 0.035-0.038 N/m) and that can be attributed to the instrument's error.

Moreover, the 3520 pH meter showed a pH of 2.9±0.2 whereas the company data suggests it is within this range 2.2-2.8. This value might not be good for the stability of the ink over a long

period of time, but it was reported that lower pH amounts of the PEDOT:PSS ink results in a good conductivity [191].

Finally, the contact angle and wettability measurements of the ink were carried out using CAM200 KSV NIMA goniometer and the results of ink contact angles with paper, glass, plastic coated with ITO and silicon-coated sheet are 29.5º±0.5°, 26º±1°, 30º±2° and 38º±1° respectively. As the PEL paper is the substrate of interest here, the contact angle that the PEDOT:PSS ink with it is 29.5º±0.5° which means that the ink spreads slowly on the paper as it has a porous ceramic coating that helps absorbing the ink's solvents and this can result in achieving a good printing for desired patterns. The evolution of the contact angle for the PEDOT:PSS droplets (figure 6.21) has fewer variations and is smoother than that of the silver's. This might be associated with the carrier solvents for both inks.

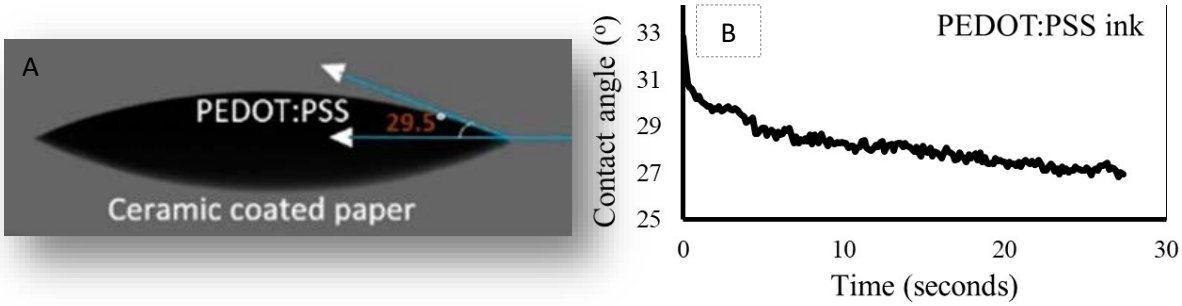

Figure 6.21: *the contact angle measurements of PEDOT:PSS ink on ceramic coated paper; a) an image shows the ink droplet making a contact angle of 29.5° with the paper and b) the time that the droplet takes to settle down.*

6.2.3 Printing the PEDOT:PSS ink

Having tested the main properties and factors that are crucial to achieve a high-quality inkjet printing of PEDOT:PSS and obtained good results which are within the range of which they should be for printing and the print head compatibility.

A piezoelectric Epson Stylus P5O desktop printer was used to carry out the printing. The printer functions by means of a piezoelectric squeeze mode printhead and its main specifications are as the same as the one used for printing the nanoparticle silver ink.

Just to mention here that there were no modifications done to the printer in order to inkjet print PEDOT:PSS. The PEDOT:PSS ink (Sigma Aldrich) was initially filtered using a 5µm filter to remove large particles (if any existed) to avoid blocking the nozzle, then ultrasonically stirred to ensure good dispersion and uniformity. The next step was to fill the ink in the cartridge which was done by using a syringe. For each colour (cartridge), some specific changes in the associated interface such as the brightness and contrast were required to obtain good printouts. Different shapes and tracks were successfully inkjet printed on ceramic coated paper with various layers ranged from 1-10 layers. Curing then took place at 70ºC for three hours (recommended by the supplier, Sigma Aldrich) to help evaporate the solvents.
The quality of the patterned PEDOT:PSS was investigated by means of LAOPHOT-2 optical microscope (fitted with Nikon camera DS-Fi1), scanning electron microscopy (SEM), IV and sheet resistance measurements, mechanical stress (bending) test and scotch tape test.

6.3.3 Results and Discussion

A visual evaluation using an optical microscope and SEM, electrical measurements and mechanical stress (bending) effect and an adhesion test were all performed of the inkjet-printed PEDOT:PSS for general evaluations that will be discussed in the next sections.

6.3.3.1 Optical microscope imaging and scanning electron microscopy (SEM) of the inkjet printed PEDOT:PSS

The quality of the inkjet-printed PEDOT:PSS (1-5 and 10 layers) on ceramic coated PEL paper were initially investigated using Nikon LABOPHOT-2 optical microscope, fitted with Nikon Camera DS-Fi1. The optical microscope images revealed some qualities of the printed layers.

It can be observed from the optical microscope images presented in figures 6.22 that the more printed layers of PEDOT:PSS, the light interference with the patterned material results in changing the colour of the deposited layers in relation with PEDOT:PSS thickness that is increased with printing more passes of the PEDOT:PSS ink. It also indicates that the PEDOT:PSS printed layers are not uniform and that might be because of the porous surface of the ceramic coated paper.

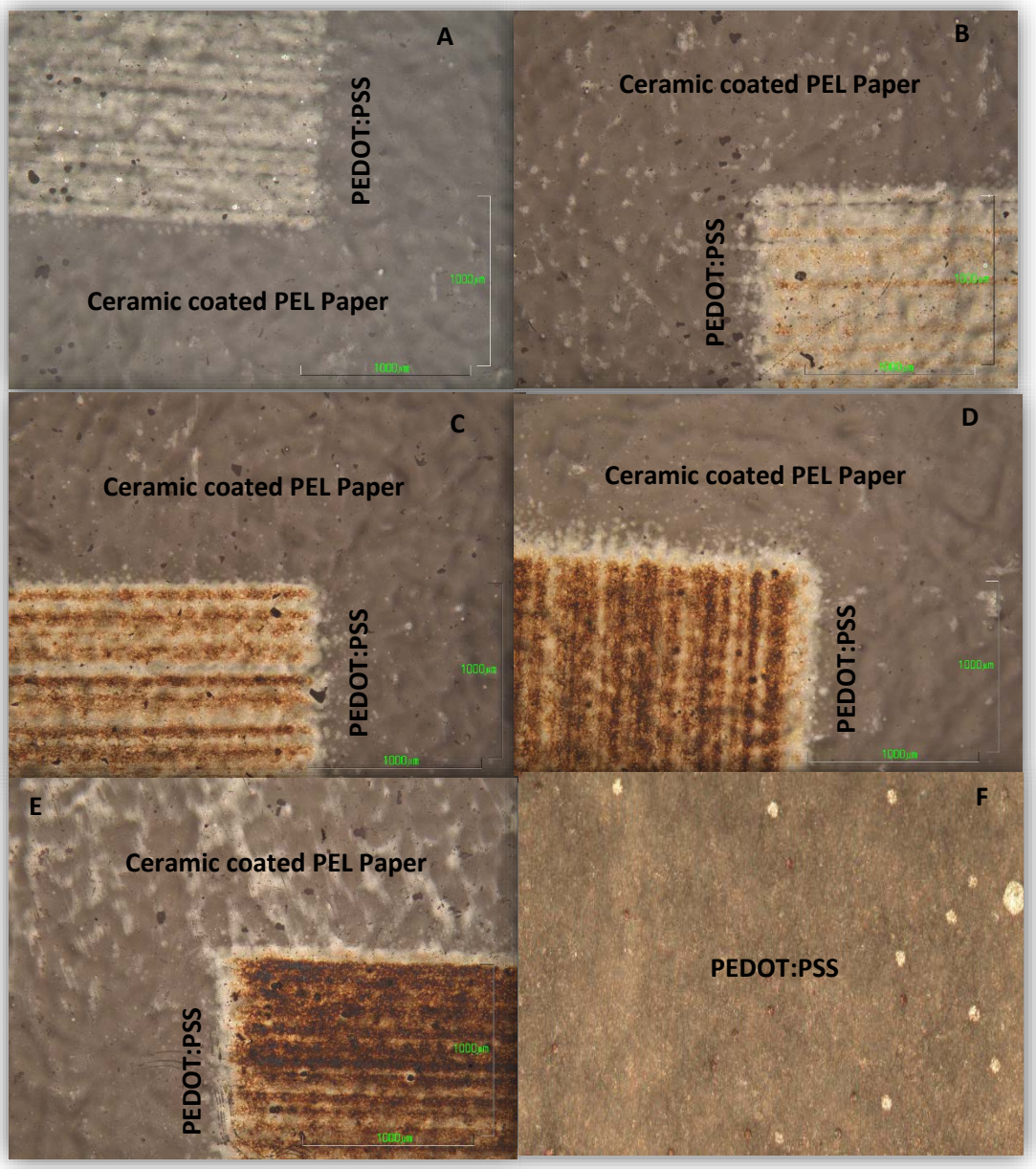

Figure 6.22: *optical microscope images of inkjet printed PEDOT:PSS layers on ceramic coated PEL paper; a) one layer, b) two layers, c) three layers, d) four layers, e)five layers and f) ten layers.*

Some samples (5 passes) were also investigated under higher magnifications using SEM both in a vertical (for a cross-section view) and a flat position (to evaluate the surface morphology of the layers) as shown in figure 6.23. Figure 6.23 a and b, where SEM with 100x and 500x magnifications respectively, are used the inkjet-printed PEDOT:PSS layers appear to be uniform, however, higher magnification (20k x) reveals the uniformity of the layers and this might be due to the porous surface of the ceramic paper.

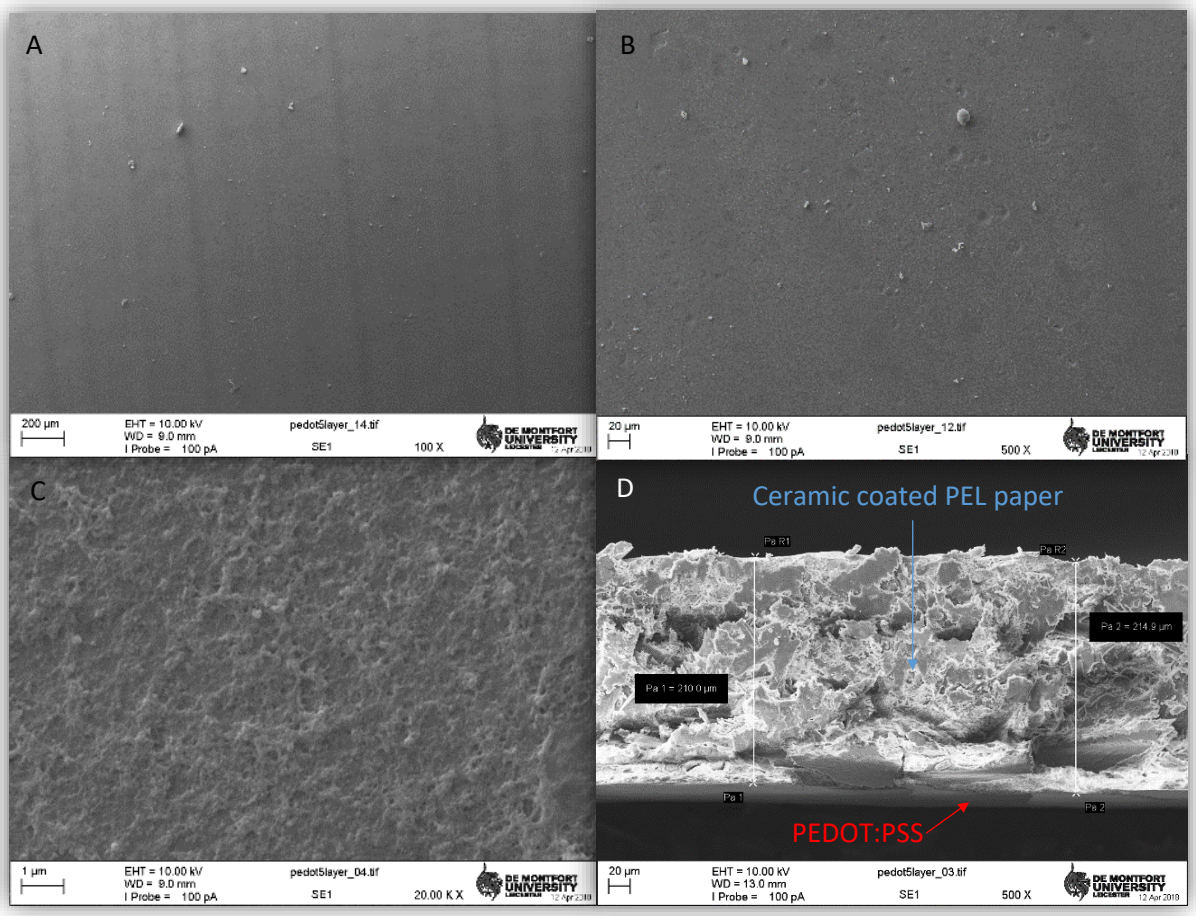

Figure 6.23: *SEM images of inkjet printed PEDOT:PSS (5 layers) on ceramic coated PEL paper; a) flat position, mag. 100 x, b) flat position, mag. 500x, c) flat position mag. 20k x and d) cross-section of paper and the PEDOT:PSS layers.*

The cross-section view (figure 6.23 d) shows the thickness of the paper (210-214 µm including the coating ceramic) with 20±2 µm layer attached to it which was expected to be the PEDOT:PSS thin film.

6.3.3.2 Electrical measurements

The electrical properties of the inkjet-printed PEDOT:PSS patterns (5 and 10 layers) were tested by two methods; 2-probe IV measurements and Van Der Pauw technique. The resistivity of the PEDOT:PSS ink used is 500-3000 Ω.cm (Supplier specifications).

In the IV measurements, a voltage was supplied to the 5-layer inkjet-printed PEDOT:PSS (maximum of 1 V), a very low current was passing through (in pico amperes) which means that the printed material has a significantly high resistance, the average calculated resistance from the 2-probe IV measurement method was 1 GΩ . The IV measurements of the 10-layer inkjet- printed PEDOT:PSS, on the other hand, presented much lower values of resistance approximately 50 MΩ. Both measurements were as exhibited in figure 6.24. The resistivity measurements based on the Van Der Pauw technique showed values of 0.2451×10^{-3}, 0.3524×10^{-3} and 0.3711×10^{-3} Ω.cm, these values are expected to be much higher.

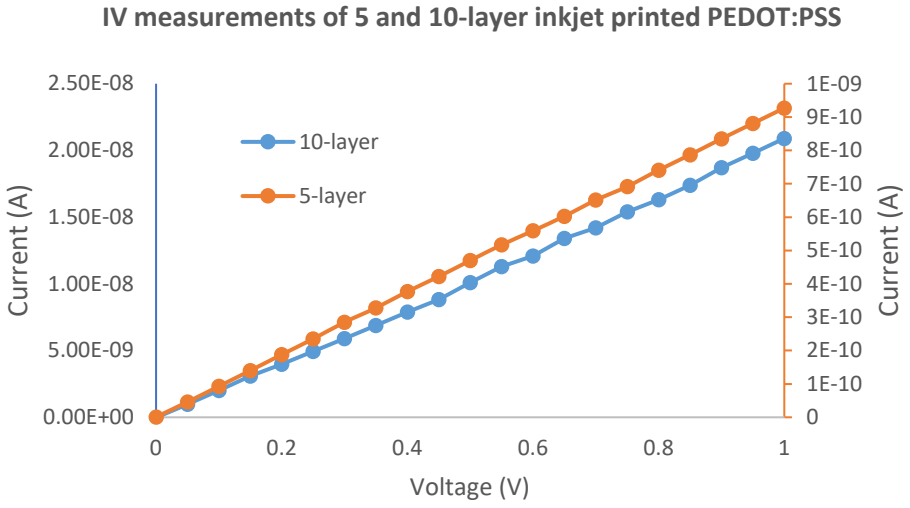

Figure 6.24: *IV measurement results of inkjet printed PEDOT:PSS (10 layers) on ceramic coated PEL paper.*

6.3.3.3 Mechanical stress (bending) test

The mechanical stress and bending effect on the 5-layer inkjet-printed PEDOT:PSS on ceramic coated PEL paper was tested to evaluate the resistance of the printed organic material to bendability and the structural strength of the inkjet-printed material.

Prior to commencing the test, the ceramic coated PEL paper surface behaviour was analysed using an optical microscope to estimate the effect they might have on the outcome of this test. Figure 6.25 shows images of the ceramic coated paper in different states; flat, smooth bending (approximately 45), and sharp bending (approximately 75°). It is observed that the surface of the paper has undergone some changes, especially, in the sharp bending, which might affect the printed material on it. Hence, this should be taken into consideration when performing the test.

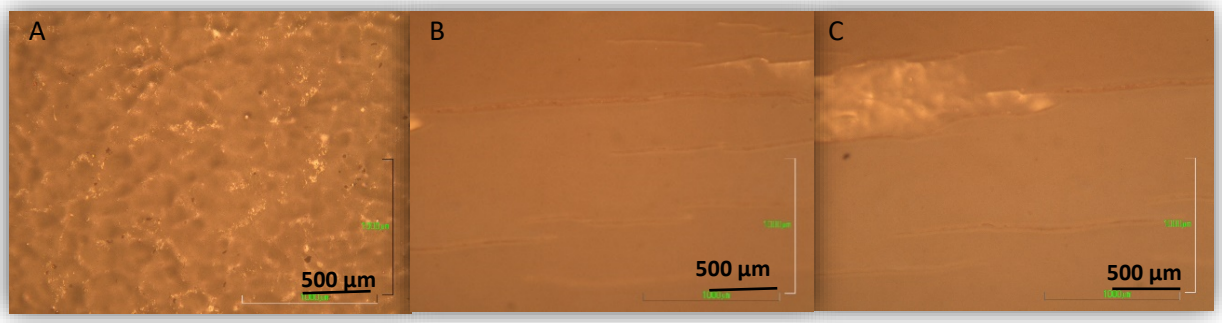

Figure 6.25: *optical microscopic images of the ceramic coated paper in flat state (a) and bending state; smooth (b) and sharp (c).*

Firstly, before performing the mechanical stress test, the surface of the sample was investigated using an optical microscope as shown in figure 6.26 to be as a reference for the test images. Then, a smooth bending (approximately 45°), as presented in figure 6.27, was carried out on the 5-layer inkjet printed (IJP) PEDOT:PSS on ceramic coated paper.

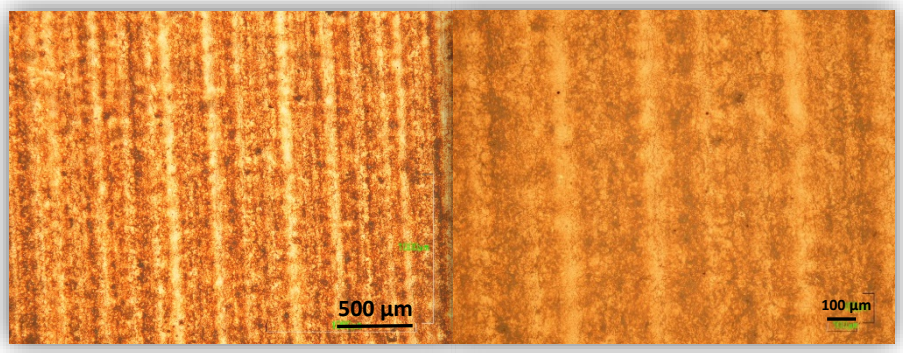

Figure 6.26: *optical microscopic images with different magnifications of inkjet printed PEDOT:PSS before performing the bending test.*

Figure 6.27: *photograph of smooth bending test set up on the IJP PEDOT:PSS.*

Having left the samples for 5 days, optical microscopic images were taken in two states; when the samples remained in the bending state and the other one when it was brought to a flat state. In the bending state, it is observed in all samples that the inkjet-printed PEDOT:PSS encountered small cracks and slight deformations as shown in figure 6.28. In the flat state, on the other hand, these cracks and deformations have disappeared and this might be due to the fact that the damage was too small so when the inkjet-printed PEDOT:PSS was straightened back to the flat position, it retained most of its shape (rejoined together) and the deformation could not be observed by an optical microscope and more sophisticated instrument is required. The thickness variations of the bent inkjet PEDOT:PSS along with small cracks and trivial deformations occurred caused visible colour changes as different levels of microscope light interference happened which resulted in different reflections.

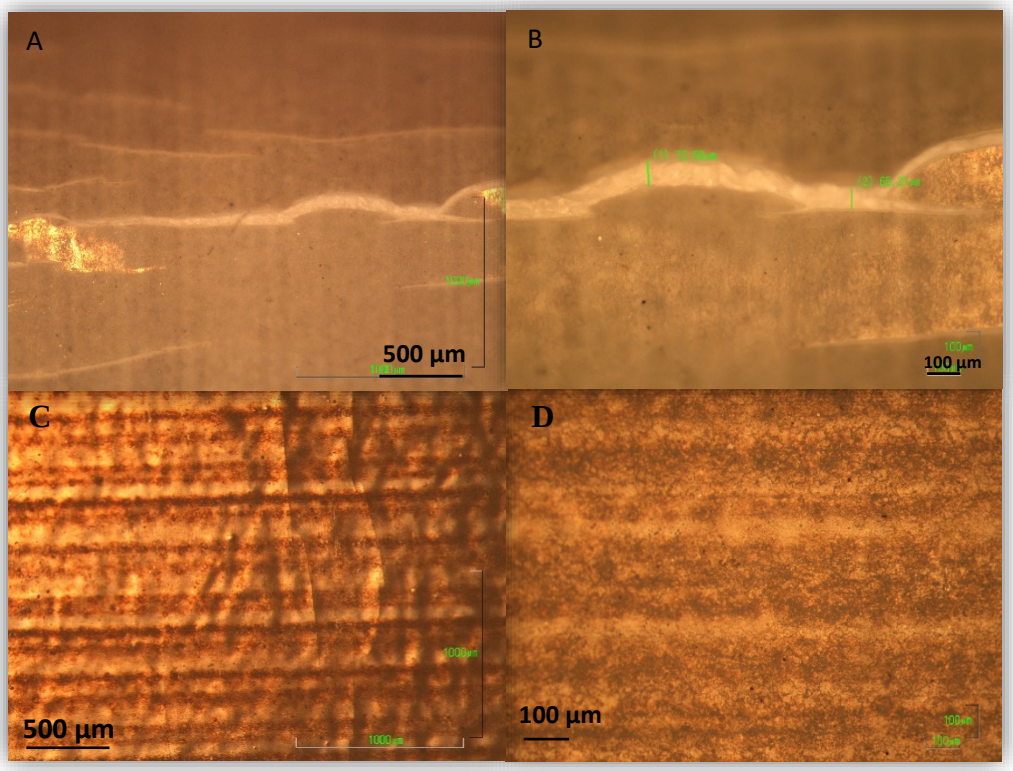

Figure 6.28: *optical microscopic images of IJP PEDOT:PSS after performing the smooth bending test when samples on the bending state a) and b) and in the flat state c) and d).*

To test higher mechanical stresses, a sharp bending (approximately 75°), as shown in figure 6.29, was performed on different 5-layer inkjet-printed PEDOT:PSS on ceramic PEL paper. Again, reference optical microscopic images were taken for the two samples prior to the test as seen in figure 6.30.

Figure 6.29: *photograph of sharp bending test set up on the IJP PEDOT:PSS.*

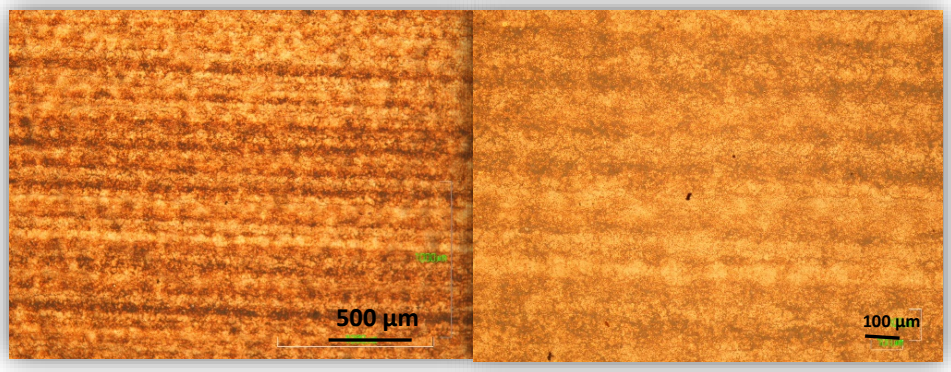

Figure 6.30: *optical microscopic images with different magnifications of inkjet printed PEDOT:PSS before performing the bending test.*

As been done in the smooth bending, the samples were left for 5 days before investigating the effect of the bendability over a long period. Both bending and flat states of the tested samples show some cracks in the PEDOT:PSS layers (as shown in figure 6.31) and this means that the inkjet-printed PEDOT:PSS might not be able to withstand strong mechanical stress and applications that include bending such as in flexible electronics. Having said that the ceramic coated paper might have affected the behaviour of the inkjet-printed PEDOT:PSS during this test, more investigations are required to come to a conclusion on whether the IJP PEDOT:PSS can stand high mechanical stresses or not.

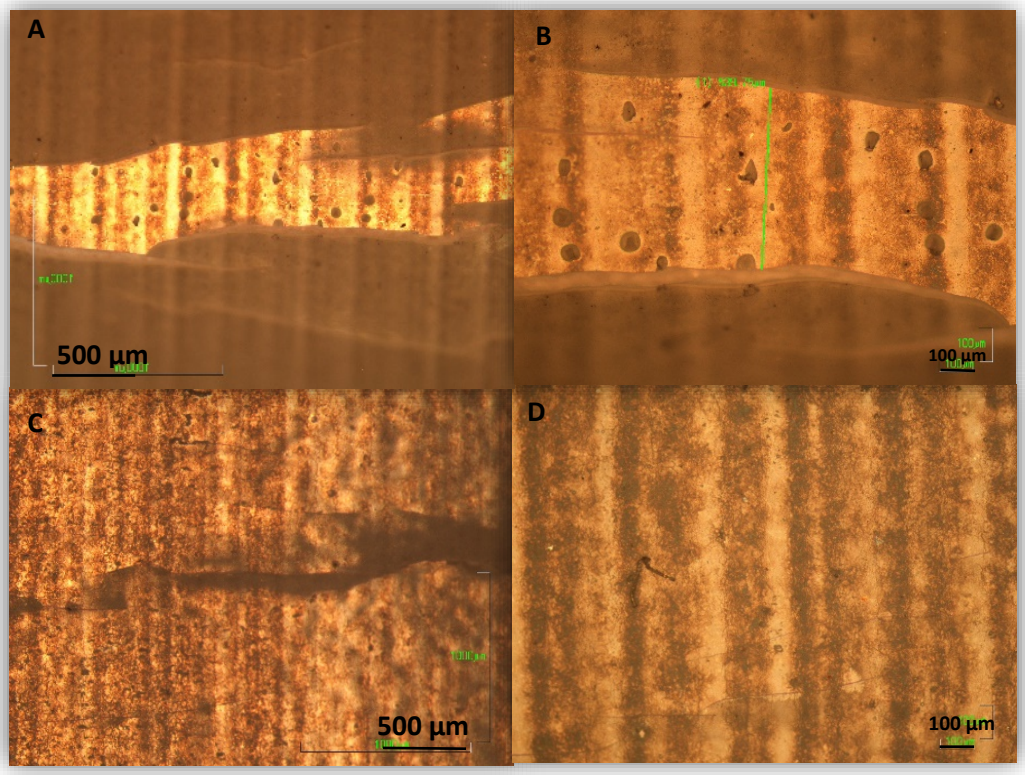

Figure 6.31: *optical microscopic images of IJP PEDOT:PSS after performing the sharp bending test when samples on the bending state a) and b) and in the flat state c) and d).*

6.3.3.4 Adhesion test

This test is not considered as the most precise test for the evaluation of adhesion as it is prone to human error susceptibility when applying and peeling out the tape, but it provides a general indication and understanding of the adhesion of a material to another material using a simple tool. This quick and easy test was aimed to provide a quick indication on how strong the inkjet-printed PEDOT:PSS layers adhered on the ceramic coated PEL paper.

Two samples were chosen to be investigated by this test; 1-layer and 5-layer inkjet-printed PEDOT:PSS both deposited on ceramic coated PEL paper. The first one was tested to evaluate the first layer adhesion strength on the surface of the ceramic coated paper while the second one to understand the effect of multiple PEDOT:PSS layers on the adhesion of all layers with the substrate`s surface and with each other.

The scotch tape (approximately 30 mm) was placed on areas where the PEDOT:PSS was deposited till the edge where the interface between the printed PEDOT:PSS and the PEL paper can be seen. To ensure good contact between the tape and tested material, gentle smooth pressure was applied along on the tape by hand/finger. Moreover, within a few seconds the tape peeling process started from that interface with a single but fast motion. The amount of tested materials visible on both the tape and substrate is the basic method when analysing the scotch tape adhesion test. So, as can be seen in figure 6.32, the 1-layer inkjet-printed PEDOT:PSS failed to survive the scotch tape test, especially, near the area where the tape was first pulled out/peeled where some parts of the printed PEDOT:PSS were removed from the sample and remained stuck to the tape. However, good adhesion and no traces of damage were observed at the bottom area where less pressure was applied during the tape removal. It can be concluded that unless high pressure is applied on the inkjet-printed PEDOT:PSS, it shows good adhesion to the substrate’s surface.

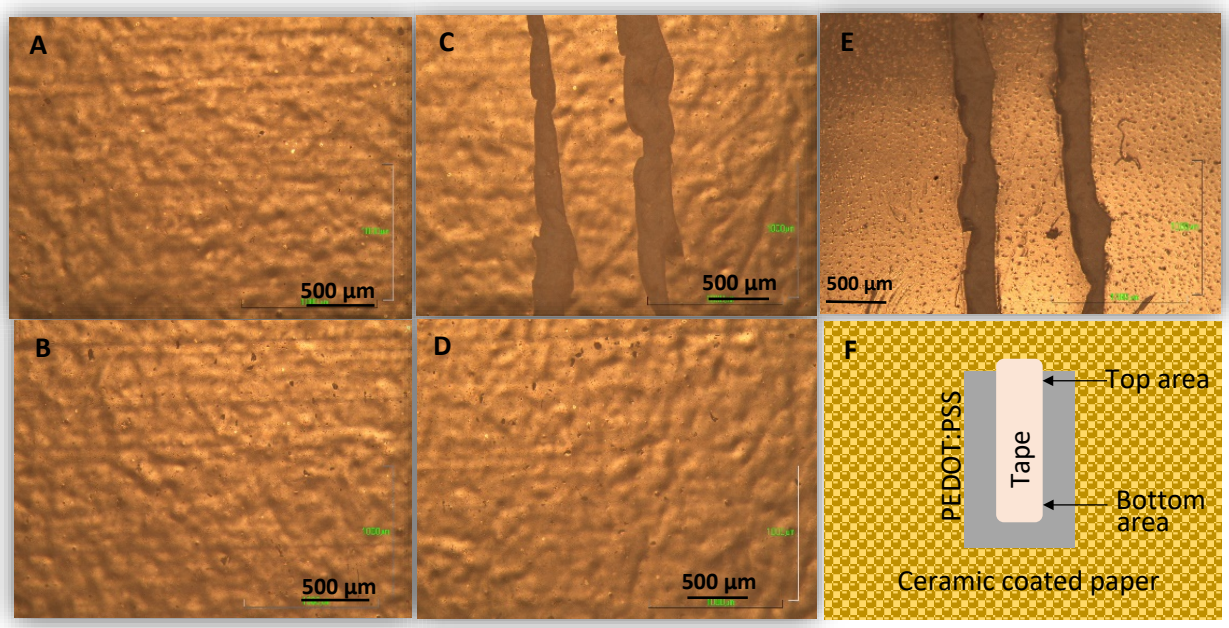

Figure 6.32: *optical microscopic images of IJP PEDOT:PSS (1 layer)* ***before performing the adhesion test;*** *a) top area of the layer and b) bottom area of the layer, and* ***after the adhesion test;*** *c) top area, d) bottom area and e) what remained in the tape. A schematic diagram showing the adhesion test set up.*

In the 5-layer inkjet-printed PEDOT:PSS scotch test, more parts of the patterned materials were removed both near and away from the starting of the tape removal points as noticed in figure 6.33. This can be attributed to the weak interconnection between the multiple layers of PEDOT:PSS and also with the surface of the ceramic coated PEL paper. Quick printing of the multiple layers can promote strengthening their adhesion to each other and the surface of the substrate.

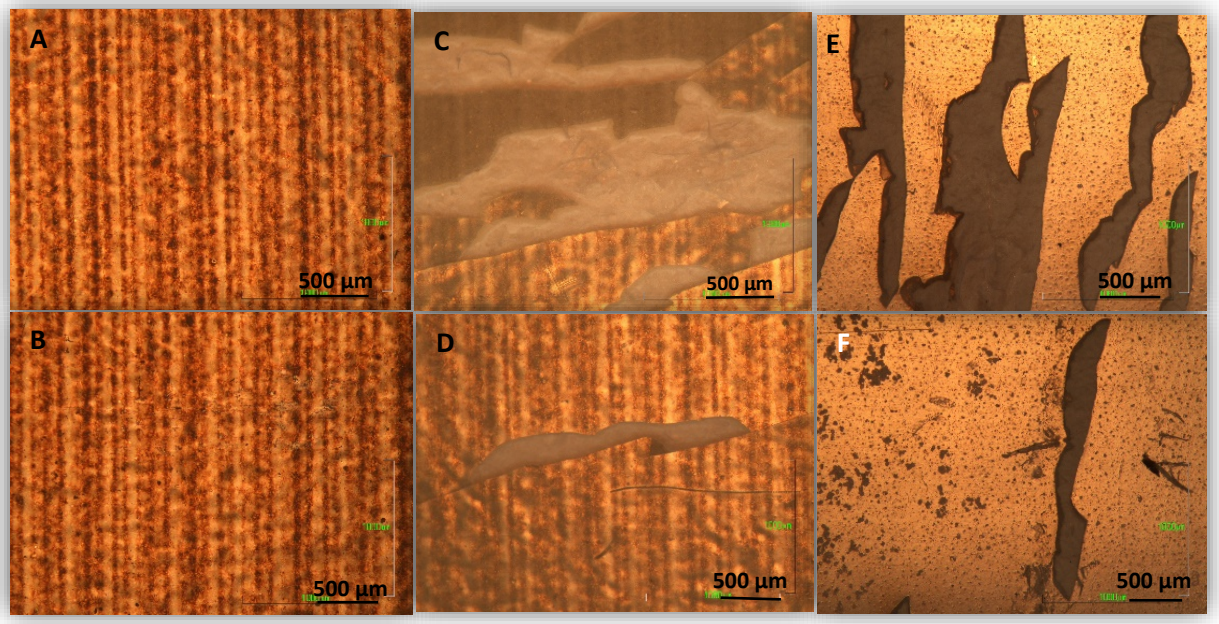

Figure 6.33: *optical microscopic images of IJP PEDOT:PSS (5 layers)* ***before performing the adhesion test;*** *a) top area of the layers of PEDOT:PSS and b) bottom area of the PEDOT:PSS, and* ***after the adhesion test;*** *c) top area, d) bottom area, e) what remained in the tape from top area and f) what remained in the tape from bottom area.*

When tape placed further to the edge of the printed PEDOT:PSS before covering the deposited PEDOT:PSS layers, more damage took place both in the top and the bottom areas of the PEDOT:PSS layers as shown in figure 6.34.

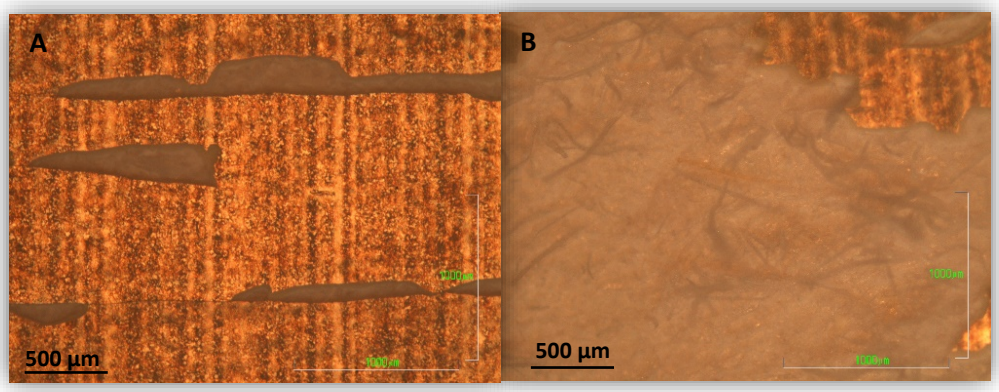

Figure 6.34: *optical microscopic images of IJP PEDOT:PSS (5 layers) after applying the adhesion test further to the edge of PEDOT:PSS before covering the deposited PEDOT:PSS; a) top area of the PEDOT:PSS layers and b) bottom area of the layers.*

Just for more information, figure 6.35 presents optical microscopic images for the a pure tape that was used in the adhesion test and the tape after performing the test on the ceramic coated PEL paper and it was observed that some materials were left on the tape which means that the adhesion between the coated ceramic layer and the surface of the paper was not strong enough and that might have affected the test results when applied on the inkjet-printed PEDOT:PSS on ceramic coated paper.

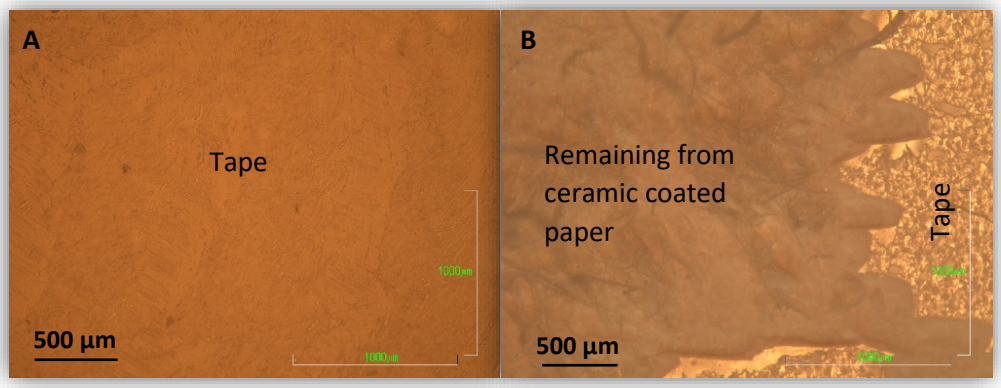

Figure 6.35: *optical microscopic images of; a) a pure tape that was used in the adhesion test and b) tape after performing the adhesion test on a ceramic coated PEL paper.*

6.3 Inkjet Printing (IJP) of Graphene Oxide

6.3.1 Background on the inkjet printing of Graphene Oxide (GO)

Graphene, as described by International Union of Pure and Applied Chemistry (IUPAC) [192] is a single carbon layer of the graphite structure, describing its nature by analogy to a polycyclic hydrocarbon of quasi-infinite size. It possesses some interesting properties including the high electrical conductivity, high thermal conductivity and high stiffness and strength (the mechanical stability). For these outstanding properties, the material has been widely studied and researched and has found applications in the field of electronics like in transparent conducting electrodes, gas sensors and the fabrication of transistors and organic solar cells [193]. Moreover, it has the ability to be an alternative to silicon in many electronic applications. Graphene has been extensively researched recently as a conductive ink for printed electronics as it is cheaper than some metals like gold (Au) and silver (Ag), not easily oxidised like copper (Cu), has much better dispensability than the widely used carbon nanotubes (CNTs) conductive ink and finally more conducive and thermally and chemically stable than the conductive polymer inks. Due to all these advantages, it has been employed in the fabrication of many electronic devices such as graphene supercapacitor electrodes [194] by inkjet printing of the ink of hydrophilic GO dispersed in water on Ti foils, flexible electric circuits and hydrogen peroxide chemical (H_2O_2) sensors [195] by means of inkjet printing of water-soluble single and few-layered graphene oxide ink on flexible substrates including paper, poly(ethylene terephthalate) (PET) and polyimide (PI). Graphene can be synthesised by different techniques such as chemical vapour deposition (CVD) and plasma enhanced chemical vapour deposition (PECEVD), these processes are considered to be quite expensive. Moreover, the inkjet printing of graphene is a cheaper alternative, some surfactants and dispersants used in the graphene ink for inkjet printing usually require high thermal treatment. The requirement a cost-effective alternative process formulating the ink for inkjet printing has led to the usage of some graphene

derivatives that have been derived from graphene including fluorinated graphene (fluorographene) and oxidised graphene (graphene oxide) (GO) which show similar properties to the graphene when they undergo some modifications such as reducing the oxygen from the graphene oxide. The latter (GO) can be synthesised cheaper than the graphene by chemically converting the graphite to GO. Graphene oxide (GO) has emerged and now considered to be one of the most popular materials that have graphene-based precursors due to low cost, simplicity and efficiency. GO is an electrical insulator because of the disruption of the sp^2 carbon-carbon bonding network by oxygen groups and the reduction of these groups is required to gain its electrical conductivity. The GO is easily dispersed in water and many other organic solvents which has made it widely used in the formation and deposition as inkjettable inks [196, 197].

6.3.2 PEL thermal inkjet printer

Here, a different inkjet printer, PEL Printing & Coating Platform from Printed Electronics Ltd, as shown in figure 6.36, was used to inkjet print the graphene oxide ink. This inkjet printing machine working principle is based on thermal printheads with a built-in controlled heating coating platform. The printheads are attached to motors that move them in x, y and z directions (3D). Moreover, it is interfaced with a packaged software which provides the control of many important parameters including the driving voltage, firing frequency, pulse width, the temperature of the substrate and the printheads (nozzles) locations in the three planes which play a major role in the ejection of the ink, the droplet formation and the evaporation of vehicle solvent as explained in chapter 5. One more advantage of this printer is that the printheads are integrated into the cartridge. However, the disadvantage of this type of printer is that the inability in printing inks with easily evaporated solvents as they might evaporate quickly before the ejection due to heating and block the nozzle because of the agglomeration of the particles

in the ink. Moreover, these kinds of built-in cartridges are usually designed for a single-use purpose which limit their usage and working time.

6.3.3 Testing the graphene oxide ink

The ink that was used here was purchased from Sigma Aldrich, graphene oxide (2mg/mL) dispersed in water. Prior to the inkjet printing process, the main properties of the ink were tested because they are crucial to achieve high-quality printed patterns as explained in chapter 5. These properties included the viscosity of the ink, the surface tension, contact angle and the pH. All measurements of each of these properties were carried out at least 3 times and an average amount was taken into consideration.

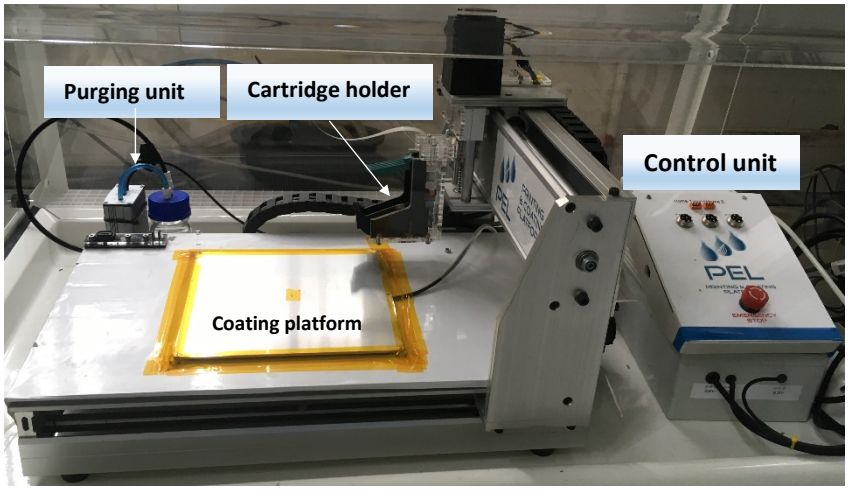

***Figure 6.36**: the main components of the PEL Printing & Coating Platform from Printed Electronics Limited.*

Firstly, the viscosity measurements were performed using a viscometer (Brookfield DV2T viscometer) and it was 14±2 cP at an angular velocity of 200 rpm and a shear rate of 264 in one minute. Then, tensiometer (Torsion Balance) was used to measure the surface tension of the ink which it was 46±2 mN/m while the pH was found to be 8.1±0.5 by using a pH meter. Finally, the contact angle and wettability measurements were carried out on PEL ceramic coated paper, glass, plastic coated with ITO and silicon substrates using a CAM200 KSV

NIMA goniometer and the results were 35°±2°, 26°±1°, 70°±3° and 66°±1° respectively. The contact angle of the GO ink with the substrate of interest (PEL paper) is 35°, as exhibited in figure 6.37, which is a promising value as it means that the ink wettability and spreading are good enough for the inkjet printing.

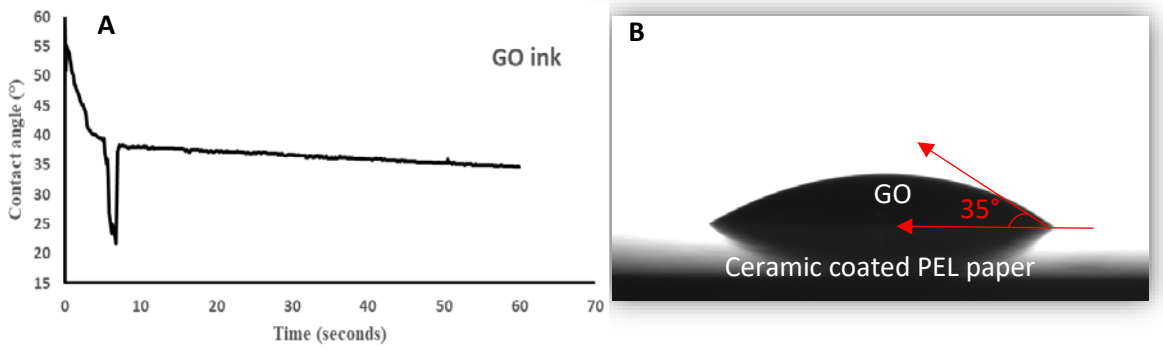

***Figure 6.37**: contact angle measurements of graphene oxide (GO) on ceramic coated PEL paper; a) the time that the droplet takes to settle down and b) an image shows the GO ink droplet making a contact angle of 35° with the paper.*

6.3.4 GO Printing

The only property here that causes some concerns for printing the GO ink is the viscosity of the ink which seems to be high for the thermal inkjet printing, however, by adjusting the driving voltage force to heat the ink through the heating element, firing frequency (FF) and pulse width (PW), the ink can be printed.

After testing the main properties of the ink, it was filtered to avoid the nozzle blockage then filled in the cartridge using a syringe. To determine the minimum and optimal parameters` values required to achieve a good quality deposition of graphene oxide patterns, different voltages 7-10 v, pulse widths (1-3.5 s) and firing frequencies (300-10000 Hz) were investigated.

It was observed that driving voltages less than 9.2 V resulted in poor depositions of the GO with all different values of other parameters. The ink started to be ejected out at voltages of 9.4

V and highest possible pulse width PW (3.5 s) and firing frequency (FF) of 10 kHz, however, the quality printed patterns was still not acceptable. Good depositions of the GO ink occurred at voltages 9.8 V and 10 V with max PW (3.5 s) and FF of 10 kHz and this might be due to the high value of the viscosity (high boiling point) of the ink which required higher threshold voltages for the heating element to generate vaporised bubbles to produce enough pressure for the ejection of the ink. Table 6.2 shows the optimal printing parameters for a good deposition of GO on ceramic coated paper.

***Table 6.2**: the optimal parameters for a good deposition of GO on ceramic coated paper. **Red:** successful deposition and **Green:** unsuccessful deposition.*

		Pulse width (s)		Firing Frequency (Hz)	
		1-3	3.5	300-1K	10K
Voltage (V)	7-9.2				
	9.4-10				

Therefore, these values of the parameters were chosen to be used for printing the desired GO patterns. The x and y planes of the desired patterns were both set to be 10 mm, 1-3 layers of the GO ink were inkjet printed on heated (60°C) PEL paper to advance the evaporation rate of the water, as shown in figure 6.38, and glass substrates. The printed GO structures were then cured at 100°C to help evaporate the ink carrier (water) before being investigated by means of an optical microscope for visual characterisation, a digital multimeter for electrical measurements and a tape test for adhesion investigation.

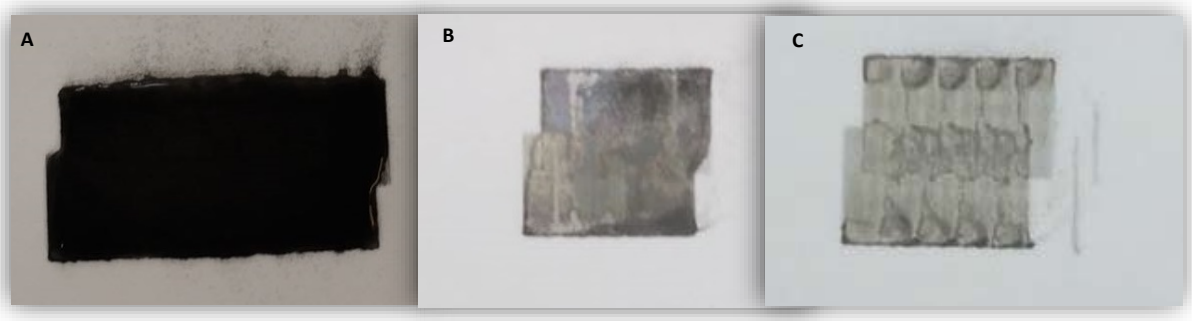

***Figure 6.38**: photographs of inkjet printed graphene oxide on PEL paper; a) 3 layers, b) 2 layers and c) 1 layer.*

6.3.5 Results and Discussion

The quality of the inkjet-printed layers of the graphene oxide was assessed by means of optical microscope (Nikon LABOPHOT-2 optical microscope, fitted with Nikon Camera DS-Fi1), while the electrical property was simply investigated by a digital multimeter.

6.3.5.1 Optical microscope imaging the inkjet printed GO

The inkjet-printed graphene oxide (1 layer, 2 layers and 3 layers) on ceramic coated paper were initially visually investigated by an optical microscope, both at the edge of the printed layers and in the centre where only GO deposition can be observed.

Figure 6.39 (a) shows the edge of 1-layer printed GO pattern where the paper substrate can be seen as well, the different colours of the deposited GO due the light interferences exhibit huge changes of the thickness of the material and that leads to poor uniformity of the printed layer which might be because it is the initial printed layer (first droplets effect) and more layers are required to form a uniform smooth surface. Moreover, the centre area of the printed GO, as exhibited in figure 6.39 (b), presents slightly more uniform (still different thicknesses appeared) film. The 2-layer inkjet printed GO shows similar results and behaviour to the 1-layer patterns as shown in figure 6.40 (a) and (b). The 3-layer printed GO, on the other hand, presents a smooth uniform and consistent layer of the printed material and this can be observed by the only one colour reflected back to the optical microscope from the deposited GO as depicted from figure 6.41 (a) and (b). It can be concluded that the GO requires more layers to be printed to have more uniform and homogenous surface and thickness as the paper has a rough porous surface and the first printed particles try to fill the porous surface and more particles required to create a uniform layer.

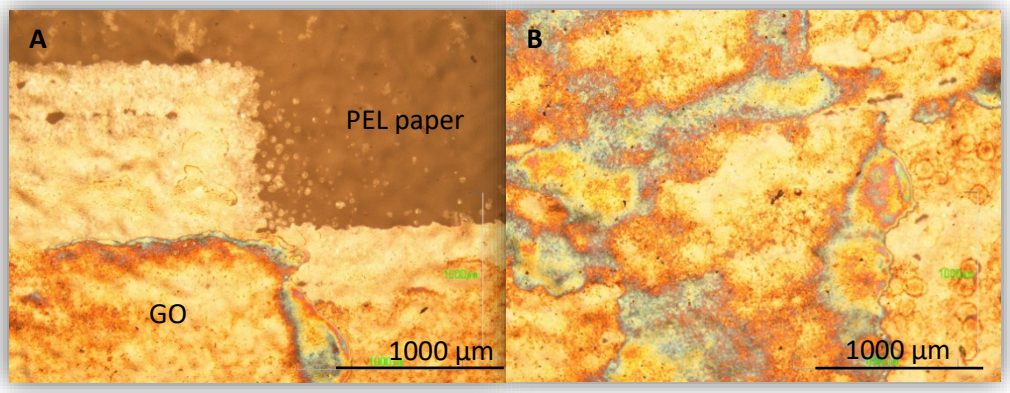

Figure 6.39**:** *optical microscope image of 1 layer of printed graphene oxide; a) at the edge (printed GO and paper) and b) in the centre of the printed GO.*

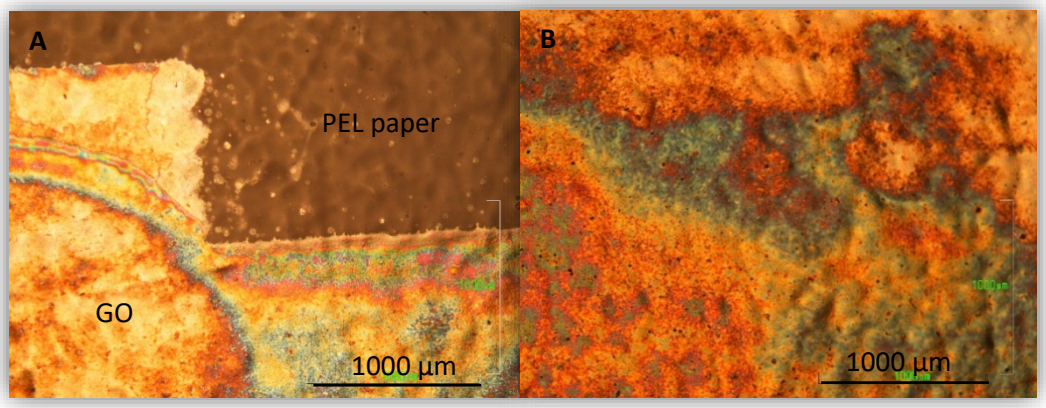

Figure 6.40**:** *optical microscope image of 2 layers of printed graphene oxide; a) at the edge (printed GO and paper) and b) in the centre of the printed GO.*

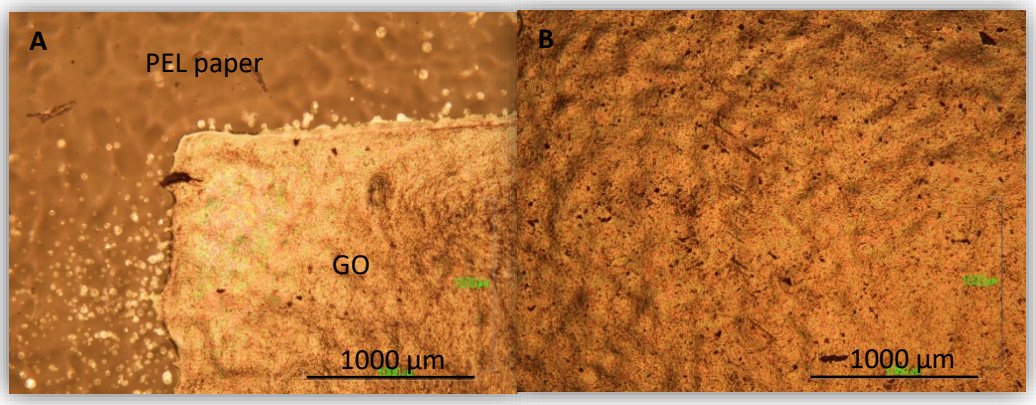

Figure 6.41**:** *optical microscope image of 3 layers of printed graphene oxide; a) at the edge (printed GO and paper) and b) in the centre of the printed GO.*

6.3.5.2 Electrical measurements

The resistance of the inkjet-printed graphene oxide on the ceramic coated paper was tested by using a simple digital multimeter (DM) set up to provide a quick indication. It is known that

the 4-probe set provides a more accurate evaluation of the electrical resistance and resistivity of the printed patterns, however, quick evaluation and simple set up were required at this stage.

The measurements were performed at several locations on all three samples, 1 layer, 2 layers and 3 layers of GO. The average measured resistances for the three substrates can be seen in table 6.3. These values are higher as expected, due to GO being an electrical insulator and the resistance might be reduced by higher curing temperature for the reduction and removal of more oxygenated functional bonds (groups) of the graphene oxide [198].

Table 6.3: *the average measured resistance values of 1-layer, 2-layer and 3-layer printed graphene.*

GO resistance/layers	***1 layer***	***2 layers***	***3 layers***
Resistance (MΩ)	***3.1***	***3.5***	***2.1***

6.3.5.3 The adhesion test

This test provides a quick and simple evaluation of the adhesion of the printed material layers both with each other and with the substrate.

The tape test was carried out on the 3-layer inkjet printed GO on ceramic coated paper. Three locations of the printed GO pattern were chosen to be investigated by an optical microscope; bottom (away from where the tape is initially removed), the centre (in the middle of the deposited material) and top (closer to the tape removal initial point). The optical micrograph images in figure 6.42 (a, d and g) of the results of the adhesion test revealed a relatively good adhesion between GO layers and the ceramic coated paper and within the layers themselves, especially, at the bottom areas.

In contrast with the centre and top areas, the adhesion was not as good as the bottom area and some of the GO layers broke and stuck to the tape, as presented in figure 6.42 (e, f, h and i) while others where all the ceramic coated layer on paper and the GO layers, were entirely removed as can be seen in figure 6.42 (e) where the paper surface can be clearly observed. This

might be because more pressure was applied at the beginning of removing the tape from the printed GO. Moreover, the adhesion between the coated ceramic layer and the paper might not be strong enough in the first place.

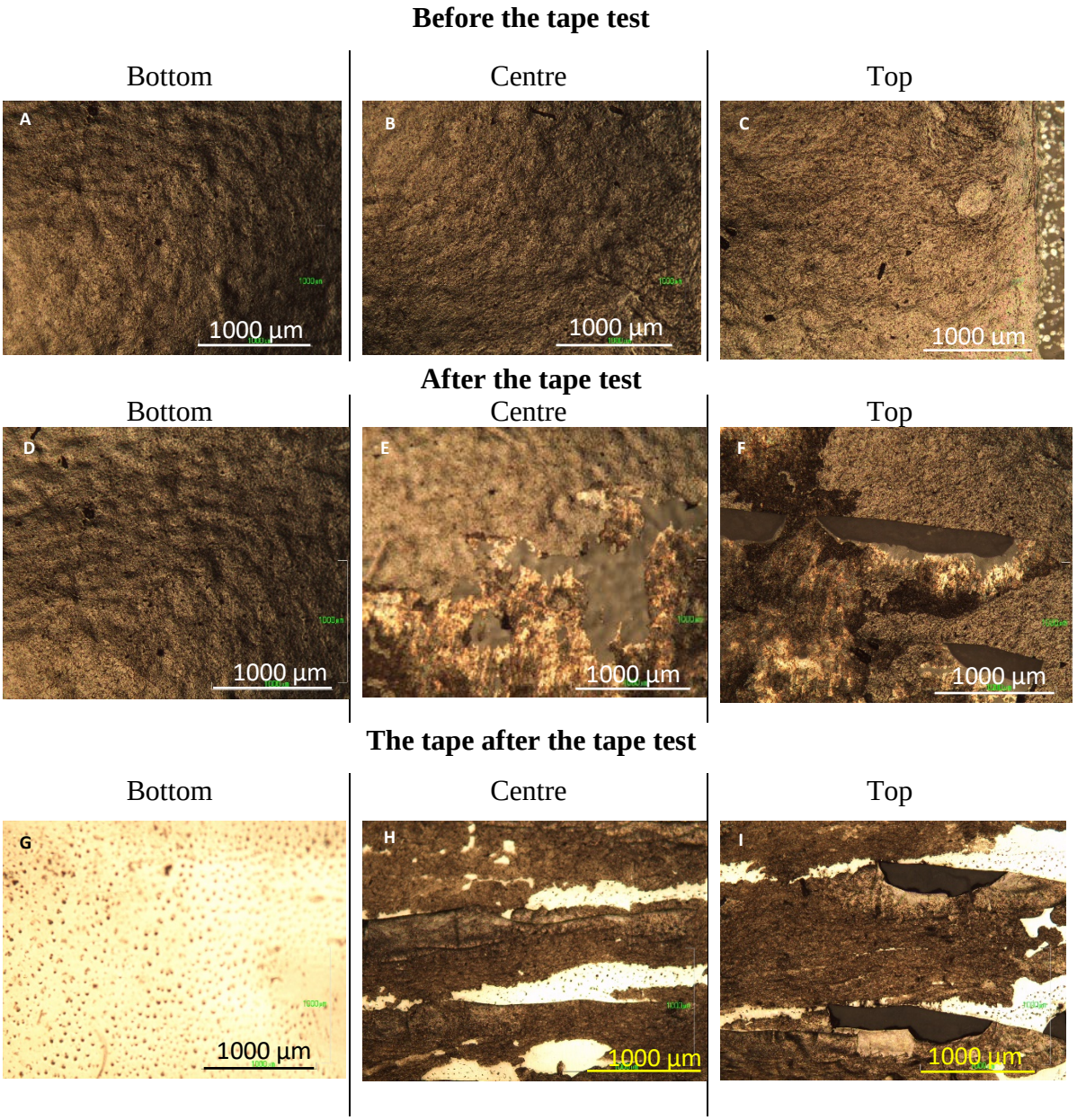

Figure 6.42: optical microscope images of the 3-layer printed GO; before the tape test (a, b and c), after the tape test (d, e and f) and the tape itself after the test (g, h and i).

3.6.6 Conclusion

Inkjet printing of GO was investigated using a thermal inkjet printer; PEL Printing & Coating Platform. Inkjet printer parameters including driving voltage, pulse width and firing frequency were investigated to obtain good deposition of GO. Voltages ranging from 9.8-10, a pulse width of 3.5 s and a firing frequency of 10 kHz were found to be the optimal printing parameters to inkjet print GO on ceramic coated paper. It was concluded that printing more GO layers resulted in uniform smooth surfaces and reduction in electrical resistance. This could be good for some applications including active layers for memory devices as the one explained in chapter 7. However, PEDOT:PSS was selected in this research work to be used as an active layer for the novel memory device for two main reasons; first, inkjet printing of PEDOT:PSS ink was easier without any modifications for the parameters of the printer and secondly, it was much cheaper than GO ink.

Chapter 7: An Application of Inkjet Printing in the Fabrication of Functional devices; Fully inkjet Printed Two-Terminal Flexible Memory

In this chapter, a novel innovative electronic device, that was fully inkjet printed by using the functional inks that have been discussed in details in the previous chapters, will be discussed as an application of inkjet printing in the fabrication of functional devices.

A commercial desktop piezoelectric inkjet printer was used to fully inkjet print information storage cells, specifically, two-terminal memory cells, on a flexible substrate; ceramic coated PEL paper. All the elements of these electronic memories were deposited by using the abovementioned inkjet printer at room temperature. To the best of our knowledge, this kind of full deposition of all elements of these types of electronic devices on ceramic coated paper using an ordinary commercial inkjet printer has not been reported.

7.1 Introduction

Organic memory devices are electronic memories that have an active organic material fabricated generally in a cross-bar structure where it is sandwiched between two inorganic electrodes as shown in figure 7.1. The electrodes are usually deposited using thermal evaporation and physical vapour deposition, while spin and dip-coatings have been the most widely used deposition techniques for the active material. When applying a voltage across the electrodes, the conductivity, caused by the nanoparticles (NPs) or molecules in the active materials, changes allowing storage of data (charge trap in the NPs/molecules) to take place. The data storage states switch between high and low states in response to the polarity of the applied voltage [199, 200]. For more information on organic memories, one can look at [201].

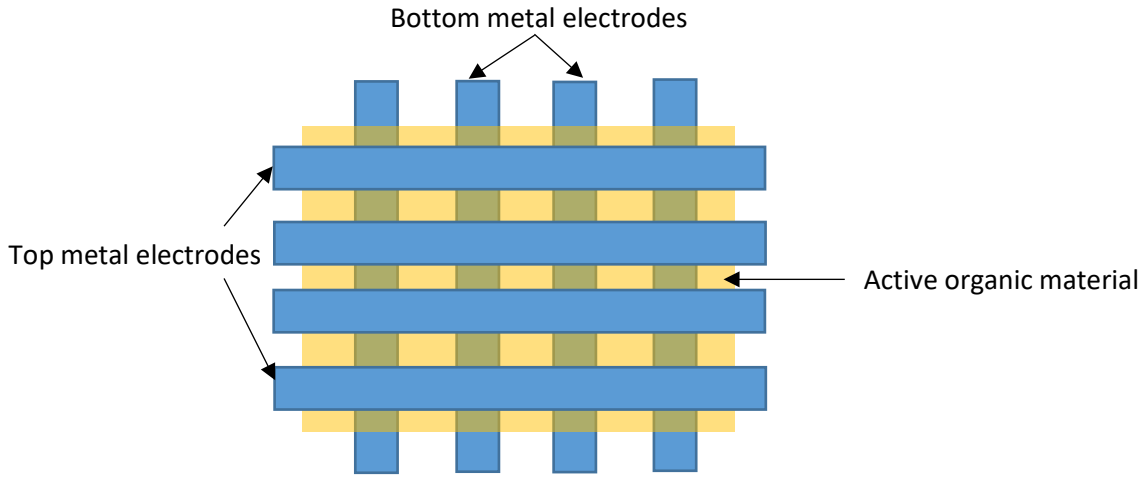

Figure 7.1: schematic diagram of an organic memory device.

In most of the current manufacturing processes of thin films, which are used in the fabrication of electronic memory devices, using conventional techniques as well as the usage of the materials in the process, the storage and the protocol system of disposing of waste materials is of a huge consideration. Moreover, heat generation is required in these thin-film fabrication techniques which might lead to the production of some chemicals and radiations that can be wasteful and harmful to the human being and the environment not to mention the amount of

the energy they are wasting during the process. All these have raised awareness among environmentally friendly researchers and scientists who they have been searching for alternative pathways and strategies for a cheap, environmentally friendly deposition of the thin films. One of these alternatives is an additive layer manufacturing technique; inkjet printing technology which is one of the most reliable environmentally friendly alternative techniques to the conventional manufacturing method of thin films. The contactless technique has been employed in the deposition of a wide range of organic and inorganic thin films on rigid and flexible substrates as mentioned in the previous chapters. This cost-effective technique is undoubtedly able to revolutionise the electronic manufacturing and industry with the broad selection of materials and the fabrication step as well as the design and the configuration of the electronic devices. There have been some studies employing this technology for the fabrication of electronic memory devices. One of which, is the inkjet printing of some components of resistive memory cells [190] previously mentioned in section 6.2.1. Furthermore, a metal/insulator/metal memristor based on graphene oxide as an active layer was reported [202], and the metal contacts for this device was deposited using a conventional thermal evaporator, while the active layer was deposited by means of inkjet printing.

In this work, the inkjet printing technology was explored to produce an innovative pathway in the fabrication of electronic devices; information storage cells on flexible substrates, seeking to fabricate and characterise a state-of-art novel fully inkjet-printed two-terminal memory cells (devices) on ceramic coated PEL paper using a commercial desktop printer at room temperature. All components (metal electrodes and the core element) of the memory cell structure (metal/active layer/metal) were fully deposited by inkjet printing. The elements (silver (Ag) electrodes and PEDOT:PSS active layer) of this memory were inkjet printed using an Epson Stylus P50 inkjet printing machine, the individual inkjet printing and characterisation of these elements was discussed in details in chapter 6. The quality of the inkjet-printed devices

was initially assessed by Nikon Labophot-2 optical microscope, fitted with Nikon camera DS-Fi1. Moreover, the electrical characterisation of the fabricated memory devices was preformed in-depth using HP41140B picoammeter.

7.2 Inkjet printing of the memory device

A commercial desktop piezoelectric Epson Stylus P50 inkjet printer was used to manufacture the two-terminal electronic memory devices (cells). Full structures (metal/active layer/metal) of the memory cells were solely deposited on ceramic coated PEL paper (Printed Electronics Ltd.). Two kinds of functional material inks were inkjet printed: firstly, a conductive ink; a nanoparticle silver (NPs Ag) ink from Printed Electronics Ltd. This ink has a viscosity of 6 cP at a shear rate of 200 rpm and a surface tension of 35 mN/m, it was used to fabricate both the top and bottom electrodes of the memory device. Secondly, a PEDOT:PSS (Poly(3,4-ethylenedioxythiophene)-poly(styrenesulfonate) ink from Sigma Aldrich with a viscosity of 14 cP at a shear rate of 200 rpm and a surface tension of 34 mN/m was inkjet printed to deposit the memory active core. In order to obtain a good wettability of the ink droplets on a substrate, the surface tension of the ink has to be at least 10-15 points lower than the surface energy of the used substrate [144]. The substrate that was used here is a ceramic coated PEL paper which has a surface energy of 50 mN/m [203] whereas the NPs Ag and PEDOT:PSS inks have lower surface tensions of 35 mN/m and 34 mN/m respectively, as presented in table 7.1 along with the number of printed layers (passes) to obtain the required conductivity, curing temperature and time. Table 7.2 presents the contact angles for Ag ink with cured 10-layer PEDOT:PSS ink and the PEDOT:PSS ink with cured 10-layer Ag ink. All these measurements were performed using a CAM200 KSV NIMA goniometer (Biolin Scientific, Sweden). The contact angle value of Ag droplets on cured PEDOT:PSS was 17°±2° while the contact angle of PEDOT:PSS ink droplets with the cured silver was observed to be 70°±5°. These values indicate a good spreading behaviour of the inks to each other and on the used substrate. Contact angle values

were provided for both sides of the droplet, however, the average value was considered. The contact angle measurement usually provides an initial high value at the first impact (contact) of the droplet before a lower level of wetting is achieved after 1s [204]. The contact angles of the silver and PEDOT:PSS inks with the ceramic coated paper, on the other hand, were discussed before in sections 6.1.2 and 6.2.2).

Table 7.1: *some physical and technical description of the used inks/process.*

Ink	Surface tension (mN/m)	Viscosity (cP)	Number of passes	Curing temperature and time
NPs Ag	34±1	4±2	4 (minimum)	120°C- 5 min
PEDOT:PSS	33±2	14±2	10 (minimum)	70°C- 3 hrs

Table 7.2**:** *the contact angle measurements of Ag and PEDOT:PSS inks with PEL paper, cured multi-layer Ag and PEDOT:PSS inks.*

	PEL paper	Cured Ag (10 layers)	Cured PEDOT:PSS (10 layers)
Ag ink	38°±2°		17°±2°
PEDOT:PSS ink	29.5°±0.5°	70°±5°	

It is worth mentioning that all inks were ultrasonically stirred for approximately an hour prior use to ensure a homogeneous ink and then filtered using 5 μm filters to remove larger particles that might block the printhead nozzles (nozzle clogging).

7.3 Characterisation of the inkjet printed device

The quality of the printed layers was assessed by Nikon LABOPHOT-2 optical microscope, fitted with Nikon Camera DS-Fi1. Electrical characterisation of the fabricated memory cells, including the current-voltage (I-V) measurements, write-read-erase and retention time behaviour were performed using an HP4140B Picoammeter.

7.4 Results and Discussion

Having tested all the main properties of the used inks and after establishing the printing requirements for each element of the electronic memory cell, the first inkjet-printed material to be fabricated for this memory cell was conducive tracks (1mm width electrodes). The

nanoparticle silver ink was used to print the bottom as well as the top electrode (later). As discussed in chapter 6, it was observed that printing few layers (less than four passes) of the NPs Ag ink will result in no electrically conductive deposited patterns due to the fact that printed NPs Ag droplets are still separated and isolated and hence, they do not form a continuous path for the electrons. Increasing the number of the prints (printed layers), more number of droplets will be deposited and they connect with each other which leads to the formation of conductive inkjet printed silver tracks. Figure 7.2 presents inkjet printed NPs Ag ink with different passes.

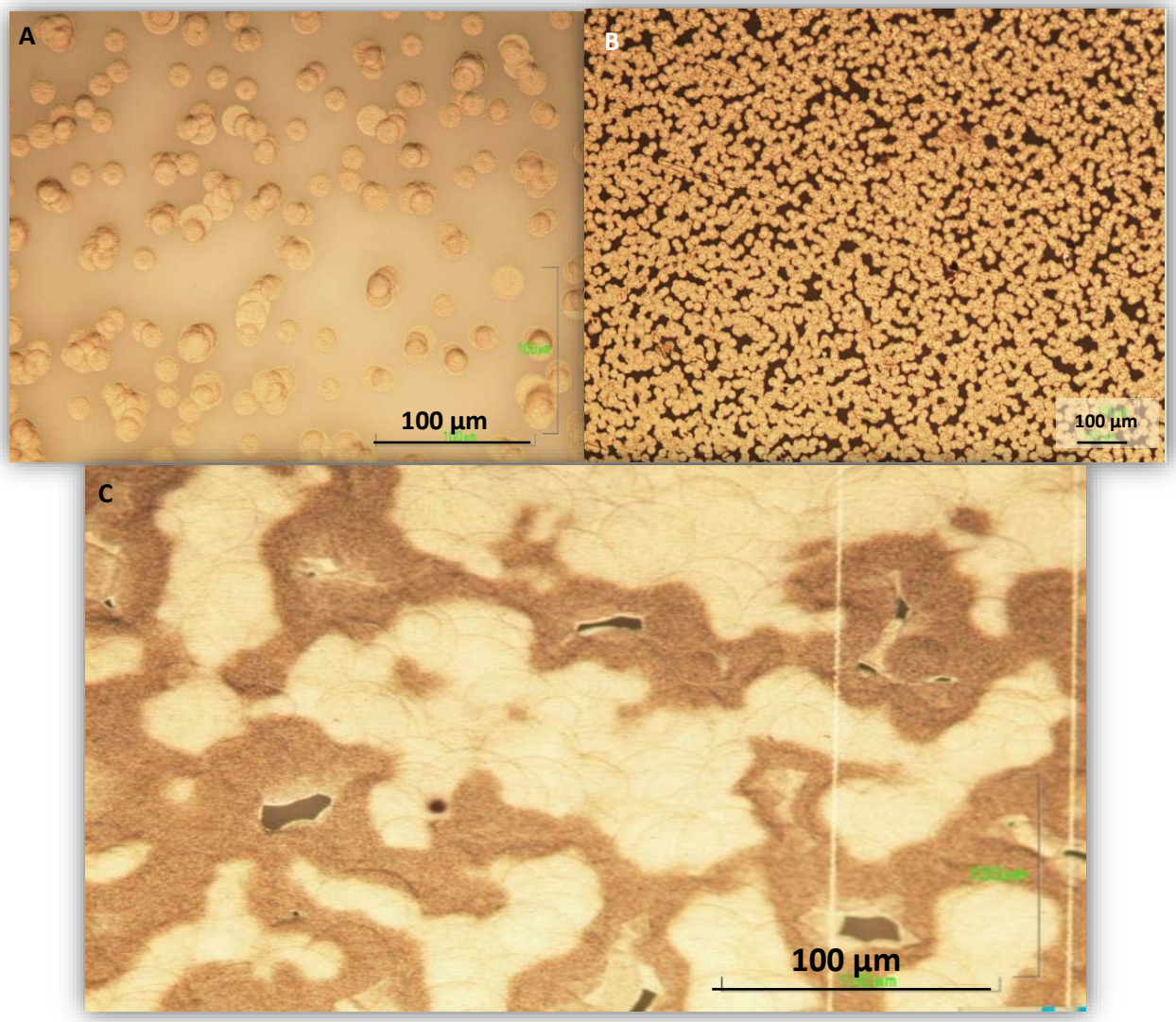

Figure 7.2: *Optical micrograph images of inkjet printed NPs Ag pattern (a) one pass, (b) 5 passes and c) 10 passes.*

An in-depth characterisation of the electrical conductivity of the silver electrodes was discussed in chapter 6. Therefore, in order to achieve the required conductivity and quality, four or more printing passes were performed and then the inkjet-printed silver electrodes were subjected to curing at 120°C for five minutes. Ten layers of PEDOT:PSS active component were inkjet printed on the top of the bottom silver electrode, ten prints (passes) were chosen to ensure a continuous uniform film of the printed layers of PEDOT:PSS. These PEDOT:PSS layers act as an active layer for the proposed memory cells. Then, the PEDOT:PSS printed layers were cured at 70 °C for 3 hours. The curing procedure was carried out for all inkjet-printed elements of the memory device, with the main scope to evaporate the solvents, improve the uniformity and hence enhance the conductivity. To finalise the crossbar structure of the printed memory device, the top Ag electrodes (1 mm width) were deposited perpendicular to the bottom electrodes and onto the active layer. Figure 7.3 shows a fully inkjet-printed Ag/PEDOT:PSS/Ag memory cell.

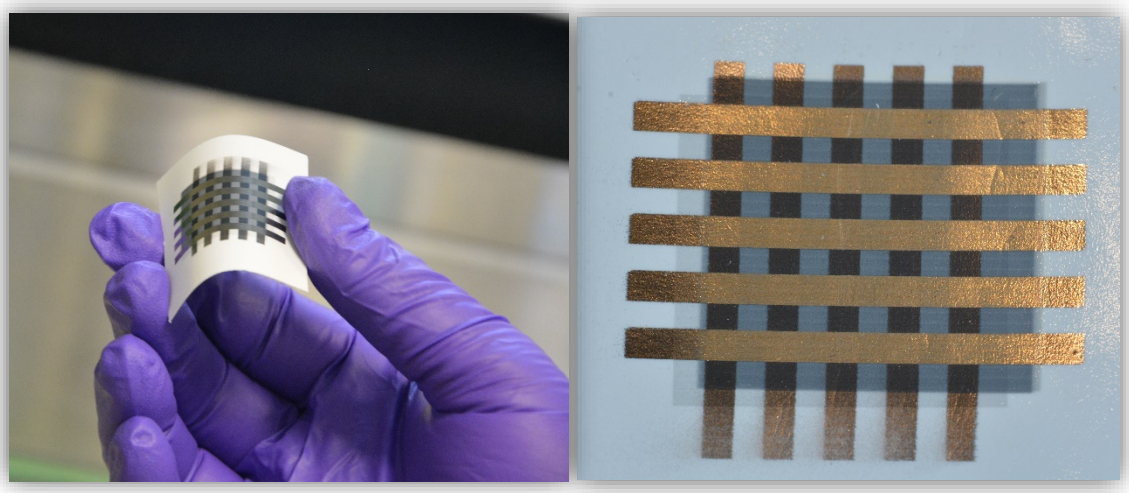

Figure 7.3: photographs of the fully inkjet printed 1mm x1 mm crossbar-type memory cell.

The typical current-voltage (I-V) behaviour of the (Ag/PEDOT:PSS/Ag) memory device is shown in figure 7.4.

.

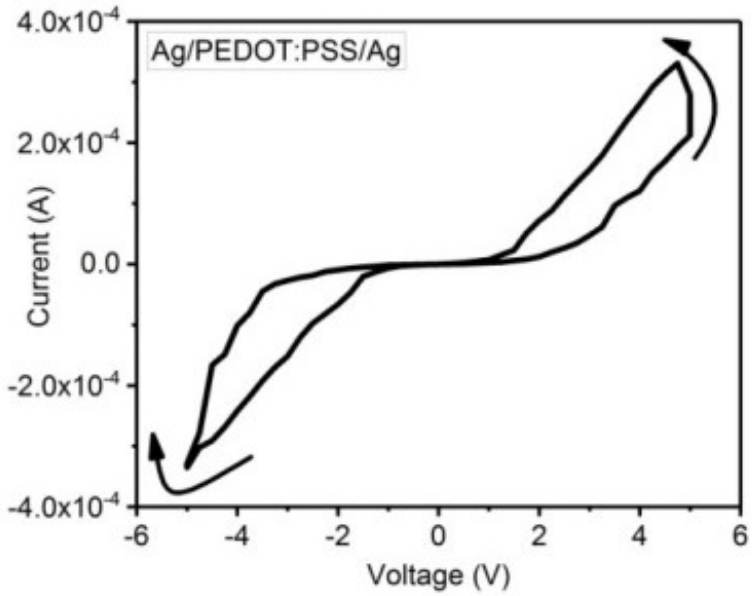

Figure 7.4**:** *Current-Voltage (IV) characterisation of (Ag/PEDOT:PSS/Ag) memory cells, the hysteresis behavior in the measurement suggests a memory behaviour.*

The memory device is originally in a high resistance state (HRS), however, a low resistance state (LRS) is obtained when the sweeping voltage bias approaching V_{SET} = 5V. Reversing the polarity of the voltage causes the device to switch back to initially HRS. As illustrated in figure 7.5, the inkjet-printed device shows a bipolar switching, with HRS and LRS attained after the device was biased with positive SET and negative RESET voltages, respectively.

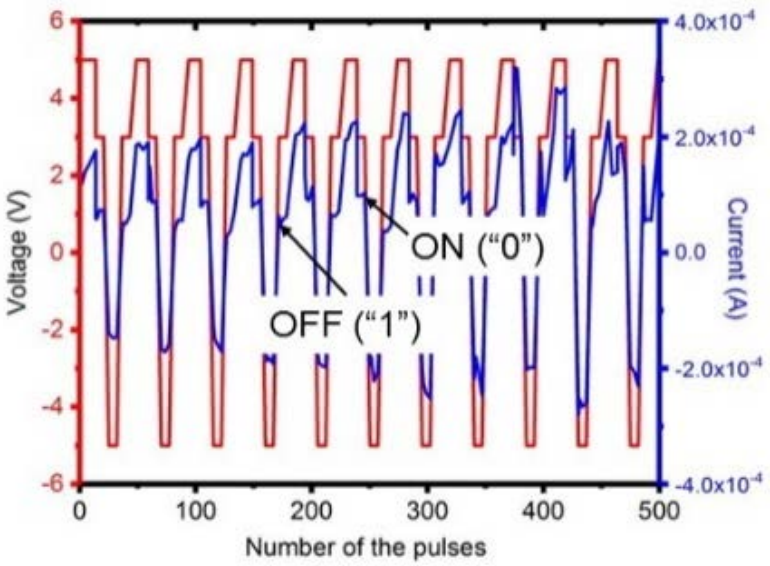

Figure 7.5**:** *Read-Write-Erase (RWE) characteristics of an Ag/PEDOT:PSS/Ag memory cell.*

The bipolar behaviour, the electrical switching between the two conductive states for the inkjet-printed memory cells, was further investigated by write-read-erase-read voltage cycles as presented in figure 7.5. The memory devices were switching between low and high conductivity states when the SET/Write pulse (5 V) was applied. These conductivity states were recorded by applying the Read pulse (3 V). The Read voltage was selected to be the point of greatest hysteresis in the I–V curve. Then, by applying a (-5 V) pulse, the stored data (information) was completely erased. The difference between the ON and OFF conductivity states is approximately 30 μA.

Moreover, the inkjet-printed memory retention time was also investigated. A single device was subjected to a SET voltage of (5 V) and (1 ms) width to allow programming the memory cells in the LRS. Furthermore, the low resistive state (LRS) was evaluated at (3 V), a low voltage which does not disrupt the state (0) or (1). After 1000 reading pulses, the inkjet-printed memory device was switched to high resistive state (HRS) by applying a pulse of (-5V/1ms) and then this state was assessed. As can be seen in figure 7.6, the printed (Ag/PEDOT:PSS/Ag) memory device exhibits a distinguishable on/off current ratio for over 1000 read pulses (cycles).

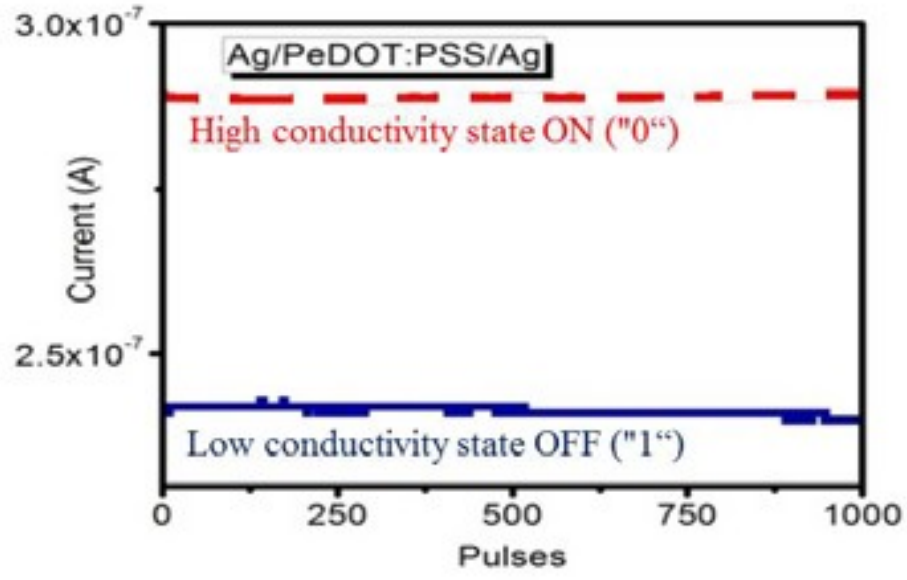

Figure 7.6: *retention time of (Ag/PEDOT:PSS/Ag) memory cells at room temperature. The plot clearly presents both the states "0" and "1" are stable for 1000 reading pulses.*

7.5 Conclusion

In summary, the fabrication of fully printed Ag/PEDOT:PSS/Ag electronic memory devices (cells) on flexible substrates, ceramic coated PEL paper, was successful. All the components of the memory device structure (metal electrode/active core/metal electrode) were deposited by a commercial desktop inkjet printer at room temperature. The two metal electrodes (the top and bottom) were inkjet printed using a colloidal nanoparticle silver ink whereas a PEDOT:PSS ink was used to inkjet print the active layer (core). The fully inkjet-printed memory devices show a bipolar switching behaviour with a distinguishable on/off current ratio for over 1000 read cycles.

Chapter 8: Conclusion and Recommendations for Future Research

8.1 Conclusion

Fabricating conducting paths for large electronic devices is one of the crucial and essential steps in realising them. A large number of methods have been employed and proposed for this purpose. The main aim of this research work was to print conducting paths using different materials in cheap, simple, easy to use and environmentally friendly techniques; a contact and non-contact printing technique. A contact printing technique was analysed by utilising a stamp printing machine manufactured using simple cost-effective apparatus to deposit aluminium tacks on oxygen plasma treated glass substrates. The investigation of these printed tracks was carried out using different techniques such as optical microscopy and SEM for the quality and morphology of the printed aluminum, profilometer for thickness measurements, the electrical properties using IV-measurements and 4-probe techniques, as well as the mechanical stability and the adhesion tests. To the best of our knowledge, this metal transfer printing from PDMS stamps to oxygen plasma-treated glass substrates using such cheap, simple, easy to use, environmentally friendly technique at room temperature has not been reported.

For the non-contact technique, on the other hand, the inexpensive environmentally friendly inkjet printing technology was selected for the deposition of some functional materials including silver, PEDOT:PSS and graphene oxide using the two commonly used drop-on-demand (DOD) methods; piezoelectric for the solvent-based silver and PEDOT:PSS inks and thermal for the water-based graphene oxide ink. The used piezoelectric printer was a desktop commercial printing machine from Epson while the thermal printer was constructed by Printed Electronics Limited (PEL). A ceramic coated PEL paper was used as the target substrate for the non-contact printing for its nanoscale porous properties to help absorbing the solvent and

dispersion agents to optimise the concentration of the nanoparticles of interest, and make the paper withstand higher temperatures (approximately 150°C). The quality and the thickness of the printed layers of the functional materials were assessed by means of an optical microscope and SEM, the electrical and mechanical properties were also investigated as well as the adhesion and bending tests. Having successfully printed and investigated these materials, the silver and PEDOT:PSS were employed to fabricate a novel flexible information storage device, electronic memory cell; all the elements of this memory device were fully inkjet printed using a cheap commercial desktop printer on ceramic coated PEL papers at room temperature.

8.2 Recommendations for Future Research

To achieve better stamping, pressure sensors are essential to determine the exact amount of the pressure required for each material to be printed, so the implementation of these sensors will have a huge impact on the quality of the printing. Moreover, the precise control of the speed of the actuator where the stamps are attached is crucial as well, as the peeling-off speed plays a major role in transferring the printed materials to the substrate. These two important factors were implemented in the late stages of the research and due to the time restrictions of the PhD time scale, the stamp printing machine was not properly investigated while they are implemented. Therefore, further in-depth investigation is suggested as these factors will definitely improve the quality of the printed patterns.

For the versatility of the simple cost-effective stamp printing machine, it will be employed to deposit other inorganic and organic materials. For example, a thick film transistor can completely be printed using the proposed machine. Moreover, viability if suitable substrate requires further investigation.

The commercial desktop inkjet printers, on the other hand, require more modifications when depositing on glass, silicon and plastic substrates. Using the CD carrier (with small

modifications) has shown promising results. Hence, further work is required to look in its potential.

List of publications and conferences attended/participated in

1. ***S. Maswoud***, S. Paul and I. Salaoru, "3-D printing of flexible two terminal electronic memory devices," MRS advances, vol 3, no 28, pp. 1603-1608, 2018.
2. ***S Maswoud*** and S. Paul “Low Cost Stamp Printer – Analysis of printed metal patterns for electronic device applications”. ICPAM conference-2016 in Romania.
3. I Salaoru, ***S Maswoud***, G Balmos, T Cimpeanu, S Paul1 “Digital Printing of Flexible Electronic Memory Devices”. Advanced Energy Materials conference-2017 in Surrey, UK.
4. ***S. Maswoud***, S. Paul and I. Salaoru, “3D Printing of Flexible Two Terminal Electronic Memory Devices”. MRS Fall Meeting-2017 in USA.
5. ***S Maswoud***, S Paul, I Salaoru “Inkjet printing of functional materials: a step forward to green electronics” ICPAM conference-2018 in Greece.
6. I Salaoru and ***S Maswoud*** “Inkjet Printing of Flexible Electronic Memory Devices” IDTechEx Show-2018, Berlin, Germany.
7. I. Salaoru, ***S. Maswoud*** and S. Paul, "Inkjet printing of functional electronic memory cells: A step forward to green electronics," Micromachines, vol 10, no 6, pp. 417, 2019.

References

1. Michael Wang. Lithography. Vukovar, Croatia: Intech, 2010, pp. 50-70.
2. A. Kumar and G. M. Whitesides, "Features of gold having micrometer to centimeter dimensions can be formed through a combination of stamping with an elastomeric stamp and an alkanethiol ‘‘ink’’followed by chemical etching," Applied physics letters, vol 63, no 14, pp. 2002-2004, 1993.
3. Z. Wang, J. Yuan, J. Zhang, R. Xing, D. Yan and Y. Han, "Metal transfer printing and its application in organic Field-Effect transistor fabrication," Advanced materials, vol 15, no 12, pp. 1009-1012, 2003.
4. S. Okazaki, "Resolution limits of optical lithography," Journal of vacuum science & technology B: Microelectronics and nanometer structures processing, measurement, and phenomena, vol 9, no 6, pp. 2829-2833, 1991.
5. Y. Xia and G. M. Whitesides, "Use of controlled reactive spreading of liquid alkanethiol on the surface of gold to modify the size of features produced by microcontact printing," Journal of the american chemical society, vol 117, no 11, pp. 3274-3275, 1995.
6. M. Wang, H. Braun, T. Kratzmüller and E. Meyer, "Patterning polymers by micro-fluid-contact printing," Advanced materials, vol 13, no 17, pp. 1312-1317, 2001.
7. Y. Loo, R. L. Willett, K. W. Baldwin and J. A. Rogers, "Interfacial chemistries for nanoscale transfer printing," Journal of the american chemical society, vol 124, no 26, pp. 7654-7655, 2002.
8. Z. Wang, J. Yuan, J. Zhang, R. Xing, D. Yan and Y. Han, "Metal transfer printing and its application in organic Field-Effect transistor fabrication," Advanced materials, vol 15, no 12, pp. 1009-1012, 2003.

9. Z. Wang, J. Yuan, J. Zhang, R. Xing, D. Yan and Y. Han, "Metal transfer printing and its application in organic Field-Effect transistor fabrication," Advanced materials, vol 15, no 12, pp. 1009-1012, 2003.
10. W. M. Moreau, "Semiconductor lithography: Principles, practices, and materials". Plenum, New York. 1988.
11. N. Stutzmann, T. A. Tervoort, K. Bastiaansen and P. Smith, "Patterning of polymer-supported metal films by microcutting," Nature, vol 407, no 6804, pp. 613, 2000.
12. M. J. Madou, "Fundamentals of microfabrication (CRC, Boca Raton, FL), " Madou Fundamentals of Microfabrication1997, 1997.
13. C. Kim, P. E. Burrows and S. R. Forrest, "Micropatterning of organic electronic devices by cold-welding," Science, vol 288, no 5467, pp. 831-833, 2000
14. X. Yu, S. Yu, Z. Wang, D. Ma and Y. Han, "Metal printing with modified polymer bonding lithography," Applied physics letters, vol 88, no 26, pp. 263517, 2006.
15. J. Yu and V. Bulović, "Micropatterning metal electrode of organic light emitting devices using rapid polydimethylsiloxane lift-off," Applied physics letters, vol 91, no 4, pp. 043102, 2007.
16. C. A. Nijhuis, J. ter Maat, S. Z. Bisri, M. H. Weusthof, C. Salm, J. Schmitz, B. J. Ravoo, J. Huskens and D. N. Reinhoudt, "Preparation of metal–SAM–dendrimer–SAM–metal junctions by supramolecular metal transfer printing," New journal of chemistry, vol 32, no 4, pp. 652-661, 2008.
17. C. Chen, T. Yu and Y. Lee, "Direct patterning of metallic micro/nano-structures on flexible polymer substrates by roller-based contact printing and infrared heating," Journal of micromechanics and microengineering, vol 20, no 2, pp. 025034, 2010.

18. S. H. Hsu, H. C. Su and Y. C. Chung, "Micro/nano-patterned metal transfer using UV-curable polymers," Journal of micromechanics and microengineering, vol 22, no 3, pp. 035008, 2012.
19. L. Fang, M. Wei, N. Wongkasem, H. Jaradat, A. Mokhlis, J. Shen, A. Akyurtlu, K. Marx, C. Barry and J. Mead, "Tin assisted transfer of electroplated metal nanostructures and its application in flexible chiral metamaterials," Microelectronic engineering, vol 107, pp. 42-49, 2013.
20. M. Zhu and C. Lee, "Facile metal transfer method for fabricating unconventional metamaterial devices," Optical materials express, vol 5, no 4, pp. 733-741, 2015.
21. Z. Wang, J. Yuan, J. Zhang, R. Xing, D. Yan and Y. Han, "Metal transfer printing and its application in organic Field-Effect transistor fabrication," Advanced materials, vol 15, no 12, pp. 1009-1012, 2003.
22. T. Granlund, T. Nyberg, L. Stolz Roman, M. Svensson and O. Inganäs, "Patterning of polymer light-emitting diodes with soft lithography," Advanced materials, vol 12, no 4, pp. 269-273, 2000.
23. Z. Wang, J. Yuan, J. Zhang, R. Xing, D. Yan and Y. Han, "Metal transfer printing and its application in organic Field-Effect transistor fabrication," Advanced materials, vol 15, no 12, pp. 1009-1012, 2003.
24. X. Yu, S. Yu, Z. Wang, D. Ma and Y. Han, "Metal printing with modified polymer bonding lithography," Applied physics letters, vol 88, no 26, pp. 263517, 2006.
25. GeSiM, MicroContact Printing Instruments, http://www.gesim.de/en/
26. Y. Xia and G. M. Whitesides, "Soft lithography," Angewandte chemie international edition, vol 37, no 5, pp. 550-575, 1998.

27. J. Cau, L. Ludovic, N. Marie, L. Adriana and P. Vincent, "Magnetic field assisted microcontact printing: A new concept of fully automated and calibrated process," Microelectronic Engineering, vol. 110, pp. 207-214, 10, 2013.
28. R. Syms, H. Zou, K. Choonee and R. A. Lawes, "Silicon microcontact printing engines," Journal of micromechanics and microengineering, vol 19, no 2, pp. 025027, 2009.
29. Y. Xia and G. M. Whitesides, "Soft lithography," Angewandte chemie international edition, vol 37, no 5, pp. 550-575, 1998.
30. G. Schmidt, M. Tormen, G. Muller, L. W. Molenkamp, Y. Chen, A. Lebib and H. Launois, "Versatile patterning process for semiconductors based on microcontact printing," Electronics letters, vol 35, no 20, pp. 1731-1733, 1999.
31. R.S. Kane, S. Takayama, E. Ostuni, D.E. Ingber and G.M. Whitesides, "The Biomaterials: Silver Jubilee Compendium," in Patterning proteins and cells using soft lithography, Anonymous Elsevier, 2006, pp. 161- 161-174.
32. J. Yu, I. Kim, J. Kim, J. Jo, T. T. Larsen-Olsen, R. R. Søndergaard, M. Hösel, D. Angmo, M. Jørgensen and F. C. Krebs, "Silver front electrode grids for ITO-free all printed polymer solar cells with embedded and raised topographies, prepared by thermal imprint, flexographic and inkjet roll-to-roll processes," Nanoscale, vol 4, no 19, pp. 6032-6040, 2012.
33. F. C. Krebs, M. Jørgensen, K. Norrman, O. Hagemann, J. Alstrup, T. D. Nielsen, J. Fyenbo, K. Larsen and J. Kristensen, "A complete process for production of flexible large area polymer solar cells entirely using screen printing—first public demonstration," Solar energy materials and solar cells, vol 93, no 4, pp. 422-441, 2009.

34. Dhingra, G. K. Padam, S. Singh, R. B. Tripathi, S. Rao, D. K. Suri, K. C. Nagpal and B. K. Das, "Study of silver addition to Y1Ba2Cu3O7− y screen printed thick films," Journal of applied physics, vol 70, no 3, pp. 1575-1579, 1991.
35. D. Sung, de la Fuente Vornbrock, Alejandro and V. Subramanian, "Scaling and optimization of gravure-printed silver nanoparticle lines for printed electronics," IEEE transactions on components and packaging technologies, vol 33, no 1, pp. 105-114, 2010.
36. Michael Wang. Lithography. Vukovar, Croatia: Intech, 2010, pp. 50-70.
37. Mijatovic, J. C. Eijkel and A. van den Berg, "Technologies for nanofluidic systems: Top-down vs. bottom-up—a review," Lab on a chip, vol 5, no 5, pp. 492-500, 2005.
38. Y. N. Xia and G. M. Whitesides, " Soft lithography," Annual review of materials science, vol 28, pp. 153-184, 1998.
39. J. Bohandy, B. Kim and F. Adrian, "Metal deposition from a supported metal film using an excimer laser," Journal of applied physics, vol 60, no 4, pp. 1538-1539, 1986.
40. K.S. Boparai and R. Singh, Advances in fused deposition modeling, Elsevier, 2017.
41. J. P. Renault, A. Bernard, A. Bietsch, B. Michel, H. R. Bosshard, E. Delamarche, M. Kreiter, B. Hecht and U. P. Wild, "Fabricating arrays of single protein molecules on glass using microcontact printing," Journal of physical chemistry B, vol 107, no 3, pp. 703-711, 2003.
42. A. Biebuyck and G. M. Whitesides, "Self-organization of organic liquids on patterned self-assembled monolayers of alkanethiolates on gold," Langmuir, vol 10, no 8, pp. 2790-2793, 1994.

43. C. Thibault, V. Le Berre, S. Casimirius, E. Trévisiol, J. François and C. Vieu, "Direct microcontact printing of oligonucleotides for biochip applications," Journal of nanobiotechnology, vol 3, no 1, pp. 7, 2005.
44. J. Tien, Y. Xia and G. M. Whitesides, "Microcontact printing of SAMs," Thin films, vol 24, pp. 227-250, 1998.
45. R. J. Jackman, J. L. Wilbur and G. M. Whitesides, "Fabrication of submicrometer features on curved substrates by microcontact printing," Science, vol 269, no 5224, pp. 664-666, 1995.
46. J. A. Rogers, R. J. Jackman and G. M. Whitesides, "Microcontact printing and electroplating on curved substrates: Production of free-standing three-dimensional metallic microstructures," Advanced materials, vol 9, no 6, pp. 475-477, 1997.
47. J. C. Huie, "Guided molecular self-assembly: A review of recent efforts," Smart materials and structures, vol 12, no 2, pp. 264-271, 2003.
48. R. M. Bright, M. D. Musick and M. J. Natan, "Preparation and characterization of ag colloid monolayers," Langmuir, vol 14, no 20, pp. 5695-5700, 1998.
49. C. D. Bain, E. B. Troughton, Y. -. Tao, J. Evall, G. M. Whitesides and R. G. Nuzzo, "Formation of monolayer films by the spontaneous assembly of organic thiols from solution onto gold," Journal of the american chemical society, vol 111, no 1, pp. 321-335, 1989.
50. C. Marzolin, A. Terfort, J. Tien and G. M. Whitesides, "Patterning of a polysiloxane precursor to silicate glasses by microcontact printing," Thin solid films, vol 315, no 1–2, pp. 9-12, 3/2 1998.
51. M. Geissler, H. Schmid, B. Michel and E. Delamarche, "Selective wet-etching of microcontact-printed cu substrates with control over the etch profile," Microelectronic engineering, vol 67–68, no 0, pp. 326-332, 6 2003.

52. J. C. Love, L. A. Estroff, J. K. Kriebel, R. G. Nuzzo and G. M. Whitesides, "Self-assembled monolayers of thiolates on metals as a form of nanotechnology," Chemical reviews, vol 105, no 4, pp. 1103-1169, 2005.
53. Malkiat S. Johal, Lewis E. V. Johnson. Understanding Nanomaterials. NewYork, usa: CRC Press, 2011, pp. 257-60.
54. A.M. Kendale and D.L. Trumper, “Microcontact Printing,” U.S. Patent 7 665 983 B2, February 23, 2010.
55. H. O. Jacobs and G. M. Whitesides, "Submicrometer patterning of charge in thin-film electrets," Science, vol. 291, pp. 1763-1766, 2001.
56. E. B. Chakra, B. Hannes, G. Dilosquer, C. D. Mansfield and M. Cabrera, "A new instrument for automated microcontact printing with stamp load adjustment," Rev. Sci. Instrum., vol. 79, 064102, 2008.
57. GeSiM, MicroContact Printing Instruments, http://www.gesim.de/en/
58. Y. Xia and G. M. Whitesides, "Soft lithography," Angewandte chemie international edition, vol 37, no 5, pp. 550-575, 1998.
59. J. Cau, L. Ludovic, N. Marie, L. Adriana and P. Vincent, "Magnetic field assisted microcontact printing: A new concept of fully automated and calibrated process," Microelectronic Engineering, vol. 110, pp. 207-214, 10, 2013.
60. R.J. Hildyard, European ceramics, University of Pennsylvania Press, 1999.
61. E. Menard, R. G. Nuzzo and J. A. Rogers, "Bendable single crystal silicon thin film transistors formed by printing on plastic substrates," Applied physics letters, vol 86, no 9, pp. 093507, 2005.
62. W. Zhou, Y. Huang, E. Menard, N. R. Aluru, J. A. Rogers and A. G. Alleyne, "Mechanism for stamp collapse in soft lithography," Applied physics letters, vol 87, no 25, pp. 251925, 2005.

63. X. Feng, M. A. Meitl, A. M. Bowen, Y. Huang, R. G. Nuzzo and J. A. Rogers, "Competing fracture in kinetically controlled transfer printing," Langmuir, vol 23, no 25, pp. 12555-12560, 2007.

64. A. Carlson, A. M. Bowen, Y. Huang, R. G. Nuzzo and J. A. Rogers, "Transfer printing techniques for materials assembly and micro/nanodevice fabrication," Advanced materials, vol 24, no 39, pp. 5284-5318, 2012.

65. K. Felmet, Y. Loo and Y. Sun, "Patterning conductive copper by nanotransfer printing," Applied physics letters, vol 85, no 15, pp. 3316-3318, 2004.

66. Y. Loo, R. L. Willett, K. W. Baldwin and J. A. Rogers, "Additive, nanoscale patterning of metal films with a stamp and a surface chemistry mediated transfer process: Applications in plastic electronics," Applied physics letters, vol 81, no 3, pp. 562-564, 2002

67. D. Kim, J. Ahn, H. Kim, K. J. Lee, T. Kim, C. Yu, R. G. Nuzzo and J. A. Rogers, "Complementary logic gates and ring oscillators on plastic substrates by use of printed ribbons of single-crystalline silicon," IEEE electron device letters, vol 29, no 1, pp. 73-76, 2008.

68. B. Furman, E. Menard, A. Gray, M. Meitl, S. Bonafede, D. Kneeburg, K. Ghosal, R. Bukovnik, W. Wagner and J. Gabriel, , "A high concentration photovoltaic module utilizing micro-transfer printing and surface mount technology," In Photovoltaic specialists conference (PVSC), 2010 35th IEEE, 2010, pp. 475.

69. K. R. Shull, D. Ahn, W. Chen, C. M. Flanigan and A. J. Crosby, "Axisymmetric adhesion tests of soft materials," Macromolecular chemistry and physics, vol 199, no 4, pp. 489-511, 1998.

70. A. Carlson, S. Wang, P. Elvikis, P. M. Ferreira, Y. Huang and J. A. Rogers, "Active, programmable elastomeric surfaces with tunable adhesion for deterministic assembly

by transfer printing," Advanced functional materials, vol 22, no 21, pp. 4476-4484, 2012.

71. A. Carlson, H. Kim-Lee, J. Wu, P. Elvikis, H. Cheng, A. Kovalsky, S. Elgan, Q. Yu, P. M. Ferreira and Y. Huang, "Shear-enhanced adhesiveless transfer printing for use in deterministic materials assembly," Applied physics letters, vol 98, no 26, pp. 264104, 2011.
72. J. D. Eisenhaure, S. I. Rhee, M. Ala'a, A. Carlson, P. M. Ferreira and S. Kim, "The use of shape memory polymers for microassembly by transfer printing," Journal of microelectromechanical systems, vol 23, no 5, pp. 1012-1014, 2014.
73. R. Saeidpourazar, M. D. Sangid, J. A. Rogers and P. M. Ferreira, "A prototype printer for laser driven micro-transfer printing," Journal of manufacturing processes, vol 14, no 4, pp. 416-424, 2012.
74. N. Ahmed, A. Carlson, J. A. Rogers and P. M. Ferreira, "Automated micro-transfer printing with cantilevered stamps," Journal of manufacturing processes, vol 14, no 2, pp. 90-97, 2012.
75. R. D. Nagel, T. Haeberle, M. Schmidt, P. Lugli and G. Scarpa, "Large area nano-transfer printing of sub-50-nm metal nanostructures using low-cost semi-flexible hybrid templates," Nanoscale research letters, vol 11, no 1, pp. 143, 2016.
76. Y. Xia and G. M. Whitesides, "Soft lithography," Angewandte chemie international edition, vol 37, no 5, pp. 550-575, 1998.
77. J. N. Lee, C. Park and G. M. Whitesides, "Solvent compatibility of poly(dimethylsiloxane)-based microfluidic devices," Analytical chemistry, vol 75, no 23, pp. 6544-6554, 2003.
78. Dow Corning Corporation, " Product Information: Sylgard 184 Silicone Elastomer," Form No. 11-3184B-01.

79. E. Delamarche, H. Schmid, B. Michel and H. Biebuvck, "Stability of molded polydime thylsiloxane microstructures," Advanced materials, vol 9, no 9, pp. 741-746, 1997.

80. Y. Xia and G. M. Whitesides, "Soft lithography," Angewandte chemie international edition, vol 37, no 5, pp. 550-575, 1998.

81. H. Schmid and B. Michel, "Siloxane Polymers for High-Resolution, High-Accuracy Soft Lithography," Macromolecules, vol. 33, pp. 3042-3049, 2000.

82. T. W. Odom, J. C. Love, D. B. Wolfe, K. E. Paul, and G. M. Whitesides, "Improved Pattern Transfer in Soft Lithography Using Composite Stamps," Langmuir, vol. 18, pp. 5314-5320, 2002.

83. X. -M. Zhao, "Soft lithographic methods for nano-fabrication," Journal of materials chemistry, vol 7, no 7, pp. 1069-1074, 1997.

84. B. A. Grzybowski, S. T. Brittain and G. M. Whitesides, "Thermally actuated interferometric sensors based on the thermal expansion of transparent elastomeric media," Review of scientific instruments, vol 70, no 4, pp. 2031-2037, 1999.

85. C. Moraes, Y. Sun, and C. A. Simmons, "Solving the shrinkage-induced PDMS alignment registration issue in multilayer soft lithography," J. Micromech. Microeng., vol. 19, p. 065015, 2009.

86. H. Schmid and B. Michel, "Siloxane Polymers for High-Resolution, High-Accuracy Soft Lithography," Macromolecules, vol. 33, pp. 3042-3049, 2000.

87. K. S. Park, E. K. Seo, Y. R. Do, K. Kim and M. M. Sung, "Light stamping lithography: Microcontact printing without inks," Journal of the american chemical society, vol 128, no 3, pp. 858-865, 2006.

88. E. Delamarche, J. Vichiconti, S. A. Hall, M. Geissler, W. Graham, B. Michel and R. Nunes, "Electroless deposition of cu on glass and patterning with microcontact printing," Langmuir, vol 19, no 17, pp. 6567-6569, 2003.
89. M.M.J. Decré, R. Schneider, D. Burdinski, J. Schellekens, M. Saalmink and R. Dona, "Wave printing (I): Towards large-area, multilayer microcontact printing," In Materials research society symposium proceedings, pp. 59-61, 2004.
90. GeSiM, MicroContact Printing Instruments, http://www.gesim.de/en/ (accessed 13 February 2014).
91. A. Bietsch and B. Michel, "Conformal contact and pattern stability of stamps used for soft lithography," Journal of applied physics, vol 88, no 7, pp. 4310-4318, 2000.
92. D.K. Schroder, Semiconductor material and device characterization, John Wiley & Sons, pp 579-584, 2006.
93. K. L. Chopra, "Thin film phenomena," 1969.
94. SMC, "Product Information: EC Series Electric Cylinders LZDBB5L-100A5" P/N. CUS10050 Rev. 1.0 07/03, available at: http://www.smcpneumatics.com/pdfs/ LZDBB5L-100A5.pdf (accessed 16 August 2014).
95. SMC, LC3F212-5A5B, available at: http://www.smcpneumatics.com/pdfs/LC3F2.pdf (accessed 16 August 2014).
96. S.J. Lee and N. Sundararajan, Microfabrication for microfluidics, Artech House, pp 120-130, 2010.
97. Dow Corning, Sylgard 184 Silicone Elastomer Kit, http://www.dowcorning.com/ (accessed 10 January 2014).
98. D. J. Campbell, K. J. Beckman, C. E. Calderon, P. W. Doolan, R. M. Ottosen, A. B. Ellis and G. C. Lisensky, "Replication and compression of bulk and surface structures

with polydimethylsiloxane elastomer," Journal of chemical education, vol 76, no 2-4, pp. 537-541, 1999.

99. W. Yuming and W. Alfred, An introduction to physics and technology of thin films, World scientific, 1994.

100. G. J. Shugar, J. T. Ballinger and L. M. Dawkins, Chemical technicians' ready reference handbook, 1996.

101. Available at: http://www.surface-tension.de/solid-surface-energy.htm (accessed on 10 February 2017).

102. A. L. Sumner, E. J. Menke, Y. Dubowski, J. T. Newberg, R. M. Penner, J. C. Hemminger, L. M. Wingen, T. Brauers and B. J. Finlayson-Pitts, "The nature of water on surfaces of laboratory systems and implications for heterogeneous chemistry in the troposphere," Physical chemistry chemical physics, vol 6, no 3, pp. 604-613, 2004.

103. S. K. Rhee, "Surface energies of silicate glasses calculated from their wettability data," Journal of materials science, vol 12, no 4, pp. 823-824, 1977.

104. F. Aviles, O. Ceh and A. I. Oliva, "Physical properties of au and al thin films measured by resistive heating," Surface review and letters, vol 12, no 01, pp. 101-106, 2005.

105. M. Ohring, Materials science of thin films, Elsevier, 2001.

106. K. Fuchs, , "The conductivity of thin metallic films according to the electron theory of metals," In Mathematical proceedings of the cambridge philosophical society, 1938, pp. 100-108.

107. E. H. Sondheimer, "The mean free path of electrons in metals," Advances in physics, vol 1, no 1, pp. 1-42, 1952.

108. A. F. Mayadas, M. Shatzkes and J. F. Janak, "Electrical resistivity model for polycrystalline films: The case of specular reflection at external surfaces," Applied physics letters, vol 14, no 11, pp. 345-347, 1969.

109. G. Cummins and M. P. Desmulliez, "Inkjet printing of conductive materials: A review," Circuit world, vol 38, no 4, pp. 193-213, 2012.

110. M. T. Plateau, "On the recent theories of the constitution of jets of liquid issuing from circular orifices," The london, edinburgh, and dublin philosophical magazine and journal of science, vol 12, no 79, pp. 286-297, 1856.

111. L. Rayleigh, "Further observations upon liquid jets, in continuation of those recorded in the royal society's' proceedings' for march and may, 1879," Proceedings of the royal society of london, vol 34, pp. 130-145, 1882.

112. L. Rayleigh, "On the instability of jets," Proceedings of the london mathematical society, vol 1, no 1, pp. 4-13, 1878.

113. E. Rune, " US Patent 2566443," Measuring instrument of the recording type, 1951.

114. R. G. Sweet, "High frequency recording with electrostatically deflected ink jets," Review of scientific instruments, vol 36, no 2, pp. 131-136, 1965.

115. S. I. Zoltan, " US Patent 3683212," Pulsed droplet ejecting system, 1972.

116. N. Mark, "US3179042A," Sudden steam printer, 1965.

117. N. Hopkinson, R. Hague and P. Dickens, Rapid manufacturing: An industrial revolution for the digital age, John Wiley & Sons, 1st Edition, pp 249, 2006.

118. B. De Gans and U. S. Schubert, "Inkjet printing of well-defined polymer dots and arrays," Langmuir, vol 20, no 18, pp. 7789-7793, 2004.

119. E. Tekin, P. J. Smith and U. S. Schubert, "Inkjet printing as a deposition and patterning tool for polymers and inorganic particles," Soft matter, vol 4, no 4, pp. 703-713, 2008

120. J. Perelaer, B. De Gans and U. S. Schubert, "Ink-jet printing and microwave sintering of conductive silver tracks," Advanced materials, vol 18, no 16, pp. 2101-2104, 2006.

121. J. Chung, S. Ko, N. R. Bieri, C. P. Grigoropoulos and D. Poulikakos, "Conductor microstructures by laser curing of printed gold nanoparticle ink," Applied physics letters, vol 84, no 5, pp. 801-803, 2004.

122. S. Ko, H. Choi, M. Kang, H. Hwang, H. Ji, J. Kim, J. Ko and Y. Kang, "Silole-spaced triarylamine derivatives as highly efficient organic sensitizers in dye-sensitized solar cells (DSSCs)," Journal of materials chemistry, vol 20, no 12, pp. 2391-2399, 2010.

123. B. De Gans, P. C. Duineveld and U. S. Schubert, "Inkjet printing of polymers: State of the art and future developments," Advanced materials, vol 16, no 3, pp. 203-213, 2004.

124. S. Jung, A. Sou, E. Gili and H. Sirringhaus, "Inkjet-printed resistors with a wide resistance range for printed read-only memory applications," Organic electronics, vol 14, no 3, pp. 699-702, 2013.

125. T. Shimoda, K. Morii, S. Seki and H. Kiguchi, "Inkjet printing of light-emitting polymer displays," MRS bulletin, vol 28, no 11, pp. 821-827, 2003.

126. F. V. López, A. Diez and A. Odriozola, "Inkjet printing of conductive and resistive coatings," International polymer processing, vol 22, no 1, pp. 27-33, 2007.

127. M. Singh, H. M. Haverinen, P. Dhagat and G. E. Jabbour, "Inkjet printing—process and its applications," Advanced materials, vol 22, no 6, pp. 673-685, 2010.

128. M. Vilardell, X. Granados, S. Ricart, I. Van Driessche, A. Palau, T. Puig and X. Obradors, "Flexible manufacturing of functional ceramic coatings by inkjet printing," Thin solid films, vol 548, pp. 489-497, 2013.

129. N. Reis, C. Ainsley and B. Derby, "Ink-jet delivery of particle suspensions by piezoelectric droplet ejectors," Journal of applied physics, vol 97, no 9, pp. 094903, 2005.

130. L. Rayleigh, "On the capillary phenomena of jets," Proc.R.soc.london, vol 29, no 196-199, pp. 71-97, 1879.

131. H. Wijshoff, "The dynamics of the piezo inkjet printhead operation," Physics reports, vol 491, no 4-5, pp. 77-177, 2010.

132. J. Brünahl and A. M. Grishin, "Piezoelectric shear mode drop-on-demand inkjet actuator," Sensors and actuators A: Physical, vol 101, no 3, pp. 371-382, 2002.

133. S. D. Howkins, " US patent 4,459,601," Ink jet method and apparatus, 1984.

134. N. Stemme, " U.S. Patent No. 3,747,120," Arrangement of writing mechanisms for writing on paper with a coloredliquid, 1973.

135. E. L. Kyser and S. B. Sears, " U.S. Patent No. 3,946,398," Method and apparatus for recording with writing fluids and drop projection means therefor, 1976.

136. K. H. Fischbeck and A. T. Wright, " U.S. Patent No. 4,584,590," Shear mode transducer for drop-on-demand liquid ejector, 1986.

137. S. I. Zoltan, " U.S. Patent No. 3,683,212," Pulsed droplet ejecting system, 1972.

138. H. Wijshoff, "The dynamics of the piezo inkjet printhead operation," Physics reports, vol 491, no 4-5, pp. 77-177, 2010.

139. S. Magdassi, The chemistry of inkjet inks, World scientific Singapore, pp 203, 2010.

140. S. Magdassi, The chemistry of inkjet inks, World scientific Singapore, pp 19-22, 2010.

141. A. Kamyshny, J. Steinke and S. Magdassi, "Metal-based inkjet inks for printed electronics," The open applied physics journal, vol 4, no 1, 2011.

142. A. W. Adamson and A. P. Gast, "Physical chemistry of surfaces," pp 3-20, 1967.

143. H. R. Kang, "Water-based ink-jet ink. I, formulation," Journal of imaging science, vol 35, no 3, pp. 179-188, 1991.

144. Pillar Technologies: The Surface Tension Phenomenon. Available at: http://www.pillartech.com/Surface-Treatment/Technical-Info/Useful-Information/Surface-Tension-Phenomenon (accessed 20 February 2017).

145. R. Rioboo, C. Tropea and M. Marengo, "Outcomes from a drop impact on solid surfaces," Atomization and sprays, vol 11, no 2, 2001.

146. A. W. Adamson and A. Gast, "Physical chemistry of surfaces,", New York, Wiley,1997

147. T. Young, "An essay on the cohesion of fluids," Philosophical transactions of the royal society of London, vol 95, pp. 65-87, 1805.

148. E. Chibowski, "On some relations between advancing, receding and young's contact angles," Advances in colloid and interface science, vol 133, no 1, pp. 51-59, 2007.

149. C. W. Extrand and Y. Kumagai, "An experimental study of contact angle hysteresis," Journal of colloid and interface science, vol 191, no 2, pp. 378-383, 1997.

150. J. E. Fromm, "Numerical calculation of the fluid dynamics of drop-on-demand jets," IBM journal of research and development, vol 28, no 3, pp. 322-333, 1984.

151. D. Jang, D. Kim and J. Moon, "Influence of fluid physical properties on ink-jet printability," Langmuir, vol 25, no 5, pp. 2629-2635, 2009.

152. Decker, "Light-induced crosslinking polymerization," Polymer international, vol 51, no 11, pp. 1141-1150, 2002.

153. S. Magdassi, M. Grouchko, O. Berezin and A. Kamyshny, "Triggering the sintering of silver nanoparticles at room temperature," ACS nano, vol 4, no 4, pp. 1943-1948, 2010.

154. I. Reinhold, C. E. Hendriks, R. Eckardt, J. M. Kranenburg, J. Perelaer, R. R. Baumann and U. S. Schubert, "Argon plasma sintering of inkjet printed silver tracks on polymer substrates," Journal of materials chemistry, vol 19, no 21, pp. 3384-3388, 2009.

155. J. Perelaer, B. De Gans and U. S. Schubert, "Ink-jet printing and microwave sintering of conductive silver tracks," Advanced materials, vol 18, no 16, pp. 2101-2104, 2006.

156. A. Kamyshny, J. Steinke and S. Magdassi, "Metal-based inkjet inks for printed electronics," The open applied physics journal, vol 4, no 1, 2011.

157. C. Yang, C. P. Wong and M. M. Yuen, "Printed electrically conductive composites: Conductive filler designs and surface engineering," Journal of materials chemistry C, vol 1, no 26, pp. 4052-4069, 2013.

158. K. K. Nanda, A. Maisels, F. E. Kruis, H. Fissan and S. Stappert, "Higher surface energy of free nanoparticles," Physical review letters, vol 91, no 10, pp. 106102, 2003.

159. R. D. Deegan, O. Bakajin, T. F. Dupont, G. Huber, S. R. Nagel and T. A. Witten, "Capillary flow as the cause of ring stains from dried liquid drops," Nature, vol 389, no 6653, pp. 827, 1997.

160. S. R. Samarasinghe, I. Pastoriza-Santos, M. J. Edirisinghe, M. J. Reece, L. Liz-Marzán, M. R. Nangrejo and Z. Ahmad, "Electric-jet assisted layer-by-layer deposition of gold nanoparticles to prepare conducting tracks," Natural science, vol 1, no 02, pp. 142, 2009.

161. P. S. Karthik and S. P. Singh, "Copper conductive inks: Synthesis and utilization in flexible electronics," RSC advances, vol 5, no 79, pp. 63985-64030, 2015.

162. P. K. Jain, X. Huang, I. H. El-Sayed and M. A. El-Sayed, "Noble metals on the nanoscale: Optical and photothermal properties and some applications in imaging, sensing, biology, and medicine," Accounts of chemical research, vol 41, no 12, pp. 1578-1586, 2008.

163. T. K. Sau, A. L. Rogach, F. Jäckel, T. A. Klar and J. Feldmann, "Properties and applications of colloidal nonspherical noble metal nanoparticles," Advanced materials, vol 22, no 16, pp. 1805-1825, 2010.

164. Y. Sun, B. Mayers, T. Herricks and Y. Xia, "Polyol synthesis of uniform silver nanowires: A plausible growth mechanism and the supporting evidence," Nano letters, vol 3, no 7, pp. 955-960, 2003.

165. B. J. Wiley, Y. Chen, J. M. McLellan, Y. Xiong, Z. Li, D. Ginger and Y. Xia, "Synthesis and optical properties of silver nanobars and nanorice," Nano letters, vol 7, no 4, pp. 1032-1036, 2007.

166. K. Rajan, I. Roppolo, A. Chiappone, S. Bocchini, D. Perrone and A. Chiolerio, "Silver nanoparticle ink technology: State of the art," Nanotechnology, science and applications, vol 9, pp. 1, 2016.

167. S. B. Fuller, E. J. Wilhelm and J. M. Jacobson, "Ink-jet printed nanoparticle microelectromechanical systems," Journal of microelectromechanical systems, vol 11, no 1, pp. 54-60, 2002.

168. H. Lee, K. Chou and K. Huang, "Inkjet printing of nanosized silver colloids," Nanotechnology, vol 16, no 10, pp. 2436, 2005.

169. M. M. Menamparambath, C. M. Ajmal, K. H. Kim, D. Yang, J. Roh, H. C. Park, C. Kwak, J. Choi and S. Baik, "Silver nanowires decorated with silver nanoparticles for low-haze flexible transparent conductive films," Scientific reports, vol 5, pp. 16371, 2015.

170. https://www.epson.co.uk/products/printers/inkjet-printers/for-home/epson-stylus-photo-p50?productfinder=p50#specifications (accessed 22 March 2017).

171. J. Perelaer, A. W. De Laat, C. E. Hendriks and U. S. Schubert, "Inkjet-printed silver tracks: Low temperature curing and thermal stability investigation," Journal of materials chemistry, vol 18, no 27, pp. 3209-3215, 2008.

172. T. H. Joubert, P. H. Bezuidenhout, H. Chen, S. Smith and K. J. Land, "Inkjet-printed silver tracks on different paper substrates," Materials today: Proceedings, vol 2, no 7, pp. 3891-3900, 2015.

173. D. Kim and J. Moon, "Highly conductive ink jet printed films of nanosilver particles for printable electronics," Electrochemical and solid-state letters, vol 8, no 11, pp. J33, 2005.

174. M. Bolduc, C. Trudeau, P. Beaupré, S. G. Cloutier and P. Galarneau, "Thermal dynamics effects using pulse-shaping laser sintering of printed silver inks," Scientific reports, vol 8, no 1, pp. 1418, 2018.

175. A. Denneulin, A. Blayo, C. Neuman and J. Bras, "Infra-red assisted sintering of inkjet printed silver tracks on paper substrates," Journal of nanoparticle research, vol 13, no 9, pp. 3815-3823, 2011.

176. E. Rocha-Rangel, A. P. la Fuente, J. A. Rodríguez-García, I. Estrada-Guel and R. Martínez-Sánchez, "Effect of silver nanoparticles on the microstructure and mechanical properties of alumina ceramics," Canadian metallurgical quarterly, vol 56, no 3, pp. 332-339, 2017.

177. O. Y. Posudievsky, N. V. Konoshchuk, A. G. Shkavro, V. G. Koshechko and V. D. Pokhodenko, "Structure and electronic properties of poly (3, 4-ethylenedioxythiophene) poly (styrene sulfonate) prepared under ultrasonic irradiation," Synthetic metals, vol 195, pp. 335-339, 2014.

178. A. G. Bayer, "Eur. patent 339 340, 1988. b) F. jonas, L. schrader," Synth.met, vol 41, pp. 831-836, 1991.

179. Y. Yoshioka and G. E. Jabbour, "Desktop inkjet printer as a tool to print conducting polymers," Synthetic metals, vol 156, no 11-13, pp. 779-783, 2006.

180. M. F. Mabrook, C. Pearson and M. C. Petty, "An inkjet-printed chemical fuse," Applied physics letters, vol 86, no 1, pp. 013507, 2005.

181. A. Singh, S. Mandal, V. Singh, A. Garg and M. Katiyar, , "Inkjet printed PEDOT: PSS for organic devices," In 16th international workshop on physics of semiconductor devices, 2012, pp. 854936.

182. S. Kirchmeyer and K. Reuter, "Scientific importance, properties and growing applications of poly (3, 4-thylenedioxythiophene)," Journal of materials chemistry, vol 15, no 21, pp. 2077-2088, 2005.

183. J. Y. Kim, J. H. Jung, D. E. Lee and J. Joo, "Enhancement of electrical conductivity of poly (3, 4-ethylenedioxythiophene)/poly (4-styrenesulfonate) by a change of solvents," Synthetic metals, vol 126, no 2-3, pp. 311-316, 2002.

184. D. Sankir, "Selective deposition of PEDOT/PSS on to flexible substrates and tailoring the electrical resistivity by post treatment," Circuit world, vol 34, no 4, pp. 32-37, 2008.

185. U. Lang, P. Rust, B. Schoberle and J. Dual, "Piezoresistive properties of PEDOT: PSS," Microelectronic engineering, vol 86, no 3, pp. 330-334, 2009.

186. A. Singh, M. Katiyar and A. Garg, "Understanding the formation of PEDOT: PSS films by ink-jet printing for organic solar cell applications," RSC advances, vol 5, no 96, pp. 78677-78685, 2015.

187. Z. Xiong and C. Liu, "Optimization of inkjet printed PEDOT: PSS thin films through annealing processes," Organic electronics, vol 13, no 9, pp. 1532-1540, 2012.

188. M. F. Mabrook, C. Pearson and M. C. Petty, "An inkjet-printed chemical fuse," Applied physics letters, vol 86, no 1, pp. 013507, 2005.

189. C. Srichan, T. Saikrajang, T. Lomas, A. Jomphoak, T. Maturos, D. Phokaratkul, T. Kerdcharoen and A. Tuantranont, , "Inkjet printing PEDOT: PSS using desktop inkjet printer," In Electrical engineering/electronics, computer, telecommunications and information technology, 2009. ECTI-CON 2009. 6th international conference on, 2009, pp. 465-468.

190. B. Huber, P. B. Popp, M. Kaiser, A. Ruediger and C. Schindler, "Fully inkjet printed flexible resistive memory," Applied physics letters, vol 110, no 14, pp. 143503, 2017.

191. Y. Mochizuki, T. Horii and H. Okuzaki, "Effect of pH on structure and conductivity of PEDOT/PSS," Transactions of the materials research society of japan, vol 37, no 2, pp. 307-310, 2012.

192. Available at: https://goldbook.iupac.org/html/G/G02683.html (accessed 15 April 2017).

193. J. Wu, H. A. Becerril, Z. Bao, Z. Liu, Y. Chen and P. Peumans, "Organic solar cells with solution-processed graphene transparent electrodes," Applied physics letters, vol 92, no 26, pp. 237, 2008.

194. L. T. Le, M. H. Ervin, H. Qiu, B. E. Fuchs and W. Y. Lee, "Graphene supercapacitor electrodes fabricated by inkjet printing and thermal reduction of graphene oxide," Electrochemistry communications, vol 13, no 4, pp. 355-358, 2011.

195. L. Huang, Y. Huang, J. Liang, X. Wan and Y. Chen, "Graphene-based conducting inks for direct inkjet printing of flexible conductive patterns and their applications in electric circuits and chemical sensors," Nano research, vol 4, no 7, pp. 675-684, 2011.

196. L. Huang, Y. Huang, J. Liang, X. Wan and Y. Chen, "Graphene-based conducting inks for direct inkjet printing of flexible conductive patterns and their applications in electric circuits and chemical sensors," Nano research, vol 4, no 7, pp. 675-684, 2011.

197. V. Dua, S. P. Surwade, S. Ammu, S. R. Agnihotra, S. Jain, K. E. Roberts, S. Park, R. S. Ruoff and S. K. Manohar, "All-organic vapor sensor using inkjet-printed reduced graphene oxide," Angewandte chemie, vol 122, no 12, pp. 2200-2203, 2010.

198. B. L. Dasari, J. M. Nouri, D. Brabazon and S. Naher, "Graphene and derivatives–Synthesis techniques, properties and their energy applications," Energy, vol 140, pp. 766-778, 2017

199. S. Paul, A. Kanwal and M. Chhowalla, "Memory effect in thin films of insulating polymer and C60 nanocomposites," Nanotechnology, vol 17, no 1, pp. 145, 2005.

200. D. Prime and S. Paul, "First contact-charging of gold nanoparticles by electrostatic force microscopy," Applied physics letters, vol 96, no 4, pp. 043120, 2010.

201. J. C. Scott and L. D. Bozano, "Nonvolatile memory elements based on organic materials," Advanced materials, vol 19, no 11, pp. 1452-1463, 2007.

202. S. Porro and C. Ricciardi, "Memristive behaviour in inkjet printed graphene oxide thin layers," RSC advances, vol 5, no 84, pp. 68565-68570, 2015.

203. I. Salaoru, Z. Zhou, P. Morris and G. J. Gibbons, "Inkjet printing of polyvinyl alcohol multilayers for additive manufacturing applications," Journal of applied polymer science, vol 133, no 25, 2016.

204. W. K. Hsiao, S. D. Hoath, G. D. Martin, I. M. Hutchings, N. B. Chilton and S. Jones, "Imbibition dynamics of nano-particulate ink-jet drops on micro-porous media," Nanotech 2011 Conference, Boston, 2011.

Appendix

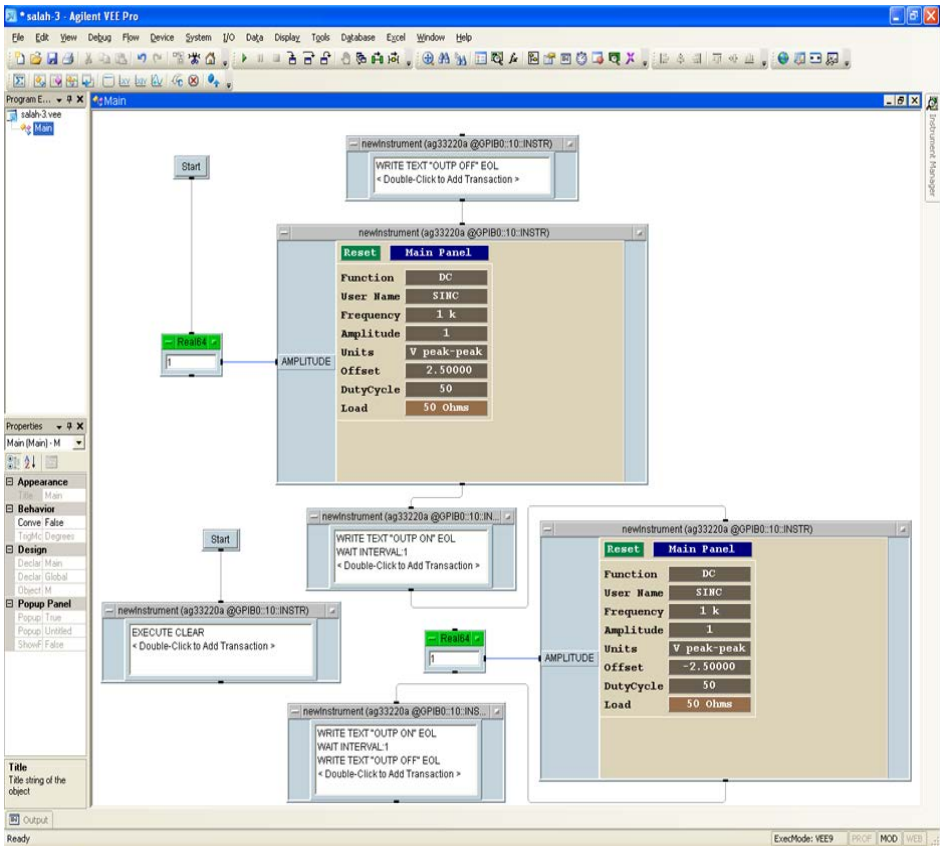

Figure A1: *Agilent VEE programme code used to automate the stamping process in the proposed printer.*

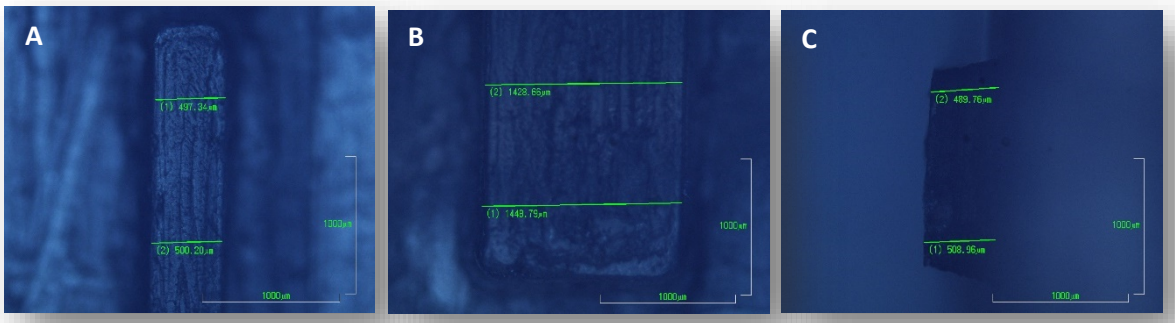

Figure A.2: PDMS stamp features resulted from the engraved base of the casting set; a) a 500 µm width track, b) a 1500 µm width track and c) the highest of the track (500 µm).

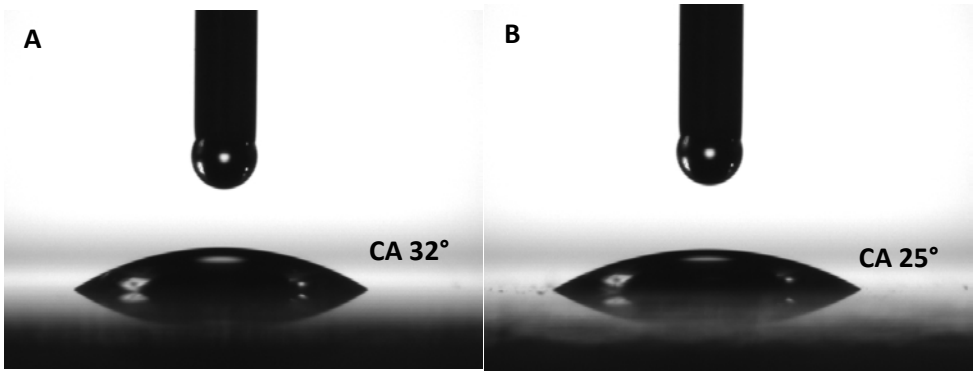

Figure A3: *water contact angle on; untreated glass and b) DI water rinsed glass*

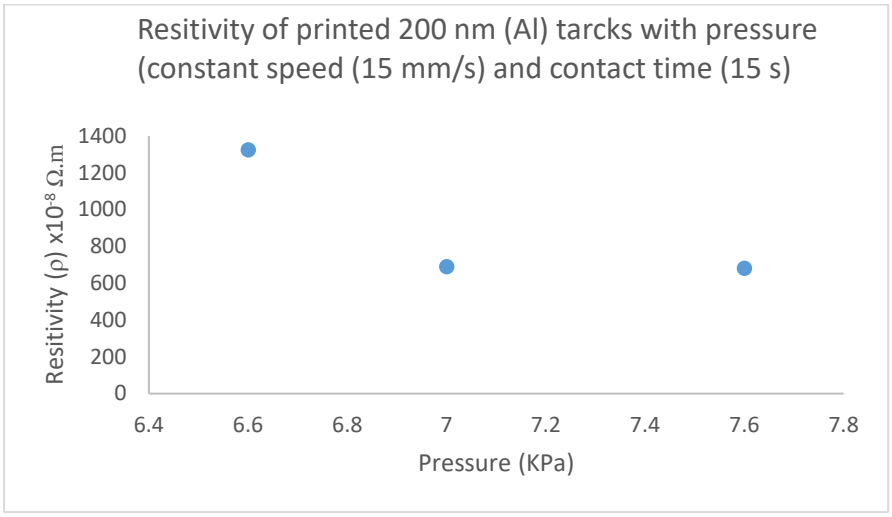

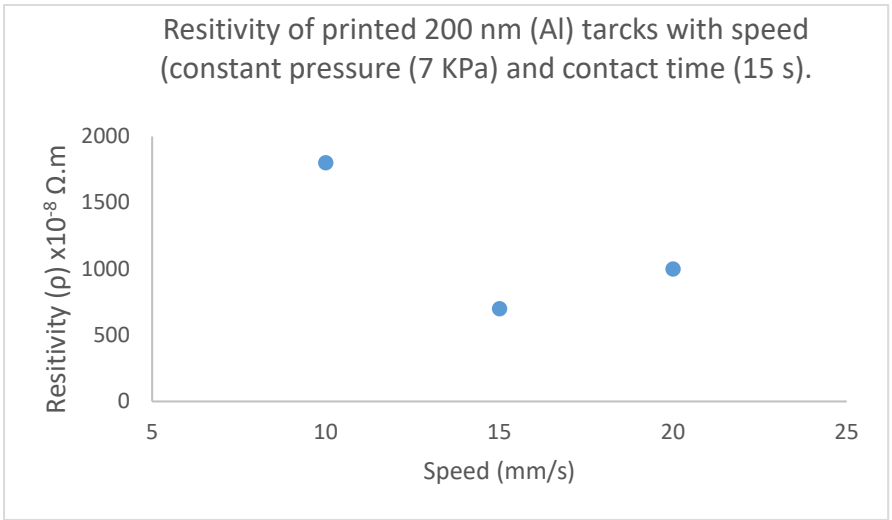

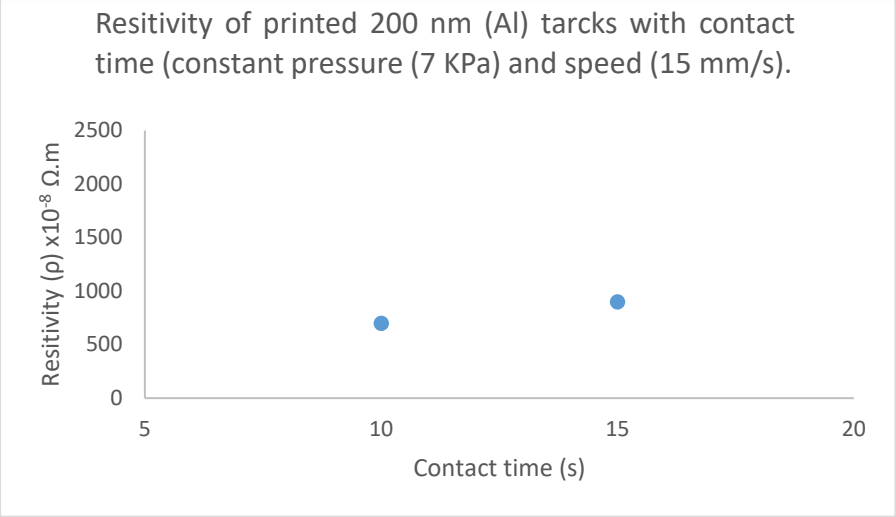

Figure A4: *some resistivity measurements on successful stamp printed aluminium (200 nm) on O_2 plasma treated glass substrates with different control parameters.*

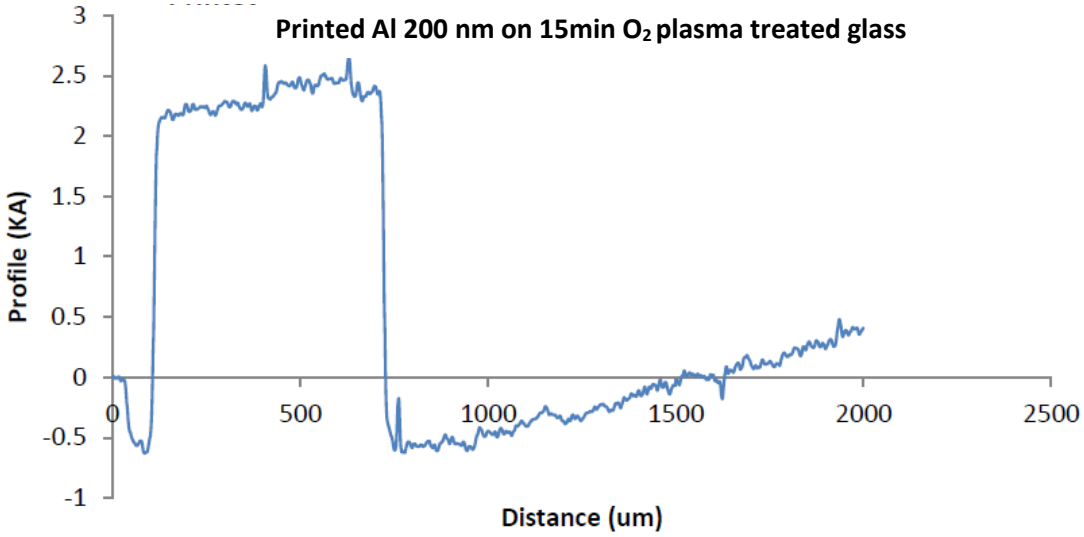

Figure A5: *a profilometer measurement of stamp printed Al (width of 600 µm) on 15-min oxygen plasma treated glass showing a thickness of approximately 200nm.*

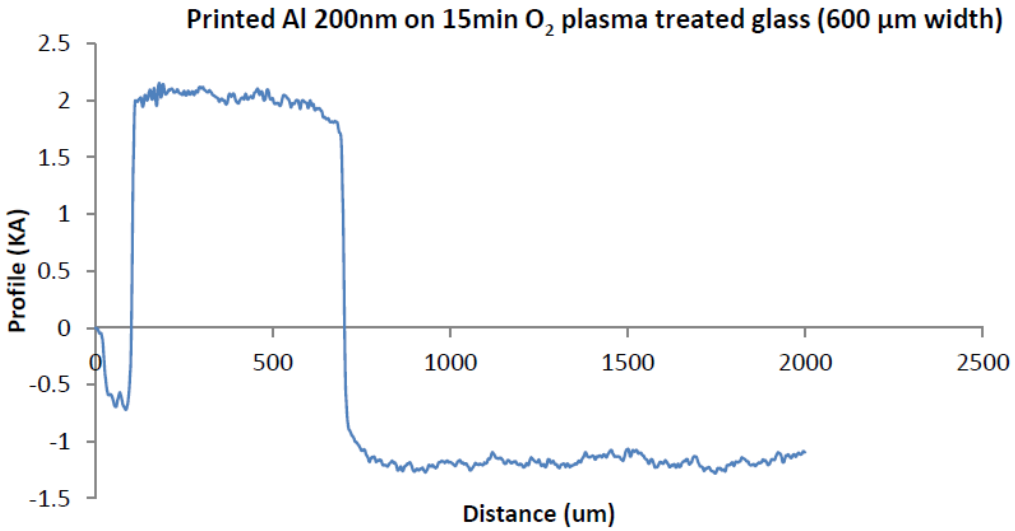

Figure A6: *a profilometer measurement of stamp printed Al (width of 600 µm) on 15-min oxygen plasma treated glass showing a thickness of approximately 200nm.*

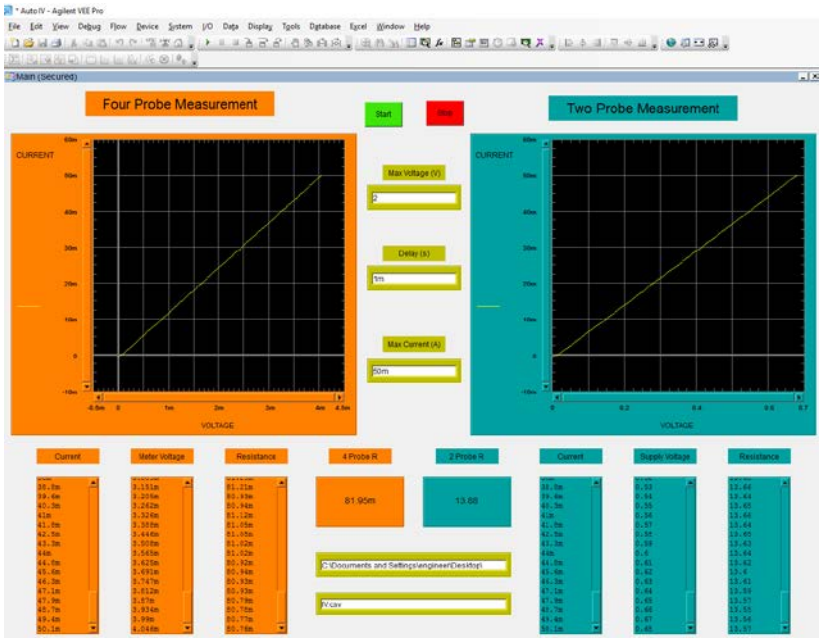

PSV: Power Supply voltage

DVM: Digital Voltmeter

Figure A7: *software (developed by J Glover at DMU) used for some 2-probe and 4-probe measurements*

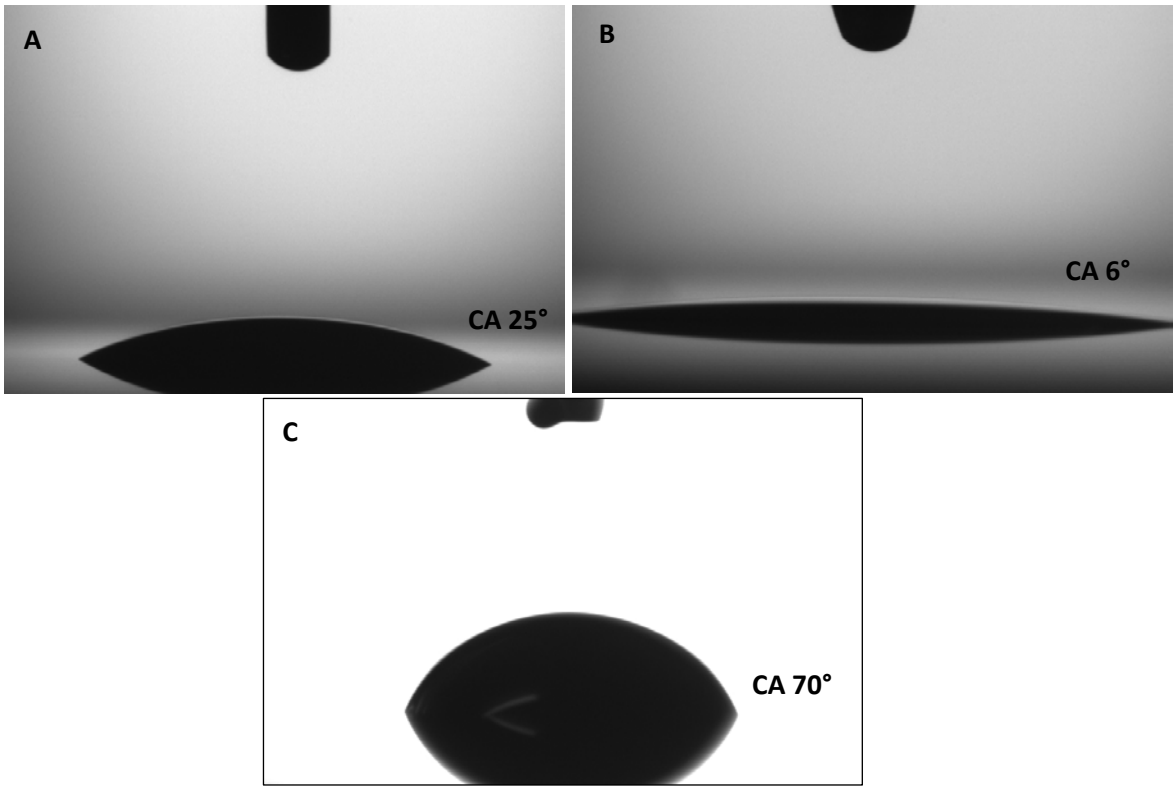

Figure A8: *contact angle of different inks with plastic covered with ITO substrate; a) silver ink, b) PEDOT:PSS ink and c) graphene oxide ink*

Information about the ceramic coated PEL paper which was used as substrate in some printings

PEL NANO P60

Electronic Grade Paper

Short description

A research-grade, electronic-rated paper. Designed to complement the range of substrates available for the development of printed electronics, PEL have released a non-organic coated paper for use with nanoparticulate inkjet inks.

The inorganic coating on the top side of the paper has a pore size of 60nm that absorbs solvents and dispersion agents thereby concentrating the nanoparticles and enhancing low temperature sintering.

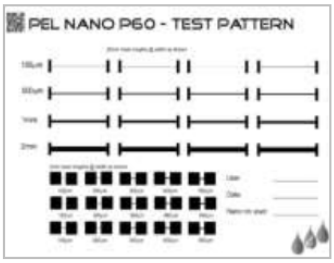

Thermal Curing/Sintering:

NanoP60 can be heated to 150°C with minimal discolouration and, for short periods, can be used at higher temperatures: sintering has been demonstrated with a wide variety of nano inks within a few seconds on PEL NanoP60.

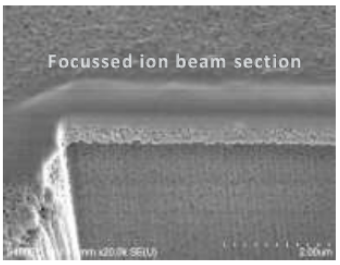

Photonic Curing:

The paper ink combinations work well with pulsed Xe flash using NovaCentrix's PulseForge and Xenon Corporation's Sinteron systems.

Data

All data is provided for information only and is not a guarantee of performance or a warranty. PEL recommend testing the Nano P60 paper using your nano particulate inks.

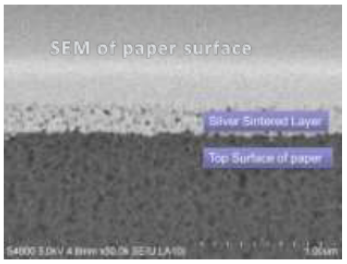

Summary

With many commercial inks full cure is achieved in less than one minute at 120°C to 150°C.

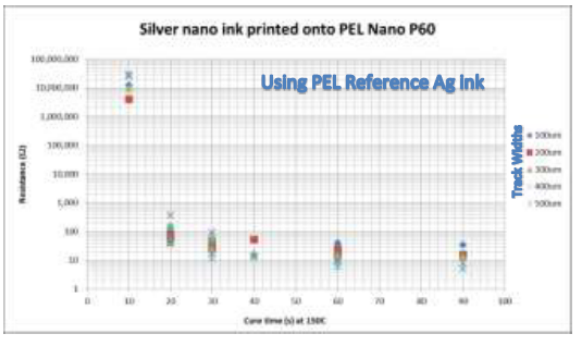

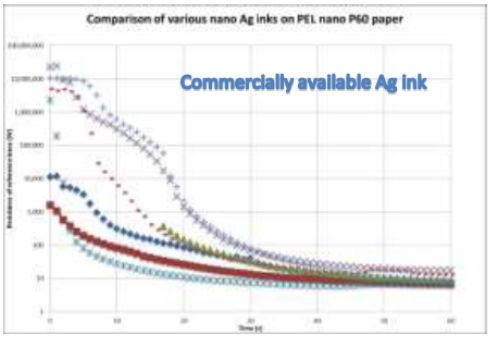

info@printedelectronics.com